Inorganic Scale Management during Shale Gas Production

Xu Wang

Submitted for the degree of Doctor of Philosophy

Institute of Petroleum Engineering

School of Energy, Geoscience, Infrastructure and Society

Heriot-Watt University

Edinburgh, UK

March 2018

Abstract

Hydraulic fracturing for shale gas production involves pumping large volumes of water; as a consequence of this, produced water management is an important topic to address in order to sustainably produce shale gas. It has been well documented that only approximately 10-40% of the pumped fluids will be produced back to the surface, and that there will be increased concentrations of various ions in the flowback water during this process. This flowback water, with high total dissolved solids and/or high concentrations of certain ions, presents a significant risk of mineral scaling.

Analysis of geochemical data is performed to address the question of whether the increase in salt concentration in the flowback water is due to the dissolution of minerals into the injected fracture fluid, or whether it is due to the interaction/reaction between fracture fluid and the *in situ* formation water. Data from both industry sources and the public domain have been used. Additionally, to understand better the fluid transport mechanisms within shale systems, and to match the volume of flowback water observed in field cases, models of fractured shale gas systems have been developed and the results are discussed.

Analysis of produced water compositional data has been performed – not only to calculate the scaling risk during shale gas production, but also to identify the *in situ* formation water composition. In general, it can be very challenging to identify the *in situ* formation water composition in shale reservoirs since samples of the formation water can be difficult to obtain. They may have been contaminated during the drilling process, reactions may have taken place due to fluid mixing between the injected fluid and the formation water, or simply they may not have been preserved appropriately. Some calculations of formation water compositions are presented based on the observed compositional data; thereafter, the predicted formation water compositions are validated by comparison with the observed total dissolved solids (TDS) data.

A mineral dissolution model was developed using PHREEQC to understand better the cause of high ion concentrations in the flowback water. Additionally, a series of single-phase 1D reactive transport models (including certain primary minerals) were developed to further analyse and validate the identification of the *in situ* water composition. In addressing the first question posed in this thesis, we conclude that the main reason for the high salinity of the flowback water is the occurrence of fluid mixing between the

fracture fluid and the high salinity formation water; it is not primarily the result of dissolution of minerals into the fracture fluid.

A two-phase 3D numerical flow model has been developed that includes a hydraulic fracture and is populated with shale reservoir properties. (This model assumes the hydraulic fracture is already established – i.e. the calculations include coupled flow and component transport, but the geomechanics are not considered). It is used to simulate fluid transport mechanisms within the shale system and to address the second question – what causes the significant retention of fracture fluid in shale reservoirs. A series of simulations was performed to achieve a history match with observed flowback water data in a western Canadian basin (the Horn River Basin). Meanwhile, given that extremely low matrix permeabilities (order nD) are measured in actual field systems, these calculations suggest that the injected fluid must propagate through secondary induced fractures or even a natural fracture network within the shale system, in order to propagate far enough from the main propped hydraulic fracture not to flow back immediately. In order to perform more representative modelling, the conductivity of the grid cells adjacent to the main hydraulic fracture must be increased, thus simulating a secondary induced fracture region. Additionally, the impact of gravity segregation and secondary fracture closure were also included to achieve a history match with field data (total volume of flowback water and the fraction of injected fracture fluid in produced water).

A further two-phase 3D flow model was developed to examine the scaling tendency due to the evolving produced brine composition over the lifetime of the well. It is based on the previously history matched model and includes the fracture fluid and formation water compositions to predict precipitation of minerals. The simulation results demonstrate that the worst scaling risk occurs during the initial period of shale gas production: this is an important consideration when designing scale control strategies. Finally, scale inhibitor injection was simulated to examine the impact of inhibitor retention on well protection. The model demonstrates that there is the potential to design a satisfactory scale inhibitor treatment as part of the pumping process.

This body of work develops a methodology for systematically analysing flowback water data and predicting *in situ* formation water compositions in shale reservoirs. It also uses modelling tools to identify scaling risks and address the causes of high salinity in the flowback water. It then introduces a simplified 3D fluid flow model that nevertheless

offers a good history match of observed data from a shale system. Further modelling studies based on this history-matched model demonstrate that the scaling tendency can be predicted and that an appropriate scale management programme can be designed.

To my parents, Yanhua Wang and Changhe Wang

Acknowledgements

Firstly, I would like to express my sincerest gratitude to my PhD supervisor Professor Eric James Mackay. Without his guidance, encouragement, enlightenment and support I would not have been able to smoothly manage my research work or even approach any valuable satisfactory research conclusions at this point of my PhD study. Albert Einstein says “In the middle of every difficulty lies opportunity”. PhD study is a complicated and difficult long-term research process for everybody, to conquer it one requires to find out every opportunity among all the difficulties. Eric’s patient edification and guidance is like a beacon in the fog which will always lead me to my correct direction on the research paths. He is not only a supervisor for me, he’s like a father who gives me good advice while I’m confused; he’s like a friend who listens and respects my ideas while we’re having technical discussions; he’s like a research partner who always inspires me and offers me help during my entire research work. It is really my greatest honour to have a supervisor like him.

Secondly, I sincerely appreciate the support and help offered by Foundation CMG (now Energi Simulation) and Flow Assurance & Scale Team (FAST) during my entire PhD study. Without their financial and technical support, it would have been definitely difficult for me to complete my research work. I also want to send my appreciation to FAST 5 and FAST 6 JIP sponsors for their valuable advice and support with regard to my presentations at each steering meeting.

In addition, I want to thank my second supervisor Ken Sorbie for his kind help and great guidance. My appreciations also extend to all the wonderful colleagues in FAST group Dr. Oleg Ishkov, Dr. Oscar Vazquez, Dr. Lorraine Boak, Mr. Mike Singleton and other people who helped and assisted me during my PhD study. I also want to send my warmest thanks to my friends Dr. Yisheng Hu and Giulia Ness who are always willing to help me to discuss and solve my questions when I needed.

I also want to offer my sincerely thanks to Associate Professor Alexander Shapiro from Technical University of Denmark and Associate Professor Dr. Jingsheng Ma from Heriot-Watt University who agreed to examine this thesis and my PhD work.

The software providers for offering me authentications to use their software during my simulation studies are also thanked – Computer Modelling Group, Schlumberger, Expro Petrotech and United States Geological Survey.

My very special appreciations will be given to Mr. Paul Bradley and his mum Jeannie Stewart Taylor Bradley, who made me feel like I've got a warm home in Scotland and offered me every support I could ever asked for. Without them, I would not have been able to get through all the difficulties and fully concentrate on my research these years. Both of them will be the most important people in my life forever and I will always appreciate and value every single moment we spent together.

Finally, my last special thanks will be given to my parents for being my shield to protect me and supporting me to continue my research for all of these years. I will always love them and be thankful for everything they did for me.

ACADEMIC REGISTRY

Research Thesis Submission

Name*:*	Xu Wang		
School:	School of Energy, Geoscience, Infrastructure and Society		
Version: *(i.e. First, Resubmission, Final)*	Final Submission	Degree Sought:	PhD, Petroleum Engineering

Declaration

In accordance with the appropriate regulations I hereby submit my thesis and I declare that:

1) the thesis embodies the results of my own work and has been composed by myself
2) where appropriate, I have made acknowledgement of the work of others and have made reference to work carried out in collaboration with other persons
3) the thesis is the correct version of the thesis for submission and is the same version as any electronic versions submitted*.
4) my thesis for the award referred to, deposited in the Heriot-Watt University Library, should be made available for loan or photocopying and be available via the Institutional Repository, subject to such conditions as the Librarian may require
5) I understand that as a student of the University I am required to abide by the Regulations of the University and to conform to its discipline.
6) I confirm that the thesis has been verified against plagiarism via an approved plagiarism detection application e.g. Turnitin.

**Please note that it is the responsibility of the candidate to ensure that the correct version of the thesis is submitted.*

Signature of Candidate*:*		Date:	

Submission

Submitted By *(name in capitals):*	
Signature of Individual Submitting:	
Date Submitted:	

For Completion in the Student Service Centre (SSC)

Received in the SSC by *(name in capitals):*			
1.Method of Submission (*Handed in to SSC; posted through internal/external mail*):			
2.E-thesis Submitted (**mandatory for final theses**)			
Signature:		Date:	

Please note this form should be bound into the submitted thesis.

Table of Contents

Nomenclature

1D	One-dimensional
2D	Two-dimensional
3D	Three-dimensional
Ba	Barium
$BaSO_4$	Barium sulphate (Barite)
$BaCO_3$	Barium carbonate (Witherite)
bbls	Barrels
b.d.	Below detection
Br	Bromide
C	Scale inhibitor concentration in solution
Ca	Calcium
$CaCO_3$	Calcium carbonate (Calcite)
cal.	Calculated
C_{fw}	Chloride concentration in the formation water
C_{ow}	Chloride concentration in the observed (flowback) brine
C_{iff}	Chloride concentration in injected fracture fluid
Cl	Chloride
CO_2	Carbon dioxide
CO_3	Carbonate
Cr	Rock compressibility
C_{sifw}	Concentration of scale inhibitor in flowback water

DFN	Discrete fracture network
EDTA	Ethylenediaminetetraacetic acid
EIA	Energy Information Administration
EOS	Equation of state
Φ_{NF}	Porosity of the natural fractures in each block
FW	Formation water
H+	Hydrogen
HCL	Hydrogen chloride
HCO_3	Bicarbonate
H_2O	Water
H_2O_{con}	Calculated solution in mg/L
H_2O_{MW}	Solution molecular weight
HRB	Horn River Basin
I_{con}	Calculated ion concentration in mg/L
$\sum I_{mm}$	Summation of ion concentrations in mmole/L
I_{mola}	Exported ion molality in flowback water in simulation results
IFFF	Injected fracture fluid fraction in the flowback water
IW	Injection water
IWF	Injection water fraction
K	Potassium
K and *n*	Constants which identify the adsorption level
Keq	Equilibrium constant

LGR	Local Grid Refinement
$L_{I \text{ or } J}$	Grid block size in I or J direction
Mg	Magnesium
MIC	Minimum inhibitor concentration
Na	Sodium
N_{fw}	Produced water volumetric rate
N_I	Numbers of fractures in I direction
N_J	Numbers of fractures in J direction
NORM	Naturally occurring radioactive materials
N_{si}	Scale inhibitor produced mass flux rate
SI	Scale inhibitor
SIT	Specific ion Interaction Theory
SO_4	Sulphate
Sr	Strontium
$SrSO_4$	Strontium sulphate (Celestite)
SR	Saturation Ratio
S_W	Seawater
Swc	Connate water saturation
T	Thickness of the grid block
Γ	Actual adsorbed amount of scale inhibitor
TDS	Total dissolved solids
V_B	Total volume of each grid block

V_I	Volume of fractures in I direction
V_J	Volume of fractures in J direction
W	Width of the fracture

PUBLICATIONS

Xu Wang and Eric Mackay. What is the Fate of Fracture Fluid during Shale Gas Production? Paper presented at the 78th EAGE Conference & Exhibition, Vienna, Austria, 30 May – 2 June 2016.

Xu Wang and Eric Mackay. Simulation Study for Inorganic Scale Management during Shale Gas Production. Paper SPE190717 presented at the SPE Canada Unconventional Resources Conference and Heavy Oil Technical Conference, Calgary, Canada, 13-14 March 2018.

Xu Wang and Eric Mackay. Simulation Study for Scale Management during Shale Gas Production. Paper SPE190717 has been presented at the SPE International Oilfield Scale Conference and Exhibition, Aberdeen, Scotland, UK, 20-21 June 2018.

CHAPTER 1 INTRODUCTION

1.1 SHALE GAS OVERVIEW

As global energy consumption is rising rapidly, exploiting only conventional energy cannot meet the demand. As a result of this, significant exploitation of unconventional energy is required. As one of the unconventional energy sources with greatest potential, the development of shale gas production has been growing very rapidly in US, and the interest of operating shale systems has also extended to other countries which potentially have large shale gas reserves (Richardson et al., 2013).

Shale gas is a natural gas which is stored within the low permeability matrix rock of the shale reservoir. The shale reservoir not only contains a high content of organic matter, but also has high content of clays of fine grain sizes (Gluyas and Swarbrick, 2009). There are three main ways for natural gas to be stored in shale reservoirs: free gas stored within pores of the rock, gas adsorbed on the organic matter and also the free gas stored within the natural fracture systems in shales (Lu et al., 1995; Allen et al., 2009). All of these natural gas storage mechanisms provide the key for different production designs for the shale gas reservoirs, and also differentiate which stimulation method should be undertaken.

Before shale gas became a popular unconventional energy source, it was considered as immobile and uneconomical to produce due to the source rock having low porosity and very low permeability. However, the application of hydraulic fracturing and horizontal drilling makes economical shale gas production possible (Slatt, 2015). If there is a system of natural fractures also existing in the shale reservoir, the transmissibility within the reservoir will be provided by both the natural fractures and the hydraulic fractures. Compared with conventional reservoirs, fractured shale is considered to be both the source rock and also the reservoir. The properties of the fractures play an important role in shale gas productivity, shale gas development and sustainable commercial shale gas production rates. Hydraulic fracturing involves large volumes of water to complete the process; as a consequence of this, the water transportation, source water treatment, as well as flowback water and produced water management are important topics for the sustainability of shale gas production.

There is significant resistance to the fluid flowing within a low permeability reservoir, of which shale reservoirs are typical. As geological time passed by, geochemical and geomechanical processes acted on the low permeability reservoir rock; some of these actions will have narrowed or even blocked the flow paths in the rock. Under these circumstances, hydraulic fracturing is the only way to stimulate flow. In many situations, especially for the low permeability shale reservoirs, they are economical only if a successful hydraulic fracturing process is designed and operated (King, 2010). A successful hydraulic fracturing treatment requires optimization of hydraulic fracture properties with regards to the reservoir conditions, and then making sure the designed programme is implemented successfully while the treatment is taking place in the field (King, 2012). By the year 2015, hydraulic fracturing had been widely applied in shale reservoirs all over the world, such as the US, Canada, China, etc. **Figure 1.1** indicates a general hydraulic fracturing process applied on Marcellus shales in the United States (RSRAE, 2012).

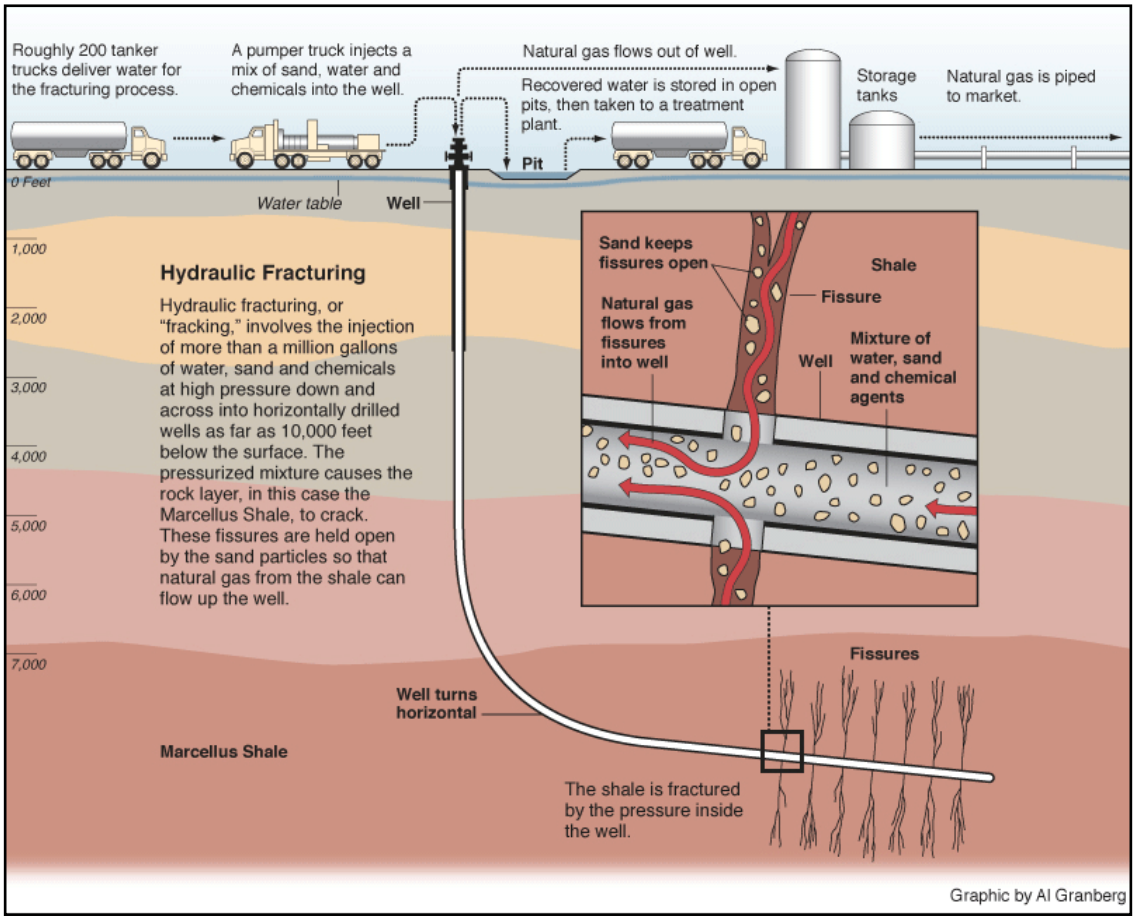

Figure 1.1 Hydraulic fracturing used for shale gas production (RSRAE, 2012)

Generally speaking, hydraulic fracturing is used to increase the production rate, which makes an uneconomical reservoir become commercial. Under usual conditions hydraulic fracturing is applied for a number of reasons (King, 2010&2012; Meyer and Bazan, 2011), such as:

- For the low permeability reservoirs (like shales), to increase the flow rate of the hydrocarbons
- For the damaged well, to increase the flow rate of hydrocarbons past the damage zone
- For the reservoir where natural fractures exist, to connect the natural fractures and create paths to the wellbore
- To prevent sand production risk by reducing the pressure drawdown around the well
- To control the risk of asphaltine and paraffin deposition by decreasing the pressure drop near the wellbore
- When hydraulic fractures are created, there is an increase of drainage area as well as the contact area between well and formation
- To build up connections between the reservoir and a directional well/horizontal well

Apart from all the hydraulic fracturing effects mentioned above, there are also other applications with hydraulic fracturing; however, the most commonly useful ones have been identified above.

Due to shale gas accumulating throughout a large geographic area as a continuous type of natural gas play, shale gas reservoirs may have longer production period than conventional production. According to data presented in **Table 1.1**, the worldwide reserves estimation of shale gas shows a significant potential (US EIA, 2013).

Table 1.1 Estimated technically recoverable shale gas by country

NO.	Country	Estimated technically recoverable shale gas (trillion cubic feet)	Proven natural gas reserves of all types (trillion cubic feet)	Report Date
1	China	1115	124	2013
2	Argentina	802	12	2013
3	Algeria	707	159	2013
4	United States	665	318	2013
5	Canada	573	68	2013
6	Mexico	545	17	2013
7	South Africa	485	-	2013
8	Australia	437	43	2013
9	Russia	285	1688	2013
10	Brazil	245	14	2013

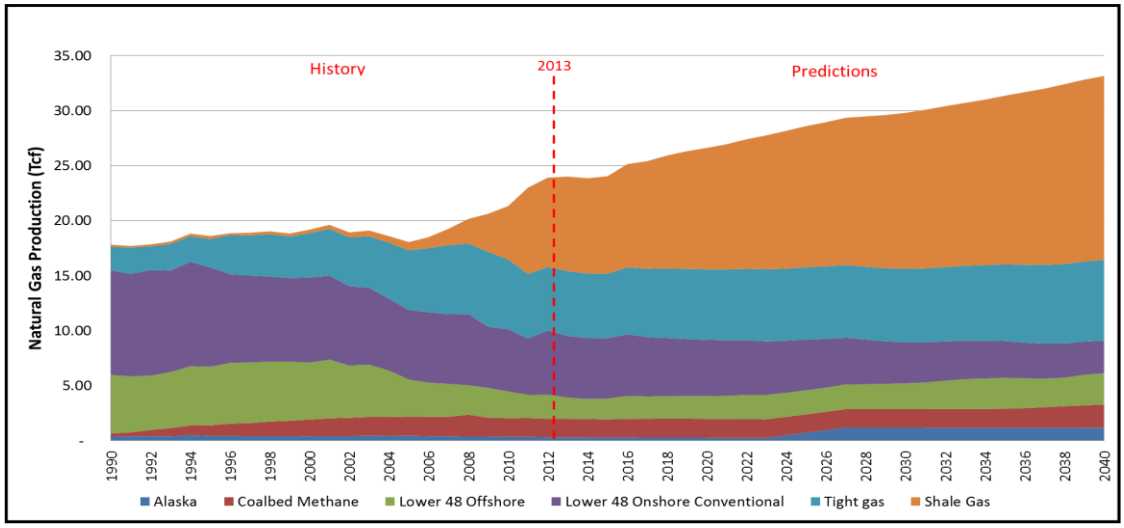

Figure 1.2 Nature gas supply and predictions within US, as of 2013 (EIA, 2013)

It has been reported that the total number of unconventional natural gas wells in 2004 in US was 18,485 and this number increased to 25,145 in 2007 and is still expected to rise until 2040 (Vidas, 2008). According to this report, it indicates that the lifetime for natural gas production in US is expected to last for 100 years; however, the proven reserves can only supply 11 years of continuous recovery from the calculation. The predicted trend plot for natural gas production in US has been indicated in **Figure 1.2** (US EIA, 2013).

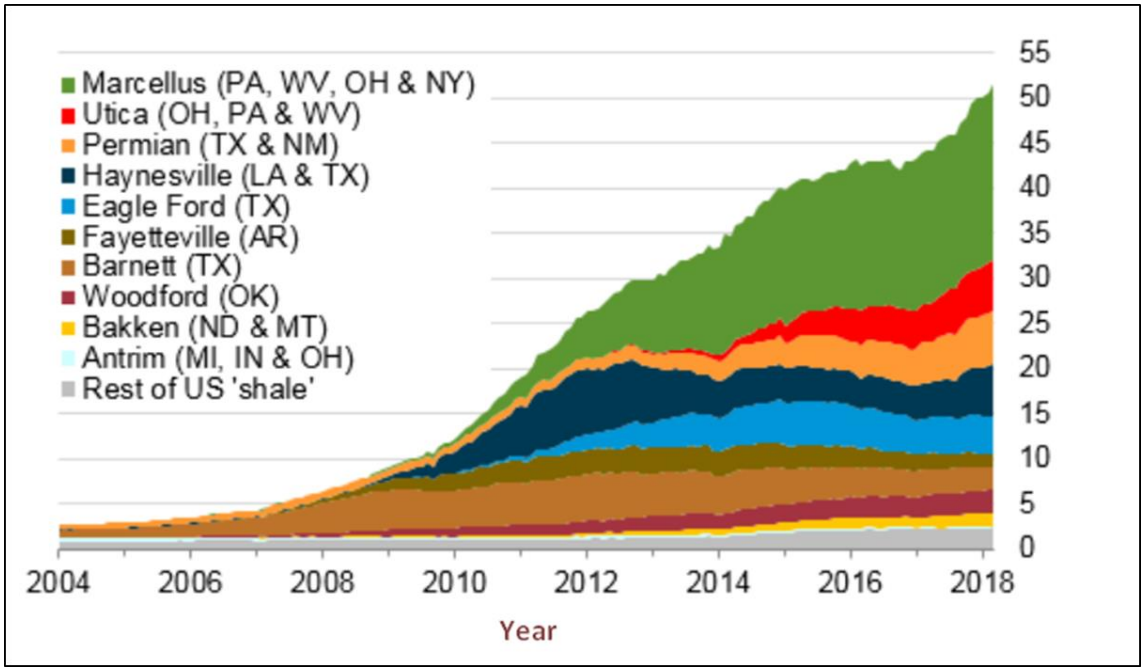

Figure 1.3 Dry shale gas productions in US from different shale plays by 2018 (EIA, 2018)

Figure 1.3 shows some plots of dry shale gas production from different shale plays in US; the data have been derived from state administrative data collected by DrillingInfo Inc. up to 19th April 2018. From the plots it can be readily seen that the overall trend of shale gas production in the last 15 years in US is increasing, in line with the discussions above; however, a decrease can be observed for most of the shale plays in 2014 and again in 2016. These declines of shale gas production can be considered as corresponding to the low oil and gas prices those years, and an increase can be observed again after 2017 due to the crisis in the oil and gas industry having largely passed.

1.2 OILFIELD SCALE OVERVIEW

It is well known that inorganic scales can be found in oilfield production due to the application of ionic brine for water flooding, hydraulic fracturing and other stimulation processes. Most of the oilfield inorganic scales are formed by chemical crystallisation

reactions. These scales are usually generated during the hydrocarbon recovery process and deposit due to the changing of the ionic concentration, temperature, pressure and other conditions (Vetter, 1976; Duccini et al., 1997).

Table 1.2 Different types of inorganic scales encountered in oilfield production

Mineral type	Composition	Relative Solubility (mg/l)	Causes of Solubility Change
Calcite	$CaCO_3$	196	PCO_2, Total pressure, TDS, Temperature
Siderite	$FeCO_3$	100	PCO_2, Total pressure, TDS, Temperature
Barite	$BaSO_4$	44	Pressure, Temperature, TDS
Celesitie	$SrSO_4$	520	Pressure, Temperature, TDS
Anhydrite	$CaSO_4$	3270	Pressure, Temperature
Gypsum	$CaSO_4.2H_2O$	6300	Pressure, Temperature
Pyrite	FeS	105	Pressure, Temperature, TDS
Galena	PbS	0.006	Pressure, Temperature, TDS
Sphalerite	ZnS	0.09	Pressure, Temperature, TDS

There are many different types of inorganic scales which can affect the normal production process; some of the common ones are presented in **Table 1.2**. The three major types of inorganic scales which can be commonly observed in many oilfields will be introduced and the deposition mechanisms will be identified as follows (Mackay et al., 2004; Guan, 2016):

- The first type of inorganic scale will deposit due to pressure and/or temperature changes. The pressure decrease and/or temperature increasing will cause the CO_2 to evolve and PH to raise, this causing carbonate scale deposition, such as calcium carbonate (the chemical equation is shown in **Equation1.1**).

$$Ca(HCO_3)_2 = CaCO_3 \downarrow + CO_2 \uparrow + H_2O \quad \text{...Equation 1.1}$$

- The second type of inorganic precipitation is due to mixing of two fluids which have incompatible compositions and this will lead to chemical reaction taking place that result in the creation of oilfield scales (the most common type is when the flooding water contains sulphate and the formation water has cations which will react with the sulphate, such as barium, calcium or strontium, resulting in the formation of $BaSO_4$, $CaSO_4$ or $SrSO_4$). Here we describe $BaSO_4$ precipitation as an example:

$$Ba^{2+} + SO_4{}^{2-} = BaSO_4 \downarrow \text{...Equation 1.2}$$

- The third type of inorganic scale is halite. This forms due to evaporation.

Due to the various deposition mechanisms discussed above, there are different potential locations for deposition (Clemmit et al., 1985; Mackay et al., 2004) : within or adjacent to injection/production wellbore and the stimulated areas within the formation (due to

the mixing of injected fluid and formation water), inside production tubing (due to the mixing between fluids produced from isolated areas with different compositions or due to pressure decrease), inside treatment facilities (such as separators, hydro-cyclones and other equipment).

If a scaling risk has been predicted or observed during oilfield development, scale depositions may not only reduce the productivity but also increase the cost of facility maintenance or even cause significant safety risks. As a consequence of this, the management of scale control is necessary for developing long-term hydrocarbon production.

1.3 SCALE CONTROL OVERVIEW

The deposition of inorganic scale is a common flow assurance problem for many hydrocarbon fields. On the one hand, many conventional reservoirs require water to be injected to maintain and to sweep oil towards producers, and this will lead to s scaling risk due to the use of high sulphate injection water (such as seawater, recycled produced water etc.) (Obinna and Frzrie, 2011); on the other hand, for most unconventional reservoirs, hydraulic fracturing is necessary to achieve a better performance of hydrocarbon production, and this may cause serious mineral precipitation on account of fluid mixing between fracture fluid and flowback water with high salinity (Guan, 2016). If a high scaling risk has been predicted or evaluated during the production, scale control is necessary to protect well and reservoir from the potential damage.

Productivity can be badly affected by the formation damage caused by deposition of mineral scales. To maximise the hydrocarbon recovery efficiency and also to extend the sustainability of oilfield development, the management of scale is important and necessary. The most common scale control management strategies are scale removal and scale inhibition (Rogers et al., 1990; Oddo et al., 1999; Ragulin et al., 2004; Jordan et al., 2005; Hernandes, 2008; Mackay, 2010; Yan et al., 2013; Guan, 2015; Tiwari et al., 2017).

1.3.1 Scale removal

1.3.1.1 Chemical treatment removal

The most widely applied scale removal operation is chemical treatment in terms of pumping acid or chelating agents. The acid flush is normally performed to deal with

carbonate mineral scales like calcite, dolomite, magnesite (Tiwari et al., 2017) and chelating agents are normally introduced to stabilize precipitation and/or remove particularly targeted mineral scales (e.g. EDTA is applied for removing barite scales) (Mahmoud and Elkatatny, 2017). The flushing of acid fluid and chelating agents is commonly conducted as a pre-treatment for the scale control process and applied in combination with a scale inhibition process to reduce/ prevent scaling risk.

The carbonate mineral scales will be dissolved through chemical reactions with acid fluid due to their high solubility at low PH conditions, whereas the chelating agent solutions can increase the saturation index of the targeted mineral so that further treatment can be managed thereafter (Frenier et al., 2000; Mahmoud and Elkatatny, 2017). With the completion of the pre-cleanout operations, scale inhibition treatments can be performed for the post scale control management (Sitz et al., 2003).

1.3.1.2 Mechanical treatment and removal

Another widely implemented scale removal method is mechanical treatment, such as milling, high pressure water jetting etc. (Brown et al., 1991; Eslinger et al., 2000; Enerstvedt and Boge, 2001). Milling tools are used for removing less compacted filter cakes or "weakly" formed depositions on the surface. Once they are broken into pieces or loosened up by the milling process, high pressure water jetting can be performed for further clean the system. The mechanical scale removal treatment is considered as an efficient method to remove those surface scales that are less consolidated and it can also be an economical option (Brown and Merrett, 1991). Nevertheless, conventional mechanical scale removal can also have some potential disadvantages – 1) if the milling process is not managed properly, unexpected damage will be caused due to long intervals between application; 2) even though high pressure water jetting is able to carry away most of the small particles, some hard bits or even large pieces are still not able to be lifted away, which could lead to further blockage due to gravity segregation (Eslinger et al., 2000). In consideration of these disadvantages, further improvements in downhole tools and milling techniques have been made to optimize the removal process as well as reduce the risk caused by a failed treatment (Kocis et al., 2015; Gajdos et al., 2016).

Although both the chemical and the mechanical scale removal treatments are able to reduce or even eliminate the appearance of mineral scale deposition, they are not able to stop or control the mineral precipitation from forming during the ensuing production.

Hence, a scale inhibition process must be conducted after the removal treatment in a mature scale environment.

1.3.2 Scale inhibition

As noted previously, scale inhibition treatments will only be performed if the oilfield is at serious risk of scaling, as determined by a dependable assessment of the scaling tendency based on compositional analysis and thermodynamic prediction (Ragulin et al., 2004; Guan, 2015). The basic principle of scale inhibition is to introduce SI (scale inhibitor) into the system so that mineral scales can be prevented from precipitating. Meanwhile, different methods can be selected in order to deliver SI into the system, such as continuously pumping SI into the injection stream, treating SI as one of the chemical additives in the injection fluid prior to the stimulation process, managing SI squeeze treatment jobs in producing wells, and so forth. A successful scale inhibition treatment will be achieved with a significant retention of inhibitor within the target location, and it can be measured by evaluating the concentration of SI in the produced/flowback water (Rogerset et al., 1990; Crowe et al., 1994).

1.3.2.1 Continuous injection of SI

Continuous injection of SI has been widely applied as one of the major scale inhibition strategies, not only for the conventional reservoirs, but also for the unconventional oilfield development (Hernandes, 2008; Guan, 2015). Before continuously injecting SI into a scaling system, selections of SI needs to be performed to identify the chemical which has the best performance in preventing mineral scales from forming. A series of laboratory tests is required to evaluate SI compatibility with injection brine, and core flood tests are needed to test for formation damage along with SI adsorption. (Samuelsen et al., 2009)

After identifying SI performance, continuous SI injection can be deployed. This involves continuously injecting SI through a chemical line into the production system. Alternatively, SI can be included as an additive in the injection brine, and will be continuously pumped into the target formation during fracking (Hernandes, 2008; Samuelsen et al., 2009). The second strategy has been widely performed to prevent mineral scales from depositing within unconventional systems (Vetter et al., 1988; Crowe et al., 1994; Norris et al., 2001; Guan, 2016).

For some unconventional oilfield scale management, SI injection is performed prior to the injection of fracture fluid as a pre-flush process to inhibit scale forming adjacent to the near wellbore zones; however, for most inhibition strategies it has been added directly into the fracture fluid due to its good compatibility and stability (Crowe et al., 1994). Another reason for adding SI into the fracture fluid is to achieve better adsorption/retention behaviour, due to the fluid propagation that can be achieved after the hydraulic fracturing process is completed (even better retention can be observed within a naturally fractured system) (Vetter et al., 1988; Spooner et al., 2014). It is known that due to the low matrix conductivity and poor communication between wells and unconventional formations, fluid transport will occur within the stimulation area where potentially there is a higher scaling risk. Therefore, injection of SI along with fracture fluid can effectively inhibit this scaling tendency (Yan et al., 2015). It is reported that the fraction of SI added in the fracturing fluid is on average 0.023% (Tollefson, 2013).

1.3.2.2 SI squeeze treatment

Another widely applied scale inhibition strategy is SI squeeze treatment (Kerver and Heilhecker, 1969; Mackay, 1999; Wang and Hung, 2006; Vazquez, 2012). A representative SI squeeze treatment design normally include five stages, which are pre-flush, injection of main SI slug, overflush, shut-in and back production (Rakhimov et al., 2010).

The pre-flush process can be considered as a preparation stage before managing the whole squeeze treatment, which helps to clean out the surfaces of target locations and also cools down the nearby areas so that SI can be delivered further into the formation without experiencing a major loss due to the adsorption within the zones adjacent to the wellbore. The main treatment is where the majority of the inhibitor chemical is injected. The overflush stage can displace the SI into deeper zones in the reservoir. The shut-in period provides extra time for SI to be fully adsorbed/precipitated in the formation so that better inhibitor retention can be achieved.

A minimum inhibitor concentration (MIC) will be determined from laboratory tests or field experience, and time for inhibitor returns to reach MIC can be used to evaluate whether or not the operated squeeze treatment is successful. A schematic of a SI squeeze treatment design is indicated in **Figure 1.4** (Kokal et al., 1996).

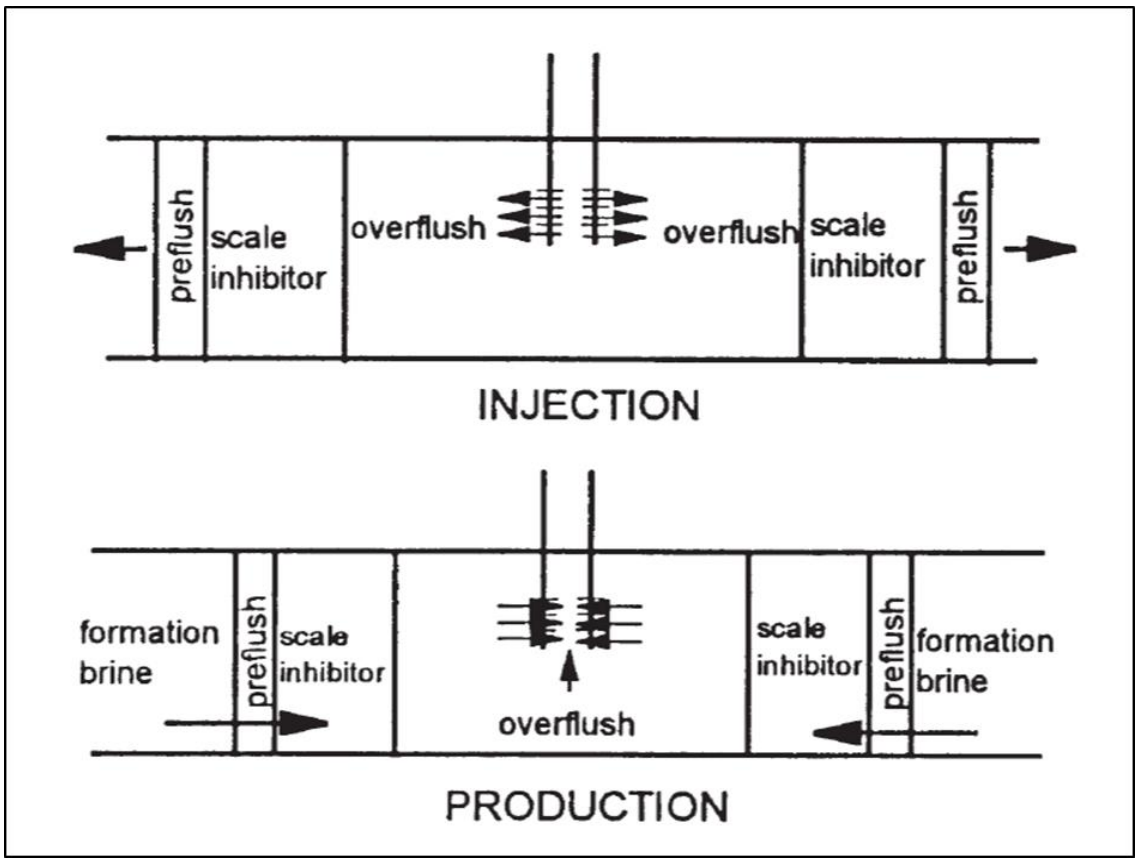

Figure 1.4 Schematic of a conventional SI squeeze treatment design (Kokal et al., 1996)

Some squeeze treatments are also applied in unconventional hydrocarbon recoveries, and one has been studied and reported by Spicka (2017). This squeeze treatment has been designed for the development in the Bakken shale play, which is a shale formation located in North Dakota, US.

For hydrocarbon recovery in conventional reservoirs, the existence of natural fractures could be considered as an enhancement of productivity, yet they cause potential difficulties for successfully managing a SI squeeze treatment due to the high conductivity of the natural fracture zones which may "steal" the injected SI and will lead to less SI being delivered to the deeper formation (Spooner et al., 2014). In contrast with conventional reservoirs, to achieve a better recovery factor the unconventional production relies on the stimulated area created by the hydraulic fracturing process, and these high conductivity fracture zones also provide a region where most of fluid transport occurs. As a consequence of this, there is potential to perform a successful squeeze treatment in unconventional reservoirs to manage scaling risk (Spicka et al., 2017).

1.3.2.3 Novel scale inhibition treatment

Due to the unique properties of unconventional reservoirs (normally with low permeability and porosity) along with the requirement of hydraulic fracturing, some novel scale inhibition treatments have been proposed for scale control during unconventional recovery in the recent decades, with a representative one being the application of proppant-based scale inhibitor (Gupta et al., 2008; Kalfayan et al., 2013; Shen et al., 2017).

The most widely applied and studied proppant to deliver SI is "a proppant sized, high internal surface area substrate impregnated with scale inhibitor" (Kalfayan et al., 2013). The reason for choosing this novel SI proppant is due to the total carrying surface being larger than the normal SI coated proppant (sand or ceramic) and also the larger contact area makes the release of SI into the system more effective. Compared with the conventional scale inhibition treatment, the application of proppant-based scale inhibitor could be more efficient and economical for scale control in unconventional reservoirs: 1) it is easier and more efficient to approach the target location and deliver SI into the system by injecting it along with fracture fluid; 2) it is able to provide longer scale inhibition lifetime since the desorption of SI is a gradual process. However, there are still some challenges to applying solid-based SI in unconventional reservoirs, one of which is the compatibility with fracture fluid. According to the conclusions presented in the relevant literatures, the application of solid-based SI could be an option for preventing scale formation in unconventional reservoirs with medium or low scaling risk. For those unconventional reservoirs which have serious scaling problems, it requires to selection of other scale inhibition strategies is required to achieve better scale control management.

1.3.3 Other scale control strategies

Apart from the scale inhibition treatment introduced previously, there are also some other scale control strategies that can be chosen in order to deal with different scaling risk scenarios. One of them is treatment desalination of injection brine (Amjad, 1996; Hutchings et al., 2010; Marquez et al., 2011; Abdul Majid et al., 2017).

The hydraulic fracturing process in unconventional reservoirs involves in large volumes of water; in some areas which have a lack of natural water supplies the usage of recycled produced water will be the only option. Meanwhile, for the development of

some offshore oilfields the requirement to inject seawater-based fracturing fluid will be inevitable. Both the flowback water produced from unconventional reservoirs and seawater has high salinities and this may lead to a serious scaling risk if performing a reinjection process without any pre-treatment. In this circumstance, desalination is required to reduce or even eliminate the relevant ions in the flowback water so that mineral deposition can be effectively controlled after the injection of recycled water. Nevertheless, the economic considerations in terms of disposing of large volumes of water, managing significant water storage and transportation could be significant.

1.4 MOTIVATIONS AND OBJECTIVES

As noted previously, compared with conventional reservoirs, scale control is also an important topic to study during the whole lifecycle of a shale gas reservoir development. This is due to the large volume of injected fracture fluid that is involved in the hydraulic fracturing process to stimulate the shale matrix along with the fact that only a small fraction of the injected water flows back (from 10% to 40%), and this has altered (high) salinities. Both of these factors can lead to the precipitation of inorganic scales introduced previously (inorganic scale deposits due to the mixing of two brines with incompatible compositions and due to self-scaling) and this scaling risk can be quite serious (considering one million gallons of water or more may have been introduced into the shale system).

Although, shale systems have been studied and researched for decades, and significant improvements have been made recently, inorganic scale management during shale gas production still not well performed. This body of research aims to identify an optimised scale management approach for preventing wellbore and formation damage throughout the life cycle of a shale gas development. To approach the final objective of this study, five questions require to be addressed:

- Which mechanisms account for significant retention of injected fracture fluid?
- How to set up a simplified fluid flow model that accounts for the major mechanisms proposed to represent the whole hydraulic fractured shale system?
- What causes the altered high salinity in flowback water produced after the injection of low salinity water in fracture fluid?
- Where and when will the worst scaling risk take place during shale gas production?

- How best to apply inhibitor to prevent this scale?

1.5 OVERVIEW OF SIMULATION CODES USED IN THIS STUDY

A brief overview of the simulation codes used in this study is presented as below:

MultiScale is a thermodynamic computer simulator to predict mineral deposition. It develops a multiphase equilibrium description and includes the phase distribution of the scale relevant gases, such as CO_2 and H_2S. In addition, water evaporation can also be considered in the model. This simulator is designed to predict most inorganic mineral scales such as calcite, gypsum, barite, anhydrite etc. It predicts the scaling tendency on the basis of pure mixing and on the basis of changes in pressure and temperature.

PHREEQC is a computer program developed for simulating aqueous geochemical reactions (Parkhurst and Appelo, 1999). It includes different varieties of aqueous models, such as two ion-association aqueous models, Pitzer activity models with specified ion interactions and the SIT (Specific ion Interaction Theory) aqueous model. By developing simulations for all of these models, it can be used to perform different calculations such as: 1) speciation and saturation index calculations; 2) one dimensional reactive transport calculations (reversible and irreversible), these calculations could refer to but are not confined to mineral dissolutions, mixing of solutions, kinetic reactions, ion exchange processes and pressure and/or temperature changes; 3) inverse calculations to identify the initial minerals and gas compositions that account for the compositions changing from two different specified brines. Compared with MultiScale, its advantage is that it is capable of reactive transport modelling, which means it is able to simulate more complex situations than MultiScale.

CMG IMEX is a three phase black-oil simulator with gravity and capillary terms. It can be run in explicit, fully implicit and adaptive implicit modes to adapt to the complexities of different simulations. It is capable of simulating various systems such as dual porosity and permeability models, solvent models by applying a pseudo-miscible option, polymer injection models, faulted/natural fractured models etc. It is designed with a user friendly visualisation interface. One important function related to this study requires to be discussed with IMEX simulation is the theory is that it can be used to simulate hydraulic fractures. The simulator assumes the hydraulic fractures are already established (with the application of local grid refinement, LGR). These calculations

include coupled flow and component transport calculations, but the geomechanics are not considered.

CMG CMOST is a CMG application that works in conjunction with other CMG simulators to develop sensitivity, optimization, uncertainty and history matching studies. It is capable of running multiple cases at the same time with the optimization of CPU usage, so that it is able to provide better comparisons between different cases and also it enhances the efficiency for history matching and uncertainty studies.

CMG GEM is a multidimensional, equation-of-state (EOS) compositional simulator which can simulate the important mechanisms of a reservoir under complicated conditions. The most important function used in this study is geochemical modelling. It allows users to input chemical compositional data for the brines along with defining initial minerals in place. The coupling between dynamic chemical reactions and mineral dissolutions/precipitations provides more flexibility on scaling tendency prediction and scaling risk assessment which is very valuable information for the study of scale control management.

1.6 THESIS OUTLINE

Chapter 1 provides an introduction to the whole thesis in terms of a brief overview on shale gas production and oilfield scale risk, along with an introduction to scale inhibition and an overview of simulator codes used for this study.

Chapter 2 includes an overview of the literature survey with regards to data collection. It presents the types of data collected for analysis. It then provides some discussions on chemical compositional data analysis to achieve a better understanding of scaling tendency prediction and formation water composition calculation. According to the calculation results for *in situ* formation water composition prediction, it presents a method to initially address one of the key questions – what causes the altered high salinity of the brine produced back during shale gas production. Meanwhile, Chapter 3 also provides further calculations on the fraction of injected fracture fluid in the flowback water as the basis of the history matched fluid flow modelling.

Chapter 3 introduces a methodology to develop a simplified fluid flow model to represent a typical hydraulic fractured shale system. The development of this modelling is based on the major fluid flow mechanisms proposed from relevant research

previously conducted and combines the major theories to model a case history matched against field data. As a consequence of the development of this fluid flow modelling methodology, another key question has also been addressed – which mechanisms can account for the significant retention of injected fracture fluid in a hydraulic fractured shale system.

Chapter 4 presents some simulation results obtained from the geochemical simulations developed for a shale system. It delivers further improvements in addressing the question of "what caused the altered high salinity brine produced back during shale gas production" by presenting the results of a mineral dissolution model developed in PHREEQC, and a geochemical 1D compositional model in CMG GEM. It then uses the geochemical 3D GEM modelling as a tool to predict the scaling tendency and identify scaling risk during the whole process. All of these geochemical simulations aim to provide a better understanding of how to target the worst scaling risk scenario during shale gas production, so that further scale damage can be reduced or even prevented.

Chapter 5 further develops a scale inhibitor injection model on the basis of the history matched fluid flow model established in Chapter 4. The aim for this scale inhibitor injection modelling study is to be used as an initial discussion of scale control management, so that further scale control modelling can be optimised and the final scale control design can be developed.

Chapter 6 briefly summarised the progress of this study and then draws some conclusions for the entire thesis, and also addresses the key questions proposed from the start of this topic. Some recommendations on potential future work are discussed and presented.

CHAPTER 2 DATA PREPARATION AND ANALYSIS

2.1 CHAPTER CONTENT AND INTRODUCTION

In some of the oilfields where operators use seawater as injection water or produce back high salinity water, scaling risks cause serious problems throughout the lifetime of recovery (Graham, 2004). To prevent scaling damage due to mineral deposition or even to minimise the scaling risk by choosing a suitable scale control plan are important subjects. Therefore, the analysis of produced water chemical compositional data becomes a necessary and routine task to help predict the scaling tendency, and to avoid formation/well damage throughout the entire conventional or unconventional production.

At the end of the recovery life of conventional reservoirs, the chemical compositions of produced waters tend to be close to the injection water composition due to the breakthrough of injected water. This means that the salinity of produced water recovered from conventional reservoirs will tend to be high during the early stages, and will decrease until the breakthrough of injection water takes place. By contrast, during the early stage of the unconventional recovery, the majority of the water produced back is fracture fluid and the fraction of fracture fluid decreases until the whole produced water consists of formation water.

Under normal conditions for shale gas production, within the first couple of weeks the recovered water is called flowback water; this is a mixed fluid containing both fracture fluid and formation water. Most of the fracture fluid recovery happens at this time, and there will only be a very small percentage recovered with the produced water after this period. This flowback water normally contains 20% to 40% fracture fluid with clays, chemical additives, dissolved metal ions and total dissolved solids (TDS) (Crafton et al, 2007; Ghanbari et al, 2013). The rest of the fracture fluid will remain in the shale gas reservoir or trapped in the fractures. Compared with the flowback water, the produced water contains only a small fraction that is fracture fluid, which means its salinity is normally much higher than that of the flowback water; and the TDS together with all the other ion concentrations should stay within a certain range which should be roughly the same as the TDS and the ion concentrations found in the formation water. Produced water has high levels of TDS and leaches out minerals from the shale including barium,

calcium, iron and magnesium; it also contains dissolved hydrocarbons such as methane, ethane and propane along with naturally occurring radioactive materials (NORM) (Kennedy, 2015).

Some of the operating companies have already put effort into collecting brine chemistry data from shale reservoirs in US, Canada and China, etc. (Spicka, 2017) However, the brine chemical data collected from various fields, even from various formations within the same reservoir, could be different. This could be due to different mineralogy from place to place, or different *in situ* formation water compositions in each reservoir or even other completely unique shale play properties. As a consequence, it is required to systematically collect and analyse these data so that further scaling tendency prediction and scale control plans can be made. Most operating companies monitor brine chemical data due to the detection of high concentrations for certain ions such as barium, calcium and bicarbonate, etc. (Guan, 2016) this provides opportunities to carry out this research and extend it into field application in the future.

In general, it can be very challenging to identify the *in situ* formation water composition since samples of the formation water can be difficult to obtain, they may have been contaminated during the drilling process, the reactions may take place by the fluid mixing between the injected fluid and the formation water, or even they may not be preserved appropriately. Especially for unconventional recovery scenarios such as shale gas production, the challenge to identify the exact formation water composition may be even greater due to the extremely low permeability of the shale matrix.

This chapter aims to present and discuss chemical compositional data to achieve a better understanding of scaling tendency prediction and formation water composition calculations. It also aims to address one of the key questions - what caused the altered high salinity brine produced back during shale gas production. The first section of this chapter provides a simple introduction about data collection prior to the discussion of geochemical compositional data. It then briefly describes information relating to a target field, along with the supplemental details of water chemistry and mineralogy in the same area. Thereafter, the chapter presents some basic field data analysis along with some brine chemistry analysis with data collected from other resources. Once basic collection and analysis have been completed, a methodology to predict the *in situ* formation water compositions has been introduced and validation for the predicted formation water composition has been performed. This methodology would be applied

as a key activity, not only to calculate the *in situ* formation water compositions in different reservoirs, but also to provide more information for the further geochemical modelling studies to develop a history match with the fraction of injected fracture fluid in the flowback water. Conclusions are drawn in the last section of this chapter.

2.2 DATA COLLECTION

Different types of data need to be collected in a variety of relevant areas, such as geological data, geochemical data, relevant reservoir conditions etc. All of these data can be collected from different sources, such as data supplied by geologists and operators, data collected from associated research and studies, and so forth.

It is necessary to collect reservoir data in order to input them into the reservoir simulation to develop a hydraulic fractured shale gas fluid flow model. Then the collection of geochemical data should be carried out, which can be used as preparation for the data analysis initially to predict the scaling tendency and to perform a geochemical modelling study. The majority of the data collected for this study comes from the literature survey, with some brine compositional data having been provided by project sponsors.

2.2.1 Reservoir data collection

To collect and set up an accurate and integrated database, in terms of hydraulic fracturing and reservoir properties, is one of the most time-consuming jobs for petroleum engineers who are responsible for developing a hydraulic fracturing design in a shale gas system.

All of these reservoir data collected, on the one hand can be divided into two varieties – shale reservoir properties and hydraulic fracturing treatment parameters; whereas, on the other hand they can be divided into the two types listed below (which has been used as the strategy for our reservoir data collection):

- Type one – data that cannot be controlled by the engineers, which need to be measured or estimated

- Type two – data that can be controlled or influenced by the engineers, so that further optimization can be performed based on these data

2.2.1.1 Type one data collection

The "Type one" data include shale gas reservoir properties along with the hydrocarbon properties. Both of them normally can be measured or estimated. The shale gas reservoir properties include matrix permeability, matrix porosity, formation depth, reservoir pressure, formation compressibility, reservoir thickness, connate water saturation, water compressibility, etc. The hydrocarbon properties include viscosity of gas, composition of gas, gas density, etc. Since the actual field data have not been supplied in terms of "Type One Data" for this study, examples of these properties have been gathered and estimated from the literature review to develop fluid flow simulation in the next step. All the relevant properties referred to as "Type One Data" have been collected and arranged. An example of shale matrix permeability collection is shown in **Table 2.1** and the result of more "Type One Data" collection can be found in the Appendix at the end of this thesis.

Table 2.1 Example of data collection for shale reservoir (matrix permeability)

Value (mD)	Reference
10^{-5}	Moridis G.J., Blasingame T.A. and Freeman C.M., 2010. Analysis of Mechanisms of Flow in Fractured Tight-Gas and Shale-Gas Reservoirs, SPE 139250
10^{-5} - 10^{-4}	Zhang, X., Du, C., Deimbacher, F., Crick, M. and Harikesavanallur, A., 2009. Sensitivity Studies of Horizontal Wells with Hydraulic Fractures in Shale Gas Reservoirs. IPTC 13338.
10^{-6} - 10^{-3}	Bustin R.M., Bustin A.M.M., Cui X., Ross D.J.K., and Murthy Pathi V.S., 2008. Impact of Shale Properties on Pore Structure and Storage Characteristics, SPE 119892.
10^{-4}	Oliver H., Eric T., Vincent A., 2010. The Analysis of Dynamic Data in Shale Gas Reservoirs – Part 1 (Version 2), KAPPA, December 2010.
10^{-5} - 10^{-3}	Darishchev L. P., and Rouvroy P., 2013. On Simulation of Flow in Tight and Shale Gas Reservoirs, SPE 163990.
$5*10^{-4}$	Mauricio F. and Emesto F., 2013. Hydraulic Fracturing Simulation Case Study and Post Frac Analysis in the Haynesville Shale, SPE 163847.
10^{-4}	Hamed L., Greg J. and Nnamdi A., 2013. A Novel Approach to Modeling and Forecasting Frac Hits in Shale Gas Wells, SPE 164898.

10^{-4}	Tunde Osholake Jr., John Yilin Wang and Tuygay Ertekin, 2011. Factors Affecting Hydraulically Fractured Well Performances in the Marcellus Shale Gas Reservoirs, SPE 144076.
10^{-4}	Cipolla, C.L., Lolon E. P., and M. J., 2009. Reservoir Modeling and Production Evaluation in Shale – Gas Reservoirs, IPTC 13185.
$1.5*10^{-4}$	Ahmad Alkouh, Steven McKetta and Robert A. Wattenbarger, 2013. Estimation of Effective Fracture Volume Using Water Flowback and Production Data for Shale Gas Wells, SPE 166279.

According to the tables of "Type One Data", the value of each property can be observed in a certain range for a typical shale reservoir, thus it is necessary to identify a representative value for each property to input in the base case of the fluid flow model in a hydraulic fractured shale system. All of these properties will assist in selection of initial conditions for shale simulation and could be tested by varying in a reasonable range so as to establish an ideal initial condition for further modelling studies. A summary of some important properties in "type one" dataset has been selected as examples and shown in **Table 2.2**.

Table 2.2 Some of the initial properties in fluid flow modelling from "Type One Data"

Important properties in "Type one	Values
Matrix permeability, K (mD)	0.0001
Matrix porosity, Φ (%)	5
Connate water saturation, S_{wc} (%)	30
Rock compressibility, C_r (1/psi)	3E-06
Hydraulic fractures conductivity, (mD*ft)	50

One important property in "Type One Data" requires to be further discussed here: capillary pressure. It is known that shale reservoirs have extremely low matrix permeability along with high capillary pressure and this high capillary pressure also plays a significant role in retaining injected fracture fluids within the shale system. The capillary pressure is normally gathered from core sample tests and the curve could be quite different for different shale plays (different wettability and pore sizes of shale matrix). The capillary pressure table applied in the base case fluid flow model has been derived from a previous relevant shale gas simulation study (and has been tested and verified by history matching with field data in the following modelling study.

2.2.1.2 Type two data collection

Well completion as well as stimulation treatment design plays an important role on unconventional recovery. As a consequence of this, the controllable/variable "Type Two Data" mainly consist of horizontal well properties and hydraulic fracturing design parameters. All of these properties have a large impact on the fluid production in unconventional systems, thus the optimization of "Type Two Data" could be a key to achieve economical shale gas production. Hence, part of the discussions in terms of fluid flow transport will be based on changing hydraulic fracture properties in fluid flow modelling study in the next step.

These properties in "Type Two Data" include, but are not confined to well completion details (such as length of the horizontal well, perforation status etc.), treatment volume, injection rate, fracturing fluid viscosity and density, composition of fracturing fluid, hydraulic fracture width, the hydraulic fracture orientation, hydraulic fractures spacing, height and half-length. Considering that these data can be optimized by running fluid flow simulations, therefore some sensitivity cases should be run. All the properties should be controlled within a reasonable range for the sensitivity test and these suggested ranges are indicated in the tables in the Appendix. Also, as is true for the collection of "Type One Data", most of them are collected from the relevant old researches or the literatures up to now.

2.2.2 Geochemical data collection

The geochemical data collection is a major part for this study due to its importance for scaling tendency prediction and the geochemical modelling study (Ashkan et al., 2015; Iman et al., 2016). To systematically develop a geochemical database can contribute to a better identification of the scaling risk, easier predicting of formation water composition and a more accurately developed geochemical model of the shale systems.

Shale gas reservoirs are rich in organic matter, and also most of the gas shales are found to have no more than 50% clay content (Bowker, 2007). Over geological timeframes the processes of biodegradation and aqueous percolation took place within all the different mineral shale layers, which released different ions into the formation water creating high ionic brines. Therefore, the *in situ* brine chemistry as well as mineralogy plays an important role in a shale gas geochemical study and the scaling risk prediction.

According to the literature review (Lensie, 2008; Patrick et al., 2011), a normal shale reservoir contains clay minerals, non-clay minerals and organic carbon along with calcite, minor dolomite and illite within most of the shale layers. Gas is present in all of these layers, as well as free and bound water (water is bound to the surface of clay minerals), trapped by capillary pressure.

The shale reservoir can be generally divided into three groups, which are rock matrix, shale and organic carbon. Here, "shale" is considered to be all the clay minerals together, which are confirmed by geochemical logging, such as smectite, illite, kaolinite, chlorite and glauconite. The "rock matrix" group consists of all the remaining minerals which including dolomite, pyrite, calcite, anhydrite, siderite, plagioclase and quartz. Since the water is trapped together with the various minerals mentioned above, as geological time passes this water in the reservoir becomes increasingly saturated with different ions (Mg^{3+}, Fe^{2+}, Ca^{2+}, etc.) released from these minerals. As a consequence of this, in some circumstances, the minerals within shale reservoirs define which kinds of ions we can find in the formation water (LeCompte, 2009).

As introduced briefly in Chapter 1, there are three most common sources of scale during field production. Carbonate scales are usually created in the near wellbore areas, pipelines and downhole/surface equipment. Sulphate deposition is usually formed because of two incompatible fluids mixing together (sulphate reacts with barium, strontium or calcium) and can be normally found at the locations where the most fluid transport and mixing takes place, such as within fracture network, within wellbore, wellbore perforations, stimulated formation matrix and even the downhole equipment.

Since significant volumes of water involved in hydraulic fracturing, the risk of scale precipitation can be quite serious, even worse by the altered high salinity of produced water flow back. Engineers also normally add different chemicals to the hydraulic fracture fluid, such as biocide, acid, breaker, clay stabilizer, inhibitors (corrosion inhibitor, scale inhibitor), friction reducer, surfactant etc. to control formation and wellbore damage so that fluid flow can be assured within the shale system.

Approaching better understanding in terms of composition of hydraulic fracture fluid (source water), formation water (can be predicted/calculated from flowback water compositional data) and produced water, is very important for scale risk assessment and scale control management. All the relevant data collection for scaling tendency prediction has been listed below:

- Flowback water composition as a function of time (after the hydraulic fracturing treatment is completed – shorter period of collection, within 3 months)
- Produced water composition as a function of time (compositional data collected for longer production period)
- Injected fracture fluid composition (can be taken as being fresh water in the absence of measured compositions)
- Formation water composition (can be difficult to obtain because of contamination with fracture fluid)
- Fracture fluid injection rate
- Water production rate since well started production
- Cumulative produced water volume since well started production
- Total volume of injected fracture fluid
- CO_2 content in produced gas/brine phase as a function of time since well starts production
- H_2S content in produced gas/brine phase as a function of time since well starts production

Most of data collected from public resources are from shale gas reservoirs located in the US - such as Bakken, Barnett, Marcellus, Eagle Ford, etc. (Lensie, 2008; Blauch et al., 2009; Patrick et al., 2011; James and Jeffrey, 2012; Fedotov et al., 2013; Ashkan et al., 2015; Iman et al., 2016; etc.). Some flowback water compositional data in the Marcellus shale will be reviewed and analysed as an example case study in a later section (Elisabeth, 2015) and some relevant data collected from Western Canadian Basin will also be discussed in an account of an additional study towards field data analysis in the same area (Ashkan et al., 2015). All the other compositional data have also been reviewed as comparison cases for developing scaling tendency prediction in shale systems; however, the discussions are not included in this thesis.

Table 2.3 is an example of compositional data collected from five wells in South Texas, US. All the wells have been stimulated by injecting the same fracture fluid for the

hydraulic fracturing treatment. There is potential to have $CaCO_3$ scaling risk due to the existence of high calcium and bicarbonate concentrations in the flowback water and also the scaling tendency of $SrSO_4$ is found in well 5 due to the mixing of two brines containing high strontium and sulphate concentrations. All the other relevant data collected can be found in the Appendix.

Table 2.3 Example of flowback water analysis for well in south Texas

	Injection fracture fluid	Injection fracture fluid	Flowback Well 1 - AF1				
			Flowback water				
	07/08/2013	19/02/2014	13/01/2012	18/07/2012	19/02/2013	10/05/2013	23/10/2013
Sample Point			Heater	Heater	Separator	Separator	Wellhead
Dissolved CO_2 (mg/L):	0	0	154	220	480	810	352
Bicarbonate (HCO_3) mg/L:	1384.7	1384.7	134.2	122	366	854	322
Lead (Pb) mg/L:	0.54	0.54	0.88	0.04	0	0.1	0.02
H_2S in Gas (%):	no data	no data	0.03	0.07	0.0006	0.001	0.002
H_2S in Water (mg/L):	2.5	2.5	1.5	1	1	2	4
pH:	8.1	8.1	6.7	6.7	7.3	7.3	7.4
Calculated TDS (mg/L):	2570.57	2570.57	43855	39655	26430	38104	41723
Cations	mg/L	mg/L	mg/L	mg/L	mg/L	mg/L	mg/L
Calcium (Ca):	4.19	4.19	1060	1864	1237	1885	2151
Barium (Ba):	0.26	0.26	4.47	4.79	5.63	8.43	8.41
Iron (Fe):	1.02	1.02	9.03	66.09	214.81	480.05	105
Magnesium (Mg):	1.13	1.13	107.21	174.73	111.17	171.52	192.14
Manganese (Mn):	0.01	0.01	0.25	7.18	3.58	7.58	1.52
Sodium (Na):	761	761	15650.79	12932.19	8435.69	11814.1	13255
Potassium (K):	2.53	2.53	304.76	147.14	85.33	121.72	154.06
Strontium (Sr):	0.65	0.65	15.69	236.96	168.22	258.19	337.97
Zinc (Zn):	14.36	14.36	0.13	0	0.04	0.04	0.03
Anions	mg/L	mg/L	mg/L	mg/L	mg/L	mg/L	mg/L
Sulfate (SO_4):	0	0	67	0.1	3	2	97
Chloride (Cl):	400	400	26500	24100	15800	22500	25100

2.3 HORN RIVER BASIN AREA INTRODUCTION

2.3.1 Introduction to the field

The shale gas reservoir used for data collection is located in the Western Canadian Sedimentary basin (Mossop, 1994). The horizontal laterals of the two wells are located in the Muskwa Formation and the Evie Formation. The Muskwa Formation is composed of bituminous shale and occurs in northern Alberta, north-eastern British Columbia and in the southern part of the Northwest Territories; it is a subunit of the Horn River Group and is conformably overlain by the Fort Simpson Formation and conformably underlain by the Otter Park Member, with a typical thickness of 34 metres (110ft) (Natural Resources Canada, 2009).

The Horn River Group is made up of dark siliceous and calcareous shale and it is a stratigraphic unit of Devonian age (early Givetian to late Fransnian age) (BCMEMPR, 2003). It is subdivided into the following members, from top to base: Muskwa Member- bituminous, mildly radioactive shale; Otter Park Member- grey calcareous shale; Evie Member- black silty limestone (BCMEMNEB, 2011).

Gas is produced from the Muskwa Formation shales in the Horn River Basin in north-eastern British Columbia (National Energy Board, 2009). Horizontal drilling and hydraulic fracturing techniques are used to extract the gas from the low permeability shales. The cross-section of the Horn River Basin is shown in **Figure 2.1** below.

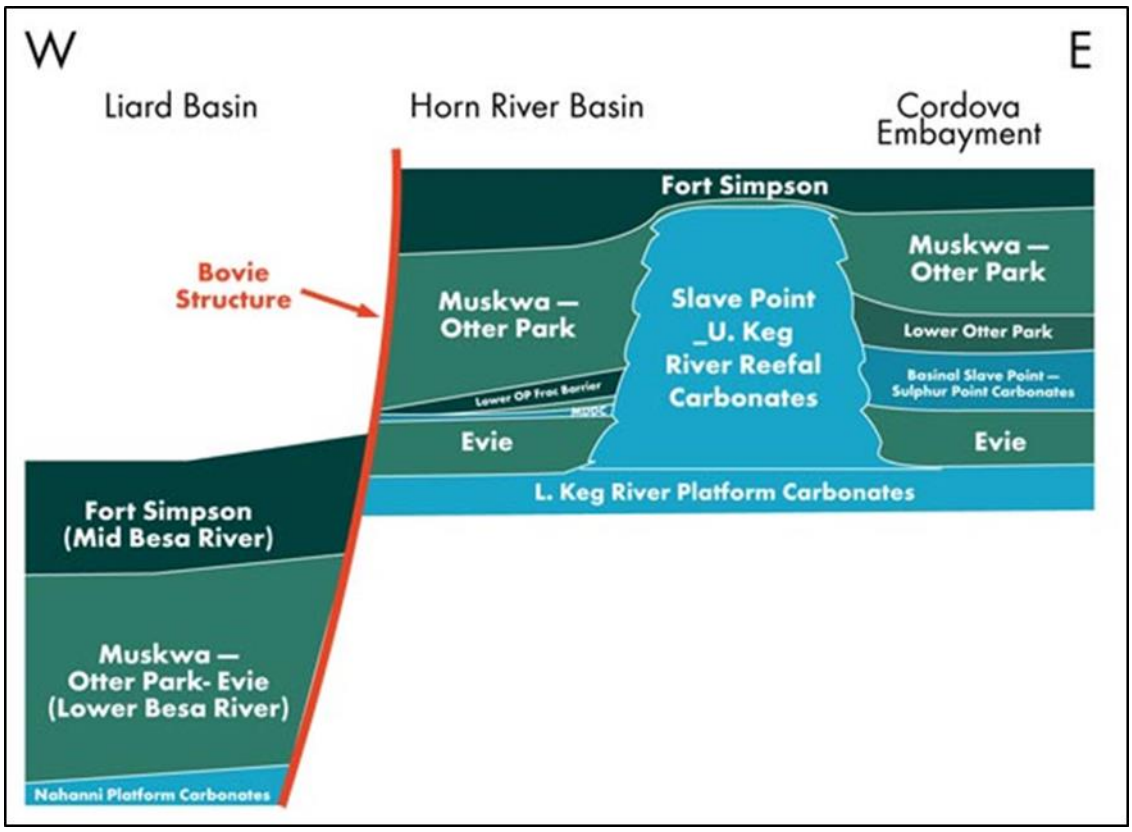

Figure 2.1 The cross-section diagram of the Horn River Basin (National Energy Board, 2009)

It is reported that the original-gas-in place volumes are estimated to be up to 500 Trillion cubic feet (HRN, 2009), which makes it as the third largest North American natural gas accumulation discovered prior to 2010 (Simon, 2011). There are several energy companies involved in the extraction of natural shale gas from the Horn River Shale Basin, which include Apache, EnCana, Devon Energy, Exxon, EOG, Nexen, Quicksilver Resources and Stone Mountain Resources (HRN, 2012). Hydraulic fracturing technology has been widely applied in Alberta by the energy companies since the late 1970s. It is used successfully in developing the shale gas production with Horn River Formation in British Colombia. The distribution of energy companies operating shale gas production on Horn River Shale Basin is indicated in **Figure 2.2** (HRN, 2012).

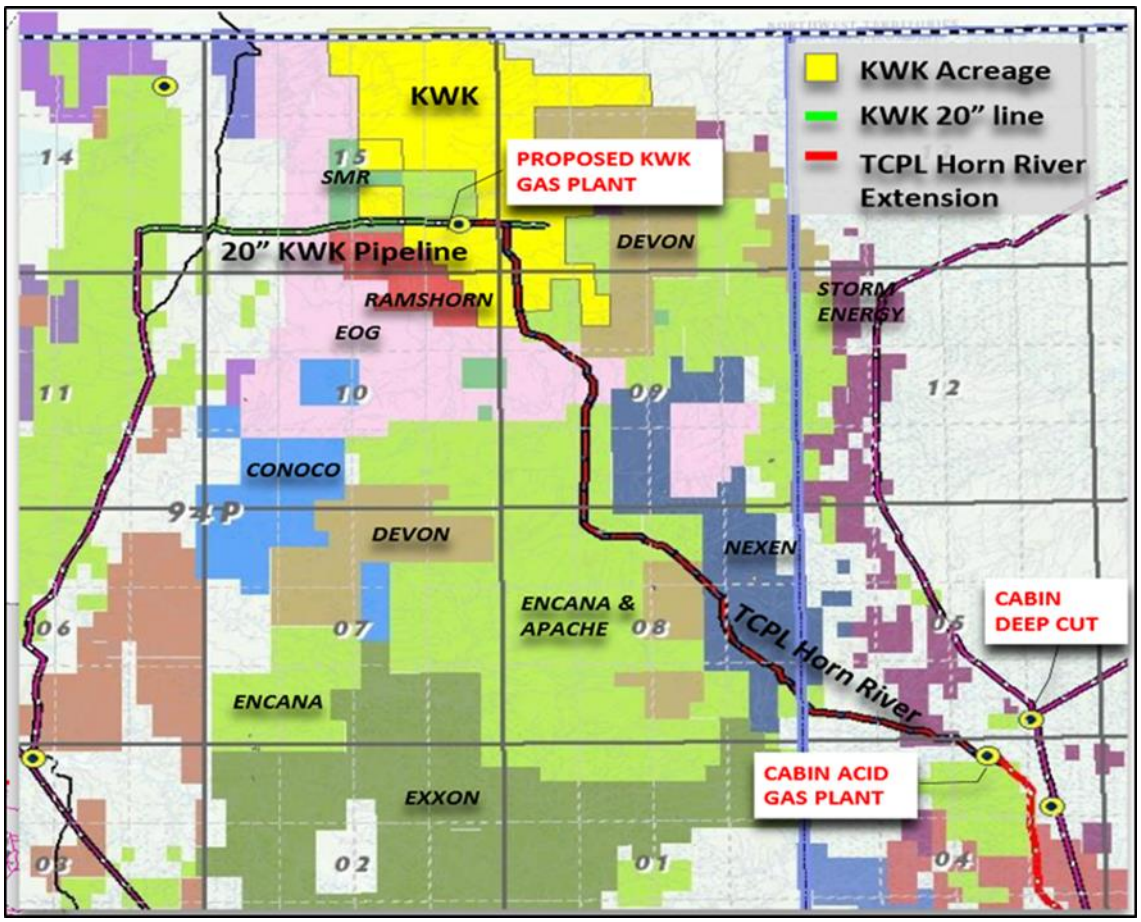

Figure 2.2 Distribution of energy companies in Horn River Shale Basin area (HRN, 2012)

2.3.2 Supplemental information in HRB area

This section briefly introduces some of the supplemental information in the HRB to help develop a better understanding of the geochemistry in this area. At first, the discussion will be around the potential source water used for the injected fracture fluid, and then we introduce some potential factors which may have impacts on the formation water salinity, such as the mineralogy, presence of aquifers etc.

The regional water quality will have a significant impact on the shale gas development (Gregory and Vidic, 2011). To have a better comprehension of the potential source water used for hydraulic fracturing in the HRB it is necessary to study the fracture fluid composition. It is reported that the wells in the HRB area are stimulated with fresh water sourced from snow melt or spring runoff and stored in pits, or river or lake water (sourced directly from the North Tsea River). It has been documented that the TDS of the surface water in HRB in the year 2015 is generally within the range from 107 ppm to 504 ppm. However, concentrations could increase due to the low flow period, and elevated metal ion concentrations are observed in the water during the high flow events,

such as when erosional processes take place (Geoscience BC, 2016). The TDS in the fracture fluid provided for our data analysis is higher than the normal surface water reported: this could be due to the contamination during the water transportation or it could also be because of the different water storage conditions and climatic reasons.

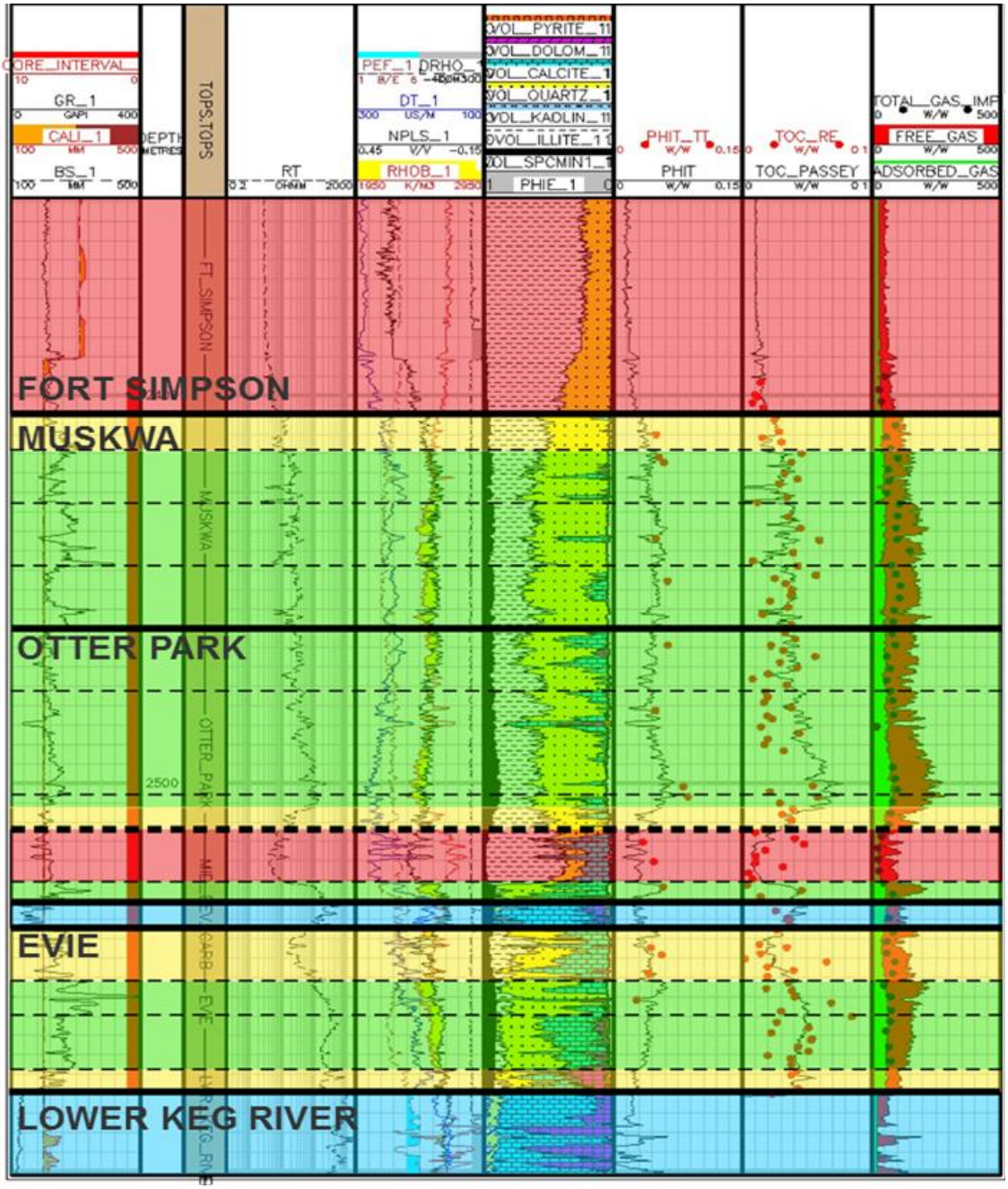

Figure 2.3 Well log response chart in HRB (Dresser Atlas, 1983)

Figure 2.3 is the diagram for the well log response chart in the HRB. It is known that the gas shales in the HRB date from the middle Devonian period, which is comparable to the age of the Barnett Shale in US (Reynolds, 2010). It has been reported that the

Muskwa / Otter Park shale has an averaging depth of 2440 m, and the thickness of the organic rich shale is around 130 m.

In terms of the mineralogy overview, it can be observed that the Muskwa member has higher clay content than Evie; however, both of them are considered as high quartz and low clay content shale. It is also documented that the major mineral in the clay content in Evie is illite. Illite contains the greatest amount of potassium of the common clays, which will lead to higher potassium radioactivity observed than in clays made up essentially of kaolinite or smectite (Dresser Atlas, 1983).

One of the studies shows that the amount of clay-bound water held by a clay system increases significantly when the water salinity is reduced, as would happen near the fracture face with fresh frac water and a high salinity reservoir. According to our previous study, the conditions across the HRB could be considered as the same case since fresh water is used as fracture fluid and high salinity formation water is predicted. Over long time periods, diffusion will cause a redistribution of this additional clay-bound water as the salinity in the reservoir comes to equilibrium. The exact amount of frac water immobilized by this mechanism depends on the amount of clay and the clay types, fracture face surface area, the permeability of the clay zones, the salinity and the effective Cation Exchange Capacity (Rezaee, 2015).

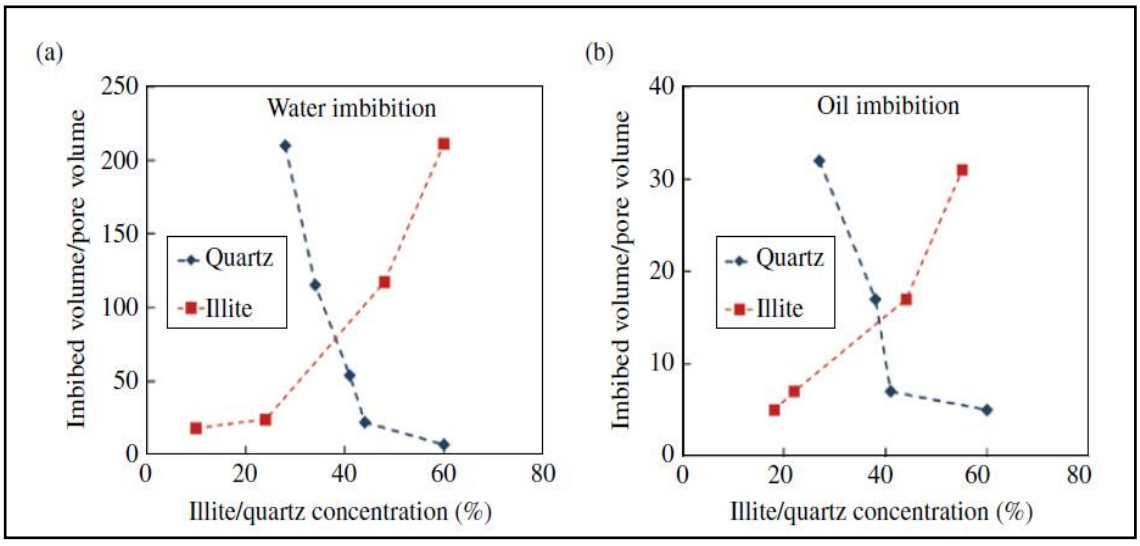

Figure 2.4 Normalized volume of fluid gained by HRB samples versus illite and quartz concentrations (Hassan et al., 2015)

Another study shows that the clay minerals in shales can adsorb a large volume of water, and the degree of adsorption depends on clay chemistry and water salinity (Chenevert,

1970; Hensen and Smit, 2002). **Figure 2.4** indicates the plots of the water and oil as a percentage of the dry sample initial pore volume versus the quartz and illite concentration for Fort Simpson, Muskwa, and Otter Park samples in the HRB area. The water uptake is strongly correlated to the concentration of illite, which is the dominant clay mineral. In conclusion, higher clay content in Muskwa could also be one of the reasons that account for the lower fraction of fracture fluid that flows back.

It is reported that the lower Evie member contains slightly higher calcite content (5 ~ 15% by weight), which could be one of the reasons for higher bicarbonate concentration in the flowback water after the prewash of the acid fluid (Towers, 2011). It is also observed that there is a significant difference in the total dissolved solids in Muskwa (40,000 ppm) and Evie (90,000 ppm); this could be caused by the clay rich Otter Park formation located in between, and which isolates the upper Muskwa/Otter Park member from the Evie member (Hayes, 2010).

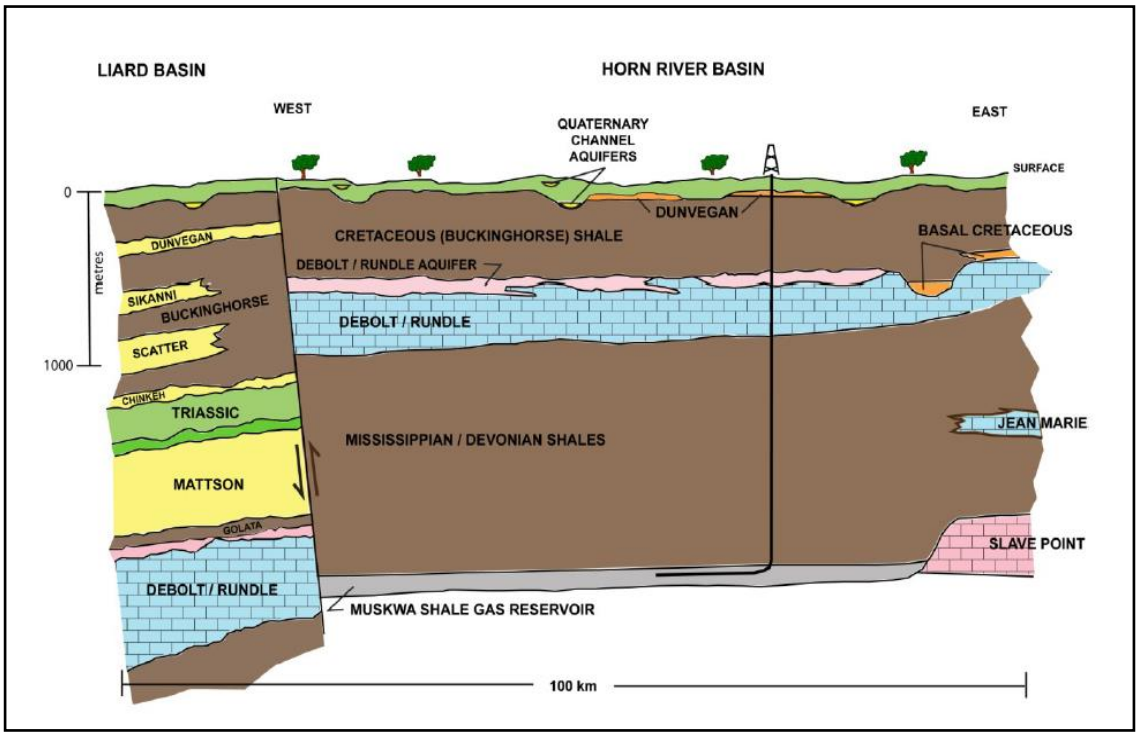

Figure 2.5 Schematic west-east cross-sections across HRB (Hayes, 2010)

Figure 2.5 indicates the west to east cross section in the HRB area. It is known that a deep subsurface aquifer exists in the HRB, which has been named the Debolt / Rundle aquifer (Hayes, 2010). As shown in the figure above, the Debolt / Rundle aquifer is mainly located above the Mississippian/Devonian Shales, and part of it is located to the west of the Horn River Basin, which is part of the Mattson formation. It is also reported

that the average TDS in the formation water for the Debolt / Rundle aquifer is in the range from 15,000 to 40,000 ppm, as illustrated in **Figure 2.6,** and the salinity values are reported to be similar across the entire vertical section. The communication between the Debolt / Rundle aquifer and the Muskwa member could be quite poor due to the intervening fault; however, there is still the possibility of fault movements taking place over geologic time, which means that the Debolt / Rundle aquifer may potentially account for the high saline formation water in Muskwa (the calculated TDS in the formation water in Muskwa is 41,500 ppm).

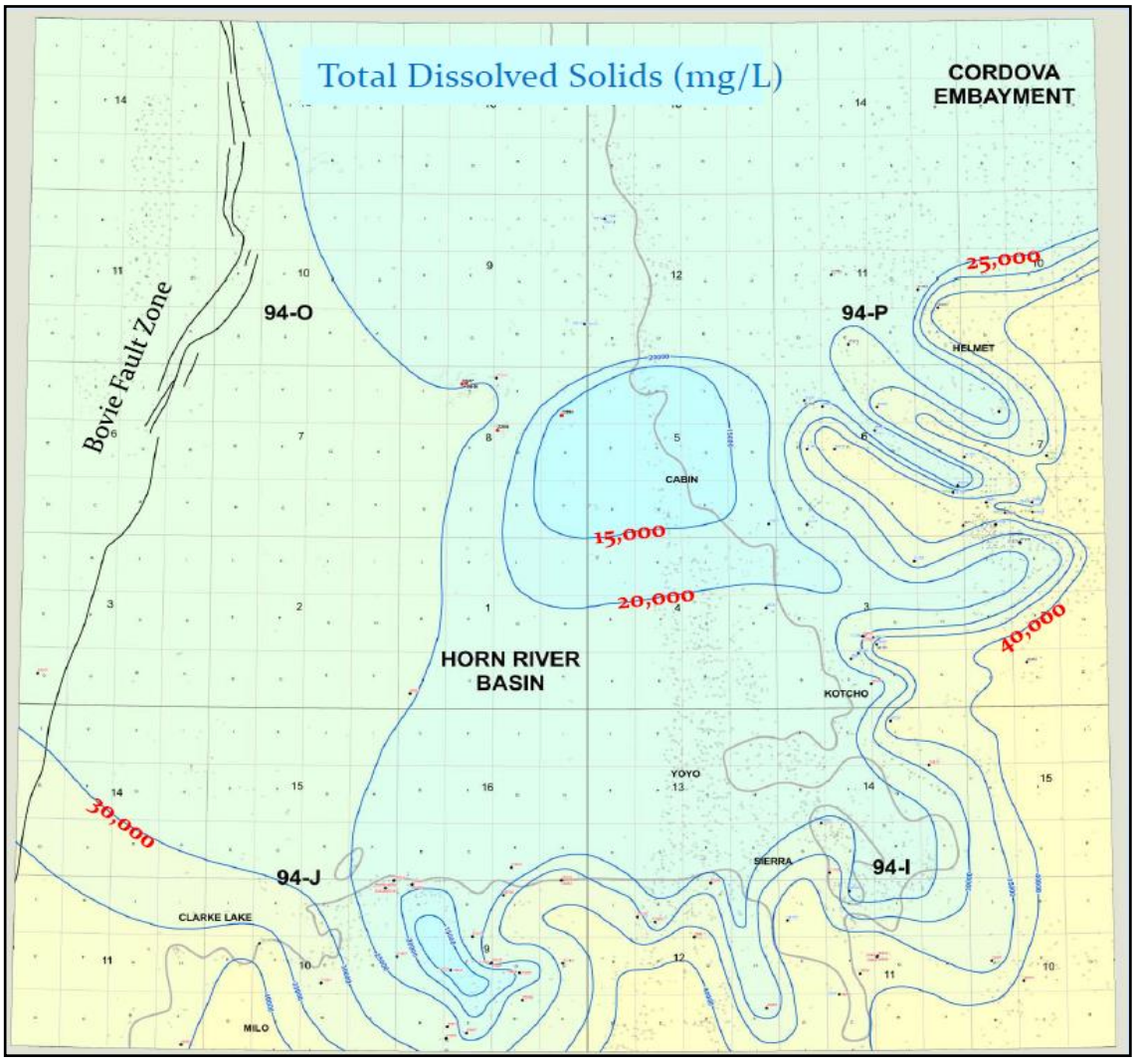

Figure 2.6 Isosalinity map for the deep saline subsurface aquifers in HRB (Hayes, 2010)

2.4 PRESENTATION AND BASIC ANALYSIS OF FIELD DATA

2.4.1 Presentation of field data

The data to be analysed are from the shale reservoir located in the western Canadian sedimentary basin and they contain a number of key contents: 1) The formation characteristics of the shale gas reservoir; 2) Mineralogy information from core samples around target wells; 3) The composition of fracture fluid; 4) The composition of flowback produced fluid; 5) The gas composition; 6) The production information for target wells (produced water rates/ gas rates, pressure information, etc.).

Some of the data are from the samples collected in several wells located in this area; however, most of the data are collected from two specific horizontal wells (wells located in Muskwa and Evie members). All the shale gas compositional data were collected and measured at two labs (AGAT Laboratories – a commercial lab and Protechnics Lab). The flowback produced water compositions for these wells were collected from 1st Dec 2011 to 21st Mar 2012 and the fracture fluid composition was collected in July 2011. The well in the Evie member was put on production on 29th Nov 2011 and the production date for the well in Muskwa was 5th Jan 2012. All wells are initially flowed full bore up casing. Tubing is installed later to maintain lift of water (otherwise wells load up and die). Each well is completed with plug and perf, and the plugs were drilled out with coiled tubing. There are two depth ranges for core sample information, one is from the depth of 2538.5 m to 2706.15 m and the other is from 1303.6 m to 1328.42 m. In addition to this information, the core samples collected from deeper (around 2,600 m) could locate at the same level as the horizontal section of the well in Evie.

The example table for flowback produced water composition of the well in the Evie member is shown in **Table 2.4** (some measured ion compositions are not included in this table for ease of viewing).

Table 2.4 Example table for flowback water composition of the Evie well (b.d.-below detection)

Date	Water Recovered %	Ba	Ca	Cl	Mg	K	Na	SO_4	HCO_3	CO_3	TDS
		mg/L	mg/L	mg/L	mg/L	mg/L	mg/L	mg/L	mg/L	mg/L	ppm
01-12-11	1.216	481	477	14800	65	73	9090	6.4	1030	<6	26262
02-12-11	1.731	613	560	17000	75	75	9980	b.d.	946	<6	29542
03-12-11	2.445	654	636	18000	86	78	11000	b.d.	867	<6	31640
04-12-11	3.093	652	658	17900	89	75	11200	16	807	<6	31709
05-12-11	3.750	718	692	19300	93	87	11600	23	774	<6	33647
06-12-11	4.386	756	696	20200	94	80	11500	99	769	<6	34554
07-12-11	5.117	786	621	19600	86	74	11000	b.d.	582	<6	33061
08-12-11	5.955	741	698	19500	91	72	11500	28	678	<6	33634
09-12-11	6.551	784	738	20200	89	68	11300	66	661	<6	34228
10-12-11	6.997	700	738	20100	91	64	11300	9.4	674	<6	34044
11-12-11	7.493	786	782	21300	100	75	12500	b.d.	624	<6	36492
12-12-11	7.849	809	782	21500	100	76	12600	b.d.	623	<6	36834
13-12-11	8.230	813	818	21500	100	76	13000	6.2	627	<6	37314
14-12-11	8.510	815	788	21600	100	80	12500	b.d.	595	<6	36810
15-12-11	8.878	830	800	22000	100	75	12800	b.d.	613	<6	37558
16-12-11	9.218	870	834	21900	100	76	13100	b.d.	605	<6	37848
18-12-11	9.818	842	844	22000	110	77	13400	9.4	576	<6	38218
19-12-11	10.10	880	834	22200	100	78	13000	b.d.	591	<6	38050
20-12-11	10.39	880	839	22200	100	77	13200	12	595	<6	38290
21-12-11	10.63	867	836	22300	110	76	13100	9.0	572	<6	38238
22-12-11	10.88	882	848	22200	110	76	13100	b.d.	632	<6	38251
23-12-11	11.12	772	783	21600	100	90	12500	b.d.	542	<6	36625
28-12-11	12.29	668	625	22493	95	122	13000	0	569.3	<6	36614
25-02-12	20.31	858	890	23993	1100	87.9	12400	2.9	453.4	<6	38696

It is reported that the fracture fluid used for stimulating the horizontal wells is as clean as fresh water, being sourced from snow melt/ spring runoff stored in pits and river/ lake water nearby. The total dissolved solids in the source water, before addition of chemicals is around 1,000 ppm. Some of the fracture fluid samples show low

concentrations of calcium and iron (the latter being as high as 30 mg/L). It is most likely that this can be attributed to there being surrounding rock formation fragments in the burrow pits within the formation where the water was stored, and also, possibly, from corrosion products from the machinery used in the operations (Towers, 2011). The slickwater hydraulic fracturing fluid has friction reducer added (polyacrylamide) and HCL acid was also pumped ahead of some stages of the hydraulic fracturing process after the time of well perforation. It is confirmed that there was no scale inhibitor pumped with the hydraulic fracturing fluid to prevent or reduce scale precipitation (HRN, 2011). The example of the fracture fluid composition collected from Evie well is shown in **Table 2.5**.

Table 2.5 Injected fracture fluid composition used for two wells

Fracture fluid composition						
Short Name	SAMPLE PT.	Na	K	Ca	Mg	Cl
c-D1-J	Water (Pre-Frac)	818.0	4.0	413.0	20.0	2055.0

The production profile and some mineralogy information from core samples have also been provided for the Horn River Basin area. These include some basic elements (produced water rate, produced gas rate, etc.) to support future history match modelling and to provide more information about the complexity of the natural fracture system between different shale formations. All the relevant information not only covers the descriptions for the two wells we aim to analyse but also include some additional details for better understand the Horn River Basin area.

All the produced data have been collected within a 16 month period of time. Meanwhile, the core sample analysis also provides some information to learn about the mineralogy in the HRB area, even though none of the core samples were collected from the target formations (some deeper core samples may overlap with the same level as wells locate at Evie member). An example table for part of the core sample analysis (the units indicate in the table is mass fractions in percentage) is shown in **Table 2.6** and another example plot to illustrate the supplied production data in the Evie formation is shown in **Figure 2.7**.

Table 2.6 Whole core samples analysis from depth of 2692 m to 2706 m

SAMPLE ID	DEPTH (m)	QUARTZ	K-FELDSPAR	PLAGIOCLASE	CALCITE	SIDERITE	ANKERITE/FE-DOLOMITE	DOLOMITE	PYRITE	FLUORAPATITE	BARITE	MAGNETITE	TOTAL NON-CLAY	SMECTITE	ILLITE/SMECTITE (I/S)	ILLITE+MICA	KAOLINITE	CHLORITE	TOTAL CLAY	GRAND TOTAL
58R	2692.70	56.00	7.00	6.00	7.00	0.00	2.00	0.00	3.40	0.10	0	0	82	0	7	11	1	0	19	100
59	2693.99	62.90	5.30	4.40	10.30	0.00	0.00	2.00	2.80	0.00	0	0	88	0	3	9	0	0	12	100
60	2694.10	68.00	3.70	4.20	12.20	0.00	0.00	1.20	1.70	0.00	0	0	91	0	4	5	0	0	9	100
61	2694.20	68.60	3.50	5.00	11.60	0.00	0.00	1.00	1.60	0.00	0	0	91	0	3	6	0	0	9	100
62	2694.30	50.90	8.50	6.10	10.20	0.00	0.00	0.60	1.70	4.60	0.00	0	83	0	5	12	0	0	17	100
63	2694.40	67.90	3.50	4.90	10.90	0.00	0.00	1.70	1.60	0.00	0	0	91	0	3	6	0	0	9	100
64	2694.50	64.70	3.20	5.70	10.30	0.00	0.40	1.00	2.60	0.00	0	0	88	0	2	10	0	0	12	100
65	2694.60	55.00	6.60	5.70	10.40	0.00	0.00	3.90	4.30	0.00	0	0	86	0	4	10	0	0	14	100
66	2694.70	50.30	3.70	6.20	25.90	0.00	0.00	2.90	1.70	0.00	0	0	91	0	0	9	0	0	9	100
67	2694.79	69.40	3.30	4.90	9.50	0.00	0.00	1.30	1.50	0.00	0	0	90	0	3	7	0	0	10	100
68	2694.91	72.90	2.80	4.20	9.30	0.00	0.00	1.70	1.50	0.00	0	0	93	0	1	6	0	0	7	100
69	2695.52	41.90	3.60	2.00	43.70	0.00	0.00	2.80	1.20	0.00	0	0	95	0	1	4	0	0	5	100
70	2696.42	69.20	3.60	4.80	9.70	0.00	0.00	1.60	2.00	0.00	0	0	91	0	2	7	0	0	9	100
71	2697.27	22.00	5.20	2.40	62.60	0.00	1.10	1.70	1.30	0.00	0.10	0.00	96	0	1	2	0	0	4	100
72	2698.45	68.30	4.80	5.30	9.00	0.00	0.00	1.60	2.40	0.20	0.10	0.00	92	0	1	7	0	0	8	100
73	2699.78	54.90	0.90	1.30	36.90	0.00	0.00	1.30	0.80	0.00	0.00	0.00	96	0	1	3	0	0	4	100
74	2700.53	59.40	6.60	6.50	11.60	0.00	0.00	1.80	3.50	0.10	0.30	0.00	90	0	2	9	0	0	10	100
75	2701.68	40.20	1.60	1.60	51.70	0.00	0.00	1.50	0.70	0.00	0.00	0.00	97	0	0	3	0	0	3	100
76	2703.41	68.50	4.70	5.60	9.30	0.00	0.00	1.50	2.60	0.00	0.00	0.00	92	0	1	6	0	0	8	100
77	2705.35	28.90	4.90	2.30	54.70	0.00	0.00	3.80	1.80	0.30	0.00	0.00	97	0	0	3	0	0	3	100
78	2706.15	72.60	3.60	5.10	7.30	0.00	0.00	1.10	2.00	0.00	0.10	0.00	92	0	1	7	0	0	8	100

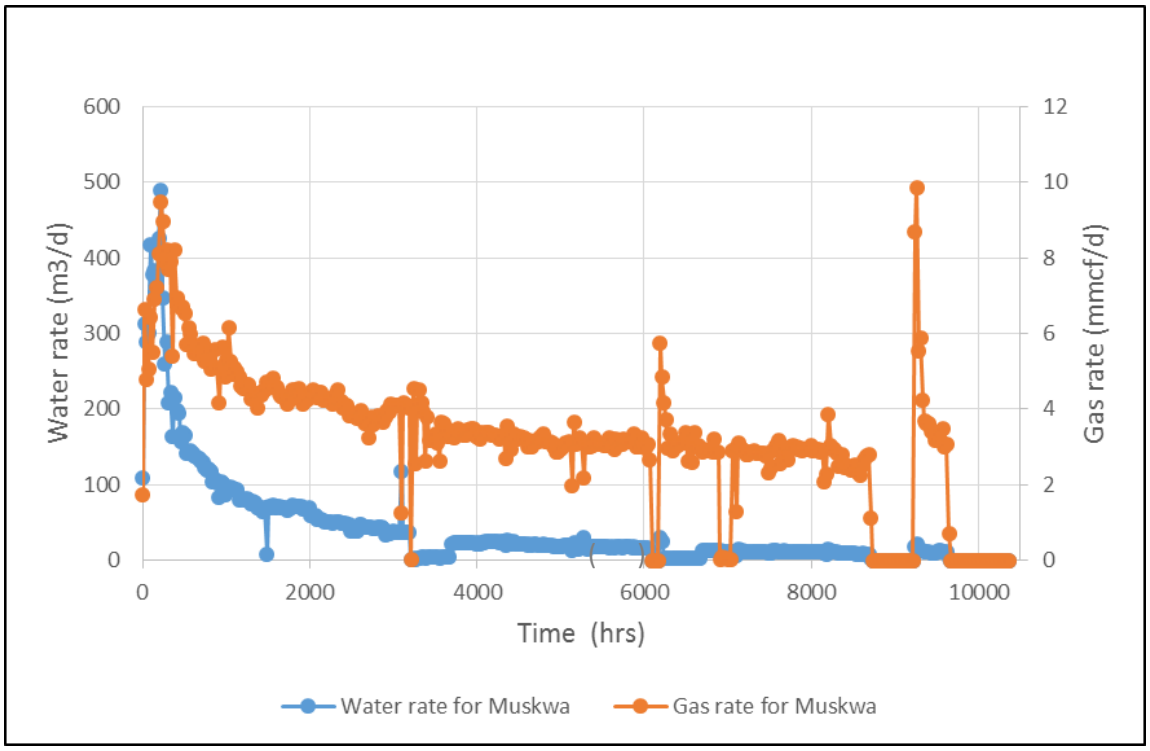

Figure 2.7 Produced water and gas rate from well in Evie member

As shown in **Table 2.6** it can be seen that the core samples have been collected from within a narrow range of depth intervals, but nevertheless they indicate a high degree of heterogeneity for some minerals, like calcite. This high calcite heterogeneity at certain intervals can potentially result in different calcium and carbonate/bicarbonate

concentration levels in the flowback water, which can cause serious scaling risk with $CaCO_3$ precipitations and the detailed analysis and discussion will be presented in the following section.

From the production profile plotted in **Figure 2.7**, some significant variations can be observed for both of produced water and gas rate. It can be considered that these produced fluids rate changes can be due to different stages of the hydraulic fracturing process being performed. According to the limited operation information collected from suppliers, the wells located in the Muskwa member are applied with 16 frac stages treatment during the entire production and the wells that penetrate the Evie member are stimulated by 18 hydraulic fracturing jobs through the life time (the timing for each hydraulic fracturing treatment is not supplied in details) (Towers, 2011).

2.4.2 Basic field data analysis

2.4.2.1 Fracture network discussion based on production profile data analysis

It is known from both our shale gas geochemical data collection and the relevant shale gas research from the public journals/ papers that the concentration of dissolved salt in flowback water significantly increases with time not only in the Horn River Basin but also with other gas producing shale reservoirs worldwide. This increase in salt concentration of flowback water could be due to the dissolution of shale minerals from the injected fracture fluid or the interaction/reaction between fracture fluid and the *in-situ* formation water. This section aims to interpret the increase in TDS of flowback water by discussing the complexity of fracture system in shale reservoir according to the analysis of field production profile.

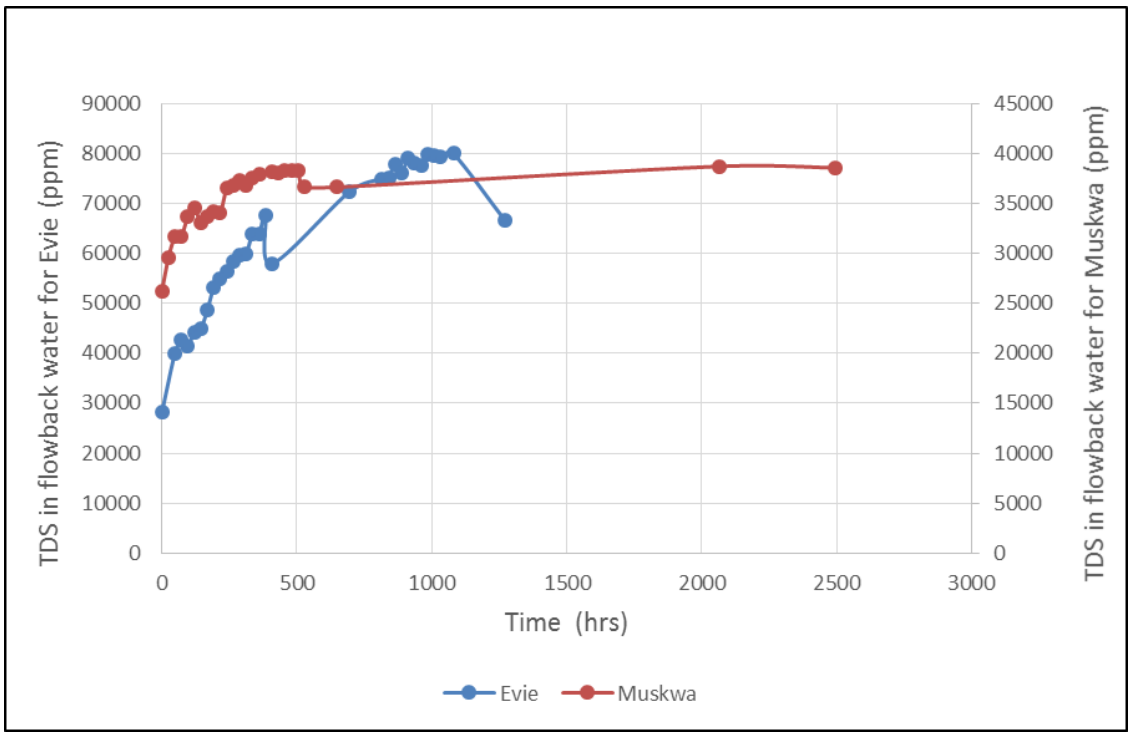

Figure 2.8 TDS of flowback water in Evie/Muskwa vs. time

Figure 2.8 is the plot of TDS in flowback water in Evie and Muskwa members in Horn River Basin against time. It can readily be found that the TDS in the flowback water in the Evie member has eventually reached a plateau at around 40,000 ppm two months after the hydraulic fracturing process was completed. By comparison, the TDS in the flowback water in the Muskwa formation reaches a level of nearly 80,000 ppm.

Compared with the TDS trends of the Muskwa member, the TDS in flowback water in the Evie member sharply increases after the first 20 days and this is followed by a transition zone to a gradual increase in the next month. The reason is that the water flowed back from the primary fractures does not show much mixing between injection water and connate water compared to the secondary fractures. The secondary fractures have a smaller aperture size to the primary ones which will increase the ratio of fracture surface area and fracture volume. In addition, the secondary fracture also contains the formation water coating the surface of shale gas minerals which makes it easy to mix with the injected fracture fluid (Bearinger, 2013). As a result of both reasons, the salinity of formation water in secondary fractures is higher than in the primary fractures. The more complex the fracture system is, the larger the contact area between injected fracture fluid and shale gas system will be, which will lead to maximize the ion transportation from shale matrix to the injected fracture fluid.

To discuss the fracture system complexity of the two members in Horn River Basin, some basic analysis on production profile data with each member needs to be observed. The water rate and gas rate of each member against the production time are shown in **Figure 2.7 and Figure 2.9.**

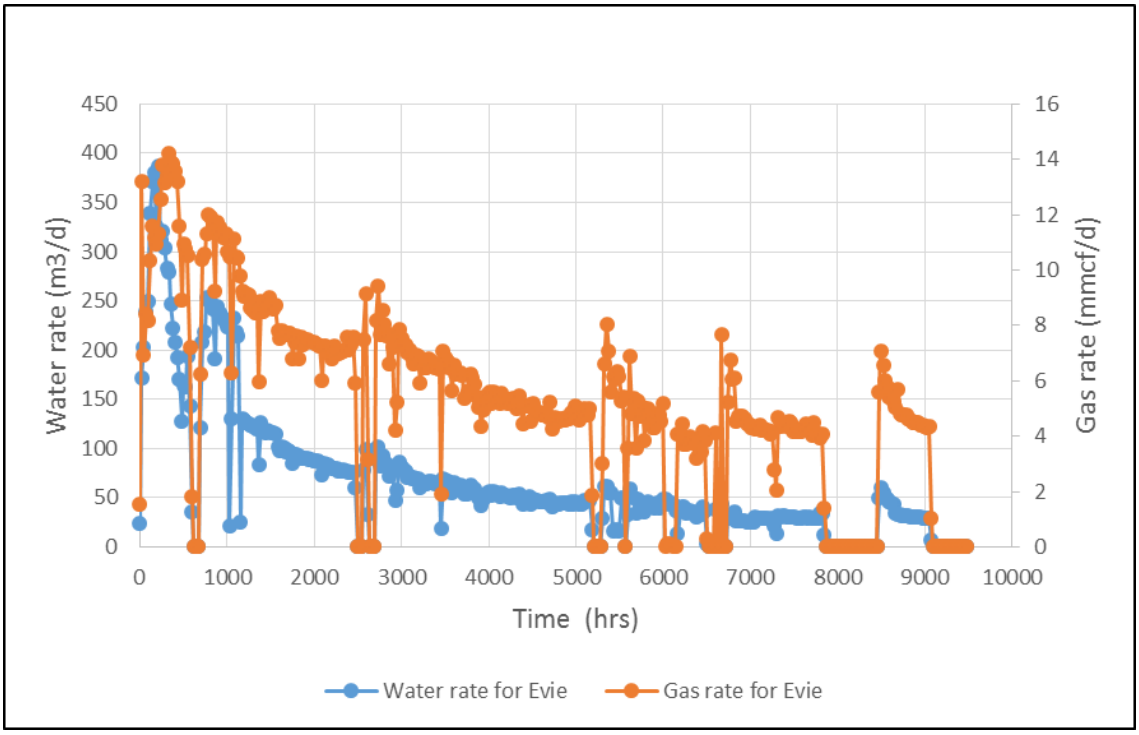

Figure 2.9 Produced water and gas rate in Evie

While at the beginning the well is put back on production, the fluid in the primary fractures created by hydraulic fracturing process will flow back due to the higher fracture conductivity and pressure draw down. With lower fracture conductivity and pressure draw down in the secondary fractures, water can be trapped within or even imbibed into the matrix due to the high matrix capillary pressure (Ebrahim, 2013). All of these processes result in the free gas existing in the active fractures or matrix being replaced and flowing up to the well through the fracture paths (Passey, 2010). As a consequence of this, as the complexity of the fracture system is increasing, it is producing back more gas and less water (more water could be trapped or imbibed within the shale gas fracture system) after the hydraulic fracturing process is performed (Rogers, 2010). It is also reported from the previous research that the imbibition into the small pores can help to account for the low volume of injection fluid flowing back (Bearinger, 2013). Furthermore, gravity will also have an impact on the amount of produced water only if there is water trapped above the horizontal well section, this occurs in certain shale gas production cases (Parmer, 2013).

Based on the thesis introduced above, as shown in **Figure 2.10**, it can be seen that compared with the production profile of the Muskwa formation, the Evie formation has a relatively higher produced gas water ratio at the beginning of production. The Evie formation has a more complex fracture system than the Muskwa formation (Blauch, 2009). Meanwhile, the salinity of connate water in secondary fractures is much higher than in the primary fractures (Ebrahim et al, 2013), therefore, it is expected that the TDS of flowback water in Evie can reach a higher value than in Muskwa. From **Figure 2.8**, it can be easily seen that the total dissolved solids of the flowback water in the Evie member does reach a higher value (80,000 ppm) compared with the Muskwa formation (40,000 ppm), which is consistent with the assumption of the fracture system complexity discussed above.

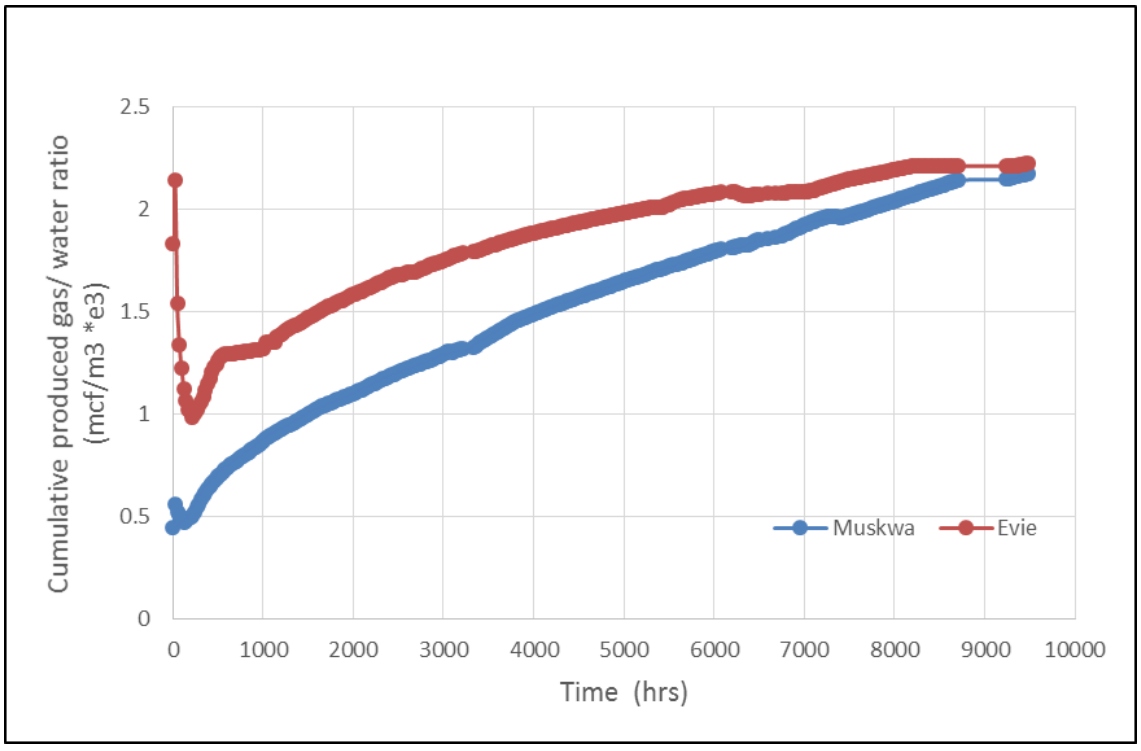

Figure 2.10 Cumulative produced gas/ water ratio for Muskwa and Evie formations vs. time

2.4.2.2 Geochemical data analysis

As a start to the geochemical field data analysis, water composition data for the two wells are processed and plotted. There are some plots of various ion concentrations in flowback water against fraction (as %) of total water recovered shown in **Figure 2.11**. **Figure 2.12** is the plot of TDS in flowback water vs. fraction (as %) of total water recovered. Both of plots are from the samples collected in the Evie well. (Not all the

ions concentration are presented here, only for some ions related to the analysis in this section; as the two wells are located in the same area and also the flowback water composition and ion concentration for both wells have similar trends, only the plots for the Evie well are shown here for ease of analysis)

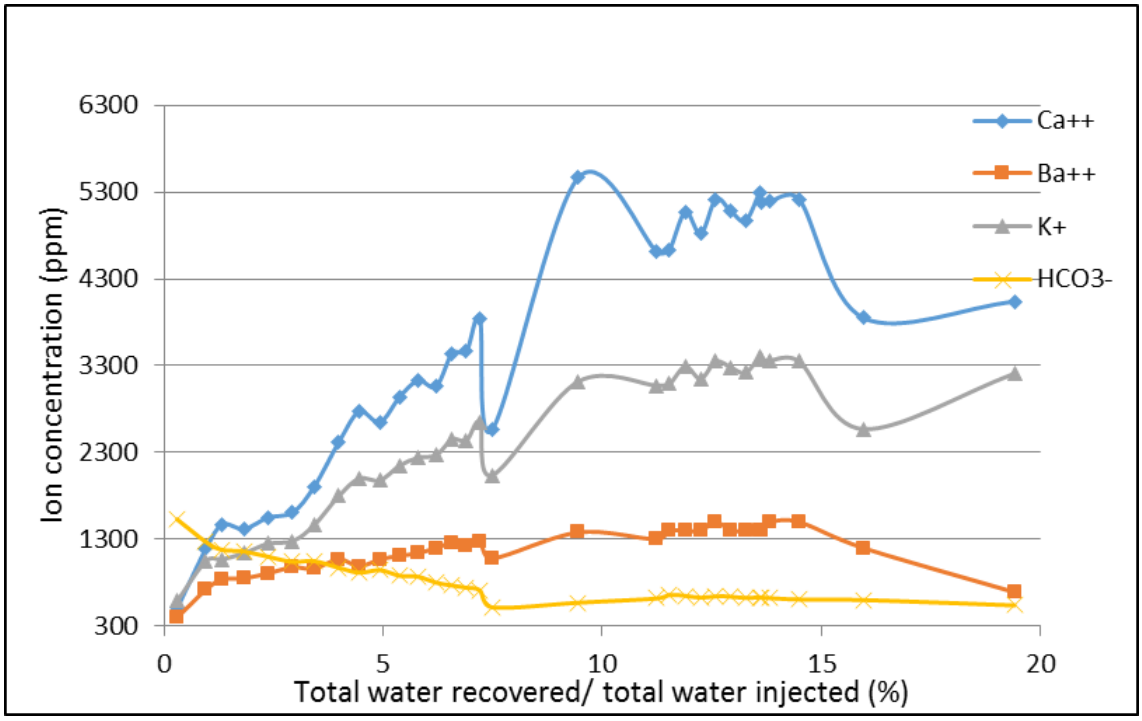

Figure 2.11 Flowback water ions concentration vs. fraction (as %) of total water recovered for well in Evie member

From the flowback water compositional data, it can readily be seen that there is an increase in the concentrations for most of the ions detected, especially for some cations like Na, Ca, and Ba. The reasons for flowback water composition changing during shale gas production could primarily be caused by three conditions, as follows: 1.) Mixing between fracture fluid and formation water; 2.) The geochemical reactions between fracture fluid and minerals within shale gas formation; 3.) Both of the conditions mentioned above. Therefore, one of the reasons above could be used to explain the great ion concentration changes between the fracture fluid and the flowback water. Among all the ions which experience large concentration changes, the change of Ba, Ca and HCO_3 in the flowback water are the most important in predicting the scale risk, as discussed in the following section.

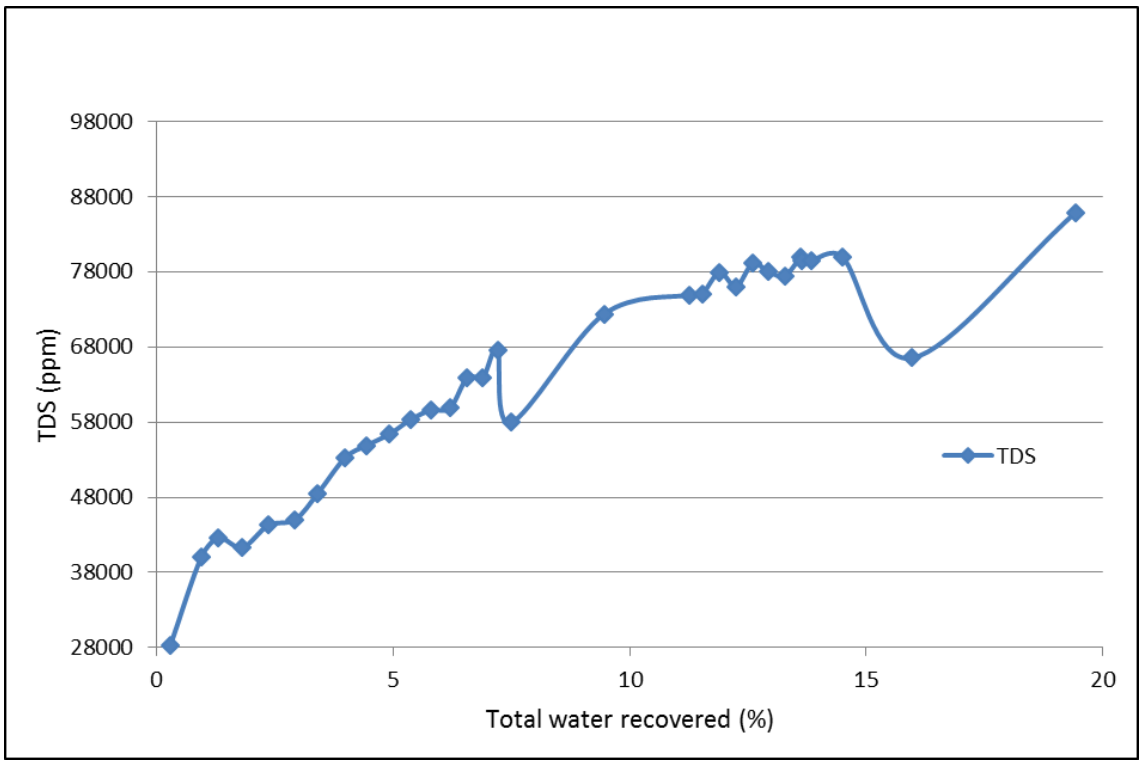

Figure 2.12 Flowback water TDS vs. fraction (as %) of total water recovered for well in Evie member

From the plot of TDS in flowback water against total water recovered, it can be found that the TDS increases during the entire period of water flow back. This is accounted for by the increase in the fraction of formation water produced back. As introduced previously, the brine produced back at an early stage is described as "flowback water", and during the later stages of production it is defined as "produced water" and contains almost 100% formation water, with higher salinity compared with the fracture fluid composition. At some point, the water that is recovered from a gas well makes a transition from flowback water to produced water. This transition point can be hard to discern, but it sometimes identified according to the rate of return measured in barrels per day (bbls/day) and by looking at the chemical composition. Flowback water produces higher flow rates over a shorter period of time, and declines rapidly to a few 100 bbls/day. Further decline is gradual, estimated at 10-20 bbls/day after a few months (HRN 2011; Towers, 2011). The chemical composition of flowback and produced water is very similar, so a detailed chemical analysis is recommended to distinguish between flowback and produced water.

As the flowback water contains high total dissolved solids and all the ions dissolved from the minerals along with other gases such as carbon dioxide, hydrogen sulphide and

so on, the risk of scale precipitation is significant. Flowback water treatment is also important before the water is disposed. To evaluate the risk of scale precipitation, the concentration of barium, calcium, bicarbonate and sulphate should be analysed as a key objective of the project.

2.4.2.2.1 Barium study

From the field chemical data it can be observed that barium concentration is very high (around 1500 ppm) compared with its value in fresh water fracture fluid (almost zero). It is known that barium has been identified in over 80 minerals, but it is never found as a free metal in nature. It only occurs in significant quantities in barite ($BaSO_4$) and witherite ($BaCO_3$) (CCME, 2013). According to the mineralogy data provided, the only mineral which contains barium is barite in this shale gas reservoir. However, it is known that the solubility for barite is extremely low, so barite dissolution cannot be the main source of the high concentrations of barium observed.

Barium concentration in water is determined by the solubility of barium salts and the adsorption of barium on active surfaces. Soluble barium compounds are mobile in the environment and have been detected in surface water, groundwater, drinking water, and sediment. Aqueous environments containing chloride, nitrate and carbonate anions will increase the solubility of barium sulphate and at pH 9.3 or less, the barium ion will be controlled by the sulphate ion concentration. Natural and treated waters generally contain sufficient sulphate to limit barium concentrations to <1500 mg/L. At pH levels >9.3, barium carbonate becomes the dominant species and limits barium solubility (CCME, 2013).

High levels of barium can be found in groundwater due to leaching and eroding of barium from sedimentary rocks and coal. Barium occurs naturally in soils with high levels associated with limestone, feldspar and shale deposits (Davis, 1992). It is reported that in the Horn River Basin area, there are also unusual minerals appearing such as barium rich k-feldspar, hyalophane and iron rich dolomite (Thomas and Ronald, 2012). Additionally, it does contain around 5 to 10 weight percentage feldspar referred to in the mineralogy table from the database. As a result, one possible source for the high barium concentration appearing in flowback water is the barium ion dissolved from the barium rich potassium feldspar.

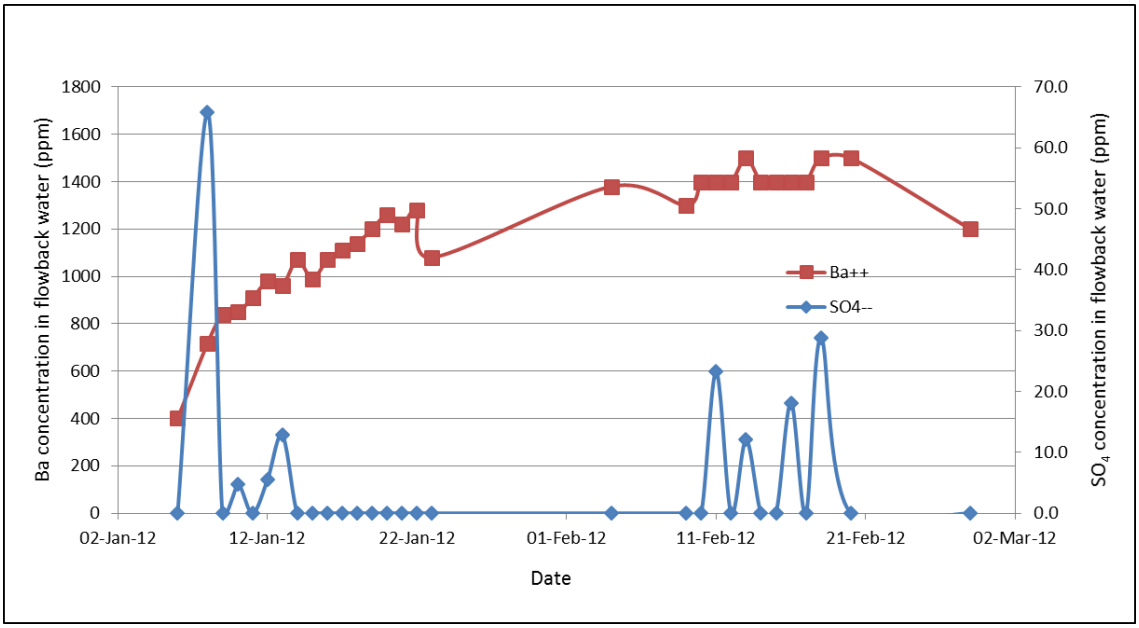

Figure 2.13 Ion concentrations in flowback water vs. date

As illustrated in **Figure 2.13** that the barium concentration in the flowback water is high at around 1,500 ppm after one month of production, although there are quite a few samples with sulphate concentrations below the detection limit (the data for sulphate concentrations are stated as being uncertain in the supplied report), in fact the sulphate concentration in the beginning is still relatively high. As a result, there will be high $BaSO_4$ scaling risk due to the commingled flow produced back between the multi-stage hydraulic fracturing process (the commingled flow consists of the flowback water produced at the end of the first hydraulic fracturing stage and the flowback water produced at the beginning of the second hydraulic fracturing stage). It is assumed that the two stages have the same production profile (high Ba produced back at the end of the first production profile and high SO_4 produced back at the beginning of the second production profile). The illustration of the multi-stage hydraulic fracturing model and the return production profiles for the two stages of the hydraulic fracturing process is shown in **Figure 2.14**.

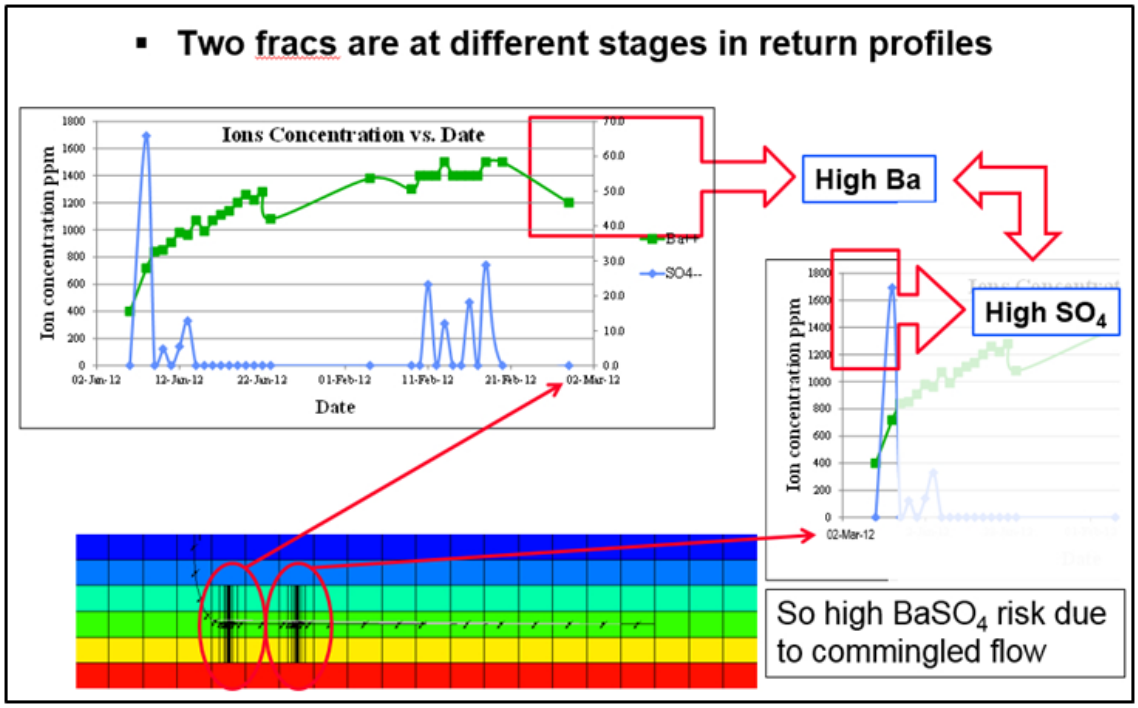

Figure 2.14 Scaling risk prediction for the multi-stage hydraulic fracturing

Due to the difficulties in obtaining shale samples from the shale gas fields and doing the experiment on testing shale gas mineral dissolution, some literature review related to the studies up to date have been carried out to identify what causes the significant change of total dissolved solids in the flowback water with shale gas systems.

From the relevant experimental studies on testing mineral dissolution and water imbibition rate into different shale samples (collected from the Horn River Basin), some key questions can be addressed (Ebrahim et al, 2013). Deionized water was used here for imbibition and mineral dissolution experiments. **Figure 2.15** (Ebrahim et al, 2013) illustrates the schematic diagram for the mineral dissolution and water imbibition tests.

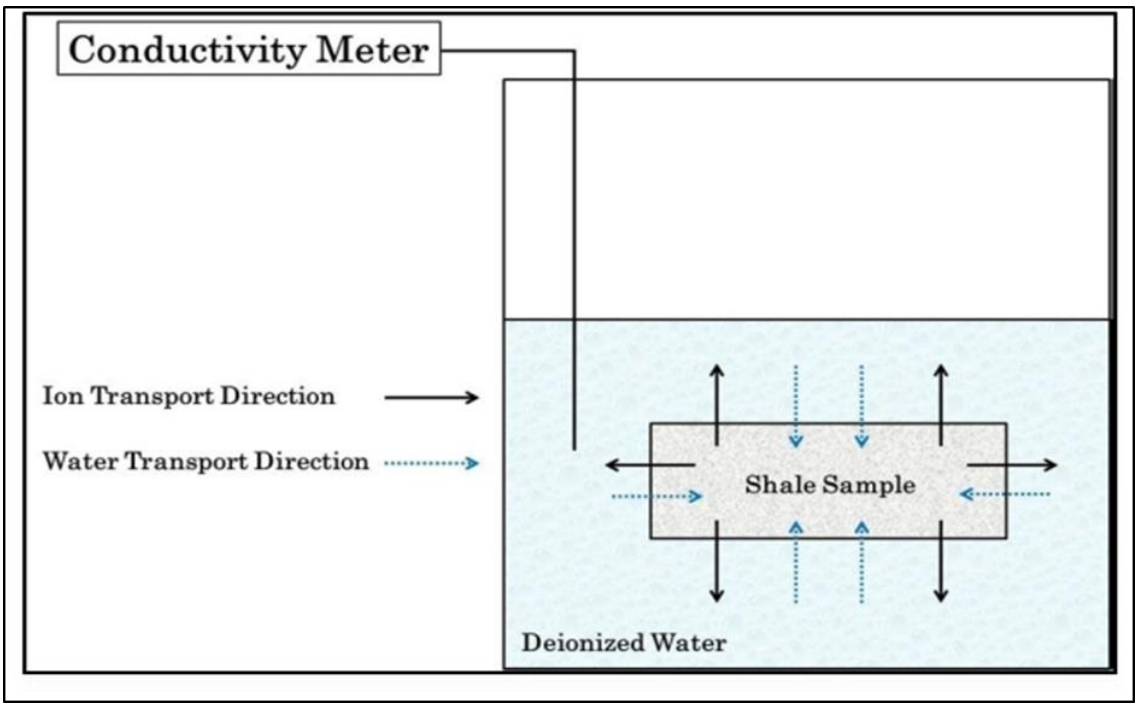

Figure 2.15 Schematic diagrams for the mineral dissolution and water imbibition tests

From the results of the experiments on shale samples in the Horn River Basin (Ebrahim, 2013), the conclusions can be drawn as below: 1) The water imbibition process can induce shale sample swelling and create micro-fractures and also lead to expelled air bubbles on the sample surface (Ebrahim et al, 2013; Blauch et al, 2009); 2) Shale samples with higher clay content have higher water imbibition and ion diffusion rates (Byrnes, 2011); 3) From the mineral dissolution test, it can be shown that Na and Cl are the dominant ions dissolved from minerals; other high concentrations of ions in flowback water can be caused by fluid mixing with the higher salinity formation water. It is considered that the imbibition process leads to dissolution of some original salts in place and followed by a diffusion process to release ions from rock sample into the brine. It is reported that the shale samples in HRB area mainly contains illite, quartz, chlorite, pyrite, dolomite and plagioclase. Therefore, plagioclase can be the main mineral source of observed Na and Cl otherwise it can be from the dissolution of precipitate salts off pore-water (Ebrahim et al, 2013; Blauch et al, 2009).

2.4.2.2.2 Calcium & bicarbonate study

As shown in **Figure 2.16**, calcium and bicarbonate concentrations are plotted against chloride concentration. It is known that the calcium concentration increases continually with time; by contrast, the bicarbonate concentration decreases throughout the period of shale gas production. It can also be seen that calcium concentration reaches a high level

of around 5,500 ppm; however, the bicarbonate concentration reduces to around 600 ppm. As discussed previously in section 3.3.1, this high concentration of calcium in Evie can be accounted for by the high content of calcite within deeper formations (heterogeneity of calcite mineral); by way of contrast, the calcium concentration in the flowback water produced from Muskwa member is 900 ppm and also there was zero detection of bicarbonate (lack of calcite exists in the shallow formations). It is also reported that there is around 12% carbon dioxide in the gas composition for the well in the Evie member; and for the well in Muskwa member the carbon dioxide percentage decreases to around 9%. There is potential to generate calcium carbonate precipitation during shale gas production. In order to better understand the relationships between calcium, bicarbonate and carbon dioxide, a simple zero dimensional thermodynamic calculation is performed using a thermodynamic scale prediction model. In this case, MultiScale was used (Kaasa, 1998).

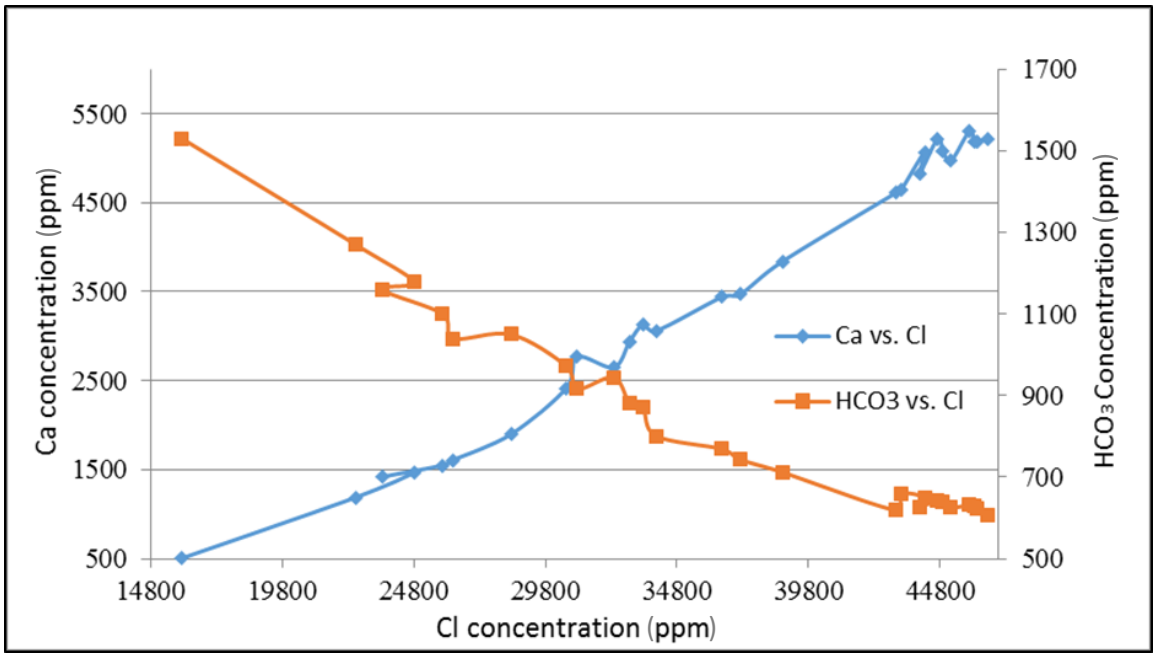

Figure 2.16 Ca and HCO_3 concentrations vs. chloride concentration

Two compositions were entered in MultiScale to create a mixing calculation, one being the fracture fluid composition and the other being the assumed formation water composition. The volume of the two fluids in the calculation is assumed to be the same, with 500 m^3/day of each making the total water rate to be 1,000 m^3/day. (The actual volume of water is not important here as evaporation is not considered, but what is important is the ratio of the two brines.) As mentioned before, the fracture fluid is almost as clean as fresh water with only around 1,156 ppm total dissolved solids;

however, the formation water is saline with TDS up to 80,305 ppm (both of the Na and Cl ion concentrations are verified by MultiScale with ionic equilibrium). Both of the fluid compositions can be found in **Figure 2.17** and **Figure 2.18**. The analysis conditions for fracture fluid is 1 bar pressure with 15 °C temperature; and for formation water it is 335.6 bar with 138 °C - i.e. reservoir condition. Another piece of information that needs to be added in the formation water input is that there is 12 mole% carbon dioxide and 88 mole% methane contained in the gas phase. It is important to define gas composition in the table since carbon dioxide plays an important role in the final ionic equilibrium for the mixture of the two fluids.

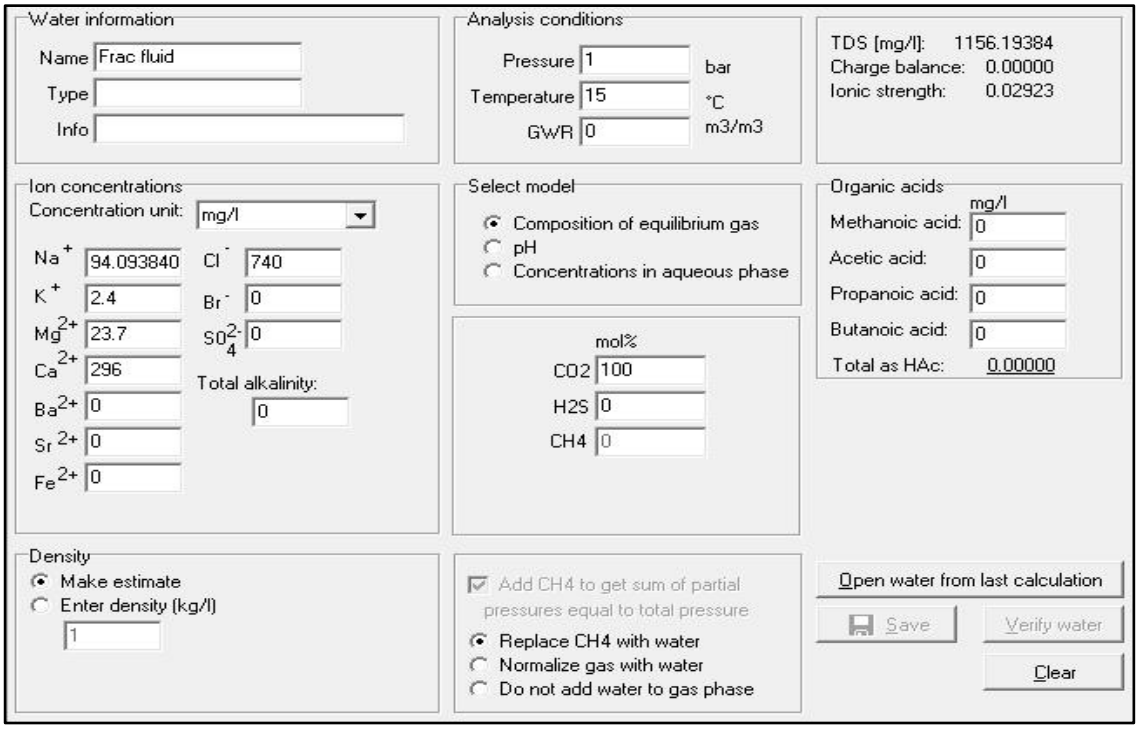

Figure 2.17 Fracture fluid composition used in MultiScale

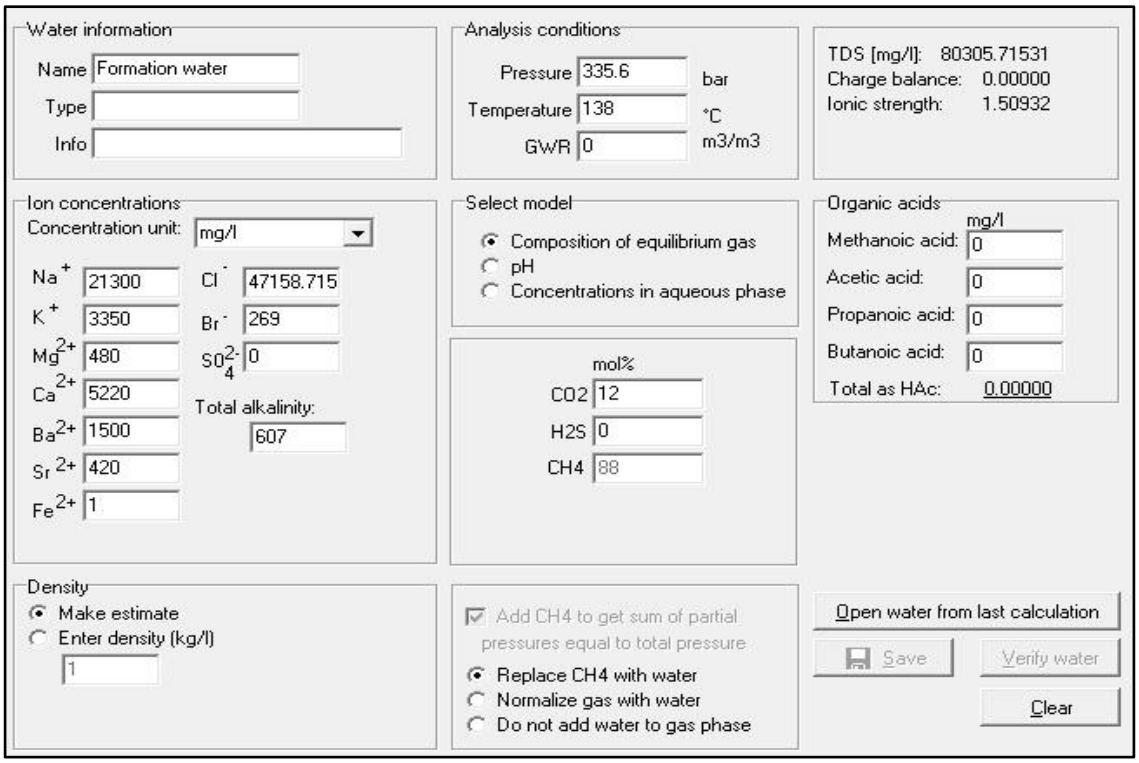

Figure 2.18 Flowback water composition used in MultiScale

After defining the fluid information table, the calculation type is set with the option of mixing profile. The analysis condition for this mixing model is set to be the shale gas reservoir condition, which are 354 bar pressure and 145 °C temperature, in order to simulate calcium carbonate precipitation/ dissolution process within the shale gas reservoir while hydraulic fracturing is taking place. The formation water is applied as base solution and fracture fluid is mixed with it. (Step 10 thus refers to 100% formation fluid.) The calculation result for this mixing model is illustrated in **Figure 2.19.**

SATURATION RATIO

Step	FeCO3	CaCO3c	NaCl	KCl	BaCO3	SrCO3
1	0.000	0.000	0.000	0.000	0.000	0.000
2	0.000	0.050	0.000	0.000	0.000	0.002
3	0.001	0.151	0.001	0.000	0.001	0.005
4	0.002	0.281	0.002	0.000	0.002	0.010
5	0.003	0.430	0.003	0.000	0.003	0.016
6	0.004	0.595	0.004	0.000	0.004	0.022
7	0.005	0.773	0.006	0.001	0.005	0.028
8	0.007	0.964	0.008	0.001	0.006	0.035
9	0.008	1.168	0.011	0.001	0.007	0.043
10	0.009	1.386	0.014	0.001	0.009	0.051

PRECIPITATION (kg/day)

Step	FeCO3	CaCO3c	NaCl	KCl	BaCO3	SrCO3
1	0.000	0.000	0.000	0.000	0.000	0.000
2	0.000	0.000	0.000	0.000	0.000	0.000
3	0.000	0.000	0.000	0.000	0.000	0.000
4	0.000	0.000	0.000	0.000	0.000	0.000
5	0.000	0.000	0.000	0.000	0.000	0.000
6	0.000	0.000	0.000	0.000	0.000	0.000
7	0.000	0.000	0.000	0.000	0.000	0.000
8	0.000	0.000	0.000	0.000	0.000	0.000
9	0.000	32.784	0.000	0.000	0.000	0.000
10	0.000	74.525	0.000	0.000	0.000	0.000

Figure 2.19 Calculation result for MultiScale model (step 1 is pure fracture fluid and step 10 is 100% formation water in reservoir condition.)

From the calculation results in **Figure 2.19** it can be seen that for mixtures up to 80% fracture fluid into formation water, the saturation ratio for calcium carbonate is 0.964 (i.e. below 1). It starts to generate calcium carbonate precipitation (32.784 kg/day) only after mixing 90% of formation water with the fracture fluid. The final precipitation mass for calcium carbonate reaches 74.525 kg/day at 100% formation water composition. The calculation results from Multiscale illustrate that the system does have a calcium carbonate precipitation risk due to mixing between formation water and fracture fluid at reservoir conditions.

As there was no formation water composition provided, the formation water composition used here is picked from the flowback water composition data by using the second last sample analysed in the database. From our data analysis, it can be considered this flowback water composition may be quite close to the formation water composition. However, under different circumstances, fracture fluid can be produced back with flowback water for multiple weeks. The water flow rate may still be quite high on the date the sample was collected; there is insufficient evidence to state that this

is produced water and does not contain some flowback water – i.e. the asymptote in the concentration curve may not have been reached. Therefore, it cannot be said for sure that the water composition used in the formation water table is exactly the composition it should be. If the data used from this sample is confirmed as flowback water, the real compositions for formation water could be even higher than that which was used. In that case, the discussion and calculation of formation water composition will be predicted and presented at the end of this chapter. This is significant, in that chemical equilibrium conditions dictate that 100% formation water cannot be oversaturated.

To better predict the scaling tendency with $CaCO_3$, an extended Ca and HCO_3 study using the MultiScale model was developed with the fluid mixing between fracture fluid and each of the flowback water samples. These modelling cases are used to calculate the final ionic equilibrium for the mixture of the two fluids with the minimum fraction of CO_2 in the gas phase required.

Table 2.7 Table of flowback water compositions of well in Evie

Collected Date	Ba	Br	Ca	Cl	Mg	K	Na	Sr	SO_4	HCO_3
	mg/L	mg/L	mg/L	mg/L	mg/L	mg/L	mg/L	mg/L	mg/L	mg/L
6-Jan-12	400	78.7	506	16000	62	590	8900	47.8	b.d.	1530
8-Jan-12	718	122.2	1190	22600	120	1050	12600	93.7	66	1270
9-Jan-12	839	120.6	1470	24800	130	1070	12700	126	b.d.	1180
10-Jan-12	851	125.8	1420	23600	140	1140	12600	137	4.8	1160
11-Jan-12	908	111.2	1550	25900	150	1250	13000	150	b.d.	1100
12-Jan-12	979	125.6	1610	26300	160	1280	13200	158	5.5	1040
13-Jan-12	962	141.3	1900	28500	180	1460	14000	178	13	1050
14-Jan-12	1070	158.3	2420	30600	240	1800	15600	200	b.d.	972
15-Jan-12	990	179.9	2770	31000	270	2000	16400	210	b.d.	916
16-Jan-12	1070	195.5	2650	32400	250	1980	16500	230	b.d.	945
17-Jan-12	1110	165.4	2940	33000	270	2150	17400	240	b.d.	880
18-Jan-12	1140	173.1	3130	33500	290	2240	17800	250	b.d.	870
19-Jan-12	1200	205.2	3060	34000	290	2270	17600	270	b.d.	801
20-Jan-12	1260	218.6	3440	36500	320	2450	18500	280	b.d.	769
21-Jan-12	1220	189.0	3470	37200	320	2440	17900	280	b.d.	743
22-Jan-12	1280	241.8	3840	38800	360	2650	19200	320	b.d.	712
9-Feb-12	1300	222.3	4610	43100	440	3070	21000	354	b.d.	619
10-Feb-12	1400	223.3	4640	43300	430	3090	20800	350	b.d.	660
11-Feb-12	1400	219.4	5070	44200	470	3290	22000	373	23.2	650
12-Feb-12	1400	215.7	4820	44000	440	3150	20800	377	b.d.	627
13-Feb-12	1500	280.8	5220	44700	470	3350	22300	390	12.0	644
14-Feb-12	1400	234.7	5080	44900	470	3280	21400	391	b.d.	640
15-Feb-12	1400	281.0	4970	45200	460	3220	20700	395	b.d.	625
16-Feb-12	1400	226.2	5300	45900	490	3410	21900	400	18.1	632
17-Feb-12	1400	305.7	5180	46100	480	3370	21400	420	b.d.	630
18-Feb-12	1500	283.9	5190	46200	480	3360	21100	440	28.8	623
20-Feb-12	1500	268.9	5220	46600	480	3350	21300	420	b.d.	607

Table 2.7 shows different ion concentrations in flowback water for the well in Evie member within two months after the hydraulic fracturing process. Some ion compositions in the flowback produced water are not shown in this table for the reason that they are nonessential parameters in the MultiScale model.

Instead of only using the second last flowback water sample as the base solution, the flowback water compositions collected from different samples on each production date will be applied in the MultiScale mixing model. The analysis condition of the fracture fluid remains 1 bar pressure with 15 °C temperature; and for formation water it is 335.6 bar with 138 °C - i.e. the reservoir condition (the analysis condition of the two fluids mixing is also the reservoir condition).

It is reported that the original CO_2 content in the gas phase is 12%; however, for different mixing cases with varied flowback water compositions, there is an appropriate CO_2 content in the gas phase to ensure that there is no $CaCO_3$ precipitation generated after the calculation of each ionic equilibrium state. By testing the different CO_2 content values in the various cases, the minimum value of CO_2 content of each case to prevent precipitating has been identified. All the minimum values of CO_2 content and the ratio of calcium and bicarbonate for each different flowback case are shown in **Table 2.8** (the highlighted sample (the last flowback water sample collected in Evie formation) is used to be the formation water sample for the MultiScale analysis in the previous section). The plot between Ca/HCO_3 ratio and fraction (as %) of CO_2 in the gas phase is illustrated in **Figure 2.20**.

Table 2.8 Table for Ca, HCO_3, Ca/HCO_3 and fraction (as %) of CO_2 in gas phase

Date	Ca	HCO_3	Ca/HCO_3	CO_2 %	Date	Ca	HCO_3	Ca/HCO_3	CO_2 %
	mg/L	mg/L				mg/L	mg/L		
8-Jan-12	1190	1270	0.937008	37%	21-Jan-12	3470	743	4.670256	23%
9-Jan-12	1470	1180	1.245763	37%	22-Jan-12	3840	712	5.393258	21%
10-Jan-12	1420	1160	1.224138	35%	9-Feb-12	4610	619	7.447496	17%
11-Jan-12	1550	1100	1.409091	32%	10-Feb-12	4640	660	7.030303	20%
12-Jan-12	1610	1040	1.548077	29%	11-Feb-12	5070	650	7.8	19%
13-Jan-12	1900	1050	1.809524	33%	12-Feb-12	4820	627	7.6874	18%
14-Jan-12	2420	972	2.489712	33%	13-Feb-12	5220	644	8.10559	19%
15-Jan-12	2770	916	3.024017	31%	14-Feb-12	5080	640	7.9375	19%
16-Jan-12	2650	945	2.804233	32%	15-Feb-12	4970	625	7.952	18%
17-Jan-12	2940	880	3.340909	29%	16-Feb-12	5300	632	8.386076	19%
18-Jan-12	3130	870	3.597701	29%	17-Feb-12	5180	630	8.222222	19%
19-Jan-12	3060	801	3.820225	24%	18-Feb-12	5190	623	8.330658	18%
20-Jan-12	3440	769	4.473342	24%	**20-Feb-12**	5220	607	8.599671	17%

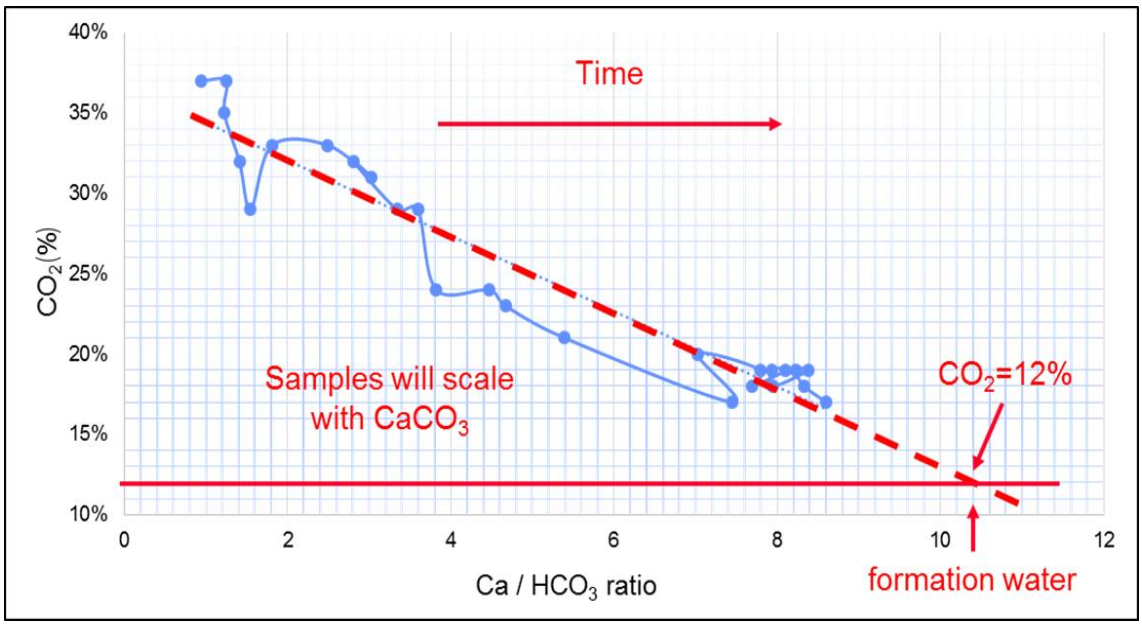

Figure 2.20 Ca/HCO_3 vs. fraction (as %) of CO_2 in gas phase

From **Table 2.8** and **Figure 2.20**, it can be found that the calcium concentration is increasing and bicarbonate concentration is decreasing. However, at the beginning of shale gas production, the rate of calcium concentration increasing is much faster than the rate of bicarbonate concentration decreasing; after a month of shale gas production, the rate of concentration with calcium and bicarbonate are tending to be the same. The reason for that is that after the hydraulic fracturing process is completed, there will be a transition time from flowback water to produced water (formation water). At the beginning of shale gas production, the flowback water composition normally has changed due to the mixing between fracture fluid and formation water or even the dissolution process between fracture fluid and minerals within the shale gas reservoir; as time passes by, less fracture fluid is included in the flowback water and after multiple weeks on production, the composition of flowback water will tend to be the same as the formation water composition and the value of it will vary in a small constant range before the next hydraulic fracturing stage is operated.

From **Figure 2.20** it can be found that during the process of shale gas production, the minimum fraction of CO_2 content in the gas phase is roughly decreasing with each case to balance the ionic equilibrium status without any $CaCO_3$ precipitation generated. Meanwhile, compared with the sample collected two months later, the requirement of CO_2 content for the sample collected at the beginning of the production has more than double the amount in the gas phase just to prevent $CaCO_3$ precipitation. As the requirement of minimum CO_2 content in the gas phase changes significantly during the

shale gas production process, it can be shown that CO_2 plays an important role in predicting the scaling tendency of $CaCO_3$ in the shale gas reservoir system. It also demonstrates that all the minimum CO_2 fractions in gas phase for each case are higher than the CO_2 content at reservoir conditions, which verifies that there is scaling risk to generate CaCO3 precipitation during the whole process. Another important finding that can be deduced from the plot is – The ratio of calcium and bicarbonate concentrations must be 10.4 to balance the ionic equilibrium status under the initial reservoir conditions (which contains 12% CO_2 content in the gas phase).

2.5 PRESENTATION AND BASIC ANALYSIS OF DATA FROM OTHER RESOURCES

To further study the scaling tendency risk during shale gas production and illustrate the reason for the high salinity of the flowback water in shale gas systems, some further review of the literature has been conducted and more chemical compositional data have been collected and analysed.

All the geochemical data presented in this section are from the Marcellus shale – one of the best studied and explored shale plays worldwide. The specific location for the target shale reservoir is in the southwest and north central Pennsylvania. Since sufficient shale gas geochemical data are available, it is observed that the composition of the flowback water sample collected 1 year (long-term) after the hydraulic fracturing process reaches a stable plateau value and the salinity of which is considered to be the same as the *in situ* formation water. It is also reported that is less than 50% of the injected water volume has been recovered back, which is consistent with the thesis that most of the injection fluid was trapped or imbibed within the shale gas system. Several wells are used to collect time-series samples of flowback water compositions. Some of the data are shown in **Table 2.9** as examples (Elisabeth, 2015).

Table 2.9 Sample table of shale gas geochemical data in southwest Pennsylvania, Well A

WELL A, GREENE COUNTY, SOUTHWEST PENNSYLVANIA												
Sample Point	Day	Na	K	Mg	Fe	Ba	Ca	Sr	Cl	SO4	HCO3	TDS
		mg/L										
Injected Water	**–**	**20,900**	**682**	**567**	**16**	**393**	**4,380**	**1,390**	**41,900**	**63**	**0**	**70,600**
Well head	1	26,000	275	776	43.7	1,110	6,530	1,400	63,700	<225	209	100,000
Well head	2	30,100	247	828	44.9	1,560	7,900	1,820	65,000	<225	193	108,000
Well head	3	26,800	258	866	49.2	1,490	7,370	1,720	67,300	<225	206	106,000
Well head	4	30,900	298	755	38.1	1,760	8,870	2,010	70,200	<225	192	115,000
Well head	5	28,300	309	762	1.1	1,640	7,950	1,870	71,200	<225	174	113,000
Well head	7	32,800	1210	841	26.6	962	8,790	2,420	81,900	<225	98.8	130,000
Well head	15	32,400	308	953	28.1	2,270	9,630	2,280	86,500	<225	115	135,000
Storage Tank	20	34,500	311	976	36.1	2,520	10,400	2,480	87,700	<225	116	140,000
Storage Tank	212	43,800	281	1,170	96.6	3,690	14,500	3,100	98,900	<30	76.9	167,000
Storage Tank	**297**	**39,200**	**251**	**1,160**	**133**	**3,420**	**13,500**	**2,890**	**99,000**	**<30**	**107**	**161,000**
Storage Tank	393	40,300	290	1,510	107	3,360	14,300	2,890	99,300	<10	0	163,000
Separator	438	40,400	280	1,410	194	3,970	14,200	3,130	98,100	<20	0	163,000
Storage Tank	438	42,400	310	1,440	174	4,150	14,800	3,260	101,000	<20	0	169,000

Compared with the geochemical data collected from different wells of the Marcellus shale play, it can be seen that the injected fracture fluid used for hydraulic fracturing is saline water and the salinity is between 20,000 and 50,000 ppm for Well B; meanwhile for the injected fracture fluid salinity of Well A, it even reaches around 70,000 ppm, which is much higher than the fracture fluid used for the hydraulic fracturing process in the Horn River Basin area. There is also barium in the fracture fluid used for Well A and sulphate in the fracture fluid used for Well B. It is reported that the source of the fracture fluid in this case is recycled produced water. Furthermore, it can be also observed that the salinity of flowback water for each well reaches a plateau value around 160,000 ppm after a few months of production (shown in **Figure 2.21**). There is high calcium concentration (over 10,000 ppm) and barium concentration (around 4,000 ppm) in the flowback water as well (normally the barium concentration in shale gas systems is ranging from 500 ppm to 1,000 ppm).

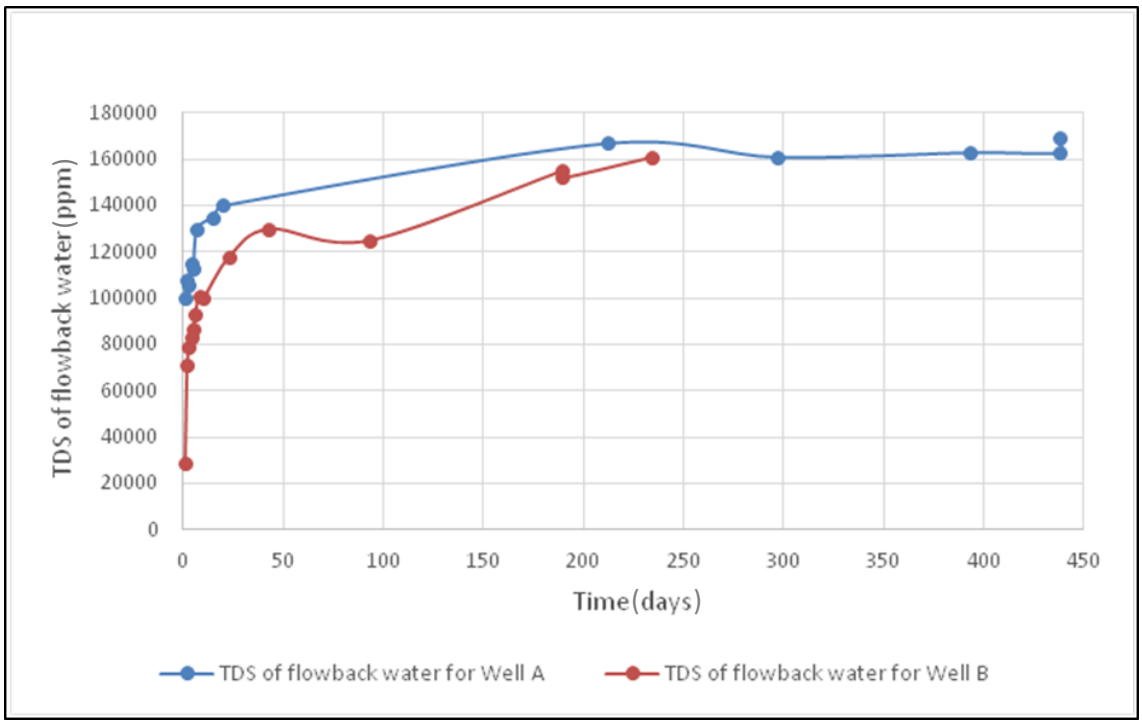

Figure 2.21 TDS of flowback water for Well A and Well B

As high barium concentrations were flowing back and also sulphate is observed in the fracture fluid used for the hydraulic fracturing process, the scaling tendency should be predicted by using MultiScale. The highlighted rows indicated in **Table 2.9** are the fluid compositions used in the MultiScale fluid mixing model. As indicated in the table, the bicarbonate concentration is not available for the fracture fluid composition analysis for both of the wells. The formation water compositions input into MultiScale are selected from the last produced water samples for which the bicarbonate concentration is available (around 1 year later). The calculation results of the MultiScale mixing model for Well A and Well B are shown in **Figure 2.22 and Figure 2.23**.

PRECIPITATION (kg/day)

Step	FeCO3	CaCO3c	BaSO4	SrSO4	CaSO4A	CaSO4G	CaSO4H	NaCl	BaCO3	SrCO3
1	0.000	0.000	72.229	0.000	0.000	0.000	0.000	0.000	0.000	0.000
2	0.000	0.000	81.016	0.000	0.000	0.000	0.000	0.000	0.000	0.000
3	0.000	0.000	89.785	0.000	0.000	0.000	0.000	0.000	0.000	0.000
4	0.000	0.000	98.527	0.000	0.000	0.000	0.000	0.000	0.000	0.000
5	0.000	0.000	107.230	0.000	0.000	0.000	0.000	0.000	0.000	0.000
6	0.000	0.000	115.873	0.000	0.000	0.000	0.000	0.000	0.000	0.000
7	0.000	0.000	124.409	0.000	0.000	0.000	0.000	0.000	0.000	0.000
8	0.000	0.000	132.730	0.000	0.000	0.000	0.000	0.000	0.000	0.000
9	0.000	0.000	140.498	0.000	0.000	0.000	0.000	0.000	0.000	0.000
10	0.000	0.000	145.899	0.000	0.000	0.000	0.000	0.000	0.000	0.000

Figure 2.22 Calculation results for MultiScale model of Well A

PRECIPITATION (kg/day)

Step	FeCO3	CaCO3c	BaSO4	SrSO4	CaSO4A	CaSO4G	CaSO4H	NaCl	BaCO3	SrCO3
1	0.000	0.000	0.099	0.000	0.000	0.000	0.000	0.000	0.000	0.000
2	0.000	0.000	208.804	0.000	0.000	0.000	0.000	0.000	0.000	0.000
3	0.000	0.000	417.455	0.000	0.000	0.000	0.000	0.000	0.000	0.000
4	0.000	0.000	626.013	0.000	0.000	0.000	0.000	0.000	0.000	0.000
5	0.000	0.000	834.372	0.000	0.000	0.000	0.000	0.000	0.000	0.000
6	0.000	0.000	1042.165	0.000	0.000	0.000	0.000	0.000	0.000	0.000
7	0.000	0.000	1246.680	0.000	0.000	0.000	0.000	0.000	0.000	0.000
8	0.000	0.000	1143.165	0.000	0.000	0.000	0.000	0.000	0.000	0.000
9	0.000	0.000	572.906	320.122	0.000	0.000	0.000	0.000	0.000	0.000
10	0.000	0.000	0.000	381.205	0.000	0.000	0.000	0.000	0.000	0.000

Figure 2.23 Calculation results for MultiScale model of Well B

The fluid mixing conditions for both of the models are set as reservoir conditions, which are 380 bars of reservoir pressure and 75 °C of reservoir temperature (Elisabeth, 2015). From the MultiScale calculation results, it can be easily found that both of the wells could have significant scaling problems during production. Well B can generate up to around 1,200 kg $BaSO_4$ precipitation every day, which is 8 times higher value than the scale precipitation that can be generated from Well A (around 150 kg/day). The reason for the high scaling tendency difference between the two wells is that the sulphate concentration in the fracture fluid used for Well B is as much as six times more than the sulphate concentration used in fracture fluid in Well A, and also more than enough barium in the flowback water is recovered for both cases which means Well B has a significantly greater scaling risk than Well A. There is thus a serious scaling risk during shale gas production with Marcellus shales in the southwest and north central Pennsylvania, unless some solutions could be found (such as adding scale inhibitor in the fracture fluid or pre-treating frac water *before* using it as a hydraulic fracturing fluid).

2.6 PREDICTION OF FORMATION WATER COMPOSITION

2.6.1 Prediction in Evie member

As a continuation of the geochemistry study in the Horn River Basin area, the prediction of formation water composition has been carried out. In general it can be very challenging to identify the *in situ* formation water composition for the reason noted earlier. In order to obtain more information on the formation water composition, some calculations have been carried out based on the given geochemistry data and previous data analysis; thereafter, the validation of the predicted formation water composition has

been made. In the end, some conclusions have been drawn to address the key question – what causes the high salinity in flowback water during shale gas production.

As mentioned previously, the calcium and bicarbonate concentrations in the flowback water has been supplied (Towers, 2011), the calcium and bicarbonate concentrations are plotted against the chloride concentration in the flowback water. Each of the equations for the trend line from both plots is illustrated in **Figure 2.24**.

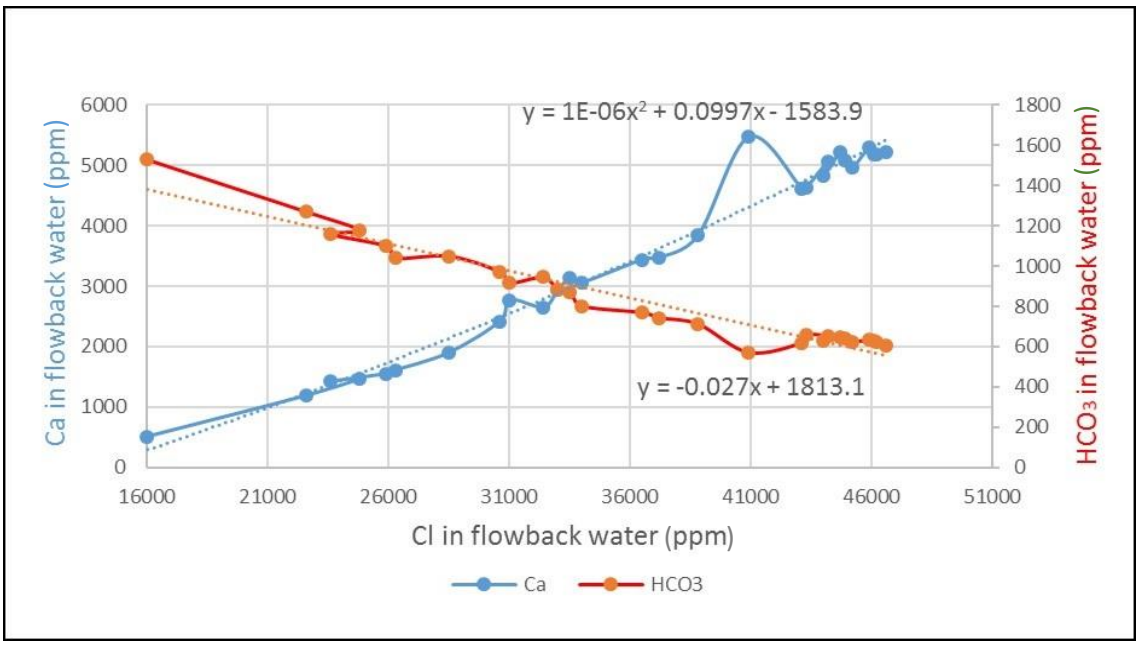

Figure 2.24 Chloride concentration vs. Ca and HCO_3 concentration in flowback water

It can be readily identified that the bicarbonate concentration in the flowback water drops during the production process. To identify the envelope of possible water compositions, it is initially assumed that the bicarbonate concentration in the formation water keeps decreasing until it reaches a near zero value. The chloride concentration in the formation water then can be calculated from **Equation 2.1**. Meanwhile, the calcium concentration could also be confirmed from the calculation result of **Equation 2.2**. The initially estimated calcium, bicarbonate and chloride concentration in the formation water will thus be: 8900 ppm, 0 ppm and 67152 ppm, respectively. Note, these are not the expected formation water concentrations, these are the extreme values that cannot be exceeded – being upper values for calcium and chloride and a lowest possible value for bicarbonate.

$$y = 1E\text{-}06x^2 + 0.0997x - 1583.9 \quad \ldots \textbf{Equation 2.1}$$

$$y = -0.027x + 1813.1 \quad \ldots \textbf{Equation 2.2}$$

Although, the bicarbonate concentration decreases during the entire production, nevertheless, according to the previous analysis of the calcium carbonate scaling tendency, it still shows the existence of bicarbonate in the formation water – i.e. it is not zero concentration. In addition, the ratio between calcium and bicarbonate concentrations in the formation water should be around 10.4, based on our previous analysis. In order to obtain more information relating to the formation water composition, the ratio of calcium and bicarbonate concentrations is plotted against the chloride concentration from each of the flowback water samples. The plot is shown in **Figure 2.25** and **Figure 2.26** indicates the potential trendline equations for this plot.

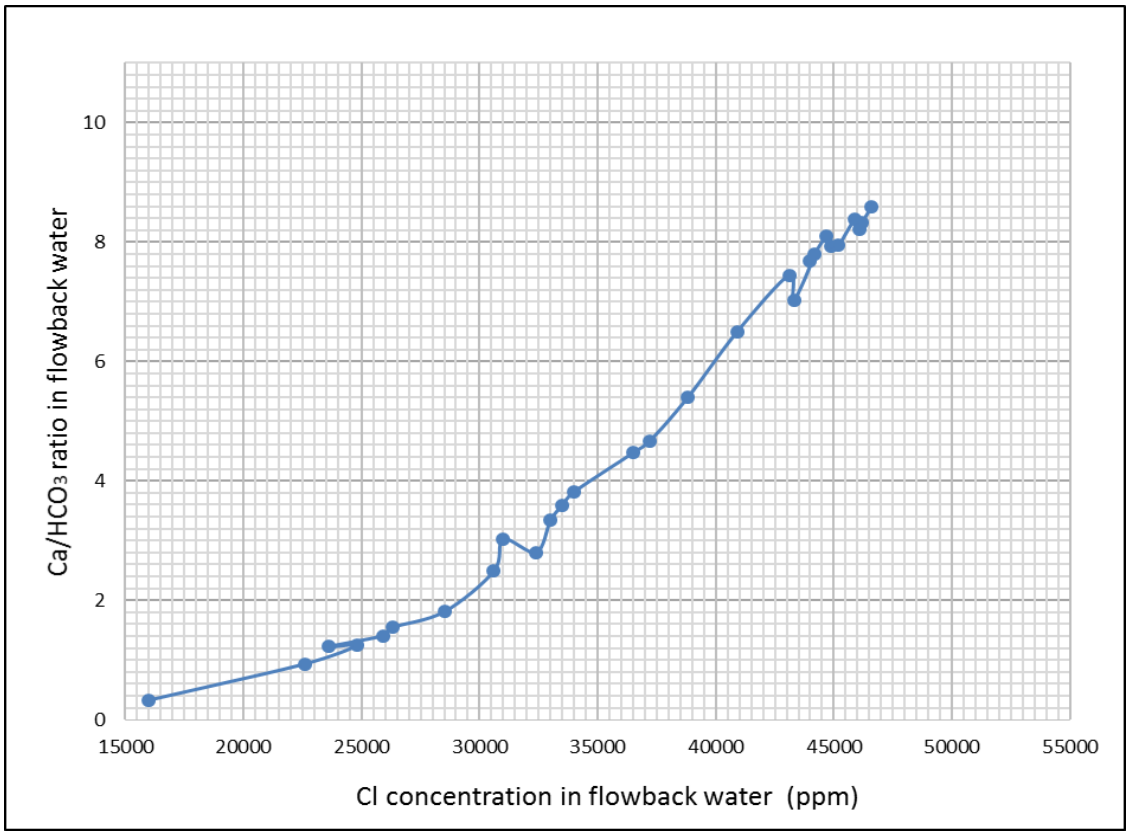

Figure 2.25 Cl vs. Ca/HCO_3 ratio in flowback water

$y = 0.0003x - 6.6249$
$y = 0.1237e^{9E-05x}$
$y = 9.8183\ln(x) - 97.83$
$y = 7E-09x^2 - 0.0002x + 0.9486$
$y = -1E-13x^3 + 2E-08x^2 - 0.0006x + 3.3924$
$y = -2E-17x^4 + 2E-12x^3 - 7E-08x^2 + 0.0012x - 7.3375$
$y = -4E-22x^5 + 4E-17x^4 - 2E-12x^3 + 4E-08x^2 - 0.0004x + 37.5363$
$y = -2E-25x^6 + 3E-20x^5 - 2E-15x^4 + 1E-10x^3 - 2E-06x^2 + 0.0269x - 2542.939$
$y = 4E-14x^{3.0714}$

Figure 2.26 Trendline equations for the plot above

In order to give an optimal prediction of formation water compositions, each of the trendline equations shown in **Figure 2.26** (it includes exponential, linear, logarithmic, polynomial and power equations) has been used to calculate the chloride concentration where ratio of calcium and bicarbonate concentration is 10.4. The calculation results for Cl concentration along with R-squared values for all the trendline equations are shown in **Table 2.10**.

Table 2.10 Calculation results for Cl concentration and R-squared value for each equation

Trendline options	Linear	Exponential	Logarithmic	Power	
R^2	0.9647	0.9655	0.8938	0.9948	
Cl concentration (ppm)	57699	52841	46532	48578	
Trendline options	Poly Order2	Poly Order3	Poly Order4	Poly Order5	Poly Order6
R^2	0.9956	0.9965	0.9971	0.9971	0.9972
Cl concentration (ppm)	47038	49238	45617	44237	49700

Among all of these trendline equations, power and polynomial equations can provide the most satisfactory match with the data sample (highest R-squared values obtained). The mean value of Cl concentration calculated from power and polynomial equations can be found at 48,639 ppm (the results are based on the calculations exclude order 4 and 5 polynomial equations since the calculated values are lower than the provided Cl concentration from the last flowback water sample (46,600 ppm)).

As a consequence, the 6 order polynomial equation has been selected for the formation water composition prediction in next step (best matching trendline and also with small error comparing with the average value). This method has been reviewed repeatedly in order to make selections of trendline equations in terms of calculating other ion concentrations in formation water (the trendline selections are not repeatedly discussed in further predictions). **Figure 2.27** shows the plot and trendline equation for this prediction and also indicates the predicted Cl concentration in formation water.

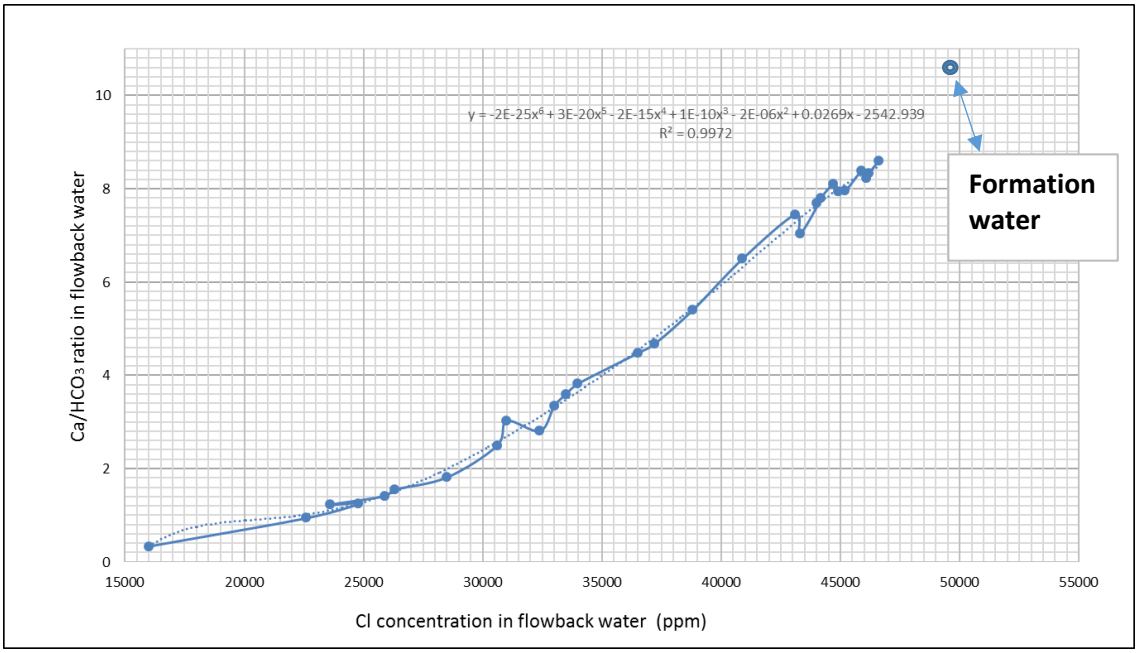

Figure 2.27 Cl vs. Ca/HCO_3 ratio in flowback water

$$y = -2E\text{-}25x^6 + 3E\text{-}20x^5 - 2E\text{-}15x^4 + 1E\text{-}10x^3 - 2E\text{-}06x^2 + 0.0269x - 2542.939$$

Equation 2.3

According to the calculation results shown in **Table 2.10**, the Cl concentration in the formation water is 49,700 ppm, where the ratio of calcium and bicarbonate concentrations in the formation water is 10.4. Once the Cl concentration is confirmed, a review of the geochemical data analysis has been carried out. It is necessary to replot the Cl concentration against other different ion concentrations in the flowback water to obtain the trend line equations for each of the scenarios. The reviewed geochemical data are plotted in **Figure 2.28** and **Figure 2.29**.

$$y = 1E\text{-}07x^2 + 0.0088x - 128.1 \quad \ldots \textbf{Equation 2.4}$$

$$y = 4E\text{-}08x^2 + 0.0098x - 132.49 \quad \ldots \textbf{Equation 2.5}$$

$$y = 0.0062x - 27.532 \quad \ldots \textbf{Equation 2.6}$$

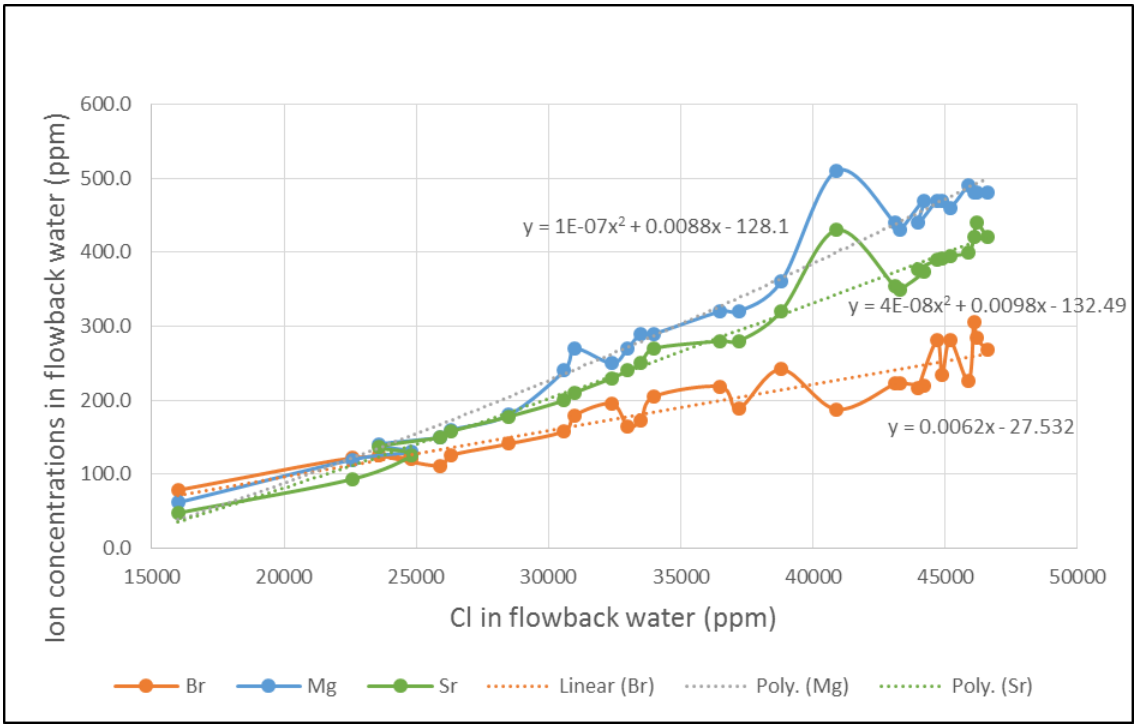

Figure 2.28 Cl vs. Br, Mg & Br concentrations in flowback water

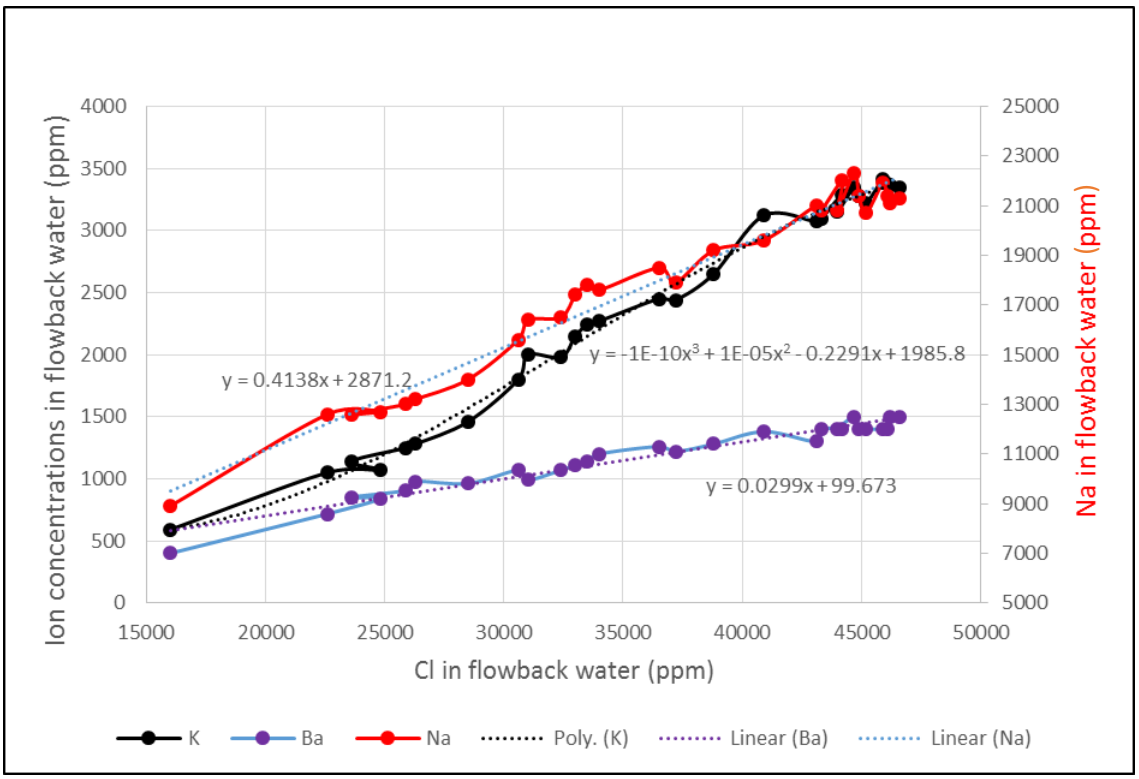

Figure 2.29 Cl vs. K, Ba & Na concentrations in flowback water

$y = 1E\text{-}07x^2 + 0.0088x - 128.1$ … **Equation 2.7**

$y = 4E\text{-}08x^2 + 0.0098x - 132.49$ … **Equation 2.8**

$y = 0.0062x - 27.532$ … **Equation 2.9**

According to these trend line equations, each of the ion concentrations in the formation water can be calculated. Some of the trend lines used the option of a polynomial equation, some of them selected the option of a linear equation. The reason for choosing different trend line options is due to the way that each equation can give a better match with the data trend. Simply by solving each of the equations assuming the chloride concentration of 49700 ppm, all of these ion concentrations in the formation water can be calculated. The calculated formation water composition in the Horn River Basin area is shown in **Table 2.11**.

Table 2.11 Calculated ion concentrations in formation water in HRB

Ion con Unit: ppm	Ca	HCO_3	Cl	Mg	Sr
Formation water (cal.)	5841	561.7	**49700**	556.3	453.4
Ion con Unit: ppm	Br	K	Ba	Na	TDS
Formation water (cal.)	272.3	3799	1585.7	23437	**86206.9**

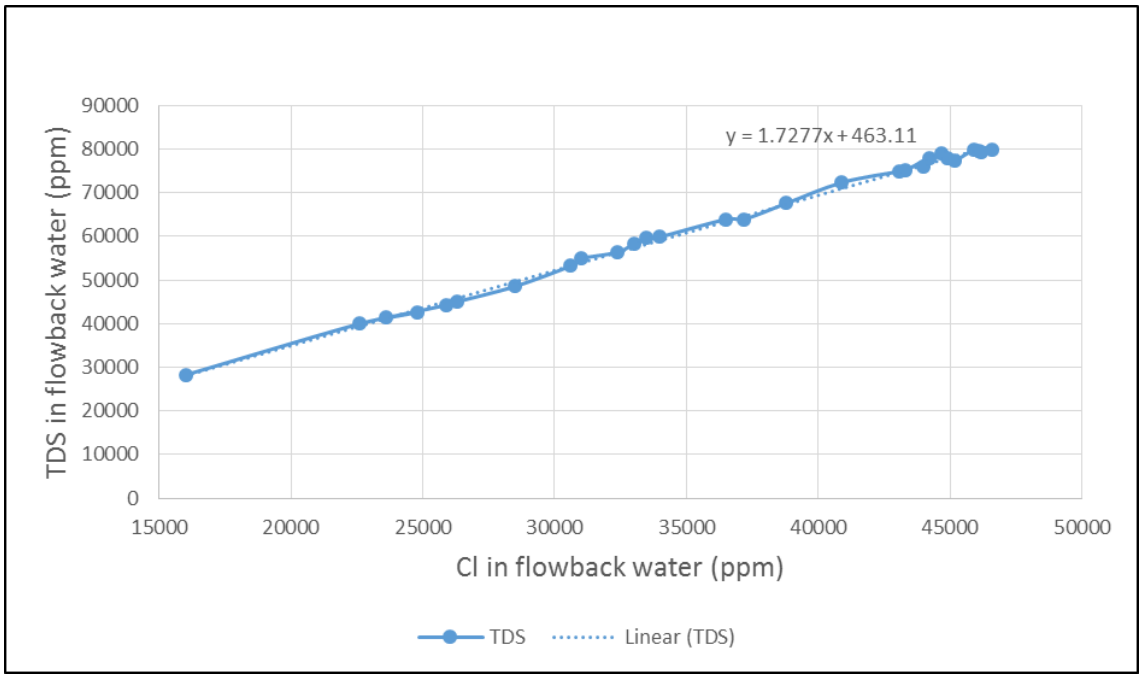

Figure 2.30 Cl vs. TDS in flowback water

$$y = 1.7277x + 463.11 \quad \ldots \textbf{Equation 2.10}$$

Figure 2.30 shows the plot of chloride concentration against TDS in flowback water. The Total Dissolved Solids in the formation water can be calculated by **Equation 2.10** as 86,330 ppm. From **Table 2.11** it can be seen that the predicted TDS in the formation water is 86,207 ppm, which is a summation of all the calculated ion concentrations in the formation water. It can be observed that the two calculated TDS values match very

well, which means the prediction of the formation water is controlled within a reasonable range.

SATURATION RATIO AND PRECIPITATION

Salt	Init SR	Precipitation mmol/kg	Precipitation kg/day	Eq SR	
FeCO3	0.0063	0.0000	0.0000	0.0063	
CaCO3c	0.9969	0.0000	0.0000	0.9969	Calcite
NaCl	0.0168	0.0000	0.0000	0.0168	
KCl	0.0018	0.0000	0.0000	0.0018	
BaCO3	0.0069	0.0000	0.0000	0.0069	
SrCO3	0.0395	0.0000	0.0000	0.0395	
NaHCO3	0.0005	0.0000	0.0000	0.0005	

*Only salts with SR higher than 0.0001 are shown

Figure 2.31 The MultiScale calculation result for the single stream formation water

An alternative way to validate the reliability of the predicted formation water composition is to check the ionic equilibrium status of the calculated formation water. MultiScale is used to perform the single stream calculation to check whether or not the formation water reaches the ionic equilibrium status in the reservoir condition. The calculation results from MultiScale are shown in **Figure 2.31**. From these results, it can be readily identified that the predicted formation water does reach the ionic equilibrium state (SR ($CaCO_3$) = 1), which also demonstrates that the calculation of the formation water composition is reliable.

2.6.2 Prediction in Muskwa member

To predict the formation water composition in the Muskwa member, a similar methodology for calculating formation water compositions as in the Evie member has been applied. As a start, the calcium and bicarbonate concentrations against chloride concentration in the flowback water in the Muskwa member need to be observed and indicated in the plot of **Figure 2.32**.

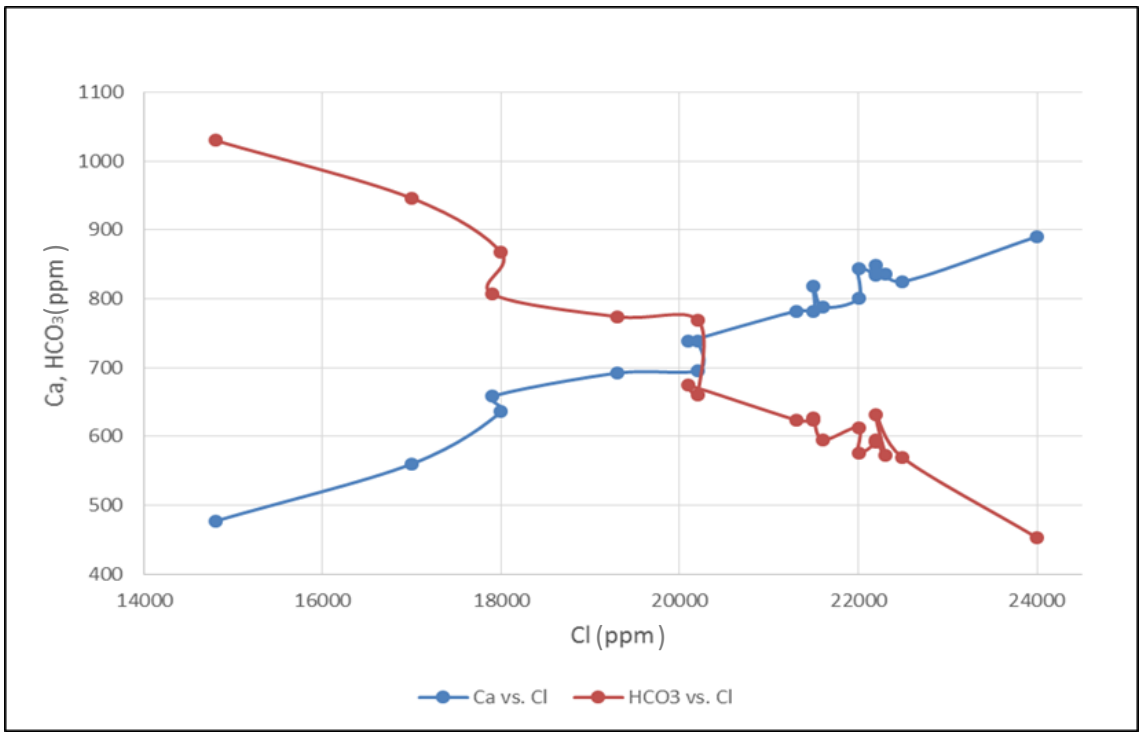

Figure 2.32 Ca and HCO_3 concentrations vs. Cl concentration in flowback water in Muskwa

From **Figure 2.32** it can be found that the calcium and bicarbonate concentrations in the flowback water in the Muskwa member have similar behaviour as in the Evie member. However, after two months production, the calcium concentration in Muskwa only increases to 900 ppm, which is much lower compared with the Evie (5,220 ppm). Since the bicarbonate concentration also decreases in **Figure 2.32**, it is considered that the formation water composition in Muskwa could be calculated by identifying the minimum CO_2 content in the gas phase for each fluid mixing sample to reach the equilibrium state.

To determine the *in situ* formation water composition in Muskwa, the CO_2 content in the gas phase needs to be calculated using the MultiScale thermodynamic model, assuming $CaCO_3$ equilibrium in the formation water and that the flowback water samples represent a mix of the injection fracture fluid and the formation water. The amount of CO_2 required for each brine sample to remain in equilibrium is then calculated.

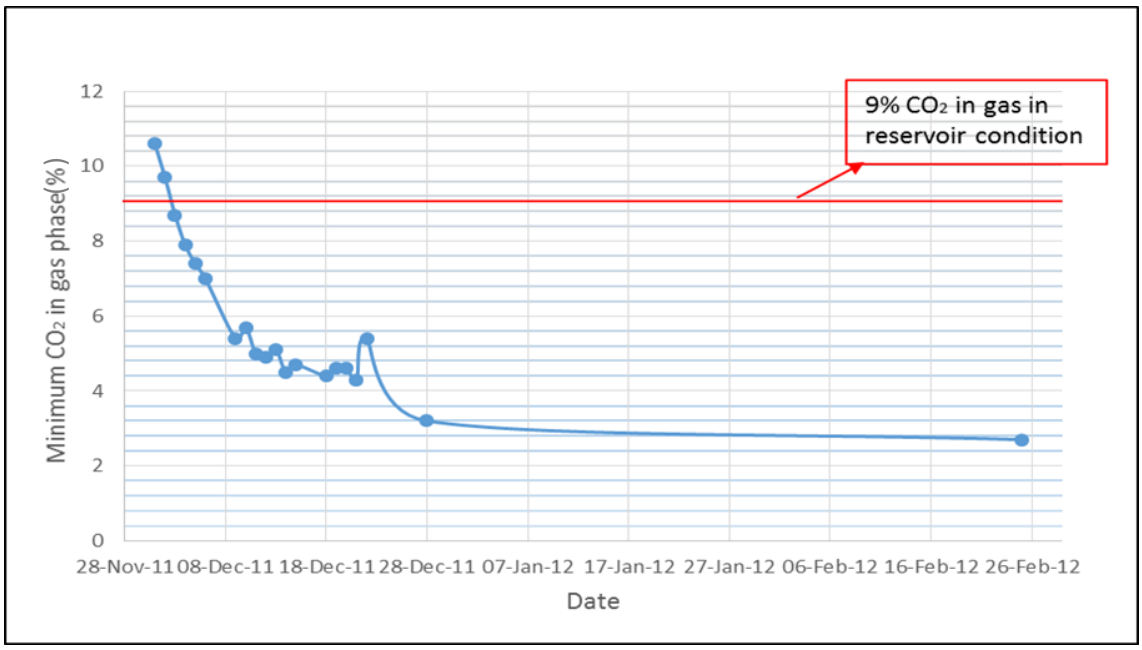

Figure 2.33 Fraction (as %) of CO_2 in gas phase in Muskwa for $CaCO_3$ equilibrium vs. Date

Figure 2.33 shows the plot of calculated CO_2 in gas phase for each mixture to reach equilibrium against production date. Each of the fluid mixing samples has been set at reservoir condition, which is 335.6 bars for reservoir pressure and 138 °C for reservoir temperature. As shown in the figure above, the red line in the plot represents the fraction of CO_2 in the gas phase at the original reservoir condition. From **Figure 2.33** it can be observed that only the first two samples have sufficient scaling tendency to generate the $CaCO_3$ precipitation, whereas most of the other samples are out of the $CaCO_3$ scaling envelope due to there being more than enough CO_2 in the gas phase compared with the actual requirement. (This does not, of course, mean that $CaCO_3$ will not form in the well as pressure reduces and CO_2 evolves.)

Another finding is that there will be a scaling tendency for $BaSO_4$ precipitation due to the presence of sulphate in some of the flowback water samples. Although the barium concentration is not as high as it in Evie (1,500 ppm), there is still sufficient barium in Muskwa (800 ppm) to enable reactions with the sulphate to deposit $BaSO_4$. Some of the studies showed that there is sulphate in the pore water of the shale samples (Ballard, 1994). It is considered it could be a process of the sulphidation from the Pyrite which leads to the existence of the sulphate (Dresel, 2010).

According to the data analysis in Evie from the discussion in the previous section, all the flowback water samples have a scaling tendency (to generate $CaCO_3$ precipitation)

because the original CO_2 concentration in the gas phase is not high enough to ensure equilibrium. The formation water can be identified where the ratio of calcium and bicarbonate concentrations in flowback water reaches 10.4. Nevertheless, the $CaCO_3$ scaling prediction for Muskwa does not give similar behaviour as for Evie: to find the end point for the formation water in Muskwa requires other constraints.

Before calculating the formation water composition in Muskwa, some assumptions need to be identified for the following calculations: The first calculation is based on the decreasing tendency for the bicarbonate concentration in **Figure 2.32**; it considers what would be the situation if the bicarbonate concentration in the original formation water in Muskwa were reduced to zero value; the second calculation is based on the analysis of the trend (the plots of required CO_2 in gas phase against the ratio of calcium and bicarbonate concentration in flowback water in Muskwa).

2.6.2.1 First prediction of formation water

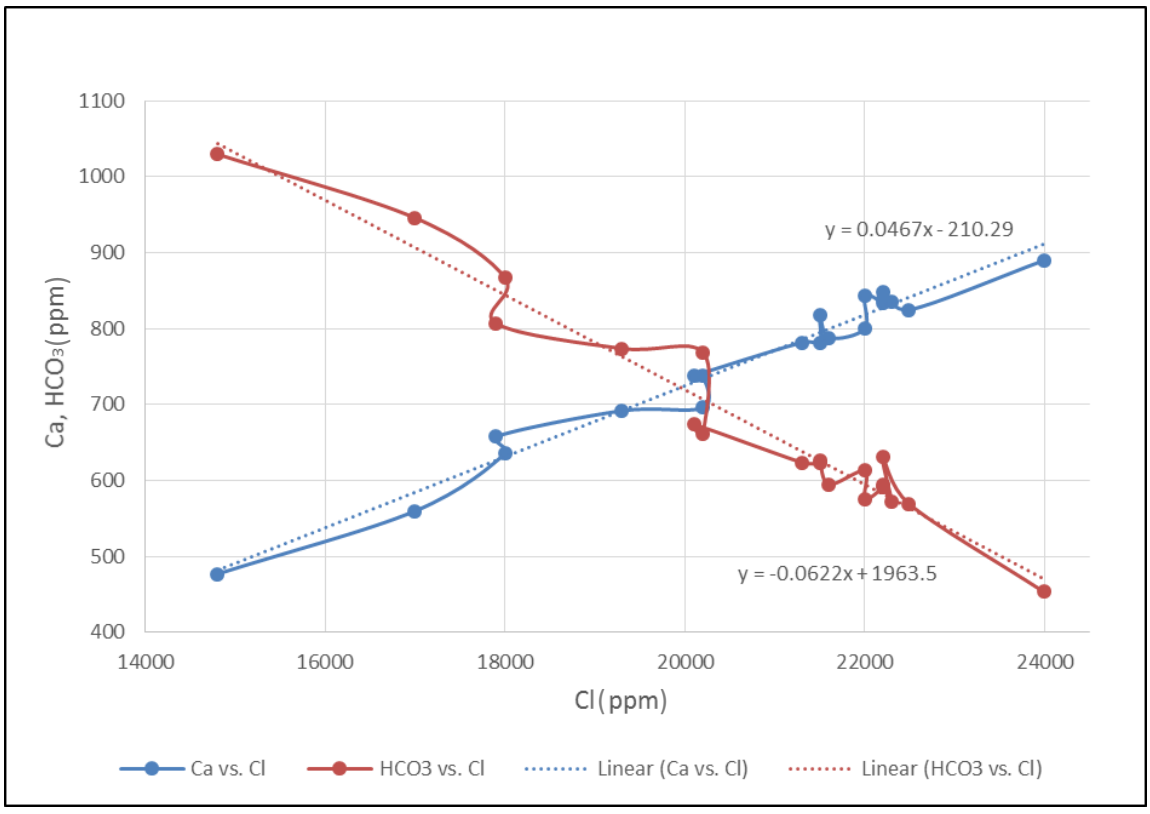

Figure 2.34 Ca & HCO_3 vs Cl concentration in flowback water in Muskwa

$$y = 0.0467x - 210.29 \quad \text{… Equation 2.11}$$

$$y = -0.0622x + 1963.5 \quad \text{… Equation 2.12}$$

Figure 2.34 gives two trend line equations for the plots between calcium and bicarbonate against chloride concentrations in the flowback water. As stated previously, it is assumed that the bicarbonate concentration in the formation water keeps decreasing until it reaches a near zero value. The maximum possible chloride concentration in the formation water then can be calculated from **Equation 2.11**. Meanwhile, the calcium concentration could also be confirmed from the calculation result of **Equation 2.12**. The initially estimated calcium, bicarbonate and chloride concentrations in the formation water will thus be: 1,264 ppm, 0 ppm and 31,568 ppm, respectively.

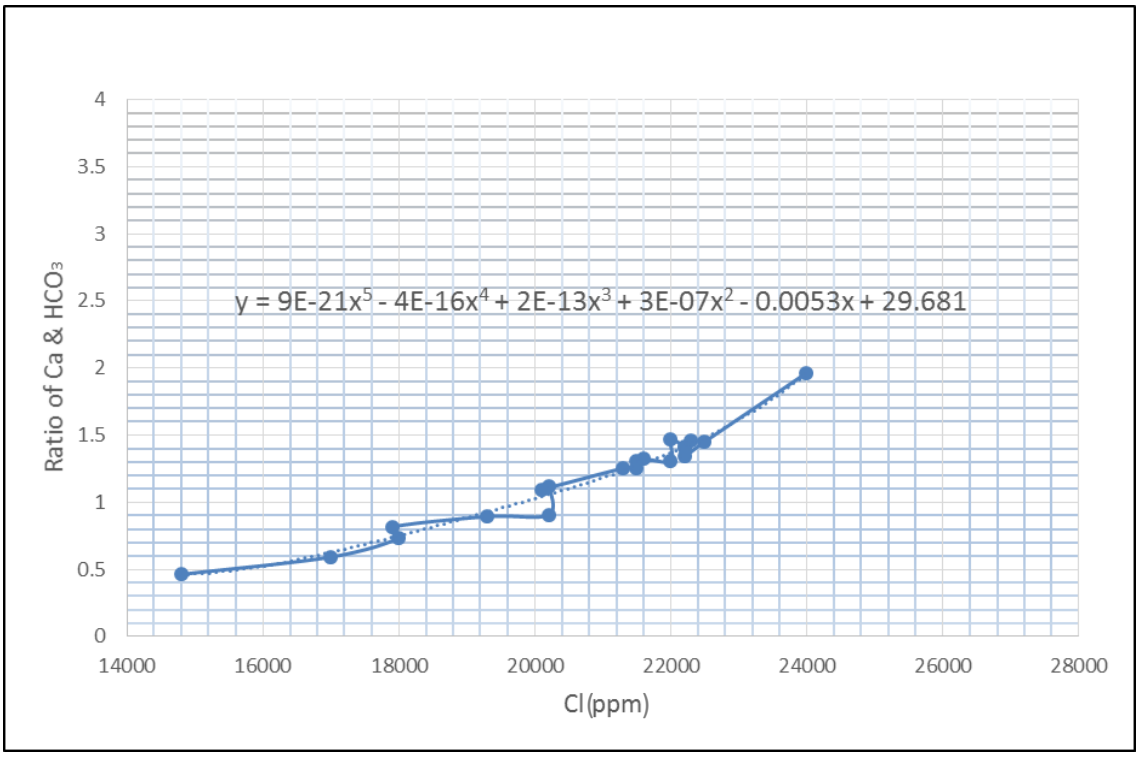

Figure 2.35 Ca/HCO_3 ratio vs Cl concentration in flowback water in Muskwa

$$y = 9E\text{-}21x^5 - 4E\text{-}16x^4 + 2E\text{-}13x^3 + 3E\text{-}07x^2 - 0.0053x + 29.681 \quad \ldots \textbf{Equation 2.13}$$

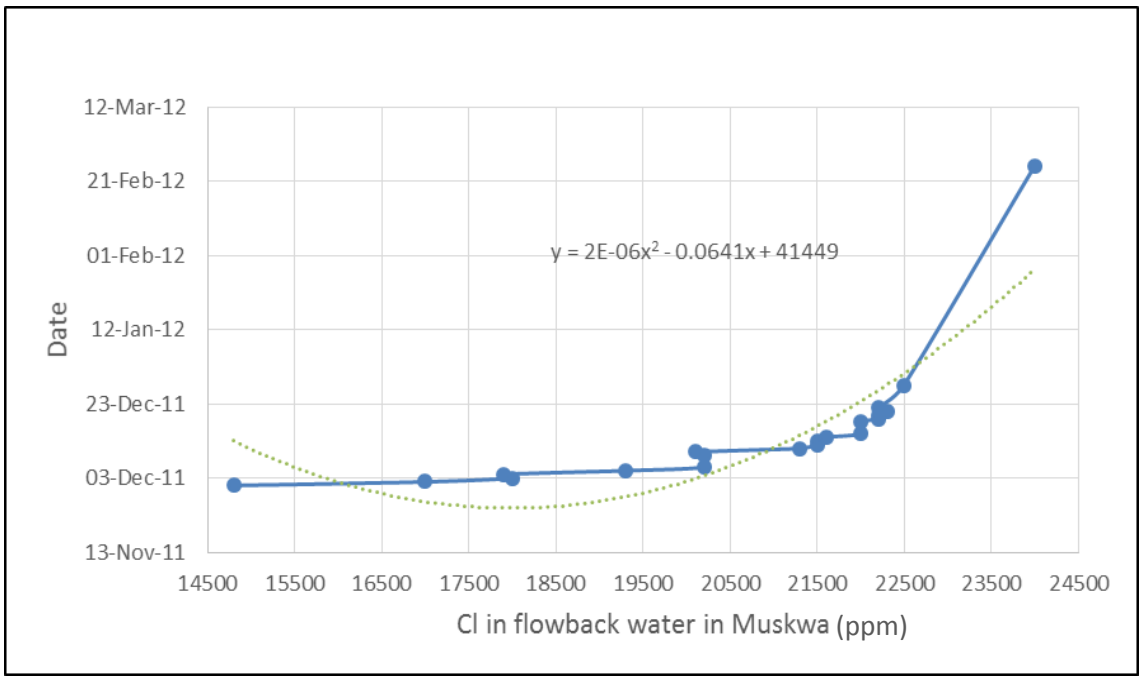

Figure 2.36 Date vs Cl concentration in flowback water in Muskwa

$$y = 2E\text{-}06x^2 - 0.0641x + 41449 \quad \ldots \textbf{Equation 2.14}$$

On the one hand, from **Equation 2.13**, it can be calculated that while the chloride concentration is 31,568 ppm, the ratio of calcium and bicarbonate concentration in flowback water is 52.5. Although this calculated ratio is much higher than the ratio observed from the last flowback water sample (1.97), the expected ratio should be even higher than this. On the other hand, from the calculation result of **Equation 2.14**, the production date of pure formation water flow back can be obtained as 24th May 2013, which is around 1.5 years after the well is brought back on production. In contrast, much research into shale gas production has shown that the flowback water process can last from weeks to months after the hydraulic fracturing operation is completed. As a consequence of the analysis above, it is believed that the first prediction of formation water in Muskwa has a significant error.

2.6.2.2 Second prediction of formation water

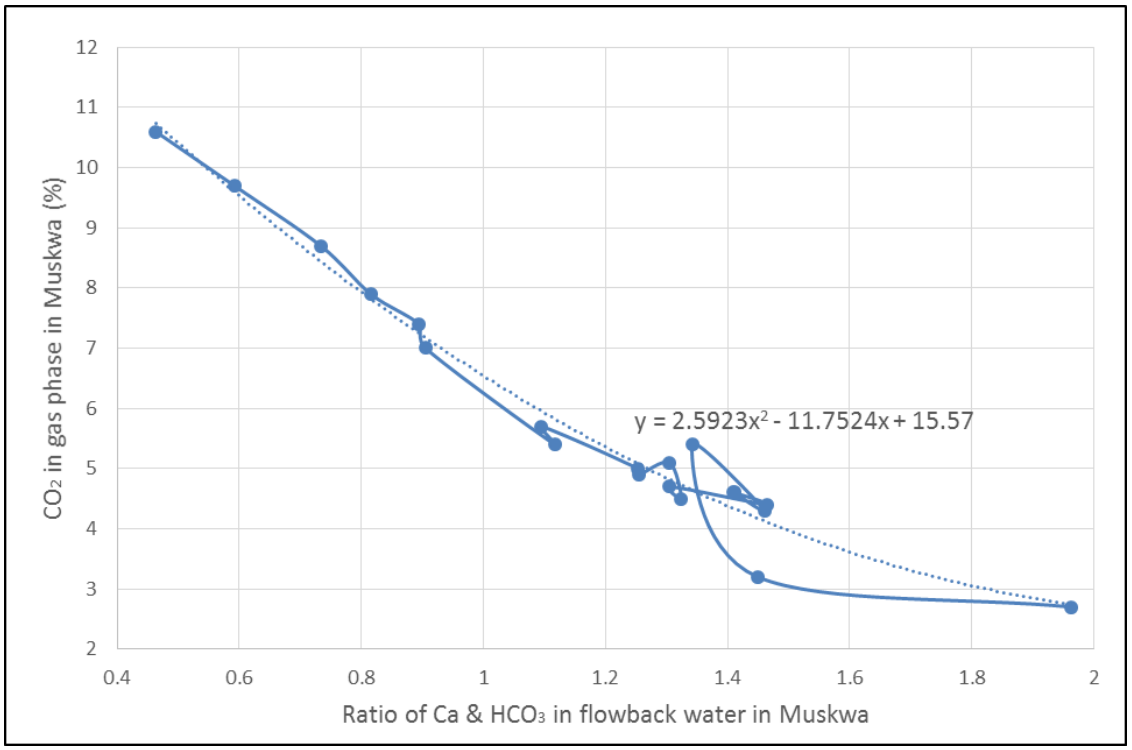

Figure 2.37 Fraction (as %) of CO_2 in gas phase vs. ratio of Ca & HCO_3 in flowback water in Muskwa

$$y = ax^2 + bx + c \quad \ldots \textbf{Equation 2.15}$$

*Where **a** = 2.5923; b = -11.7524 and **c** = 15.57*

Figure 2.37 shows the ratio of calcium to bicarbonate in flowback water in Muskwa against required CO_2 in the gas phase for the $CaCO_3$ equilibrium. It can be readily seen that the whole trend for the plot tends to reach a minimum value while the ratio of calcium and bicarbonate increases. It is known that the calcium concentration increases and bicarbonate concentration decreases, which mean the Ca/HCO_3 ratio will also increase until most of the flowback water that is produced is formation water. Meanwhile, the requirement of the CO_2 in the gas phase will also reach its minimum value. Since it is impossible to track the end point to confirm the minimum CO_2 required to calculate formation water compositions, some mathematical analysis based on the trend line equation is reviewed here to obtain some formation water compositional information.

From **Equation 2.15** it can be known that as the required CO_2 in the gas phase approaches zero, the solutions for the equation will not exist since $b^2 - 4ac < 0$ (which

means the minimum required CO_2 content in gas phase is higher than zero). Therefore, a new equation can be performed and is shown in **Equation 2.16**. It is required to find out this minimum value of the CO_2 in the gas phase where the new $b'^2 - 4a'c' = 0$.

$$0 = a'x^2 + b'x + c' \quad \ldots \textbf{Equation 2.16}$$

*Where **a' =** 2.5923; b' = -11.7524; **c' =** 15.57-y and y=minimum CO_2 content in the gas phase*

With some further calculations using **Equation 2.16**, the ratio of calcium and bicarbonate concentration in flowback water can be confirmed at 2.25. The chloride concentration can then be easily calculated from **Equation 2.11** and **2.12** with the value at 24,800 ppm. By solving **Equation 2.14**, the production date when the formation water flows back can be estimated as 29th June 2012, which is several months after the hydraulic fracturing process has been completed.

Table 2.12 Estimation of ion concentrations in formation water in Muskwa

Ion con Unit: ppm	Ca	HCO_3	Cl	Mg	Sr
Formation water (cal.)	1051	431	**24800**	114	163
Ion con Unit: ppm	Br	K	Ba	Na	TDS
Formation water (cal.)	107	85	941	14081	**41773**

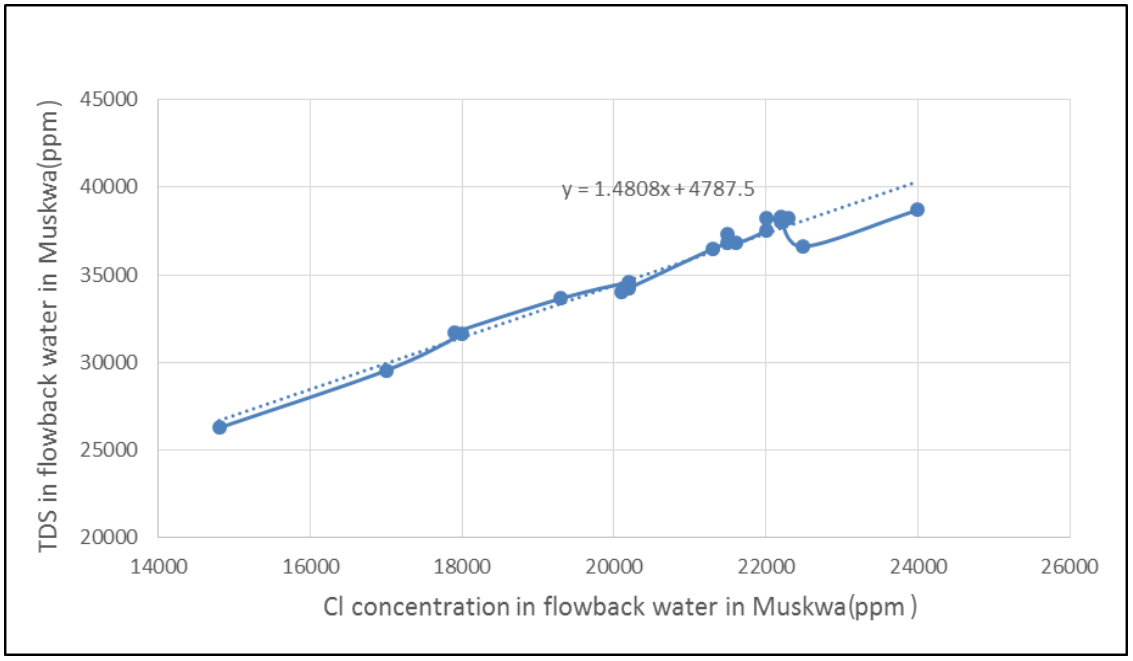

Figure 2.38 TDS vs Cl concentration in flowback water in Muskwa

Similar methods have been applied to calculate different ion concentrations in the formation water once the chloride concentration in the formation water has been identified. The estimated formation water composition is shown in **Table 2.12**. From the table it can be confirmed that the ratio of calculated calcium and bicarbonate concentrations in formation water is 2.4 which is close to the previous result (2.3). In addition, the Total Dissolved Solids in the formation water in Muskwa has also been calculated at 41,773 ppm. From another aspect, the TDS in formation water can also be predicted according to the equation shown in **Figure 2.38** and the calculated result is 41,511 ppm. According to the discussions above, the estimated formation water and the calculated formation water are consistent in terms of both of the estimated and calculated ratio between calcium and bicarbonate concentration along with the TDS in the formation water. In addition, no $CaCO_3$ precipitation has been calculated in the Multiscale fluid mixing calculation results, which also verifies that the second calculation of formation water composition for Muskwa member is reasonable.

2.7 CALCULATION OF INJECTED FRACTURE FLUID FRACTION IN FLOWBACK/PRODUCED WATER

It is necessary to identify the injected fracture fluid fraction in the flowback water to manage the history match modelling in the next step, and also to predict the scaling tendency from the geochemical modelling study in the future. By using the validated formation water composition in HRB along with the given fracture fluid composition and the flowback water composition, it is possible to calculate the injected fracture fluid fraction in the flowback water.

During conventional recovery, the injection water will take time to break through to the producers. By contrast, for unconventional recovery, the hydraulic fracturing process will be applied first to enlarge the conductivity in the low-permeability reservoir and then the well will be brought back on production. The injected fracture fluid fraction will be high at the beginning of the production and then it will decrease for weeks or even months until the flowback water composition is close to the formation water composition. The flow rate also varies during the whole process: it is very high to begin with and then keeps on reducing down to several barrels per day. It is widely reported that the total volume of the flowback water is typically only 20% - 40% compare with the volume of the injected fracture fluid (Crafton et al, 2007; Ghanbari et al, 2013).

To identify the injected fracture fluid fraction, some ions need to be selected for the calculation. It should not only be a conservative ion but also it should commonly exist in most formation waters. Chloride is an ion that commonly exists in the formation water and does not react with other ions in the fracture fluid or formation water. In addition, its concentration is high enough to help us to distinguish the formation water from the fracture fluid (Ishkov et al., 2015).

The fracture fluid and flowback water compositions are provided and the validation of the formation water has been performed in the previous section; therefore, the injected fracture fluid fraction (IFFF) in flowback water can be calculated by assuming it is a pure fluid mixing process taking place. The illustration of the calculation process is shown in **Figure 2.39 (a & b)**.

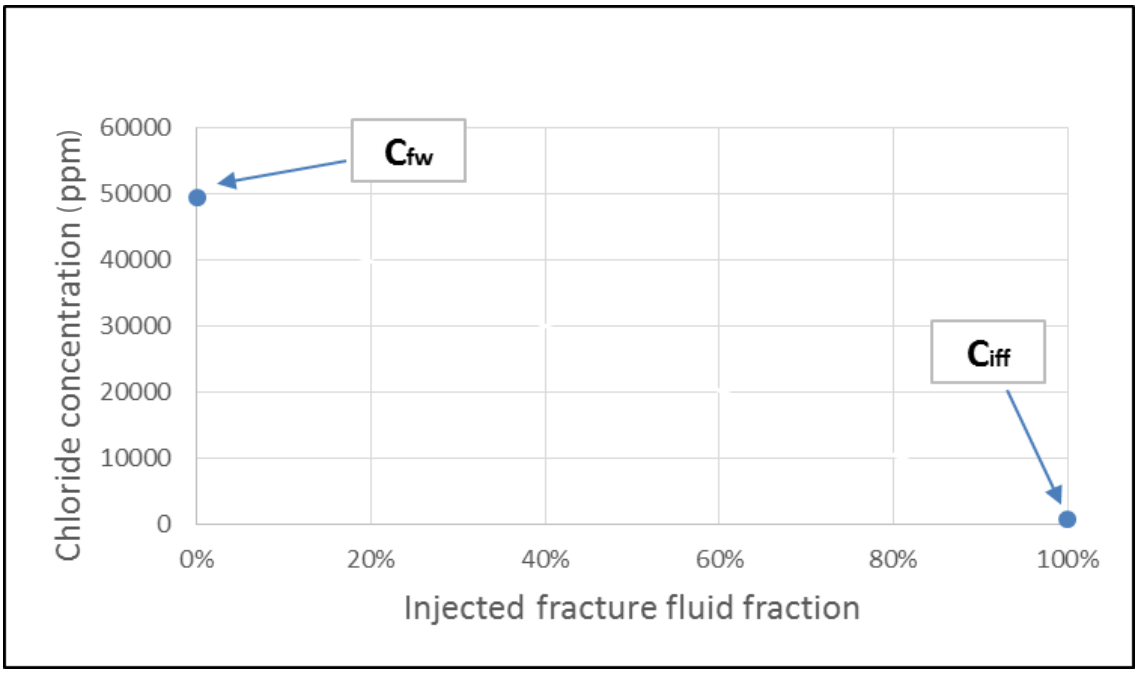

(a)

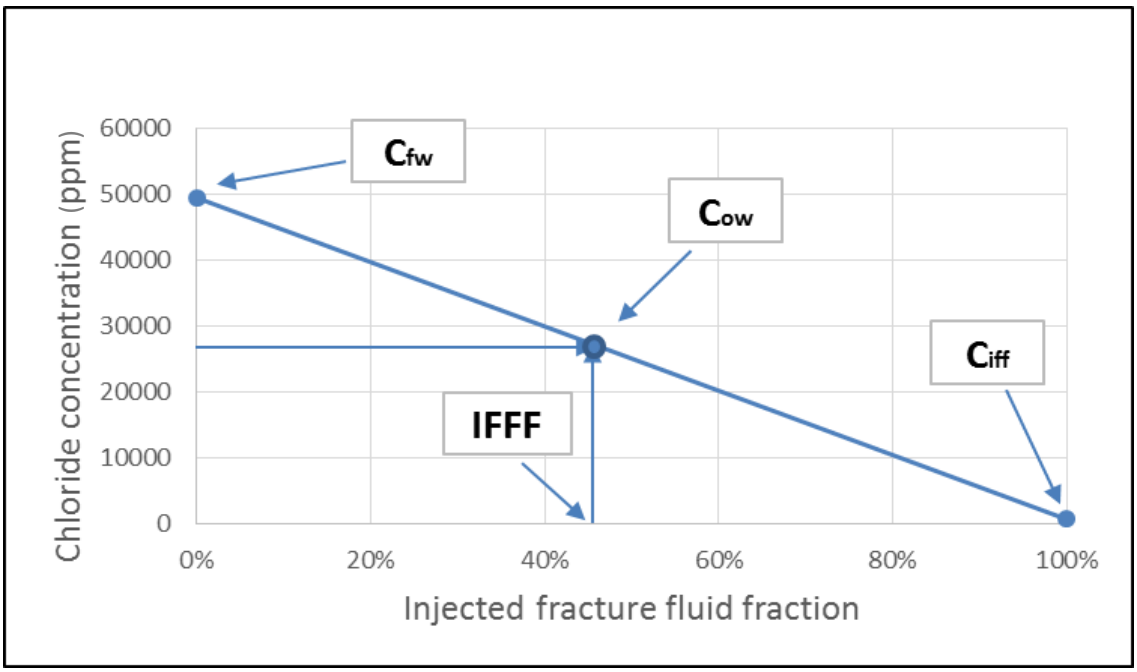

(b)

Figure 2.39 (a & b) The illustration of injected fracture fluid fraction calculation

As shown in **Figure 2.39 (a)**, the fraction of injected fracture fluid with chloride concentration has been provided at the value of 100%, i.e. pure fracture fluid; the fraction of formation water with chloride concentration has also been calculated and validated at the value of 0%, i.e. pure formation water. **Figure 2.39 (b)** shows that the chloride concentration in the flowback water identifies uniquely the fraction of fracture fluid in the flowback water during the shale gas production process. According to **Equation 2.17**, the injected fracture fluid fraction can be calculated in each of the flowback water samples.

$$IFFF = \frac{C_{fw} - C_{ow}}{C_{fw} - C_{iff}} \quad \text{… Equation 2.17}$$

where C_{fw} is chloride concentration in the formation water, C_{ow} is chloride concentration in the observed (flowback) brine, and C_{iff} is chloride concentration in injected fracture fluid. *IFFF* is thus the injected fracture fluid fraction in the flowback water.

Table 2.13 The calculation results of injected fracture fluid fraction in flowback water in Evie

Date	01/06/12	01/08/12	01/09/12	01/10/12	01/11/12	01/12/12	01/13/12
Cl (ppm)	16000	22600	24800	23600	25900	26300	28500
IFFF	68.70%	55.17%	50.66%	53.12%	48.40%	47.58%	43.07%
Date	01/14/12	01/15/12	01/16/12	01/17/12	01/18/12	01/19/12	01/20/12
Cl (ppm)	30600	31000	32400	33000	33500	34000	36500
IFFF	38.76%	37.94%	35.07%	33.84%	32.81%	31.79%	26.66%
Date	01/21/12	01/22/12	02/04/12	02/09/12	02/10/12	02/11/12	02/12/12
Cl (ppm)	37200	38800	40900	43100	43300	44200	44000
IFFF	25.23%	21.94%	17.64%	13.13%	12.72%	10.87%	11.28%
Date	02/13/12	02/14/12	02/15/12	02/16/12	02/17/12	02/18/12	02/20/12
Cl (ppm)	44700	44900	45200	45900	46100	46200	46600
IFFF	9.84%	9.43%	8.82%	7.38%	6.97%	6.77%	5.95%

Using calculations based on **Equation 2.17**, the injected fracture fluid fraction in each of the flowback water samples has been identified. The result is shown in **Table 2.13** and has been plotted against the production date in **Figure 2.40** (**Figure 2.41** indicates the plot of calculation results in Muskwa). From the calculation results it can be readily observed that at the initial period of the stated data, the fraction of injected fracture fluid in the flowback water is up to 70%, while after two months of production it has decreased to 6%. It is expected that several weeks later, the fraction of injected fluid will reach a steady but low value (around 2.5% from the calculation) and most of the produced water will be the formation water.

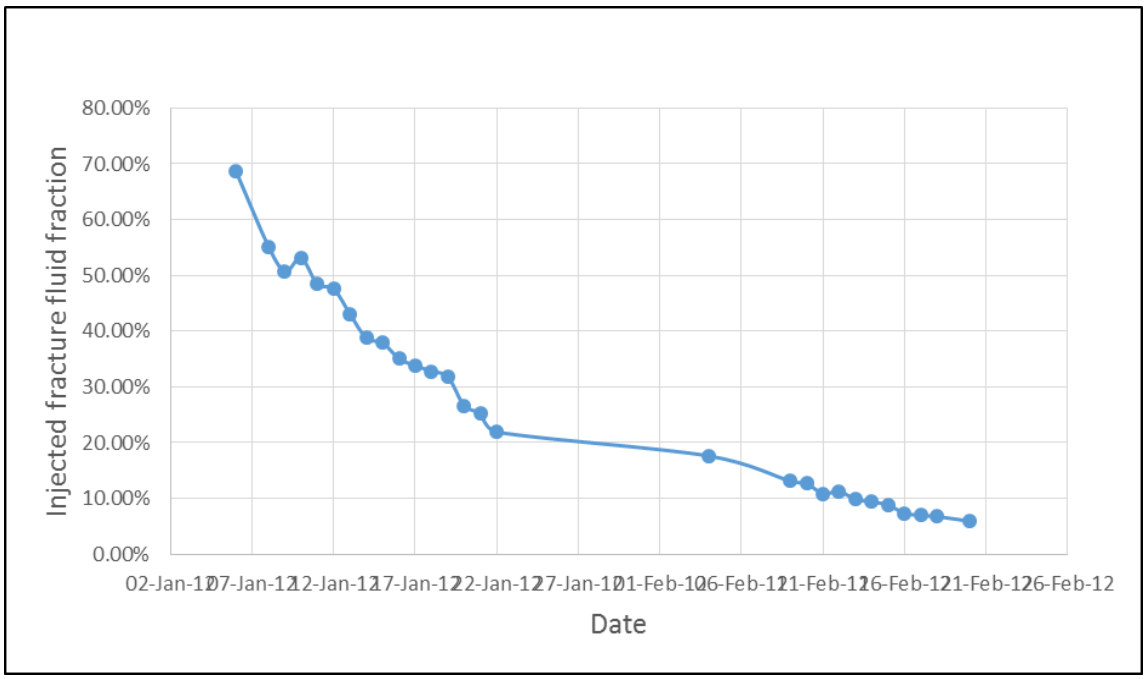

Figure 2.40 Injected fracture fluid fraction vs date in Evie

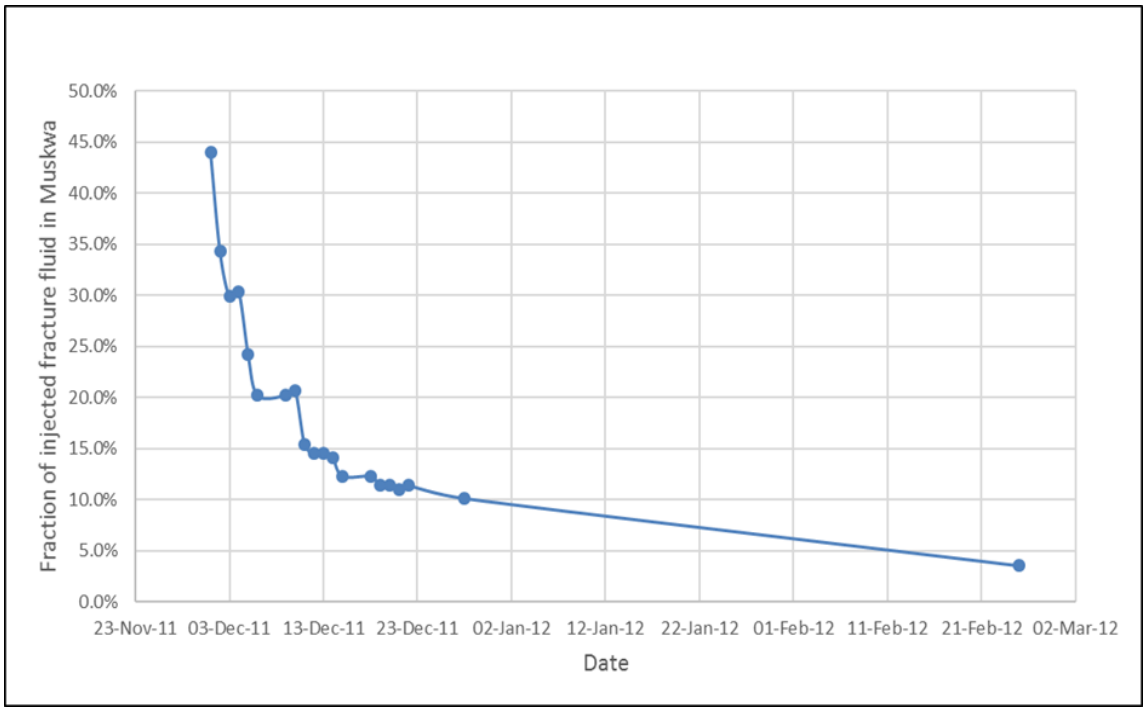

Figure 2.41 Injected fracture fluid fraction vs date in Muskwa

From the calculation results in **Figure 2.41**, it can be readily observed that for the initial period of the stated data, the fraction of injected fracture fluid in the flowback water is 44%, while after three months of production it has decreased to 3.5%. It is expected that several weeks later, the fraction of injected fluid will reach a steady but low value (around 2% from the calculation) and most of the produced water will be the formation water. Compared with the calculated fraction of injected fracture fluid in flowback

water in Evie, it is assumed that the stated data in Muskwa possibly was not collected from the early period of the production, whereas the flowback water in Evie could have been sampled at the beginning of the production in terms of the first value of injected fracture fluid fraction in flowback water in Evie (70%) is much higher than Muskwa (44%). Another assumed reason for the fraction difference between the two members could be the different hydraulic fracturing stimulation approach applied in each of the formations – it is reported that the horizontal well located in the Evie has more fracturing stages (stimulation processes) than the Muskwa, which will lead to more hydraulic fracture fluid being pumped into the shale formation. As a consequence, the injected fracture fluid in the produced water could be higher in the Evie member. Additionally, micro fractures may connect different hydraulic fractures, also affecting the overall flow backs.

According to the previous discussion, the identification of the injected fracture fluid in flowback water can be useful for establishing the fluid flow history matched model, and also it can help in the better understanding and prediction of the scaling tendency, which will be undertaken as part of the geochemical modelling activity later.

2.8 CONCLUSIONS

The data preparation and analysis, especially the prediction of *in situ* formation water composition, are important topics to be addressed – not only provide information for scaling tendency prediction but also help to address the question – what causes the altered high salinity in flowback water during shale gas production. This chapter also builds up a basic framework for better understanding the scaling risk during shale gas production and offers some evidence from data analysis results to develop some potential scale control strategies. The conclusions of this chapter are summarised below:

- The collected data do not only provide support for scaling tendency prediction, but they also offer evidence to improve the accuracy of the following study on fluid flow and geochemical reactions.
- CO_2 content plays an important role in determining the scaling tendency of $CaCO_3$ precipitation in shale gas systems.
- $CaCO_3$ scaling risk is also serious in Horn River Basin area due to the high concentration of Ca and HCO_3, and also the presence of the CO_2 content in the gas phase.

- There is a tendency to generate $BaSO_4$ precipitation in the Horn River Basin area due to the commingled flow in return profiles of the multi-stage hydraulic fracturing process.
- From the example analysis on data collected in the literatures, shale gas production in Marcellus shales has a high potential of scale risk with $BaSO_4$ precipitation due to the use of recycled formation water as the injected fracture fluid (high sulphate and barium included). As the formation water composition is confirmed by sufficient produced water composition data, it is considered that mixing with the high salinity formation water *in situ* can be the major reason causing the significant change of TDS in flowback water in Marcellus shales.
- The *in situ* formation water composition in the Evie & Muskwa member in HRB has been predicted and validated.
- According to the analysis, in terms of the calculated *in situ* formation water composition and the mineral dissolution experiment analysis (from literature review), it is shown that Na and Cl are the dominant ions dissolved from minerals, which means that the fluid mixing between the fracture fluid and the high salinity formation water is the dominant factor that leads to the high ion concentrations in the flowback water in HRB area.
- The injected fracture fluid fraction in flowback water in HRB area has been calculated and could be used as the field data history matching base case for the next reservoir simulation study.

CHAPTER 3 FLUID FLOW MODELLING

3.1 INTRODUCTION AND CHAPTER CONTENT

As the demand of energy consumption has been rapidly increasing around the world, the need to explore for unconventional hydrocarbon reservoirs has become more and more urgent. Since shale gas is one of the largest reserves of unconventional energy, research on shale gas production has been widely developed. This unconventional reservoir exploitation not only covers initially developed shale plays in America such as the Marcellus shale, the Barnett shale, etc. but also extends into some newer explored shale plays located in the west of Canada, the southwest of China and other countries (Staff, 2010). In the recent decades, the significant development in advanced drilling technology and application of unconventional seismic imaging has made commercial unconventional production achievable (Williams-Stroud et al., 2013). In order to maximize the economics of unconventional recoveries, a successful stimulation or hydraulic fracturing process is required, followed up by an optimal design of production strategy (Edwards et al., 2011). Many of the commercial unconventional reservoir recoveries have learnt from the successful experience of thousands of horizontal wells produced in America. However, numerical modelling has also become an increasingly important tool in regards to obtaining an optimal design before any stimulation or production processes are brought into operation.

The shale reservoir simulation not only provides history matching with field data, as it does for the more mature shale reservoirs, but also offers assistance with well designs and field development plans, in terms of making future production predictions. Nevertheless, accurate numerical modelling can be very difficult due to the lack of understanding of complex properties, with extremely low permeability shale matrix and also the complicated *in situ* fracture networks creating challenges (Difficult features to model include the hydraulic fractures, the induced secondary fractures and also the natural fractures already existing in the reservoir).

Another challenge for numerical modelling of unconventional is to simulate the fluid flow within the shale system by fully accounting for the fluid transport mechanisms. Fluid flow transfer mechanisms within the shale system are complicated, and it is still not completely studied and understood. This could be due to the lack knowledge of the

pressure variations due to conductivity changes, the impact of high capillary pressure on matrix relative permeability, and the adsorption and desorption process for gas with non-Darcy flow etc. Meanwhile, the fluid flow and proppant distribution within the fracture system can also bring some uncertainties for unconventional numerical modelling; this refers to the alteration of topology in fracture facies (from primary hydraulic fractures to the secondary fractures or even from secondary induced fractures to the micro natural fractures), to the imbibition process within micro fractures, to the impact of proppant distribution on conductivity changes in terms of pore scale geomechanics etc. (Lacazette et al., 2014)

In consideration of all the challenges, to utilize numerical modelling to develop a better well design or to achieve the ultimate hydrocarbon recovery, a reservoir engineer requires to include as many of these effects as possible to simulate the whole process of hydraulic fracturing and shale gas production. As a consequence of this, many of reservoir engineers apply themselves to obtain an accurate shale gas numerical model to try to include and solve all the potential challenges in order to achieve an optimal history match with the field data, and also to better represent the whole hydraulic fractured shale system. All of these models may involve complicated numerical calculations such as dual permeability/ porosity models, discrete fracture network (DFN) models, shale reservoir micro seismic data input field models etc.

As mentioned previously, the key study for this thesis is to address the question of whether or not the increase in salt concentration of the flowback water is due to the dissolution of minerals into the injected fracture fluid or due to the interaction/reaction between fracture fluid and the *in situ* formation water; and also to provide some recommendations for scale management based on geochemical and scale inhibitor modelling. This means the major study will be based on chemical compositional data analysis and geochemical numerical modelling studies. Each single shale reservoir has its own unique properties compared with other shale plays, and this will create more difficulties to develop an ideal history matched numerical model which can represent most of the field cases; therefore, some new questions have arisen during our research – 1) is it possible to develop a simplified numerical model (including some basic considerations instead of applying detailed full physics descriptions) to represent the whole hydraulically fractured shale system? and 2) Is this simplified numerical model able to provide an optimal history match of total volume of produced water and the fraction of injected fracture fluid in the flowback water?

This chapter aims to address the two questions proposed above – whether or not a simplified hydraulic fractured model matched to historical field production profile is achievable? And if it is successfully developed, what is the impact for the ensuing simulation of geochemical reactions?

First of all, this chapter gives a brief review of a representative model developed from literature derived data. This numerical model is discussed as part of the modelling development. The chapter then introduces a simulation workflow for setting up a simplified hydraulic fracture model to match with the field data in the HRB area. This section includes a full discussion focused on the initial preparation of the fluid flow modelling and also the development and improvement of the historical matched cases in regard to the total volume of water flow back, the fraction of injected fracturing fluid in the flowback water etc. Once the simplified history matched model setup is completed, some further fluid flow modelling study will be discussed – these discussions are from the simulation results of a series of more complicated cases which are based on the simplified model developed in the previous section. Conclusions will be drawn at the end of this chapter.

The objective for this chapter is thus to better understand the fluid flow mechanism within shale systems by developing a simplified numerical modelling which represents observed fluid flow behaviour. This simplified modelling should then address one of the questions posed – what causes the significant retention of injected fracture fluid within shale gas system?

3.2 REVIEW OF PREVIOUS NUMERICAL MODELLING STUDIES FROM LITERATURE

Significant improvements have been made in numerical modelling of shale gas systems in recent years (Zhang, 2009; Juan et al., 2010; Michele and Ivan, 2011; Peng and Roberto, 2013; Chaohua et al., 2014; Ardiansyah et al., 2015; Hao et al., 2015; Bicheng et al., 2017; etc.). These previous numerical modelling studies have been reviewed and one of the representative literatures is selected as an example to discuss in this section. The purpose to introduce this previous shale modelling study is to set up a comparison simulation so that further simplified fluid flow shale model can be developed. This review follows a paper (Zhang, 2009) published at International Petroleum Technology Conference in December 2009.

There are various known fluid flow mechanisms in shale systems; one, which has been extensively studied and simulated is a dual permeability/ porosity model to represent the natural fracture system and the matrix. This modelling method first has proposed in 1963 by Warren and Root. The purpose of this modelling is to distinguish the natural fracture system from the shale matrix so that the fluid flow can be better simulated. As a consequence of this, one of the major flow paths for fluid transport from the matrix up to surface is natural fractures. An interaction flow parameter is defined in such simulations in response to the fluid flow communications in between the matrix, and this is dependent on the total dimensions of each grid block and the natural fracture spacing. The illustration in **Figure 3.1** below (Zhang, 2009) shows this.

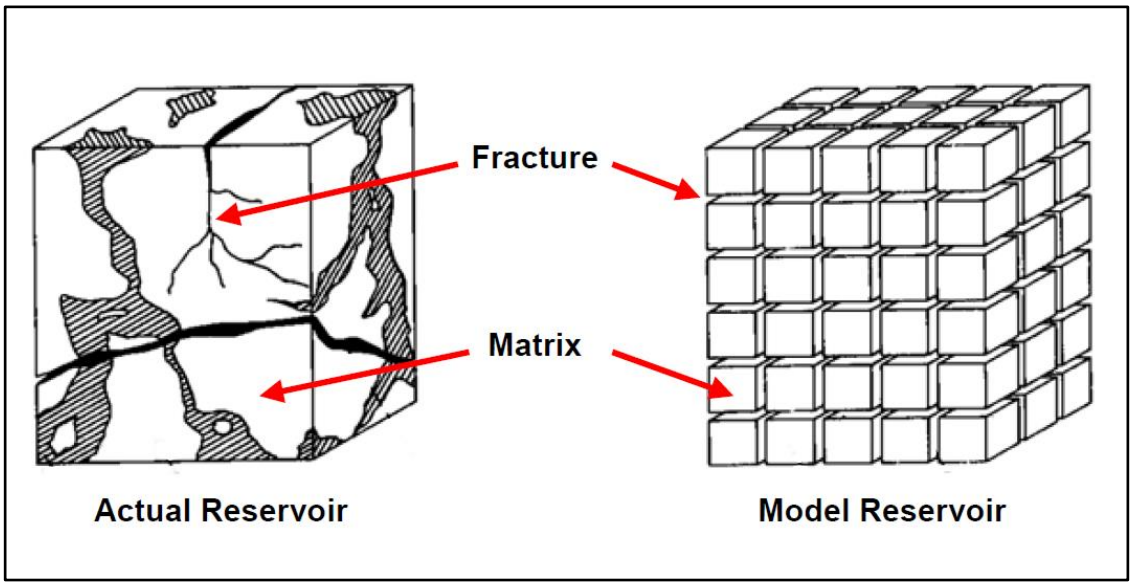

Figure 3.1 Illustration for dual porosity modelling grid block (Warren and Root, 1963)

To better represent the shale reservoirs with natural fractures, discrete fracture networks (DFN) may be applied (Dershowitz, 2010). Thus provide more flexibility to simulate the complexity of the natural fracture networks and also to upscale different reservoir and hydraulic fracture properties into the dual porosity model, so that more sensitivity cases can be developed in response to the optimization of shale gas production.

The micro seismic data used for this review of numerical modelling was collected from the Barnett Shale in the US (Du & Zhang, 2009). This has been applied in the simulations to represent the geometry and location of the natural fracture networks within the shale system (Williams-Stroud, 2008). The application of seismic mapping in the simulation will improve the history matching results. After the initial setup of the DFN model, it is then upscaled into a dual porosity model for further analysis and

discussion.

The dimensions of the dual porosity model are 4,000x 2,000x 300 ft in X, Y and Z directions and there are 10 hydraulic fractures that have been established with 300 ft spacing along the whole 3000 ft horizontal section of the well in the X direction. The model is developed for the ECLIPSE 300 simulator. The fracture width is 0.01 ft and matrix permeability and porosity are 0.0001 mD and 5% respectively. All the hydraulic fractures have conductivities of 50 mD*ft. The Zhang's (2009) paper discusses a series of sensitivity cases in terms of changing different properties, such as fracture permeability, matrix-fracture communication coefficient, natural fracture porosity etc., in addition to observing their impact on the shale gas production. However, the review of this numerical modelling study in this section will mainly focus on the basic discussion in response to the application of natural fracture networks. Some comparison plots are shown in **Figure 3.2 (a & b)** and **Figure 3.3 (a & b)**.

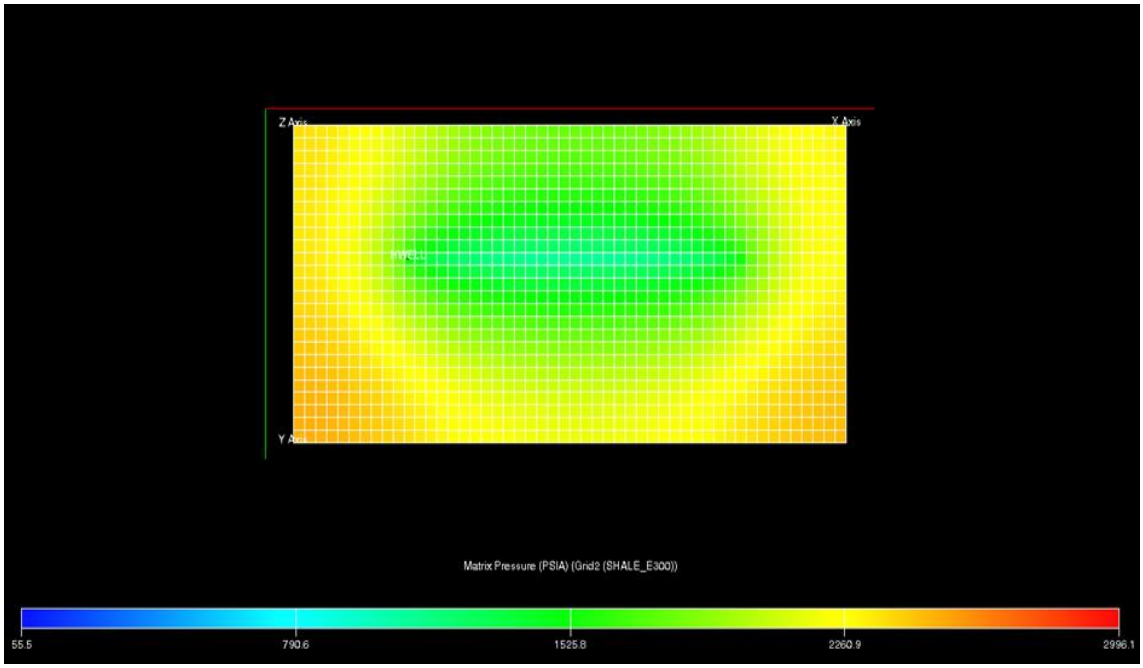

(a)

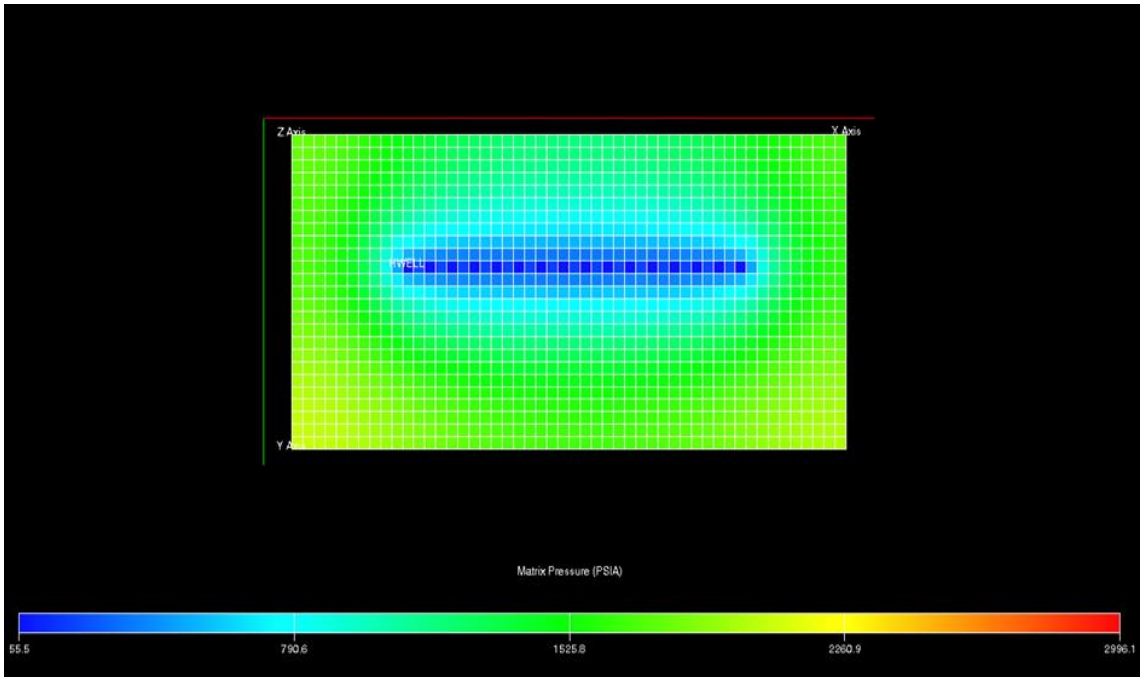

(b)

Figure 3.2 (a& b) Reservoir pressure for models (a) with and (b) without natural fractures

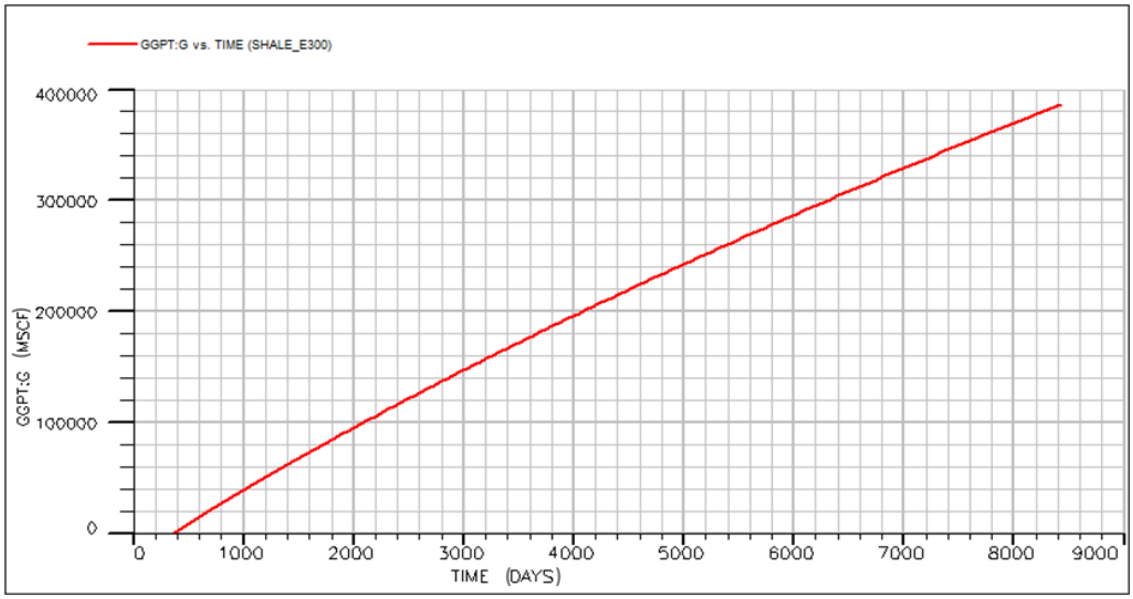

(a)

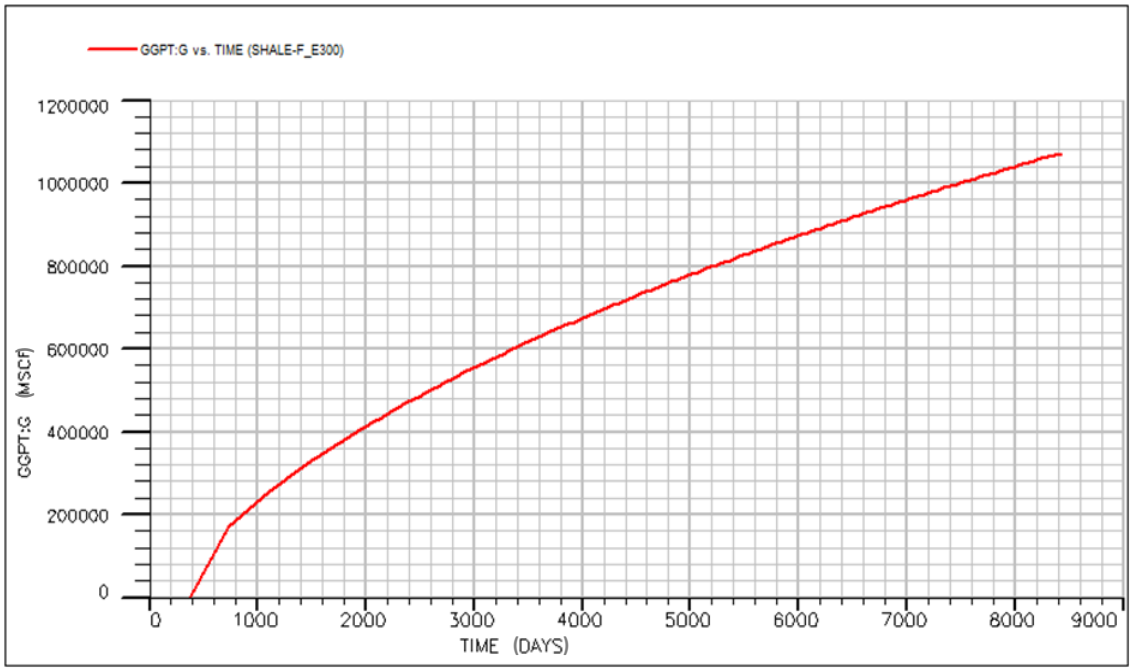

(b)

Figure 3.3 Cumulative produced gas in total vs time (a) with and (b) without natural fractures

There are no injection process is proceeded for both cases (with & without natural fractures) and the production well control for each case is constrained by low bottom-hole pressure in order to manage natural reservoir depletion. **Figure 3.2** presents a comparison of pressure calculations for the cases with and without natural fractures in shale matrix. It can be readily seen that the pressure drop for the model with natural

fractures (**Figure 3.2 a**) has got a larger variation compared with the case without it. This behaviour is even more obvious within the grid blocks adjacent to the horizontal section of the well. The explanation for this observation is that there is better communication between the well and the matrix when there are natural fractures present than when there are not. The consequence is that more gas will be produced for the case with the natural fractures. **Figure 3.3** verifies that more gas has been produced from the simulation that includes natural fractures. Another significant conclusion made in this paper regards the impact of changing hydraulic fracture parameters on cumulative gas production, and this discussion is used to initialise our numerical modelling study for the base case development in the next section.

The development of numerical simulation described by Zhang (2009) provides a typical example of a hydraulic fractured shale model used nowadays. It represents the fluid flow between the natural fractures, the shale matrix and the hydraulic fractures, and also considers the complexity of the whole natural fracture network by applying the micro seismic data collected in place (DFN model). It is challenging to develop an ideal and unique history matched model for unconventional simulation; however, with the help of the operators to collect relevant field data (such as production profiles, reservoir cores and logs, hydraulic fracturing process parameters and more), it becomes easier to characterize the whole shale system and initialise the relevant parameters.

Although the previous modelling studies indicate that it is able to approach history matching with field data by including a series of complex fluid flow mechanisms, developing a simpler fluid flow model (only considers basic shale gas petrophysical properties) for our following geochemical modelling study is still necessary – since the more complicated the fluid flow model is, the more uncertainties will be created for the geochemical simulation and analysis. The discussion of this will be presented in the upcoming section.

3.3FLUID FLOW MODELLING STUDY

3.3.1 Model setup and initialisation

A model has been set up using a commercial reservoir simulator CMG IMEX. This model is a single porosity model and developed with the typical shale gas properties collected from the previous literature review study and is designed to achieve a history match with the production profile collected in the HRB area.

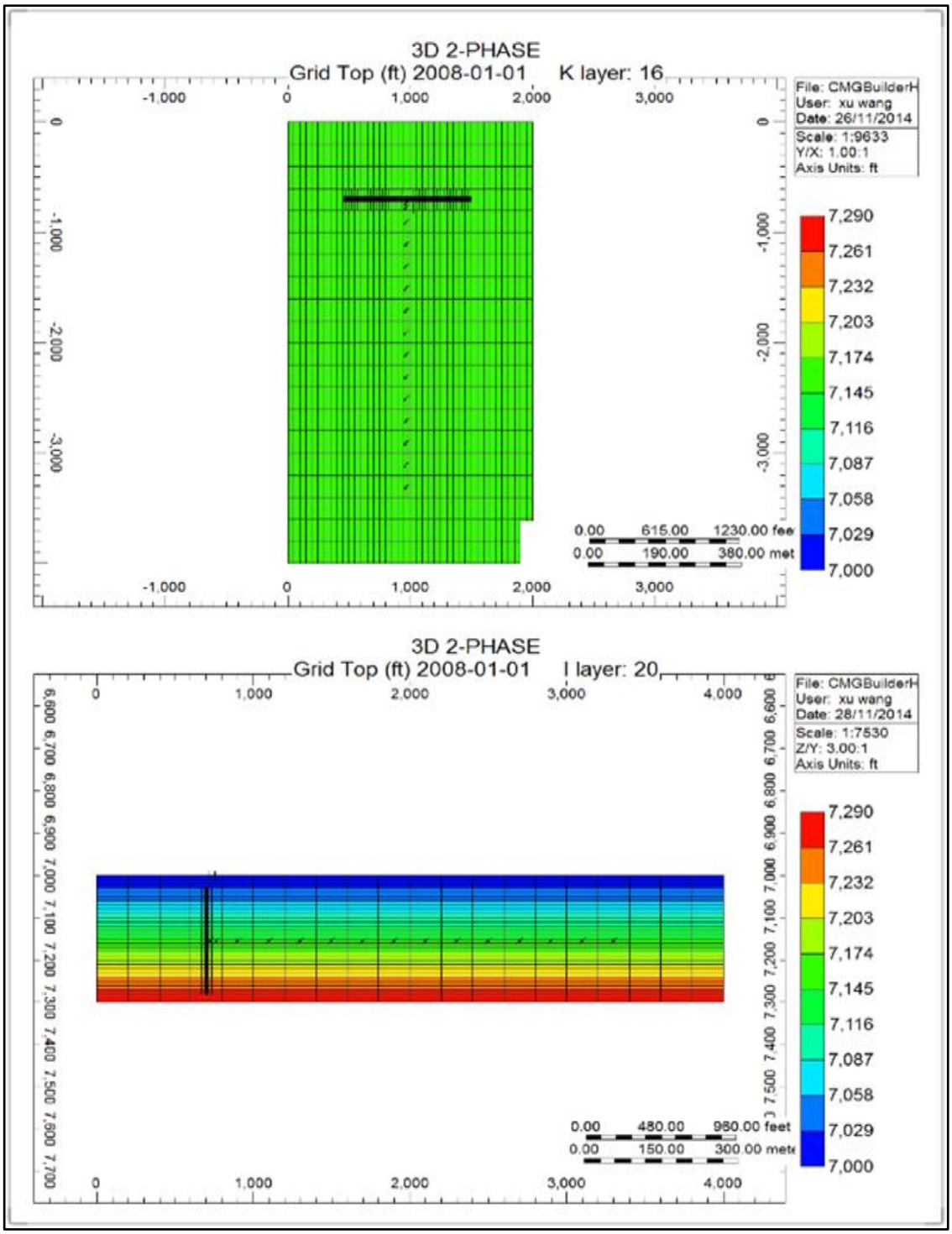

Figure 3.4 Overview of model from I-J and J-K directions

The whole view of this model from the I-J direction and the J-K direction is shown in **Figure 3.4**. The simulator considers the initial conditions are equilibrium even with the hydraulic fracture has already been established before processing injection of fracture fluid (the simulation does not involve in any modelling of hydraulic fracturing creation process). This model has 40 x 20 x 30 grid blocks in each direction with a dimensions of 50 x 200 x 10 ft for each grid block. It is a two phase fluid flow model (with gas and

water), and the top of the reservoir is set to be 7,000 ft. The Gas-Water contact is located at a depth of 10,000 ft, which means no transition zones exists in between the reservoir and the aquifer. Only one horizontal well has been included in the model, and is used as both the injection well and the production well – the whole injection process lasts for one day with a total volume of 3,000 barrels injected, and then the well is shut in and then turned into a production well for the rest of the model run time. One single hydraulic fracture is established in the model, which applied using a Local Grid Refinement (LGR) to represent the hydraulic fracture area.

The shale matrix permeability and porosity are set to 0.0001 mD and 5%, respectively. High capillary pressure of up to 1,000 psi has been applied for the shale matrix along with zero capillary pressure applied within the hydraulic fracture. The primary hydraulic fracture width is 0.01ft, with a conductivity of 50 mD*ft in each direction. The total hydraulic fracture height is 250 ft, which is set to be a vertical planar penetration through the K direction. The half-length is 500 ft and the fracture is oriented in the I direction. The parameters used in this model are shown in **Table 3.1**.

Table 3.1 Parameters for initial model setup

Parameter	Value	Unit	Definition
D	7000	ft	Reservoir top
G_p	0.5	psi/ft	Reservoir pressure gradient
K_{mi}	0.0001	mD	Matrix initial permeability
C_{fi}	50	mD*ft	Fracture initial conductivity
Φ_m	0.05	N.A.	Matrix porosity
Φ_f	0.001	N.A.	Fracture porosity
P_i	4500	psi	Reservoir initial pressure
T	135	°C	Reservoir temperature
S_{wi}	0.2	N.A.	Reserrvoir initial water saturation
H_f	250	ft	Fracture height
H_{Lf}	500	ft	Fracture half length

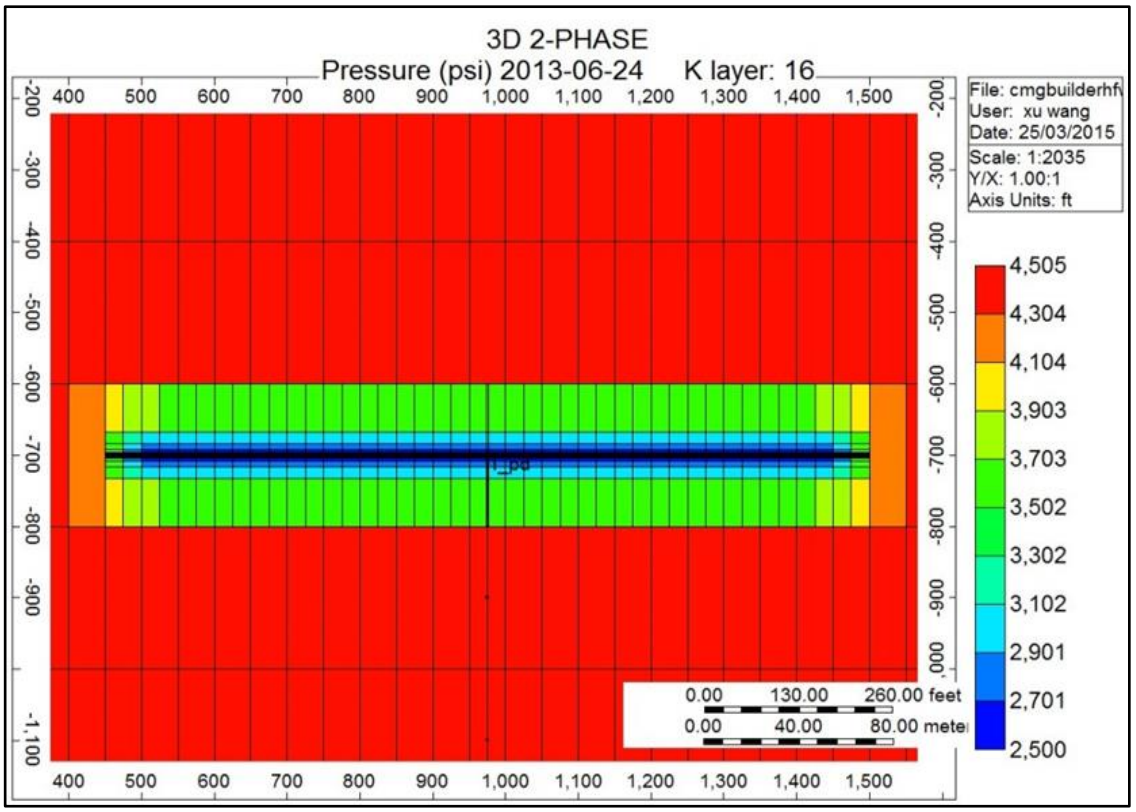

Figure 3.5 Reservoir pressure distributions around single fracture

Only one perforation (locates at the block of 20, 4, 16) is used to connect the main fracture and the wellbore during the process of fracture fluid injection. This is to ensure the model reproduces in detail part of a real well system, which may have multiple fractures, but where each fracture behaves in a similar fashion (Kurtoglu, 2013). This is also used, because of the similarity between fractures, to shorten the simulation time. The reservoir pressure distribution around the primary hydraulic fracture at the end of the production period can be found in **Figure 3.5**.

It can be readily seen that adjacent to the fracture zone, the reservoir pressure has gradually dropped due to the effect of applying different capillary pressure and conductivity between the fracture zone and the matrix zone. This reservoir pressure drop behaviour is similar to the previous numerical modelling simulation results shown in **Figure 3.2**.

To initialise this numerical modelling base case, some sensitivity runs have been developed in terms of changing different properties of the hydraulic fracture. As the conclusions presented by Zhang (2009) show, hydraulic fracture half-length has more impact on gas production than does hydraulic fracture height; therefore, the sensitivity case discussion is based on observing the impacts by changing these two parameters.

Table 3.2 Parameters for hydraulic fracturing sensitivity cases

Parameter	Unit	100%	80%	60%	40%
Hydraulic fracture height	ft	250	200	150	100
Hydraulic fracture half-length	ft	500	400	300	200

The relevant parameters for all sensitivity cases are shown in **Table 3.2**. As indicated in the table it can be seen that to enable a realistic comparison between sensitivity cases for different properties, the same relative change in value for each property will be used (e.g. all the sensitivity cases are run at 100%, 80%, 60% and 40% of the original value). **Figure 3.6** and **Figure 3.7** show some plots of produced fluid against production time for different sensitivity cases.

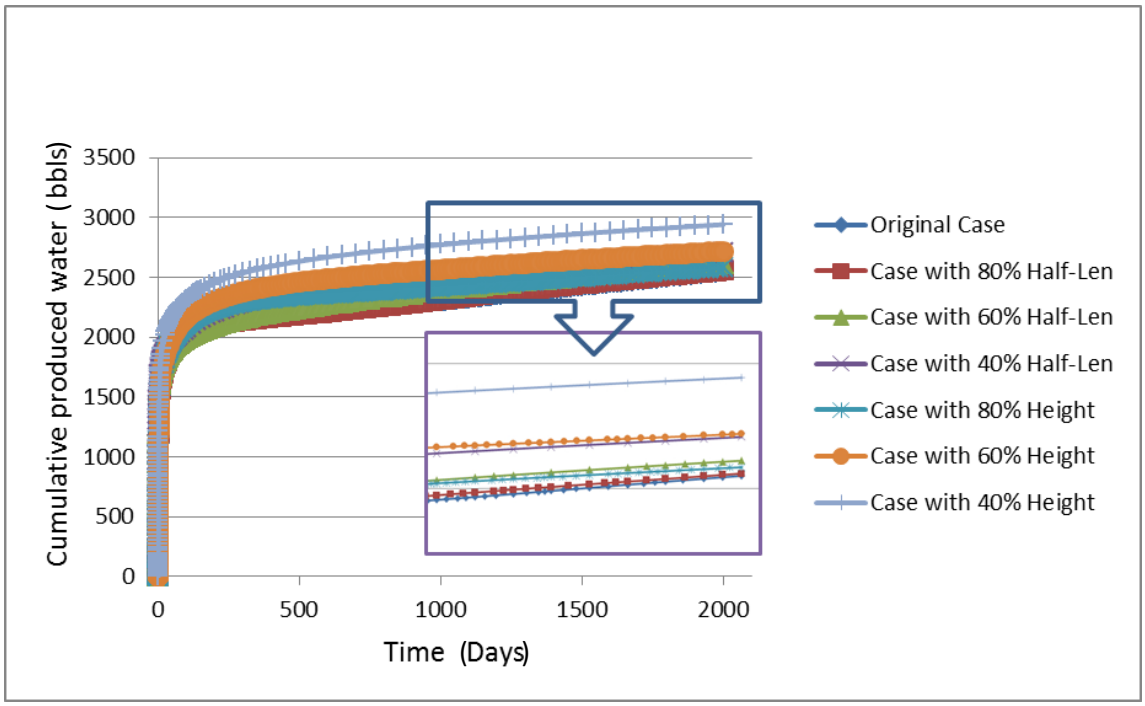

Figure 3.6 Cumulative produced water vs time for different sensitivity cases

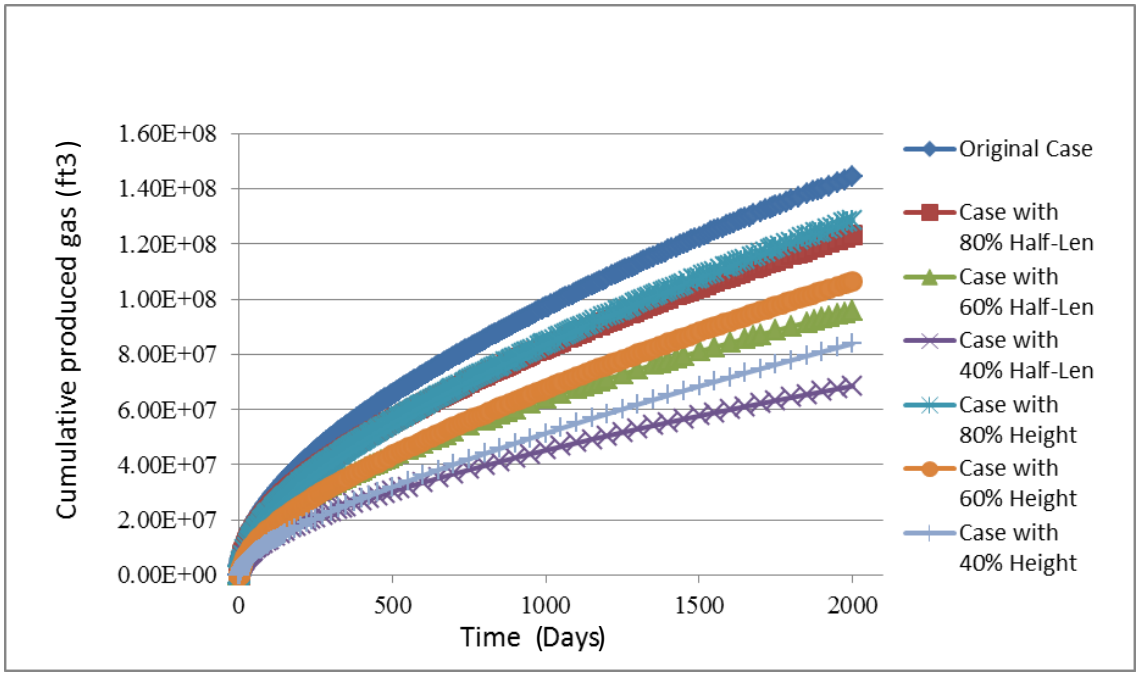

Figure 3.7 Cumulative produced gas vs time for different sensitivity cases

From **Figure 3.6**, it can be seen that the hydraulic fracture height is a more sensitive parameter than the hydraulic fracture half-length, in terms of the impact on the cumulative produced water; especially when it becomes much lower (40% of original value). However, in **Figure 3.7**, the hydraulic fracture half-length has more impact than the fracture height on the cumulative produced gas, and this agrees with the conclusions made from previous numerical modelling study (Zhang, 2009).

One reason for the different behaviour between produced water and gas in response to the changes in hydraulic fracture half-length and height is associated with gravity. In order to find out whether this assumption is correct or not, some further sensitivity cases were run to decrease the vertical permeability (from 50 mD to 0.0001 mD) to eliminate the impact at gravity. As the vertical permeability drops, the conductivity of the hydraulic fracture in the K direction decreases, and as a consequence, a much lower injection rate is needed to maintain the bottom hole pressure below the maximum constraint. The new injection rate is selected to be 600 bbls/day in these cases. The results for cumulative produced water in different cases (with extremely low vertical permeability) are shown in **Figure 3.8**.

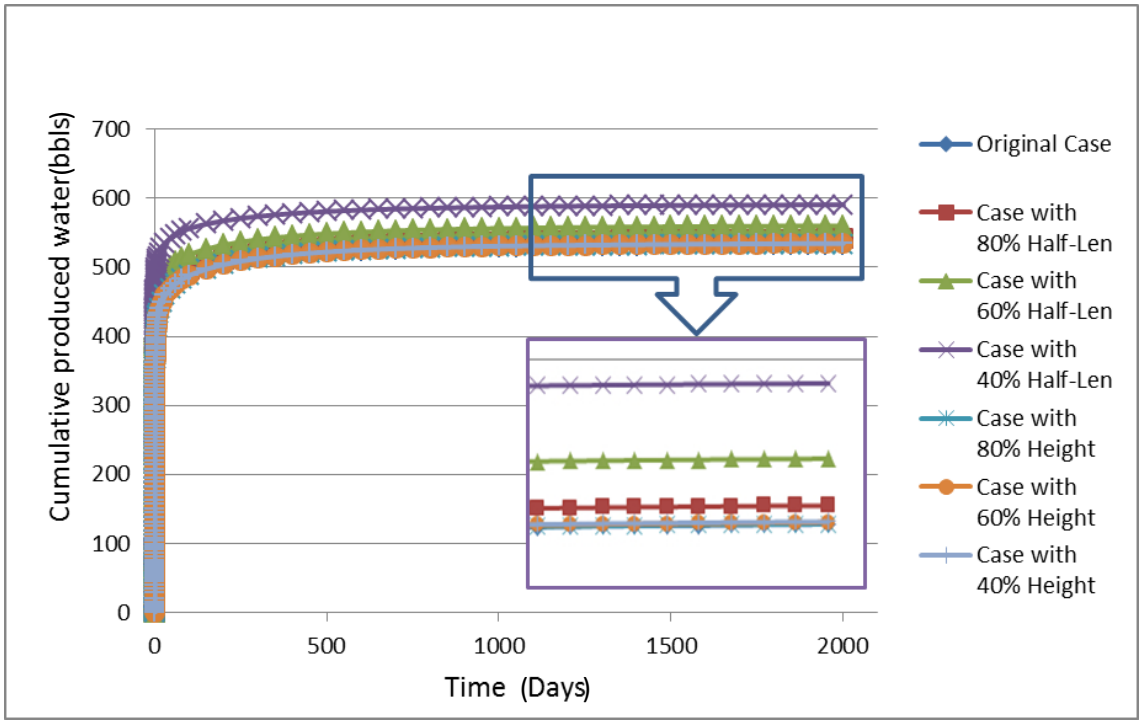

Figure 3.8 Cumulative produced water vs time for different sensitivity cases

It is evident that because of decreasing vertical permeability to extremely low values, the hydraulic fracture half-length is a more sensitive parameter in determining the cumulative produced water volume (in **Figure 3.8**). This then proves that it is correct to assume that gravity is the reason why the hydraulic fracture height is a more sensitive parameter impacting produced water volume. Further discussions will be presented later on in this section which refer to the gravity segregation impact on produced water to so that a better history match could be achieved.

3.3.2 History match with total volume of produced water

3.3.2.1 Discussions of changing critical water saturation

In the plots shown in **Figure 3.6** and **Figure 3.8**, according to the initial simulation results it can be seen that the fraction of cumulative produced water relative to the injection water volume is over 85%, which is higher than observed in actual shale gas production cases (from 10% to 40%). Considering the fact that capillary pressure of the shale matrix has already been applied with a critical maximum value (around 1,000 psi), trying to maintain any further changes in capillary pressure would not be a great help to bring the fraction of total volume of flowback water down. Instead, the water relative permeability curves have been managed to try to keep the volume of flowback water within the required ideal range (10% to 40%), by increasing the critical water saturation.

The fundamental parameters for each case are the same as shown in **Table 3.1** and the only difference between them is to apply variable critical water saturation in the matrix rel-perm table. The illustration plot for the water relative permeability curves is shown in **Figure 3.9**. These changes have been only applied with shale matrix under high capillary pressure.

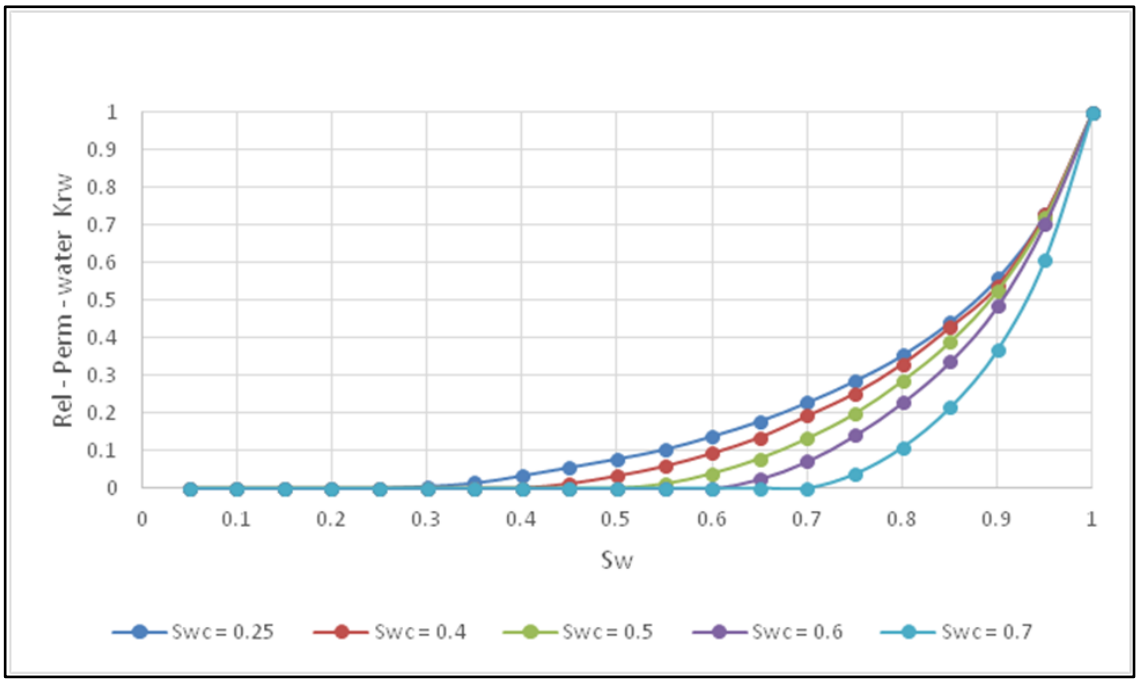

Figure 3.9 Water relative permeability curves, showing various critical water saturations used

It is known that the critical water saturation defines the maximum water saturation that a formation with a given permeability and porosity can retain without producing water (normally close to the value of the irreducible water saturation in a conventional reservoir) (Crain, 2015). This water, although present, is held in place by capillary forces and will not flow. Critical water saturation is usually determined through special core analysis. All the simulation results where different Swc are used are shown in **Figure 3.10**.

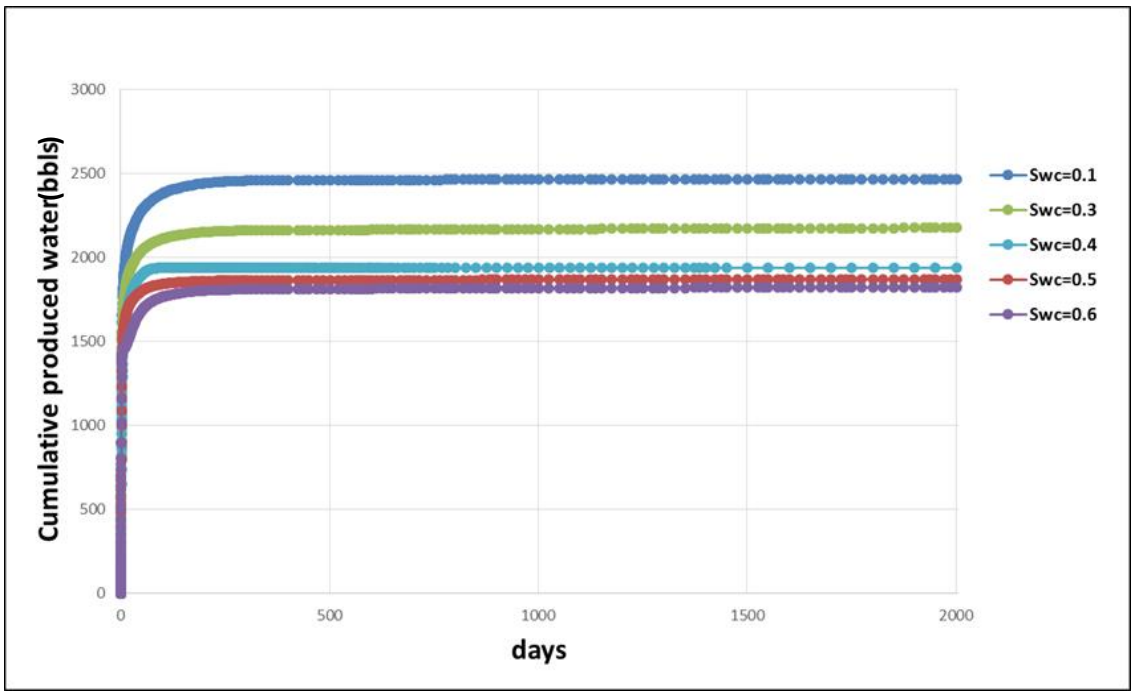

Figure 3.10 Cumulative produced water with different Swc vs time

As indicated in **Figure 3.10**, by changing the critical water saturation value of the shale matrix, it can be observed that as the Swc increases, the volume of flowback water produced reduces. From the results of these simulations it is found that even by increasing the critical water saturation to a value greater than 0.5, the fraction of flowback water relative to the injected fracture fluid varies only very slightly (between 57% and 60%). The reason is that the injected fluid cannot propagate far enough into the shale matrix due to the extremely low matrix permeability (0.1nD), which results in most of the injected fluid remaining in the rock very close to the fracture, so that even with a very high critical water saturation, the injected brine readily flows back into the fracture and from there into the well.

Cases with higher matrix permeability have been simulated only to study and discuss what the impact on the flowback water volume is when the injection fluid can propagate further into the matrix rock. This water propagation study is based on an IMEX model with two staged but adjacent hydraulic fractures (the total injection volume is 6000 bbls/day with 3000 barrels of water injected in each stage). The reason for using two stages instead of just the single one is to check for the reservoir pressure interference between the two fractures. The parameters used for this model are the same as indicated in **Table 3.1** (apart from different matrix permeability is applied in 0.0001 mD, 0.001 mD, 0.01 mD, 0.1 mD, 1mD and 10 mD) and the detailed parameters for the two hydraulic fractures are shown in **Table 3.3**.

Table 3.3 Parameters for two stages hydraulic fracturing cases

Hydraulic fractures	Center block of HF	Production time	Volume of water treatment
1st hydraulic fracture	20, 4, 5	1st day	3000 bbls
2nd hydraulic fracture	20, 5, 5	3 months later	3000 bbls

According to the results in **Figure 3.11**, it can be seen that for a matrix critical water saturation of 0.5, when the matrix permeability increases, less water is produced back. In addition, when the matrix permeability is increased to larger values, say greater than 1mD, the flowback water volume becomes more sensitive to the matrix permeability value. The simulation results show that if the water is allowed to propagate further into the reservoir, more injected fluid will be retained within the shale matrix along with applying a higher critical water saturation.

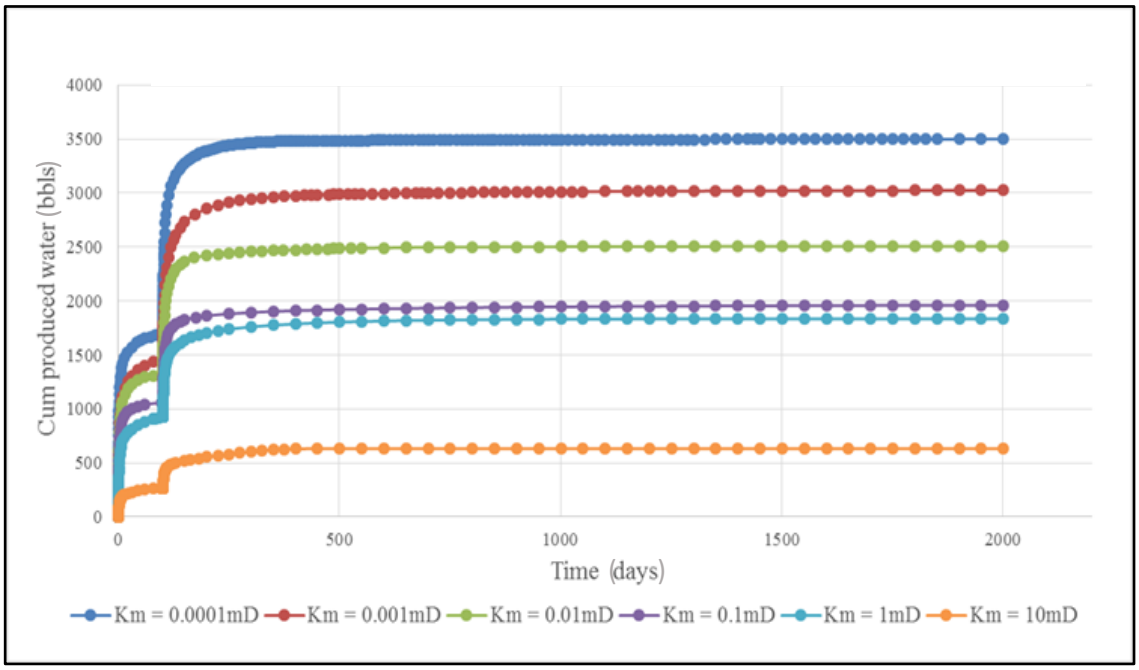

Figure 3.11 Cumulative produced water vs time in different matrix permeability

Meanwhile, given that it is known that extremely low matrix permeability (order nD) are measured in actual field systems, these calculations suggest that the injected fluid must propagate through secondary induced fractures or even a natural fracture network within the shale system, in order to propagate far enough from the main propped hydraulic fracture not to flow back immediately. In order to perform the modelling more realistically, the simulation must be updated with an enlarged conductivity zone adjacent to the primary hydraulic fracture to represent the secondary induced fracture zone or even the natural fracture networks in place.

3.3.2.2 Discussion of updated modelling to match with total volume of water flows back

3.3.2.2.1 Discussion of proposed hydraulic fracture system

The hydraulic fracturing process could induce the creation of secondary fractures if there are natural fractures existing in the shale reservoir (Rogers et al., 2010). The highly pressured fracture fluid breaks the shale matrix rocks so that the proppant can hold the cracks open to allow the hydrocarbons flow through to the well. As a consequence of this, a secondary fracture zone (also known as part of "estimated stimulated reservoir volume") is established adjacent to the wellbore and primary hydraulic fracture to increase the productivity of hydrocarbon recovery.

As discussed in the previous section in regard to the analysis of fracture system complexity, the complexity of the hydraulic fracture system could have a large impact on fluid transport within the shale system and also the flowback water geochemistry. With a more complex hydraulic fracture system, the unconventional reservoir has a greater potential for hydrocarbon recovery, since better conductivity can be provided to allow the fluids to flow into the well. To explain the impact of the fracture complexity on the amount of water flowing back, a proposed hydraulic fracture system similar to the study developed by Fan (2010) is shown here. The fracture system is illustrated in **Figure 3.12 (a & b)**.

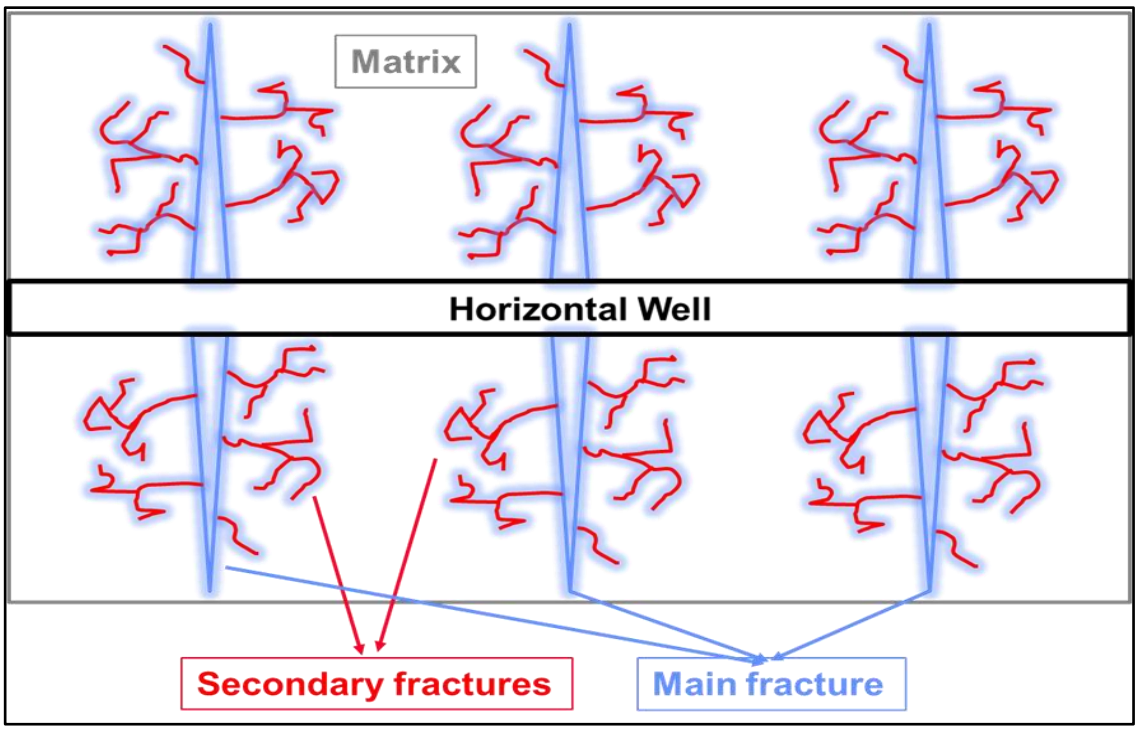

(a) Complex hydraulic fracture system

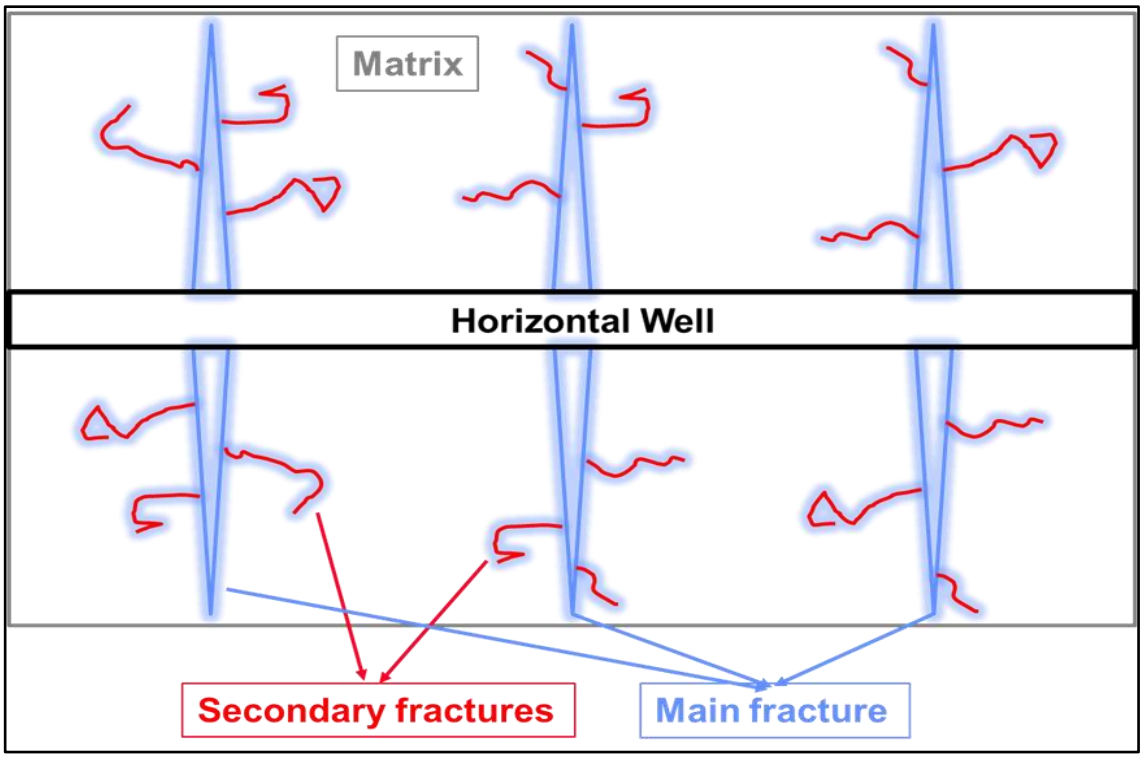

(b) Less complex hydraulic fracture system

Figure 3.12 Illustration of more and less complex hydraulic fracture systems

In **Figure 3.12 (a)** a complex hydraulic fracture system consisting of a main fracture held open by the proppant and a series of induced secondary micro fractures (or connected natural fractures in the reservoir) is depicted schematically. At the end of the hydraulic fracturing treatment, the main fracture will be filled with the proppant and the injected fluid; however, as the secondary fractures have a smaller aperture than the main fracture, they will only be filled with the injected fluid. If the secondary fractures are the natural fractures already present in the shale reservoir, they may be originally filled with the formation water before the hydraulic fracturing treatment. Once the hydraulic fracturing process starts, the fluid mixing between the injected fracture fluid and the *in situ* formation water may take place in the connected fracture system.

As soon as the well is put back on production, the large volume of injected water located in the main fracture at the end of the fracture treatment will flow straight back due to the low capillary pressure and high conductivity in the main fracture. As the reservoir pressure is drawn down, closure of some of the secondary fractures may take place. On account of the low fracture conductivity and pressure draw down in the secondary fractures, water can be trapped within or even imbibed into the matrix due to the high matrix capillary pressure (Weedmark and Spencer, 2012). The high matrix

capillary pressure additionally helps the water flowing away from the fracture system to propagate further into the shale matrix.

The gas and water originally trapped within the natural fractures can also flow into the fracture system after the hydraulic fracturing process is completed or during the period of well shut in. All of these processes result in the free gas existing in the active fractures or matrix being replaced and flowing up to the well through the fracture paths (Passey, 2010). As a consequence of this, if the complexity of the fracture system is decreasing, as illustrated in the diagram in **Figure 3.12 (b)**, the fracture will produce back less gas and more water (less water could be trapped or imbibed within the fracture system or shale reservoir) after the hydraulic fracturing process is performed, which means the produced gas/water ratio could be relatively lower (Rogers, 2010). It is also reported from the previous chapter that the imbibition into the small pores can help to account for the low volume of injection fluid flowing back (Bearingers, 2013).

3.3.2.2.2 Discussion of applying secondary fracture zone

According to the discussion of proposed hydraulic fracture system, an updated IMEX hydraulic fractured model has been developed. Several cases with different conductivities of the secondary fracture zone have been simulated to observe the impact on the flowback water volume. The parameters for the models applied with secondary fracture zones are shown in **Table 3.4** and the schematic diagram of the fracture zone for the IMEX model is shown in **Figure 3.13**.

Table 3.4 Parameters for models with secondary fracture zones

Parameter	Value	Unit	Definition
D	7000	ft	Reservoir top
G_p	0.5	psi/ft	Reservoir pressure gradient
K_{mi}	0.0001	mD	Matrix initial permeability
C_{fi}	50	mD*ft	Fracture initial conductivity
K_{sf}	0.0001 - 10	mD	Secondary fracture initial permeability
Φ_m	0.05	N.A.	Matrix porosity
Φ_f	0.001	N.A.	Fracture porosity
P_i	4500	psi	Reservoir initial pressure
T	135	^oC	Reservoir temperature
H_f	250	ft	Fracture height
H_{Lf}	500	ft	Fracture half length
S_f	0.45	N.A.	Fracture initial water saturation
S_{sf}	0.2	N.A.	Secondary fracture initial water saturation

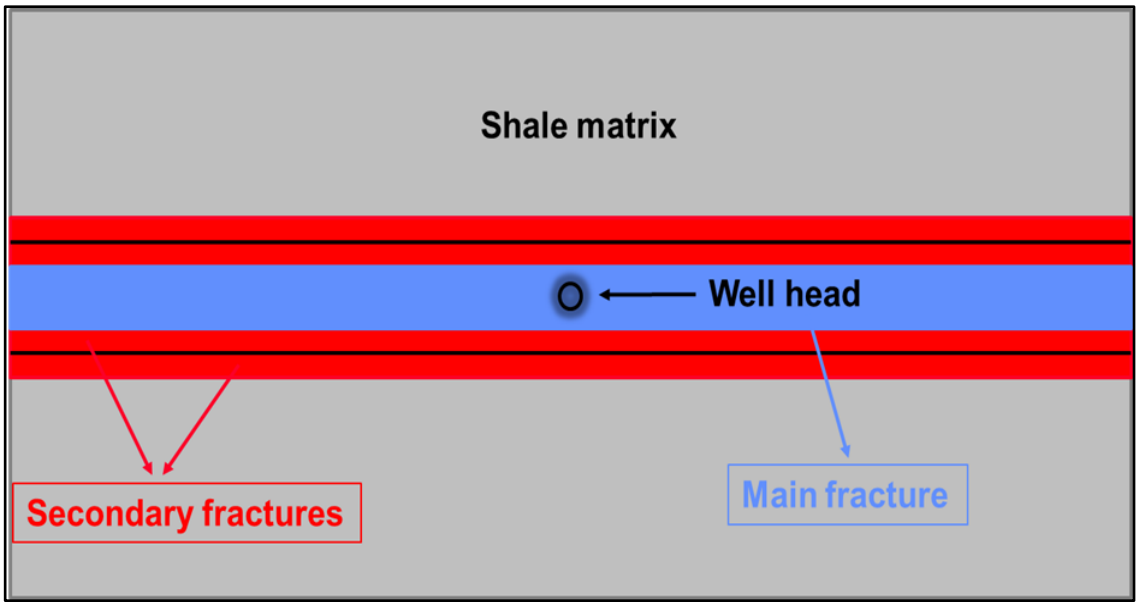

Figure 3.13 Schematic diagram of the secondary frac zone for the updated IMEX model

The new IMEX model has been updated by applying a secondary fracture zone in the system, with lower conductivity compared with the main fracture (50 mD*ft). The matrix capillary pressure has been applied in the secondary fractures, which means they are still at quite high capillary pressure compared to that applied in the main fracture (which is zero). The varied value of conductivity in the secondary fractures for each IMEX model is: 0.002, 0.02, 0.2, 2 and 20 (unit is mD*ft). The plots for the updated IMEX models are shown in **Figure 3.14**. The simulation results for each case are listed in **Table 3.5**.

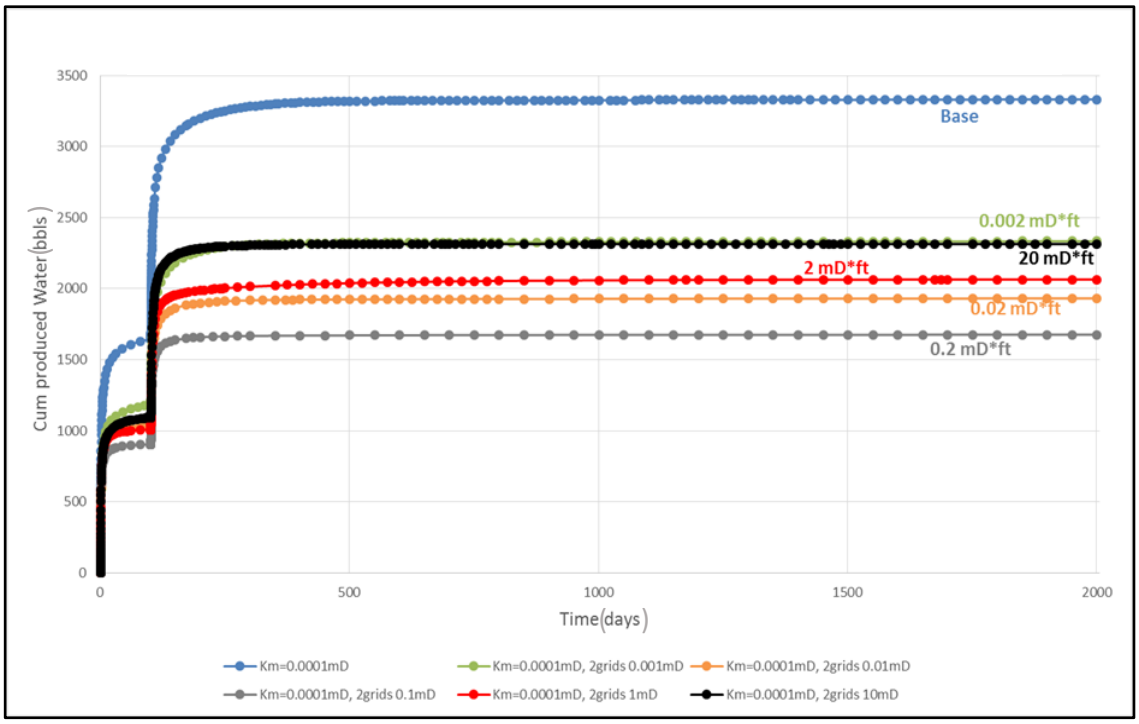

Figure 3.14 Cumulative produced water for various secondary frac conductivities vs time

Table 3.5 Cumulative produced water from different secondary frac conductivity cases

2nd frac permeability (mD)	0.0001	0.001	0.01	0.1	1	10
Cum Water (bbls)	3331.9	2333.9	1930.9	1675.4	2064.2	2313.6
Cum water/ Inj water (%)	55.5	38.9	32.2	27.9	34.4	38.6

From the simulation results of these updated cases we observe that while the matrix permeability remains 0.0001mD, by increasing the permeability of cells adjacent to the main hydraulic fracture to 0.01mD, the fraction of cumulative produced water decreases to around 30%, in keeping with observed field data. One of the interesting findings is that when the conductivity of the secondary fractures increases, less water flows back due to the high capillary pressure; however, while the permeability of the cells adjacent to the main fracture is greater than 1 mD, the volume of flowback water increases (from 27.9% to 34.4%). The reason for this flowback water increase is due to different dominant factors impacting the fluid flow. It can be observed that while the permeability of the secondary fracture zone is less than 0.1 mD, high capillary pressure is the major factor that accounts for the fluid transport; whereas when the permeability of the secondary fracture zone is more than 1 mD, the high conductivity becomes the dominant factor that allow the fluids to flow back. In other words, a critical value of permeability in the secondary fracture zone should be identified as being between 0.1 mD and 1mD, where both of the factors could be the dominant reasons to account for

the fluids flowing in the system.

Overall, the application of a secondary fracture zone provides a better history match on the total volume of water produced back so that further simulation could carry on in terms of history match on the fraction of injected fracture fluid in produced water.

3.3.3 History match with fraction of injected fracture fluid in produced water

3.3.3.1 Applying secondary fracture closures

After approached the history match with the total volume of flowback water by applying secondary fracture zones, some new IMEX models have been developed by applying the tracer in the fracture fluid to observe the injected fracture fluid fraction in the flowback water. The model with the conductivity in the secondary fracture zone at 0.02 mD*ft has been selected to be the base case of the history matching test (the parameters of the model are shown in **Table 3.4** previously). The initial results for the IMEX tracer model are shown in **Figure 3.15**. Injected fracture fluid fraction in flowback water (calculated by tracing injected fracture fluid produced) against time is plotted in **Figure 3.16**.

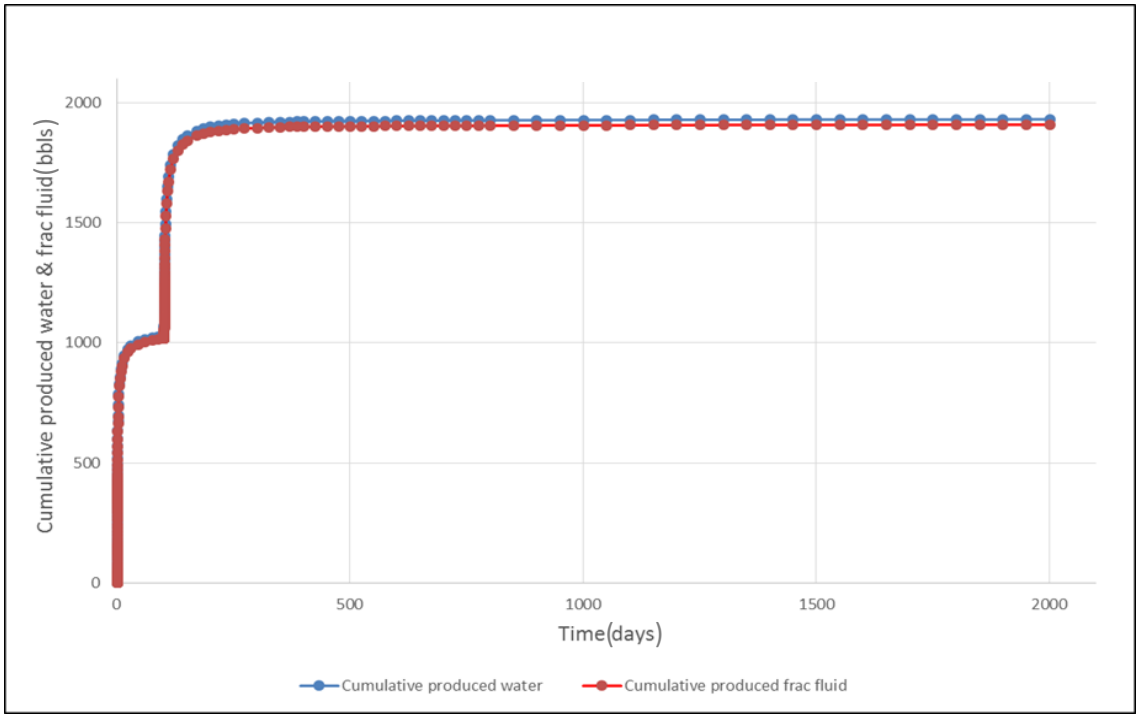

Figure 3.15 Cumulative produced water and frac fluid vs. time

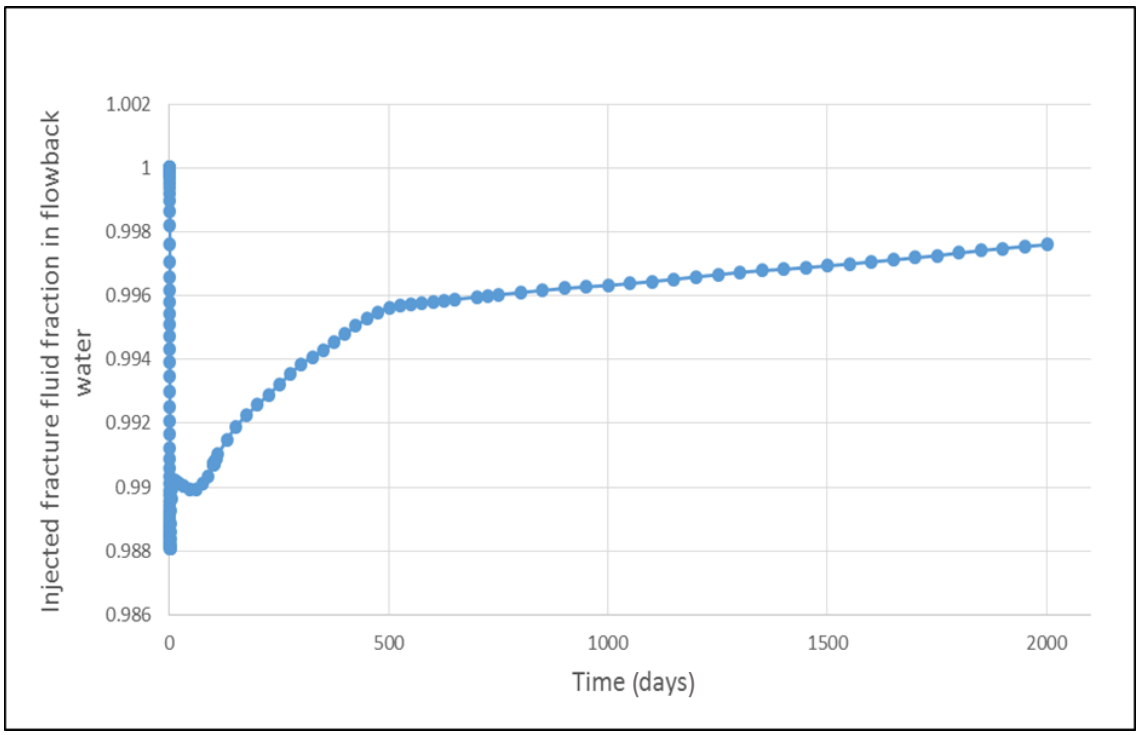

Figure 3.16 Injected fracture fluid fraction in flowback water vs. time

Figure 3.15 indicates that the volume of injected fracture fluid in this calculation is approximately the same as the flowback water volume, which means more formation water has been trapped in the matrix than expected. From **Figure 3.16** it can be observed that the fraction of injected fracture fluid increases up to 99.8% at the end of the production period, which indicates an entirely opposite behaviour to that shown in **Figure 2.40** and **Figure 2.41**. This is due to the total area of secondary fracture zones is over estimated. As a consequence of this, the next step of the modelling study is try to retain more fracture fluid in the system and produce back more formation water to match up the injected fracture fluid fraction with the field data.

As mentioned previously, there are two methods that can be used to match up the fraction of the fracture fluid in flowback water: 1. Retain more fracture fluid in the fracture system; 2. Enlarge the amount of the formation water produced back. According to the discussion of the proposed hydraulic fracture system - on the one hand, closures may take place in some of the secondary fractures due to the reservoir pressure drawdown: this will lead to more fracture fluid trapping within the system after the hydraulic fracturing process is completed; on the other hand, the water originally existing in the natural fractures can also flow into the hydraulic fracture system during the well shut in period, this will help to produce back more formation water during the production.

Considering the discussions above, there are two methods that can be used to simulate the closures within the minor fracture (conductivity change during the production): 1. Define the compaction property of the rock to simulate the conductivity decrease while the reservoir pressure is dropping. 2. Manually apply the variable conductivity zones during the production. However, after completing a series of simulations by applying different ranges of pressure dependent permeability/ porosity table in the system, the simulation results demonstrate that using the first method to simulate the secondary fracture closure is not successful - in terms of a significant fluctuation that takes place during the end period of the injection process and also the beginning period of the production, even with an observation of decrease with injected fracture fluid fraction in produced water (shown in **Figure 3.17**).

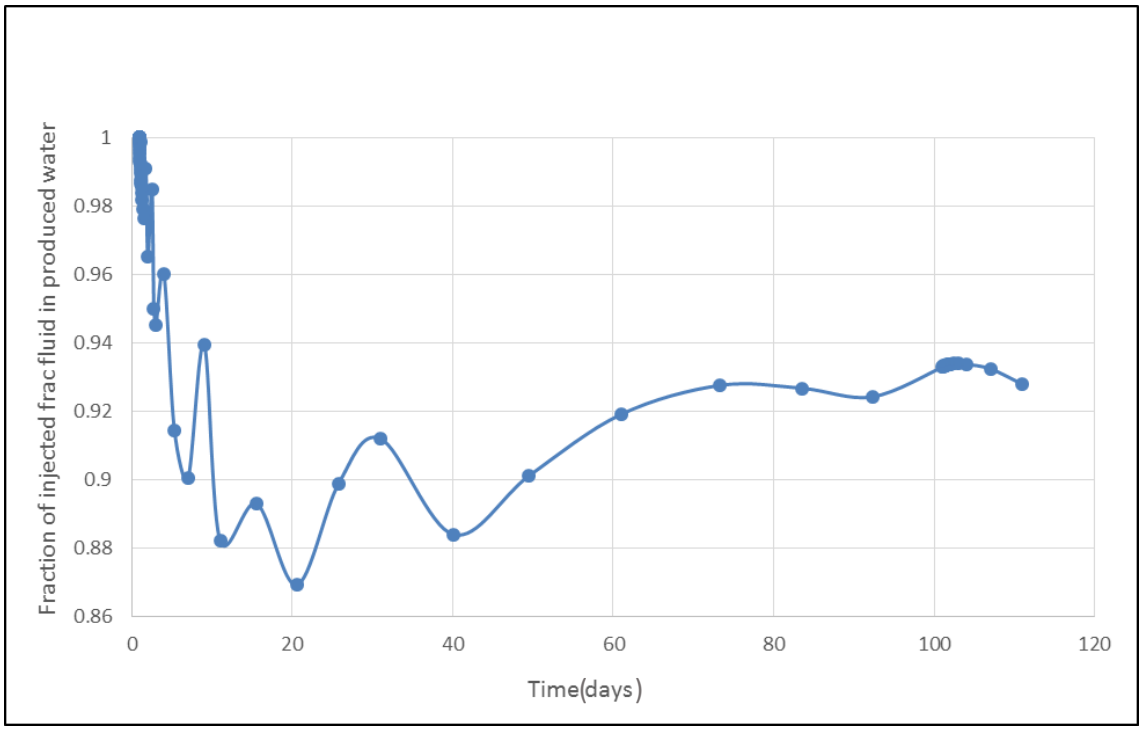

Figure 3.17 Fraction of injected frac fluid in produced water vs time with compaction table applied

Firstly, it is considered that this is because the permeability multipliers are extended with a larger range, and this will make it more difficult for the simulation to converge; and secondly, it is observed that the pressure change within or around the hydraulic fracture is quite significant and it could be quite difficult to find a suitable value for each permeability multiplier in response to the huge pressure change through the whole process. As a consequence, simply applying the pressure dependent compaction table is not enough to retain the fracture fluid into the shale system and another updated IMEX

tracer model must be developed with the second theory proposed above (the schematic diagram showing it is **Figure 3.18**). To shorten the overall simulation run time and avoid potential simulation convergence errors, the following simulation results are also based on a single fracture model and the parameters are shown in **Table 3.6**.

Table 3.6 Parameters for models with secondary fractures closure

Parameter	Value	Unit	Definition
D	7000	ft	Reservoir top
G_p	0.5	psi/ft	Reservoir pressure gradient
K_{mi}	0.0001	mD	Matrix initial permeability
C_{fi}	50	mD*ft	Fracture initial conductivity
K_{sf}	0.001	mD	Secondary fracture initial permeability
Φ_m	0.05	N.A.	Matrix porosity
Φ_f	0.001	N.A.	Fracture porosity
P_i	4500	psi	Reservoir initial pressure
T	135	°C	Reservoir temperature
H_f	250	ft	Fracture height
H_{Lf}	500	ft	Fracture half length
S_f	0.45	N.A.	Fracture initial water saturation
S_{sf}	0.2	N.A.	Secondary fracture initial water saturation
R_{sf}	10~20, 4, 8~9 (higher layers); 20~30, 4, 18~19 (lower layers)	N.A.	Secondary fracture closure zones location

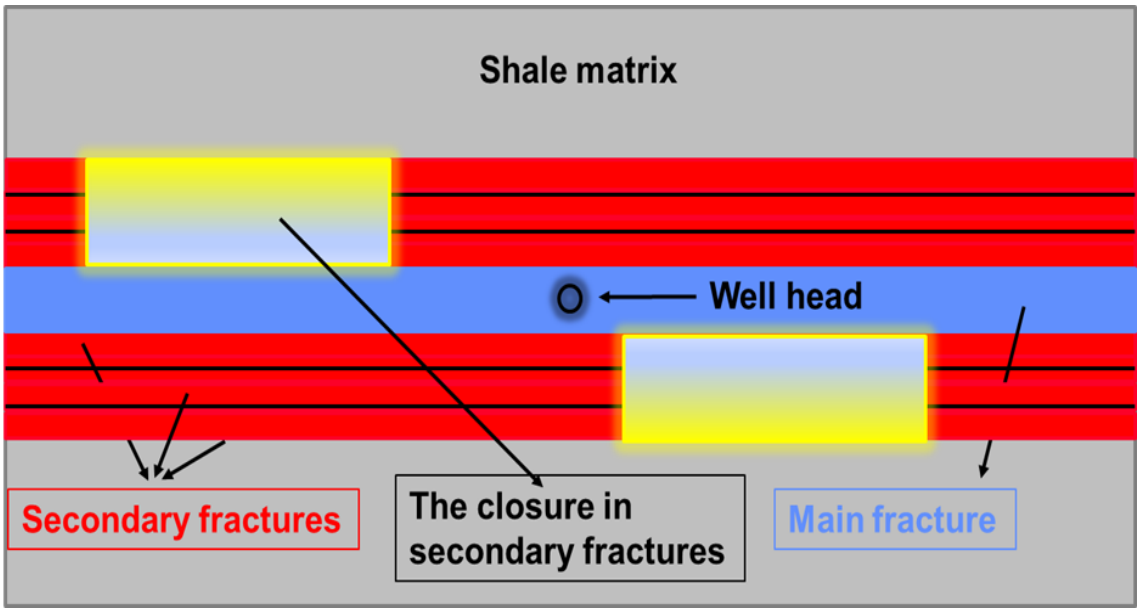

Figure 3.18 Schematic diagram of the updated IMEX tracer model

From **Figure 3.18** it can be seen that the closure of the secondary fractures (after the injection of the fracture fluid) has been included in the updated IMEX tracer model. In

addition, some of the formation water becomes mobile and flows into the fracture zone after the hydraulic fracture has been established.

The initial case of all the updated IMEX tracer models is based on two major changes: 1) The closures are applied in two upper layers and two lower layers (layers 8, 9 and layers 18, 19 – as indicated in **Table 3.6**); 2) One cell into the secondary fracture zone has been filled with mobile formation water before production is started.

The selected changes are obtained from a series of sensitivity simulations related to this particular case. As mentioned previously, to keep the petrophysical model as simple as possible, the updated IMEX tracer model only assumes a single fracture. The initial simulation results of the updated IMEX tracer model are shown in **Figure 3.19** and **Figure 3.20**.

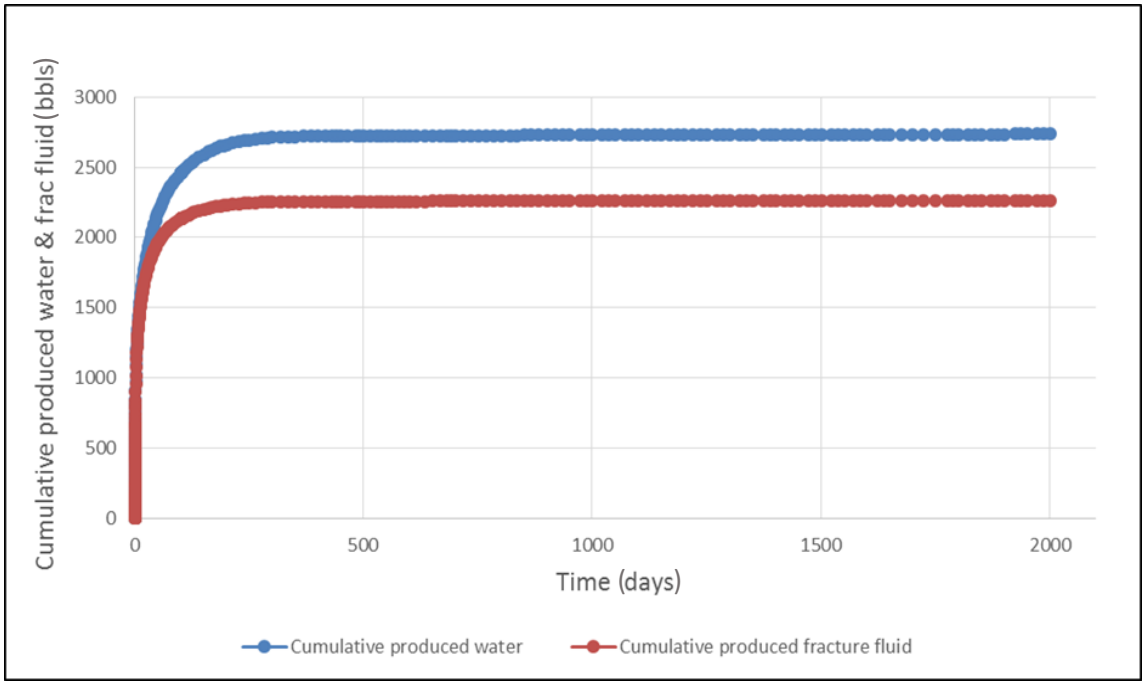

Figure 3.19 Cumulative produced water and frac fluid vs. time

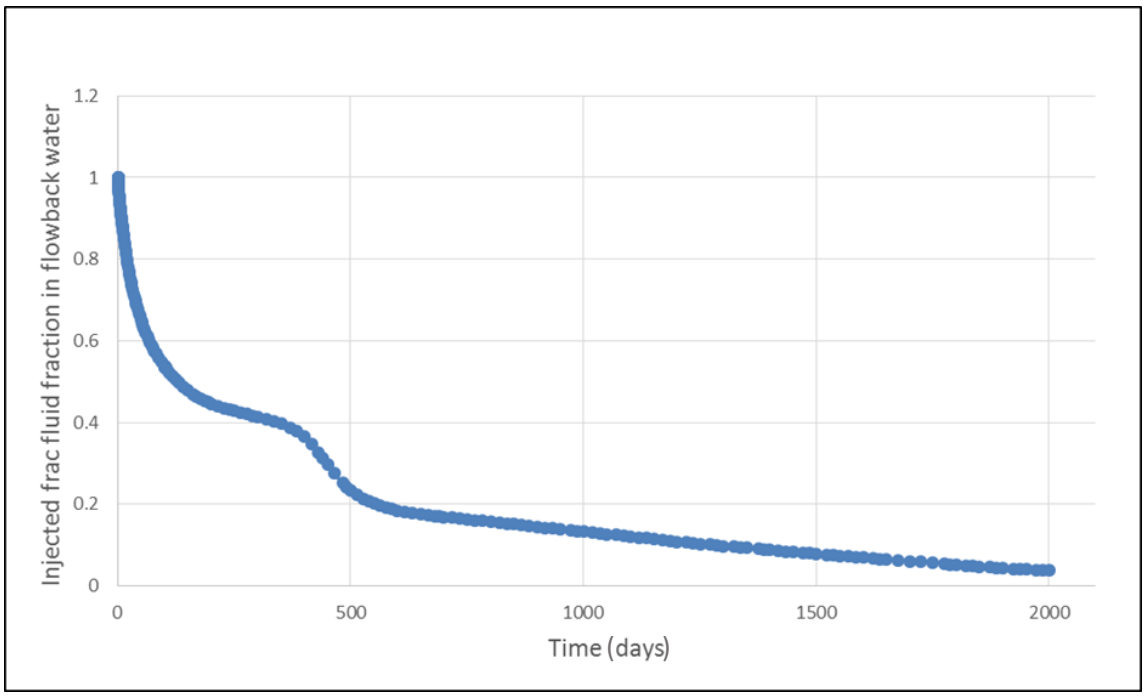

Figure 3.20 Injected fracture fluid fraction in flowback water vs. time

From the two figures above, it can be readily seen that the injected fracture fluid is better matched with the validated field data compared to the old tracer model. However, the total volume of the flowback water is still too high, almost reaching a value of 92%. In order to reduce the total volume of the flowback water, it is required to enlarge the surface area ratio of the secondary fracture closures to the main fracture. The surface area ratio for the base case is calculated at a value of 2/9. The simulation results with different surface area ratios are plotted in **Figure 3.21**. The fraction of total volume of flowback water divided by the injected fluid is shown in **Table 3.7** for each case.

Table 3.7 Cumulative produced water from the cases with different surface area ratios

Ratio of surf area	2/9	1/4	2/7	1/3
Cum Water (bbls)	2735.4	2422.9	2001.9	1002.6
Cum water/ Inj water (%)	91.2	80.8	66.7	33.4

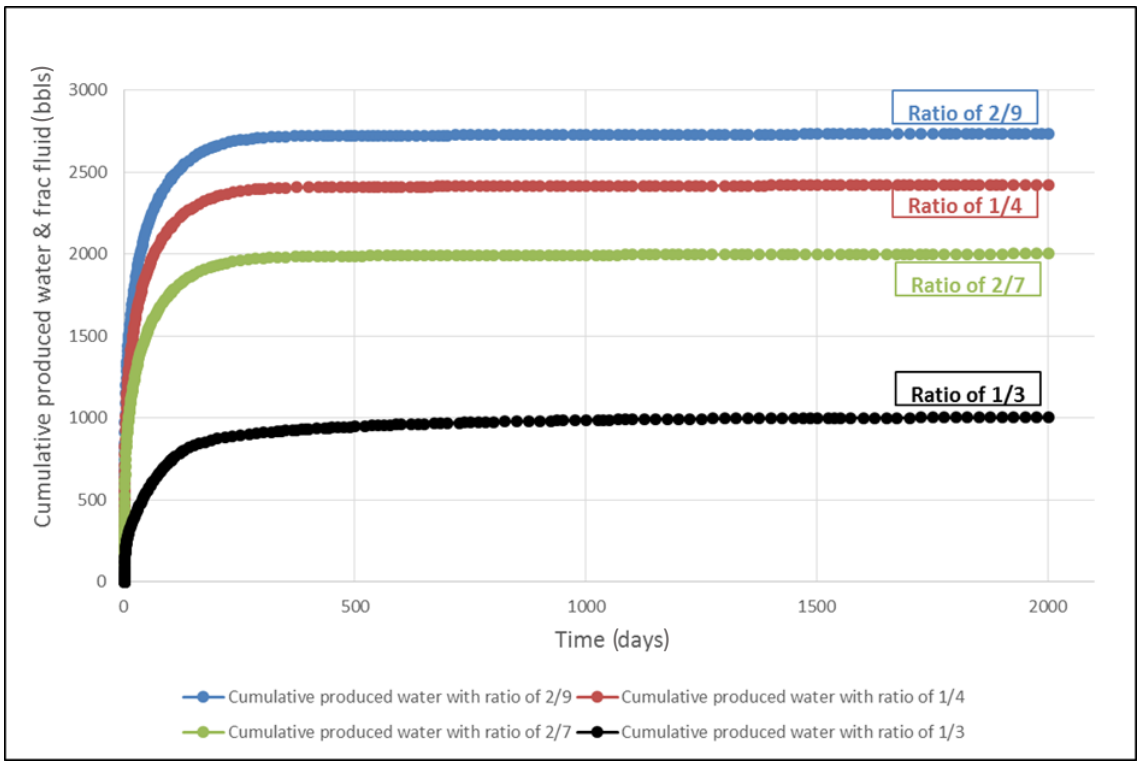

Figure 3.21 Cumulative produced water in different surface area ratio vs. time

As shown in **Figure 3.21** and **Table 3.2**, it can be seen that with the increase of the surface area ratio, less cumulative water is produced back. While the surface area ratio between the secondary closure fractures and the main fracture increases to 1/3 (locations of closure take place in the blocks of (10~20, 4 8~10) and (20~30, 4, 17~19)), the total volume of flowback water can be controlled at the value of 33%, matching with the observed field data. The comparison plots of injected fracture fluid fraction from the simulation results and calculated field data are shown in **Figure 3.22**.

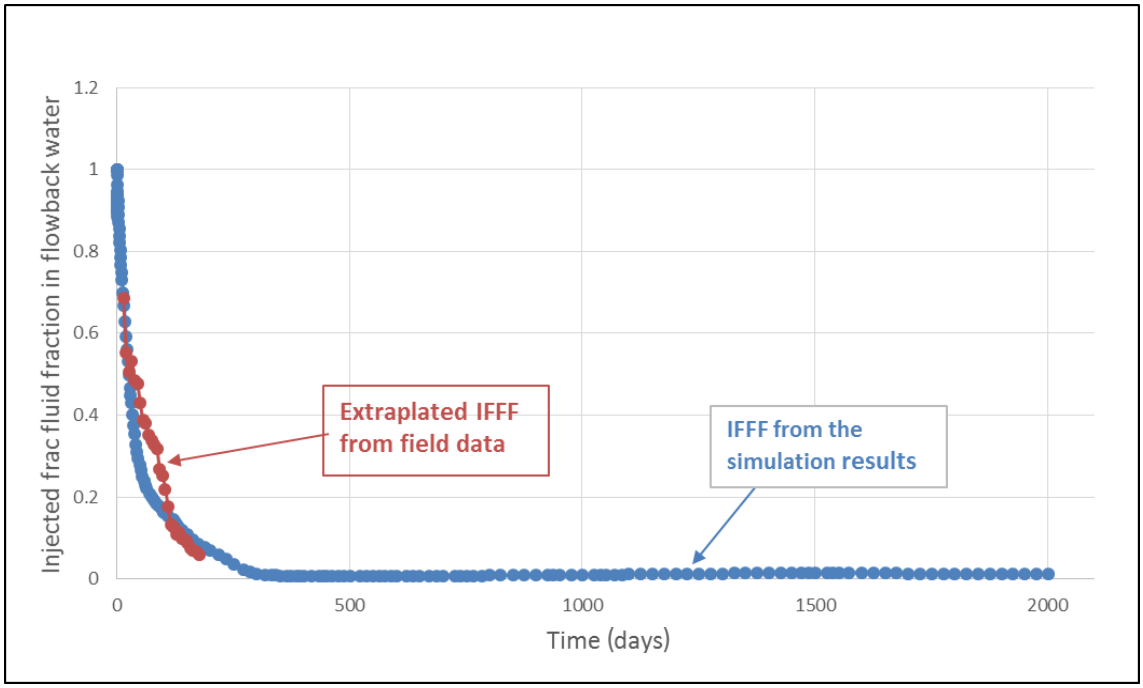

Figure 3.22 Injected fracture fluid fraction from the simulation results and the field data vs. time

From the comparison plots shown in **Figure 3.22**, it can be seen that the simulation result has a good agreement with the fracture fluid fraction field data, which means this case can be considered as the initial history matched base case for the future geochemical modelling study.

3.3.3.2 Considering the impact of gravity segregation in the fracture zone

As it is known that the impact of the secondary fracture closure can be complicated – on the one hand, it reduces the volume and surface area of the secondary fractures, which will result in more water being imbibed into the shale matrix; on the other hand, the total conductivity will decrease due to the fracture closure taking place (Fredd, 2001; Alramahi and Sundberg, 2012; Parmer, 2013). In order to keep the fluid flow model as simple as possible, these sensitivity models are based on the optimal history matched case by applying different locations for the zones of variable conductivity within the fracture zone instead of considering the volume change of the secondary fractures while the reservoir pressure drops. In specific terms, once the injection period is completed, the increased conductivity zone will become a finite but reduced conductivity zone (this will make the zones of variable conductivity almost impermeable to simulate the fracture closure process). All the 3D models include a single hydraulic fracture established with an adjacent secondary fracture zone, which has a slightly higher

conductivity compared with the shale matrix. **Figure 3.23** shows the water distribution in the fracture zone at the end of the production (the figure is exported from the simulation results of the original case, without applying any zones of variable conductivity).

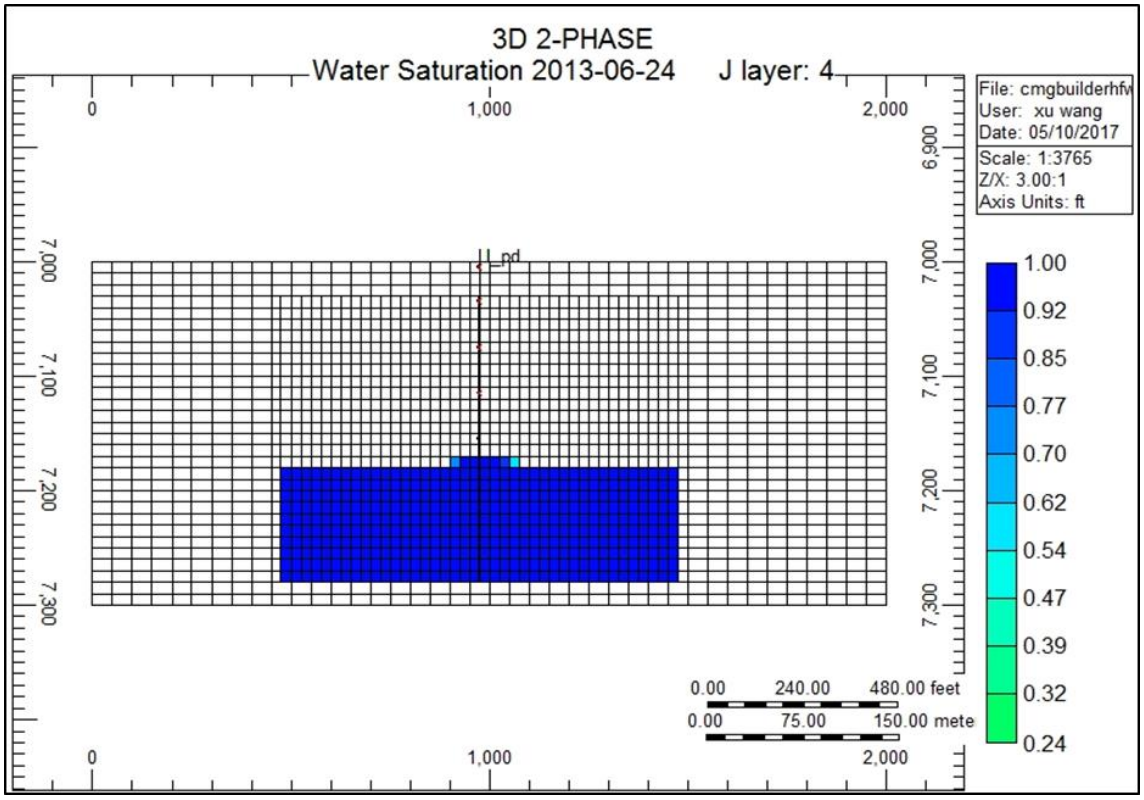

Figure 3.23 Water distributions in the fracture zone in IK view

It is known that the primary hydraulic fracture has a much higher conductivity compared with the extremely low permeability of the shale matrix (Cipolla, 2009; Gdanski, 2010). As a result, it is expected that gravity segregation will have a significant impact on the fluid flow within the fracture system (Liu, 2017). As shown in **Figure 3.23**, at the end of the production, the water tends to accumulate at the bottom of the primary fracture due to the impact of gravity segregation. This impact could be even more significant if different locations of fracture closure are included in the system.

It is well understood that water flows into the matrix due to the spontaneous imbibition process, which is accounted for by the high capillary pressure in the matrix and also the pressure differential between the fracture network and the shale reservoir matrix (Weedmark and Spencer, 2012). The fracture closure can lead to an additional amount of water being trapped in the reservoir, which results in an even lower fraction of fracture fluid flowing back (Rogers, 2010; Bearingers, 2013).

Three cases are simulated to represent different locations of the zones of variable conductivity to examine the impact of gravity segregation. The description of each case is shown in **Table 3.8** along with the detailed simulation parameters.

Table 3.8 Case descriptions and detailed parameters for sensitivity study

Parameter	Value	Unit	Definition
D	7000	ft	Reservoir top
G_p	0.5	psi/ft	Reservoir pressure gradient
K_{mi}	0.0001	mD	Matrix initial permeability
C_{fi}	50	mD*ft	Fracture initial conductivity
K_{sf}	0.001	mD	Secondary fracture initial permeability
Φ_m	0.05	N.A.	Matrix porosity
Φ_f	0.001	N.A.	Fracture porosity
P_i	4500	psi	Reservoir initial pressure
T	135	°C	Reservoir temperature
H_f	250	ft	Fracture height
H_{Lf}	500	ft	Fracture half length
S_f	0.45	N.A.	Fracture initial water saturation
S_{sf}	0.2	N.A.	Secondary fracture initial water saturation
R_{sf}	10~30, 4, 5~7 (higher layers); 10~30, 4, 11~13 (middle layers): 10~30, 4, 18~20 (lower layers)	N.A.	Secondary fracture closure zones location Three sensitivity cases

All three cases are developed with the same surface area of the zones of variable conductivity, and only one perforation is open at the horizontal section to connect with the primary hydraulic fracture during the injection process. Case 1 includes the zones of variable conductivity located in shallower formation which are above the horizontal section of the well (from layer 5 to layer 7); Case 2 targets the zones of variable conductivity in the middle of the reservoir (from layer 11 to layer 13), which are adjacent to the horizontal section, and the zones of variable conductivity of Case 3 have been applied lower down in the formation (from layer 18 to layer 20), located at the bottom of the primary fracture.

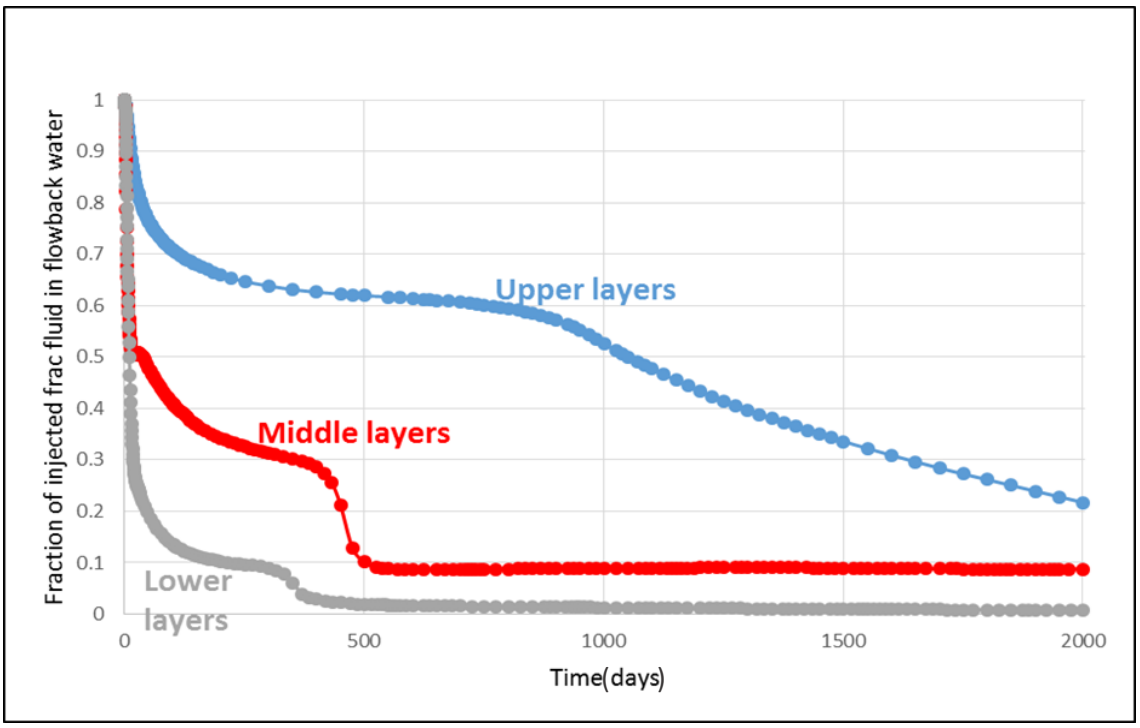

Figure 3.24 Fraction of injected fracture fluid in flowback water in different cases

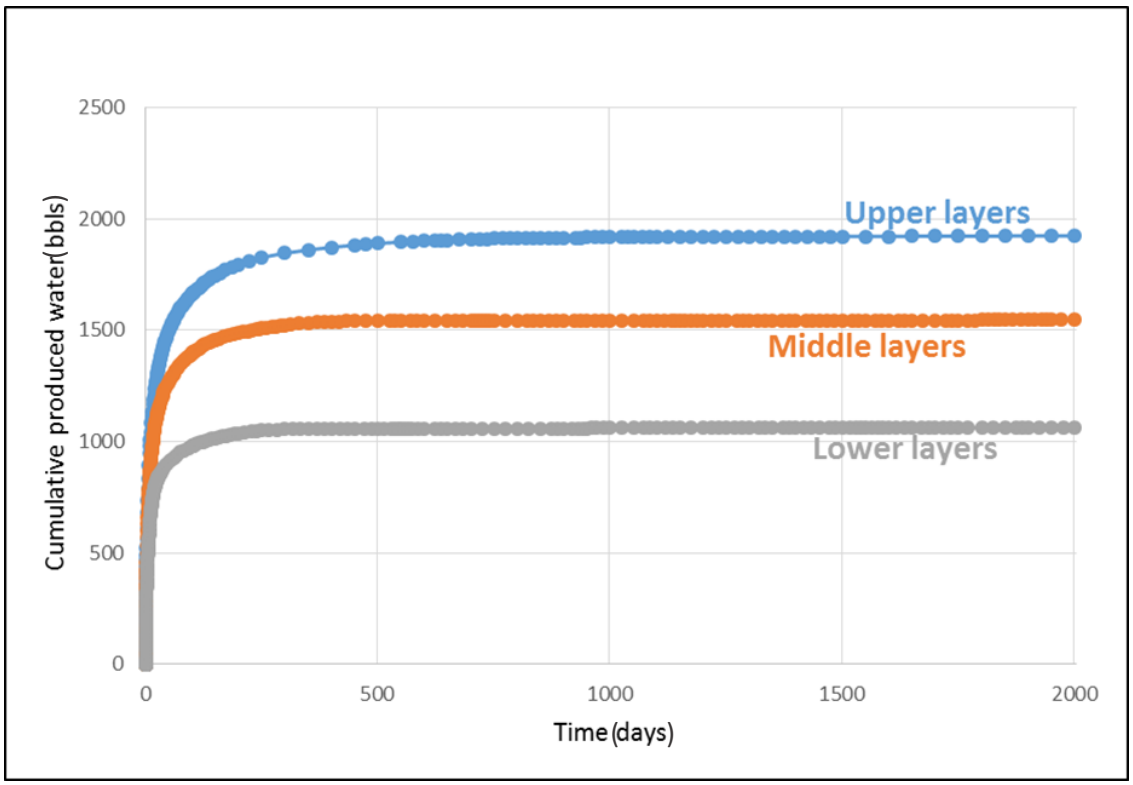

Figure 3.25 Cumulative produced water in different sensitivity cases

As shown in **Figure 3.24** and **Figure 3.25**, the simulation results from different sensitivity cases have been presented. From **Figure 3.24** it can be readily seen that the impact of gravity segregation varies with different locations of the zones of variable

conductivity, affecting the total volume of fracture fluid that flows back. With the lower zones of variable conductivity applied in Case 3, less than 1% of the fracture fluid flows back by the end of the production period; however, as a contrast, there is more than 20% of the fracture fluid produced by the same time in Case 1, which applies the zones of variable conductivity in the upper layers. It also can be seen that the deeper the location the fracture closure takes place, the more significant is the drop in the fraction of injected fracture fluid in the flowback water.

It is known that if the impact of gravity segregation is neglected, the water will be evenly distributed throughout the whole primary fracture while the reservoir pressure draws down. However, by considering the impact of gravity segregation, the water tends to be driven to accumulate at the bottom of the fracture zone, since the vertical conductivity of the primary fracture is high. This will lead to more fracture fluid instantly being trapped in the secondary fractures while the fracture closure is taking place at the bottom of the reservoir.

Additionally, it can also be seen in **Figure 3.24** that the fraction of injected fracture fluid in Case 2 and Case 3 reaches a plateau value at the end of the production, whereas in Case 1 there is still a tendency for it to continue to decrease until the simulation completed. Less fracture fluid has been trapped within the closed fractures in Case 1, which means there is still sufficient water in the system that could be potentially produced back. As a consequence, it will require a longer production period to reach the plateau value of the fracture fluid fraction for Case 1. It also can be interpreted that more water could be produced back from a case which includes the fracture closure zones in the upper layer.

The comparisons of cumulative produced water from each case are shown in **Figure 3.25**. The simulation result verifies that the largest volume of water is produced in Case 1, and, in contrast, the smallest volume of water is produced in Case 3. **Figure 3.26** is a 3D view for water distribution at the end of production in Case 3 which provides a better presentation for the theory discussed before.

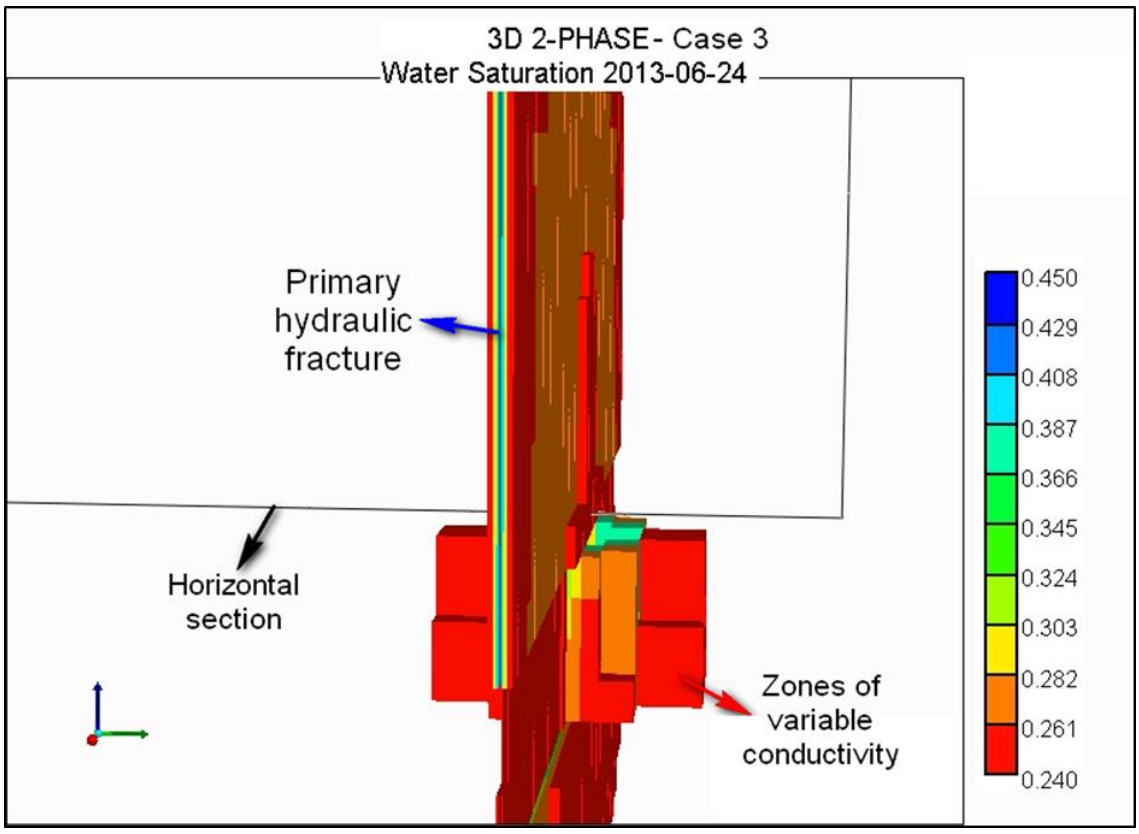

Figure 3.26 Water distributions in 3D view for Case 3

It is well known that the history match is non-unique. In other words, it is possible to achieve the fluid flow history match with various combinations of different surface areas and locations of the zones of variable conductivity. Study of the impact of gravity segregation on water flow can provide a physically justifiable way to achieve a better history match in a simplified shale model.

3.3.4 Further discussion on fluid flow modelling study

3.3.4.1 Dual porosity modelling study based on the single porosity IMEX model

3.3.4.1.1 Dual porosity IMEX modelling setup

It is known that one of the most difficult parameters to evaluate in tight and shale gas reservoirs is the drainage area size and shape; months or years of production are required for conventional well tests to identify these (Holditch, 2006; Jenkins, 2008). As a continuation of the fluid flow modelling study, a further dual porosity shale model has been developed at this step, just being used as a comparison discussion to the history matched single porosity model.

As introduced in the previous section, a shale gas reservoir with shale rock and natural fractures can be typically modelled as a dual porosity system proposed by Warren and Root (1963). The initial model has been created only containing natural fractures, and then a single hydraulic fracture has been established before production. All the matrix properties for the dual porosity model remain the same as the single porosity model, and so are the properties of the horizontal well and hydraulic fractures.

First of all, some parameter values of the dual porosity system need to be calculated and confirmed for the model initialisation. One of them is the natural fracture porosity. It is known that the naturally fractured shale reservoirs contain secondary or induced porosity in addition to their original primary porosity. Induced porosity is formed by tension or shear stresses causing fractures in a competent or brittle shale formation. The natural fracture porosity is usually very small. Values between 0.0001 and 0.001 of rock volume are typical (0.01% to 0.1%). Fracture-related porosity, such as solution porosity in granite or carbonate reservoirs, may attain much larger values, but the porosity in the actual fracture is still very small (Crain, 2015).

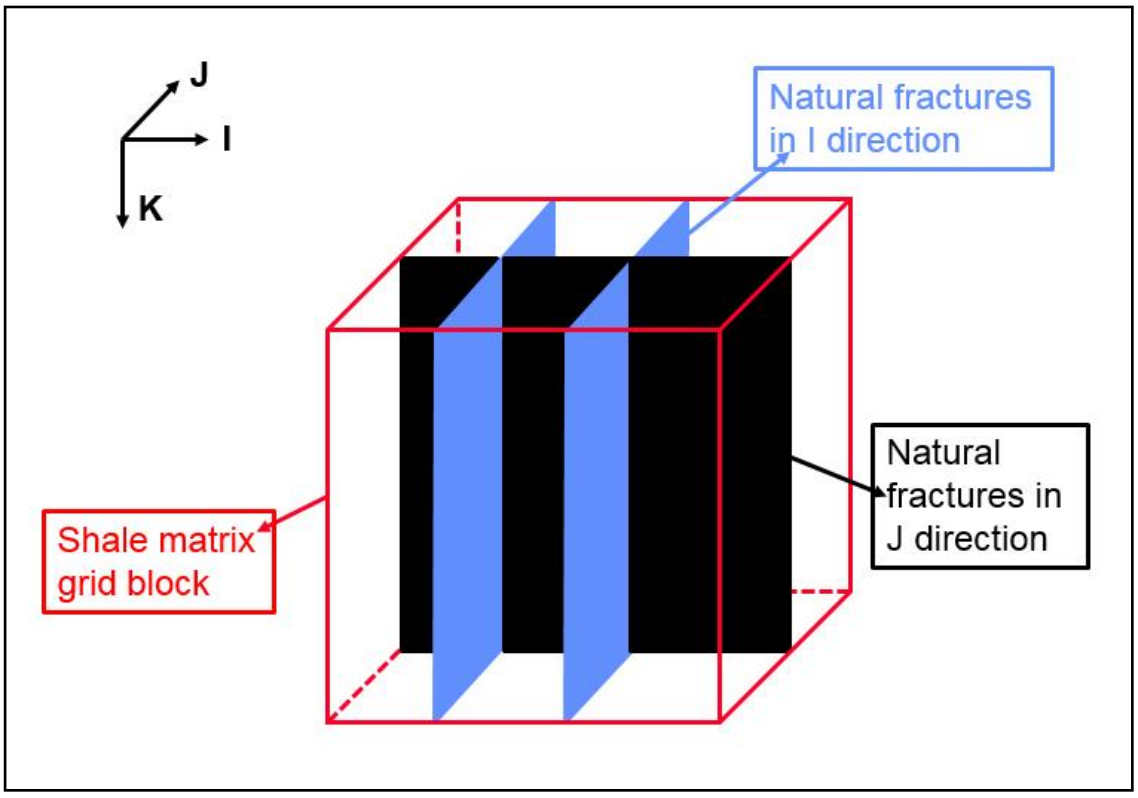

Figure 3.27 Schematic diagrams of the natural fracs in shale matrix grid block

To calculate the natural fracture property, the fracture pattern and spacing need to be addressed first. The schematic diagram for the natural fractures in each matrix grid

block is shown in **Figure 3.27**. As shown in the diagram above, the natural fracture pattern is selected as planar fractures only in the I and J directions (this is the basic assumption for the natural fracture patterns since no more information is available for the HRB and is also used as a representative natural fracture pattern to keep the dual porosity modelling as simple as possible to run). The fracture spacing in the I direction is 25ft and in the J direction is 40ft. There are no natural fractures in the K direction. The size for each matrix grid block in the I and J directions is 50 ft and 200 ft, which means there will be initially two natural fractures in I direction and five natural fractures in J direction, giving a total of seven fractures in each grid block. It is known that the accuracy of numerical simulation is better when the grid block sizes are smaller. However, when dealing with simulation of large shale reservoirs, sufficiently large grid blocks need to be used to reduce the number of blocks in order to be able to generate simulation results of practical value with reasonable computational effort and numerical accuracy. Assuming the natural fracture width is 0.001ft, the volume of fractures in each direction can be calculated using **Equation 3.1**. The total grid block volume is calculated to be 1E05 ft^3.

$$V_{I \text{ or } J} = W * L_{I \text{ or } J} * T \qquad \text{… Equation 3.1}$$

$$\Phi_{NF} = (N_I * V_I + N_J * V_J)/ V_B \quad \text{… Equation 3.2}$$

where $\boldsymbol{W}$ *is the width of the fracture,* $\boldsymbol{L_{I \text{ or } J}}$ *is the grid block size in I or J direction,* $\boldsymbol{T}$ *is the thickness of the grid block,* $\boldsymbol{\Phi_{NF}}$ *is the porosity of the natural fractures in each block,* $\boldsymbol{N_I}$ *is the numbers of fractures in I direction,* $\boldsymbol{V_I}$ *is the volume of fractures in I direction,* $\boldsymbol{N_J}$ *is the number of fractures in J direction,* $\boldsymbol{V_J}$ *is the volume of fractures in J direction and* $\boldsymbol{V_B}$ *is the total volume of each grid block.*

From the calculation of **Equation 3.2** it can be confirmed that the natural fracture porosity is 1.1E-4. As discussed previously, the natural fracture porosity is normally in the range from 1E-4 to 1E-3. The capillary pressure and the relative permeability curves for the natural fractures are the same as for the hydraulic fracture. Meanwhile, all the flows within the fractures are set as Non-Darcy flow with 0.5 ND flow coefficient with the general correlation option (Michel, 2011; Dershowitz, 2010). Tracer is added into the injected fracture fluid to identify the fraction of the fracture fluid in flowback water during the production. As all the properties have been calculated and confirmed, the

initial preparation for the dual porosity shale model is completed (parameters are shown in **Table 3.9**).

Table 3.9 Case descriptions for dual porosity model

Parameter	Value	Unit	Definition
D	7000	ft	Reservoir top
G_p	0.5	psi/ft	Reservoir pressure gradient
K_{mi}	0.0001	mD	Matrix initial permeability
C_{fi}	50	mD*ft	Fracture initial conductivity
K_{sf}	0.001	mD	Secondary fracture initial permeability
Φ_m	0.05	N.A.	Matrix porosity
Φ_f	0.001	N.A.	Fracture porosity
P_i	4500	psi	Reservoir initial pressure
T	135	°C	Reservoir temperature
H_f	250	ft	Fracture height
H_{Lf}	500	ft	Fracture half length
S_f	0.45	N.A.	Fracture initial water saturation
S_{sf}	0.2	N.A.	Secondary fracture initial water saturation
S_{nf}	0.2	N.A.	Natural fracture initial water saturation
R_{sf}	10~30, 4, 18~20 (lower layers)	N.A.	Secondary fracture closure zones location
W	0.001	ft	Width of natural fractures
Φ_{nf}	0.0001	N.A.	Natural fracture porosity
N_i	2	N.A.	Numbers of natural fractures in I direction
N_j	5	N.A.	Numbers of natural fractures in J direction
S_i	25	ft	Natural fracture spacing in I direction
S_j	40	ft	Natural fracture spacing in J direction

3.3.4.1.2 History match for Dual Porosity IMEX modelling

According to the initial simulation results of the dual porosity model, it can be observed that the total volume of flowback water is too high (around 90%) compared with the normal shale production cases (from 10% to 40%). The reason for so much water flow back is the existence of the natural fractures. The natural fractures have higher conductivity than the shale matrix, which will lead to better communications within each grid block – not only the connections between the natural fractures within each block but also the communication for the natural fractures from block to block. This will lead to more *in situ* formation water in the matrix flow back as a result of increasing the total volume of the produced water.

Compared with the single porosity model, another finding from the simulation results shown in **Figure 3.28** is that the produced water fraction keeps on increasing during the

whole production period in the dual porosity model, and this could also be due to the better communication between the grid blocks by including the natural fractures in the system in addition to the faster reservoir pressure draw down. As a contrast, the produced water increases very fast at the beginning of the production and then reaches a plateau value after a year of production in the single porosity model.

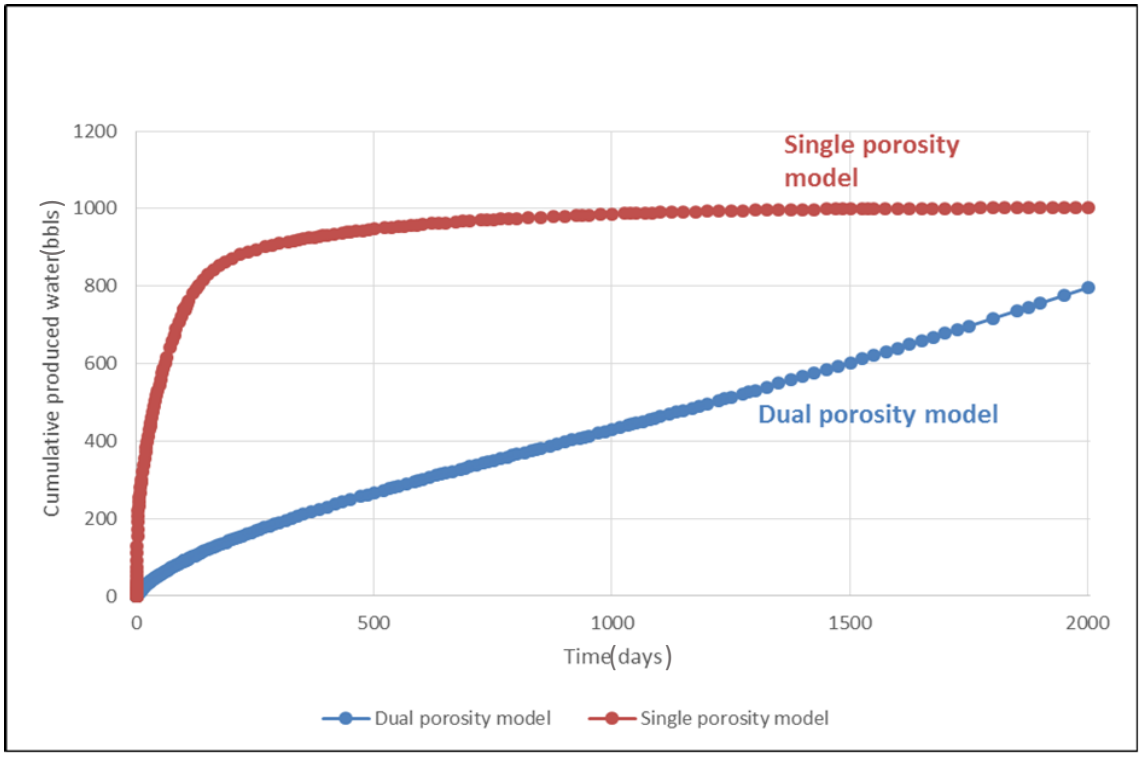

Figure 3.28 Comparison cases for the cumulative produced water in single and dual porosity models

On the basis of previously proposed hydraulic fractured shale system used for history matching in the single porosity model, the application of secondary fracture zone along with variable conductivity area requires to be included in the dual porosity model to try to history match with injected fracture fluid fraction in the produced water.

It is known that the variable conductivity models update block permeabilities and subsequent inter block transmissibilities during the simulation. The variable conductivity zones are applied at the bottom of hydraulic fracture system (as considered the impact of gravity segregation in the fracture zone discussed in section 4.3.3.2). These zones have permeability changing from 50 mD to 1E-7 mD (which makes the zone almost impermeable). The whole updated dual porosity model is developed similar to the single porosity model proposed previously in **Figure 3.18**. The simulation results are shown in **Figure 3.29**.

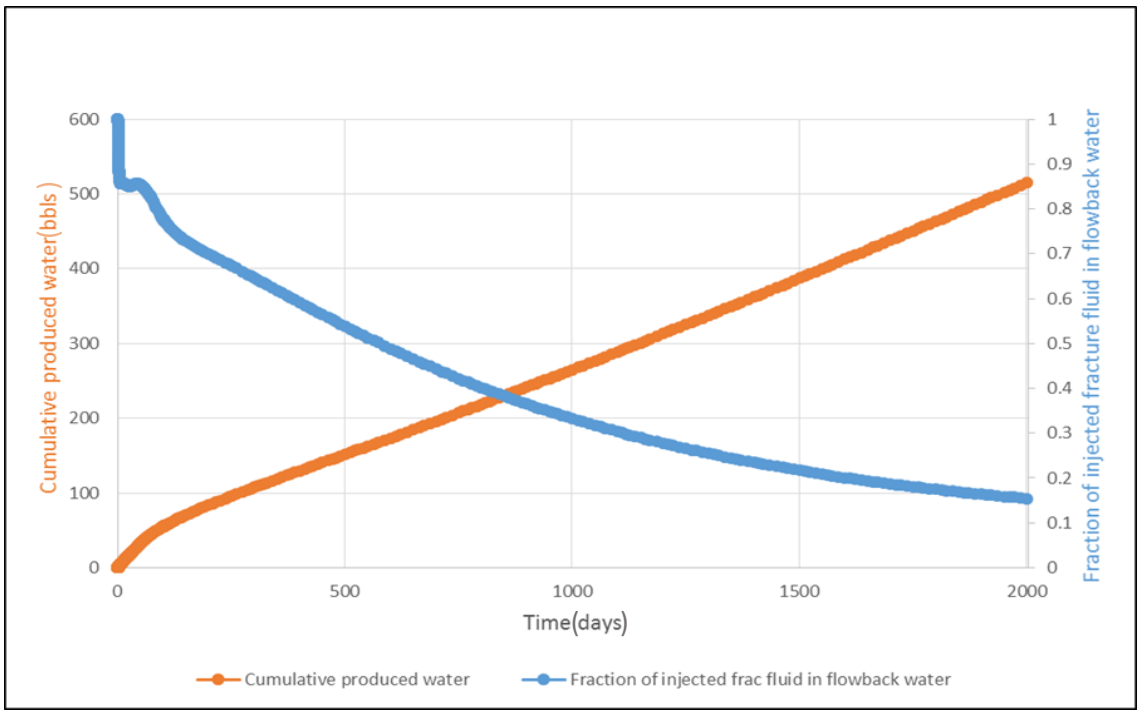

Figure 3.29 Cumulative produced water and injected frac fluid fraction in flowback water vs time

Figure 3.29 shows a decrease in both the cumulative produced water and the fraction of injected fracture fluid in the flowback water compared with the case before, which identifies that the impact of applying the closures in the secondary fracture zone on the fluid flow is significant. However, it can be readily observed that the fraction of injected fracture fluid is still too high, even under the situation that the same total surface area of the secondary closure fractures have been applied compared with single porosity model. This means a larger area of the closed secondary fracture zones must be applied in the dual porosity model.

3.3.4.1.3 Discussion of CMOST optimization study

CMG CMOST allows users to create and run numerical sensitivity experiments using a version of the base case dataset which has embedded instructions that tell CMOST where to substitute parameter values. As all the experiments are completed, the results converge to one optimal solution which should provide a satisfactory history match with the specified parameters if the parameter ranges have been appropriately defined.

The CMOST study of the dual porosity model is used to change different properties related to the natural fractures to approach a best history matching case with total

volume of produced water and also the fraction of injected fracture fluid in the flowback water.

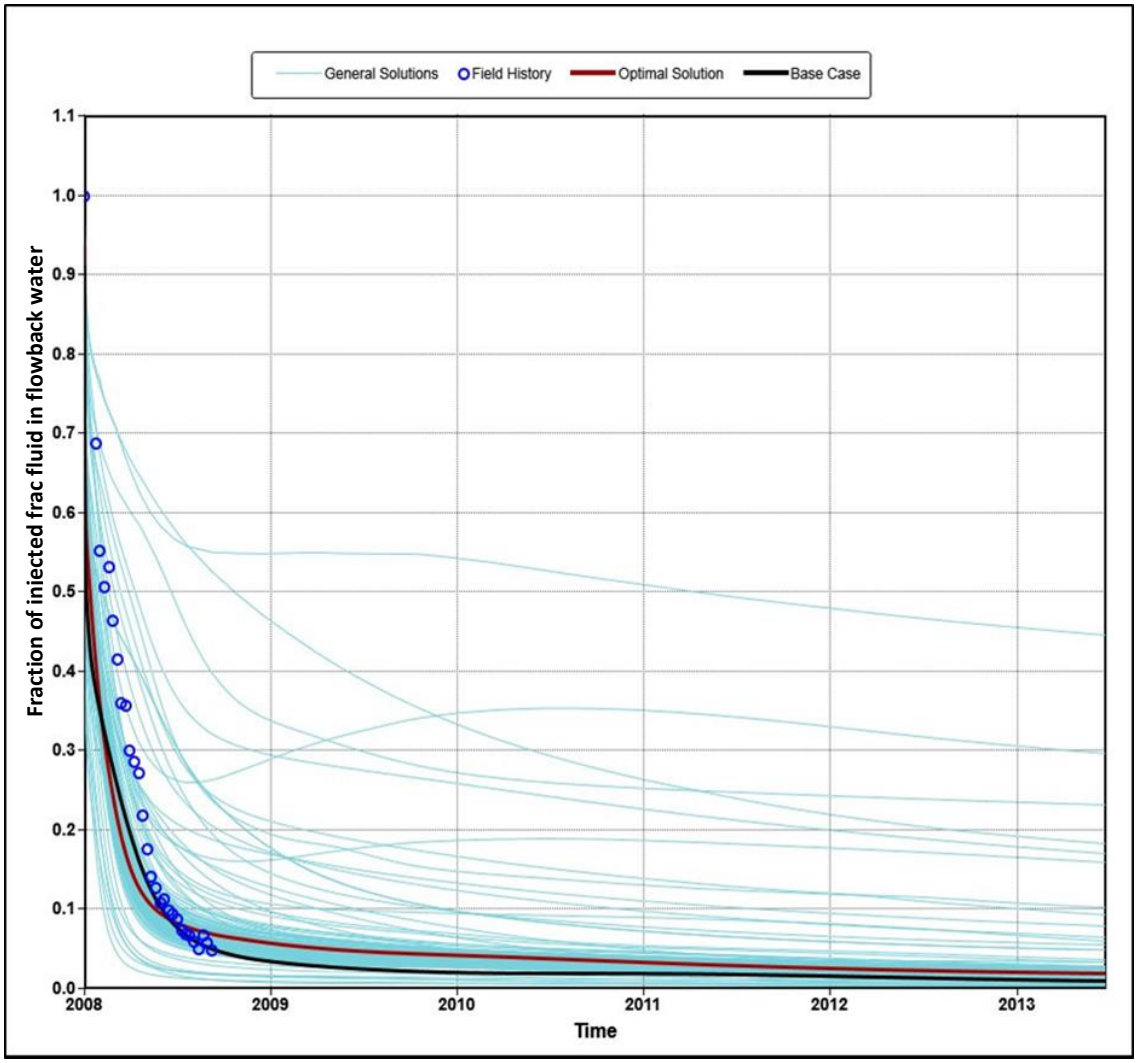

Figure 3.30 CMOST history matching experiment results

Figure 3.30 shows the simulation results from the CMOST history match study. All the green lines represent the general solutions of each experiment with different parameters applied. It can be seen that the base case (black line) gives a fairly good match with the fraction of injected fracture fluid in flowback water, but with too much total water produced (80%); in contrast, the optimal case (red line) does not only match with the injected fracture fluid fraction, but also matches with the total volume of water flows back (25%). All the experiments include the variable conductivity zones with permeability changing; these zones are applied at the bottom of the secondary fracture zone as discussed before. The optimal case is with 20ft fracture spacing in I direction and 48ft fracture spacing in J direction and also applied with slightly higher initial water saturation in natural fractures (40%) and secondary fractures (20%).

Comparing with the single porosity case, it can be identified that the surface area of the variable conductivity zones in the dual porosity model is larger. The explanation can be divided into two parts:

1. With naturally fractured matrix, each matrix block has a better conductivity, especially for the grid blocks adjacent to the primary fracture (the secondary fracture zone); meanwhile, all the natural fractures are also applied with zero capillary pressure (the same as for the primary hydraulic fracture). This will lead to relatively more water produced back before applying the variable conductivity zones in the dual porosity model compared with the single porosity model; as a result, a larger surface area must be applied;

2. As the secondary fracture zone is close to the primary fracture, the pressure drop in these grid blocks responds faster than for the blocks away from the primary hydraulic fracture. It has been reported that during the production process, not only the micro secondary fractures will close due to the pressure draw down, but also the micro cracks from the naturally fractured shale will also exhibit a similar behavior (Pervukhina et al., 2010, 2011; Shapiro, 2003). This will potentially enlarge the surface area of the closure zones during the production.

3.4 CONCLUSIONS

Before drawing the conclusions of this chapter, the two questions proposed in the introduction section at the beginning of this chapter are going to be addressed first:

1) It is possible to develop a simplified numerical modelling (including some basic considerations for hydraulically fractured shale system instead of applying them all) to represent the whole hydraulic fracturing and shale gas production processes;

2) This simplified numerical model is able to provide an optimal history match with total volume of produced water and even the fraction of injected fracture fluid in flowback water. In addition, it means the geochemical modelling study for the next step is able to be developed on the basis of this history matched simplified shale model.

Some of the conclusions drawn from this chapter list below can be used as explanations to the questions of "what causes the significant retention of injected fracture fluid within shale gas system?"

- The single porosity hydraulic fractured shale model is not a nanoscale/pore-scale geomechanical model; instead it is a simplified fluid flow model used only to study the fracture fluid retention mechanisms during shale gas production. However, the simulation results demonstrate that it is still a representative model for unconventional recovery by comparison with other complex shale models.
- The primary hydraulic fracture along with the adjacent induced secondary fractures is account for the dominant paths for fluid flow within the stimulation area after the completion of the hydraulic fracturing process.
- In order to achieve an initial history match with injected fracture fluid fraction in produced water, the closures in secondary fractures require to be simulated in terms of applying variable conductivity zones within the secondary fracture area. It is believed that a better history match can be achieved with the zones of variable conductivity located at the lower area of the fracture zone due to the impact of gravity segregation in a higher conductivity area.
- A dual porosity model can also deliver a good match for both of the total volume of produced water and the fraction of injected fracture fluid (by using the optimization function in CMG CMOST). However, it is a more complex model compared with the single porosity model already developed; furthermore, the single porosity model also provides better matching with injected fracture fluid fraction in produced water, and so this model is used for the remainder of this study.

CHAPTER 4 GEOCHEMICAL MODELLING STUDY

4.1 INTRODUCTION AND CHAPTER CONTENT

In a mature shale gas reservoir, many horizontal wells may have been drilled and stimulated with the hydraulic fracturing process. Due to the lack of knowledge of *in situ* formation water compositions, the risk of inorganic scale deposition can be difficult to quantify, but scale damage has often been shown to be very significant.

As discussed previously, both of conventional and unconventional oil and gas reservoirs may generate inorganic precipitations such as $CaCO_3$, $BaSO_4$, FeS, etc. To prevent/control the deposition of these scales can effectively maintain the hydrocarbon recovery, avoid formation damage, and extend the operating time of the production facilities. To better understand the scale forming process and also to evaluate the scaling risk, various calculations should be performed. These are not confined to the study of field data (such as produced water flows rate, flowback water compositions, mineralogy information, etc.), but also include the prediction of the scaling tendency from simulation results using reactive transport modelling.

Some of the shale gas field operators in US have already add scale inhibitor into the fracture fluid so that scale deposition during shale gas recovery could be reduced or even prevented (Spicka, 2017). However, scale inhibitor optimization is still an important topic to be addressed before performing any injection operations.

The prediction and evaluation of scaling risk needs to be undertaken prior to any decision relating to a specific scale control plan. In Chapter 3, a work flow for scaling tendency prediction, based on data analysis and calculation of *in situ* formation water composition has presented. The discussion centred on the analysis of field data collected in the HRB area, and numerical modelling was not included in that stage of the discussion.

Firstly, this chapter aims to use geochemical modelling as a tool to make further improvement on addressing the question of "what causes the altered high salinity brine produced back during shale gas production?" In order to achieve a better understanding of this question, a geochemical reaction model needs to be developed. Secondly, this chapter aims to better illustrate scaling tendency prediction from the perspective of

geochemical simulation results to provide further recommendations for scale control management.

At the beginning of this chapter, it introduces a simple mineral dissolution model developed in PHREEQC to discuss the impact of mineral dissolution on high barium concentration in the flowback water. In the following section, some further simulations have been performed based on a single phase 1D geochemical model developed in CMG GEM. This 1D GEM model provides further insights into mineral dissolution during injection and production processes and its impact on initial water compositions. A two phase 3D geochemical GEM model will be developed at the end of this chapter. It has been applied with certain chemical reactions included, to improve on the observations of scaling risks for shale production systems.

The objective for this chapter is to draw a comprehensive picture of scale deposition taking place during shale gas production.

4.2 MINERAL DISSOLUTION MODEL IN PHREEQC

The impact of mineral dissolutions on the high barium concentrations observed in flowback water is discussed in this section.

From the previous HRB geochemical data analysis in Chapter 3 it can be observed that the barium concentration is high in the flowback water (around 1500 ppm), compared with its value in fresh water fracture fluid (0 ppm). According to the mineralogy data provided, the only mineral which contains barium is barite in this shale gas reservoir. However, it is known that the solubility for barite is extremely low in the water, so barite dissolution cannot be the main source of the high concentrations of barium observed.

It is reported that barium concentration in water is determined by the solubility of barium salts and the adsorption of barium on active clay surfaces. Soluble barium compounds are mobile in the environment and have been detected in surface water, groundwater, drinking water, and sediment. High levels of barium can be found in groundwater due to leaching and eroding of barium from sedimentary rocks and coal. Barium occurs naturally in soils with high levels of limestone, feldspar and shale deposits (Davis, 1992).

Due to the limitation in obtaining samples of shale from the gas field and performing experiments to test the mineral dissolution process, some studies are going to be performed on analogue systems. Although, it is reported that the solubility of barite and witherite is extremely low in fresh water, nevertheless, a simple dissolution model was developed using PHREEQC to help better understand the high barium concentration in the flowback water. For this mineral dissolution model, witherite is used as the main barium rich mineral in the system.

Table 4.1 Fracture fluid composition used in mineral dissolution model

Ions in Frac Fluid	Na	K	Ca	Mg
Unit: mmol	4.3516	0.0767	7.4854	0.9463
Ions in Frac Fluid	Ba	Sr	S(6) as SO_4	Cl
Unit: mmol	0	0.000126	0	19.744

The fracture fluid is used as the solution and several minerals recorded in the database are introduced as the source of dissolution. **Table 4.1** shows the fracture fluid composition used in the model (the fracture fluid pH is 7 and the temperature is 140 °C - reservoir conditions). The ion concentrations in this table are the validated values by charging balanced. Some calculation results of the mineral dissolution model in PHEEQC are shown in **Figure 4.1**.

Cl_mg/kgw	Ba_mg/kgw	SO4_mg/kgw	Na_mg/kgw
7.0000e+02	0.0000e+00	0.0000e+00	1.0000e+02
7.0000e+02	1.5237e+03	2.2231e+01	1.0000e+02

Figure 4.1 Calculated ion concentrations from mineral dissolution model in PHREEQC

By changing the saturation index (SI) of the mineral at equilibrium (a technique used in the geochemical model to accommodate altered solubilities), it can be found that only when the saturation index of witherite equals to -0.3 can the barium be dissolved up to a concentration of ca. 1,524 ppm. However, it is reported that the saturation index of witherite for lake water, stream water or ground water is in the range of -3.3 to -5 (Jaremalm et al., 2013), which means this saturation index used for obtaining a high barium concentration in the dissolution model must be inaccurate and unrealistic. It also illustrates that only accounting for the mineral dissolution as the reason leads to high barium concentration in flowback water is insufficient (and barite is even less soluble than witherite).

Another interesting finding from the calculation results is the sulphate concentration in the brine. The initial sulphate concentration is set to be 0 ppm but due to the dissolution of anhydrite introduced into the system, an increase of sulphate concentration has been observed at the end of the calculation. Nevertheless the final concentration of sulphate is less than expected and this is on account of the increase in barium concentration dissolved into the brine.

Overall, on the basis of the previous validation of the high salinity of formation water (presented in Chapter 3) along with the discussion of the mineral dissolution model, a conclusion can be drawn – in the Horn River Basin area, the fluid mixing between the fracture fluid and high salinity *in situ* formation water is the dominant factor that leads to the altered high ion concentrations in the flowback water.

4.3 SINGLE PHASE 1D GEM MODELLING STUDY

Before the start of the simulation of the two phase 3D system, a series of simplified single phase (water) 1D GEM models has been developed to continue the study of the impact of mineral dissolution on initial water composition (formation water). This is a stage of preparation discussions in prior to the modelling study of scaling risk prediction within shale system and these simulations are simply conducted to further address the question of what ion concentrations could be consistent with the *in situ* water reaching equilibrium where certain minerals are included in the system. It can provide some additional justifications towards the development of compositional 3D simulations in the following section. The diagram of the model used in this study is shown in **Figure 4.2**.

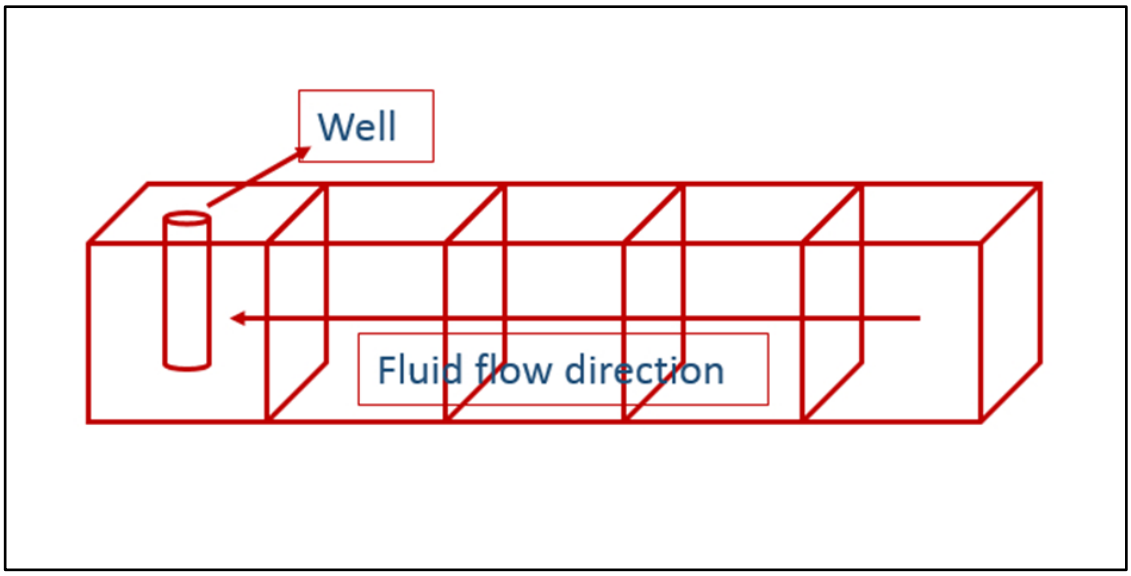

Figure 4.2 Illustration diagram of 1D GEM model

```
176
177 *MOLALITY-AQUEOUS
178  'Ba++'       'SO4--'        'Ca++'      'Na+'      'Cl-'
179  0.001597     0.00001        0.00577    0.023661    0.0499
180
```

Figure 4.3 Original ion concentrations applied in 1D GEM model

As indicated in **Figure 4.2** the base case model contains 5 x 1 x 1 grid blocks, with block sizes of 10 x 1 x 10 ft. The reservoir temperature and pressure are 135 °C and 4,500 psi, respectively, which are consistent with the initial reservoir conditions. The matrix permeability and porosity are set to 10 mD and 25%, respectively; both are much higher than the typical shale reservoir permeability and porosity (normally 0.1 nD and under 10%). No capillary pressure has been applied in the grid blocks and the initial water saturation is 25%. All the relevant parameters are shown in **Table 4.2**.

Table 4.2 Parameters for 1D GEM model

Parameter	Value	Unit	Definition
D	7000	ft	Reservoir top
G_p	0.45	psi/ft	Reservoir pressure gradient
K_{mi}	10	mD	Matrix initial permeability
Φ_m	0.25	N.A.	Matrix porosity
P_i	4500	psi	Reservoir initial pressure
T	135	°C	Reservoir temperature
S_{wi}	0.25	N.A.	Reserrvoir initial water saturation

The reason for using all of these non-shale properties in the 1D GEM model is due to the aim of these 1D GEM simulations, which is to focus on the impact of mineral dissolution on the initial brine salinity, which means to make the fluid propagation easier within the system it is not necessary to involve a more complex discussion of fluid flow in shale properties. Only reservoir pressure and temperature are required to be constant compared with the shale flow modelling (the two major factors account for the equilibrium process of mineral dissolutions).

One well is located in block 1, 1, 1 and it is controlled to be shut-in or injecting from the start and then followed by a further production period in each different simulation case. Each case is run with different minerals (anhydrite, barite or both) defined under the initial conditions, and the *in situ* water composition (the original compositions are indicated in **Figure 4.3**, the unit used is molality – mole/kgH_2O) has been repeatedly validated by using the last equilibrated ionic concentrations from each simulation result. A brief description for all the 1D models is presented in **Table 4.3**. Due to the consideration of providing sufficient brine equilibration time with minerals in place, each of the cases have been applied with adequate shut-in period to assure the brine is completely equilibrated (e.g. the maximum equilibration time for anhydrite in pure water solution requires at most 10hrs (Robert, 2005) and the equilibration time is far smaller for barite due to its extremely low solubility in pure water). The validated ion concentrations for each case compared with the original brine composition are also listed in **Table 4.4**.

Table 4.3 Descriptions for 1D GEM models

Case ID	**Case 1**	**Case 2**	**Case 3**	**Case 4**
Mineral(s) in place	Anhydrite only	Barite only	Anhydrite + Barite	
Operation strategies	Shut-in(4 years), Produce(5 years)			Shut-in(1 year), Inject(3 years), Produce(5 years)

Table 4.4 Validated molality of ions for different 1D case

Case ID	Validated molality of ions (mol/kgH_2O)				
	Ba	**SO_4**	**Ca**	**Na**	**Cl**
Original	0.0016	Finite small	0.0058	0.024	0.05
Case 1		0.0007	0.048	0.024	0.05
Case 2	6.56E-06	0.0002		0.024	0.05
Case 3	5.97E-07	0.0035	0.0053	0.024	0.05
Case 4	5.97E-07	0.0035	0.0053	0.024	0.05

As indicated in the tables above, first of all, Case 1 uses the original formation water composition as the *in situ* water composition, and applies a period of four years shut-in before production to provide plenty of time to equilibrate the brine in case the initial water is under saturated. According to the simulation results, it can be observed that there is anhydrite dissolution taking place during the shut-in period, which identifies that the original water is under saturated with respect to this primary mineral – something that is not possible. After the repeated iterations altering the initial water composition, it reaches equilibrium, and the final ion concentrations have been confirmed. It is found that the initial *in situ* water contains a higher calcium concentration (eight times more than original) and relatively low sulphate concentration, at equilibrium with the anhydrite mineral.

The simulation result for Case 2 shows a finite low barium concentration and also a reduction in sulphate concentration in the validated initial brine. By considering that Case 2 only contains barite as the mineral in place, the finite low barium in the initial water could only be accounted for by the extremely low solubility of barite in water.

Case 3 contains a combination of anhydrite and barite under the initial conditions. Due to the increase in sulphate concentration (dissolved from anhydrite), less barium and calcium are found in the validated initial water, and also the observed calcium concentration reaches the same level as is found in the original supplied water composition.

Case 4 has been developed to help to better understand the impact of injecting fracture fluid when primary mineral dissolution may take place, in a simplified 1D geochemical model. The initial water composition applied in Case 4 is the same as in Case 3, and

also the injected water composition is the same as the fracture fluid composition collected from the wells in the HRB area.

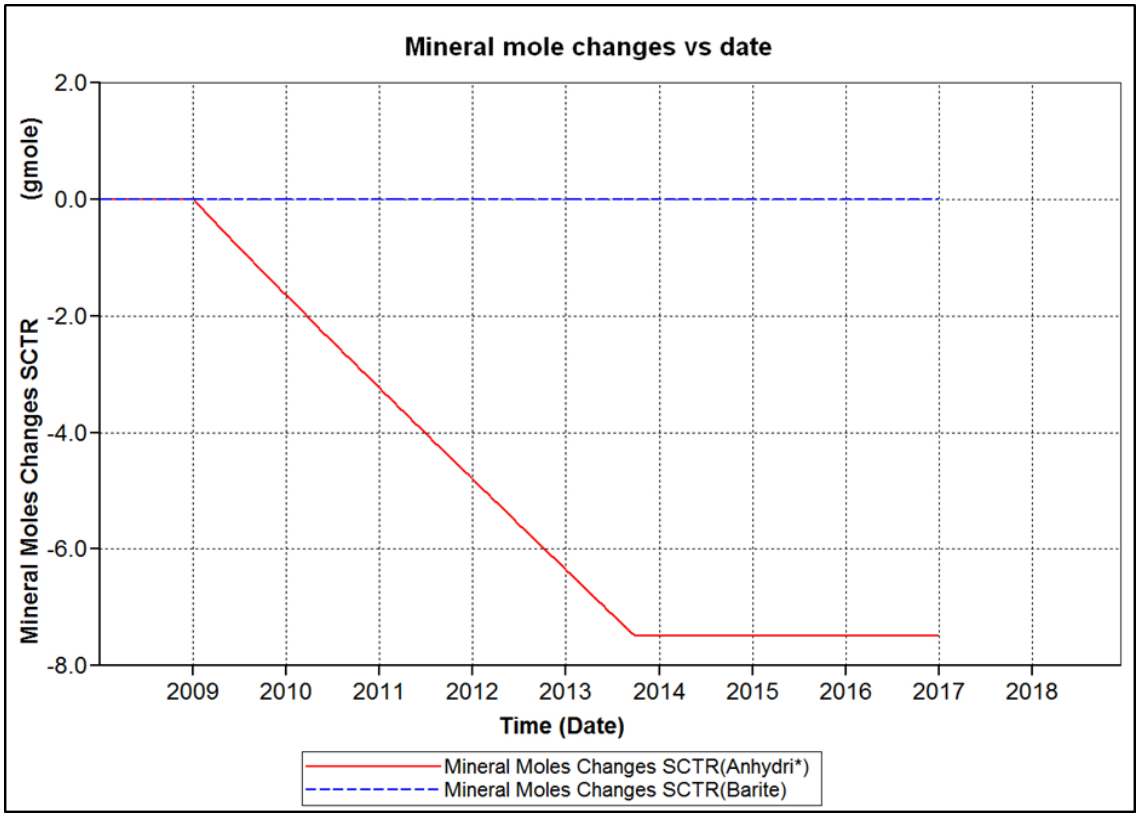

Figure 4.4 Anhydrite and barite mole changes for Case 4 vs time

Figure 4.4 shows the plot of mineral change from the simulation results of Case 4. It can be seen that mainly anhydrite and only a very small quantity of barite (the indication of barite change is not obvious in the plot since the larger scale of the Y axis has been applied) are dissolved due to the injection of low salinity/under saturated water before the production process; it is observed that the low solubility of barite relative to anhydrite explains why so little barite dissolves.

In conclusion of the 1D GEM modelling studies, with the existence of both anhydrite and barite as primary minerals in the shale system, the equilibrated initial water requires some sulphate and a finite amount of barium to be present. However, if high barium concentration has been observed in the field data then, as a consequence of this, a finite and low sulphate concentration will also be observed. A high concentration of calcium will also be observed to ensure equilibrium with the anhydrite.

The water composition discussion from the 1D simulation results is also considered as consistent by comparison with the previous calculated formation water composition.

Additionally, this can be used as further evidence to prove that the whole water chemistry prediction in Chapter 3 is justifiable. It also shows that the mineral dissolution with the injection of fracture fluid cannot be the major reason that causes high barium concentration in the formation water since the increase in barium from dissolved barite is finite and low.

4.4 TWO PHASE 3D GEM MODELLING STUDY

4.4.1 Two phase 3D GEM modelling with mineral reactions

In the previous section of this chapter, a discussion of mineralogy and shale aquifer salinity was presented to verify that the salinity of the *in situ* formation water in the Horn River Basin (HRB) could potentially be quite high. Meanwhile, an extended modelling study has been developed based on the hydraulic fractured shale system; this has been proposed previously in order to approach a more reliable model to identify the fluid flow mechanisms within the shale gas reservoir. As a continuation of the geochemical modelling study, a further two phase 3D GEM model has been developed to examine the scaling tendency during the production due to the evolving brine composition over the lifetime of the well.

This series of 3D geochemical models has been set up using the CMG GEM simulator, and consists of 40 X 20 X 30 cells, each 50 ft X 200 ft X 10 ft in size. Only one horizontal well is present in the model, and it is used as both of the injection well (during pumping of the fracture fluid) and the production well. The grid blocks have been locally refined around the well to represent the fracture zone (including primary hydraulic fracture and secondary fractures). All the parameters related to reservoir properties and hydraulic fracturing design has been applied in consistent with single porosity IMEX model introduced in Chapter 4 which is based on representative values from the HRB area (Doe, 2013; Zhang, 2009). **Table 4.5** shows a summary of some parameters used for the model.

Table 4.5 Summary of main parameters used for modelling

Parameter	Value	Unit	Definition
D	7000	ft	Reservoir top
G_p	0.5	psi/ft	Reservoir pressure gradient
K_{mi}	0.0001	mD	Matrix initial permeability
C_{fi}	50	mD*ft	Fracture initial conductivity
K_{sf}	0.001	mD	Secondary fracture initial permeability
Φ_m	0.05	N.A.	Matrix porosity
Φ_f	0.001	N.A.	Fracture porosity
P_i	4500	psi	Reservoir initial pressure
T	135	°C	Reservoir temperature
H_f	250	ft	Fracture height
H_{Lf}	500	ft	Fracture half length
S_f	0.45	N.A.	Fracture initial water saturation
S_{sf}	0.2	N.A.	Secondary fracture initial water saturation
R_{sf}	10~30, 4, 18~20 (lower layers)	N.A.	Secondary fracture closure zones location
M_r	barite, anhydrite, calcite	N.A.	Mineral reactions in model

Different from the previous model developed using CMG IMEX, the GEM compositional model includes the aqueous and mineral reactions in the system (the detailed simulation code has been included in **Appendix 3**). Initial *in situ* formation water composition has also been applied based on the calculation results from the previous study presented in chapter 3 (Ishkov, 2015). The composition of the aqueous injection fluid has also been selected to match the fracture fluid compositions from field data (Towers, 2011). Both the fracture fluid composition and the formation water composition used for the GEM model are shown in **Table 4.6**. The whole injection period still lasts for one day and there is no shut-in period before the well is brought back on production. The total volume of fracture fluid injected is 3000 bbls.

Table 4.6 Compositions of fracture fluid and formation water used for GEM modelling

Ions	Ca	HCO_3	Cl	Ba	SO_4	Na	TDS
Fracture fluid concentration (ppm)	296	0	740.4	0	100	93.9	1230.3
Fracture fluid molality (gmol of ion/kg H_2O)	0.0003	0	0.00074	0	0.0001	9.40E-05	N.A.
Formation water concentration (ppm)	5500	529	47564	1522	0	22553	82639
Formation water molality (gmol of ion/kg H_2O)	0.0058	0.0006	0.0499	0.0016	0	0.0237	N.A.

The initial GEM model includes the full brine composition definition in the formation water and in the fracture fluid, and three mineral reactions (barite, anhydrite and calcite) have also been included in the system for different simulation cases.

Meanwhile, the initial volume fraction of each mineral with respect to bulk volume of rock is set to be the same in order to observe the impact of mineral dissolution on the flowback water composition in these initial calculations. The simulation results from base case are shown in **Figures 4.5**, **4.6** and **4.7**.

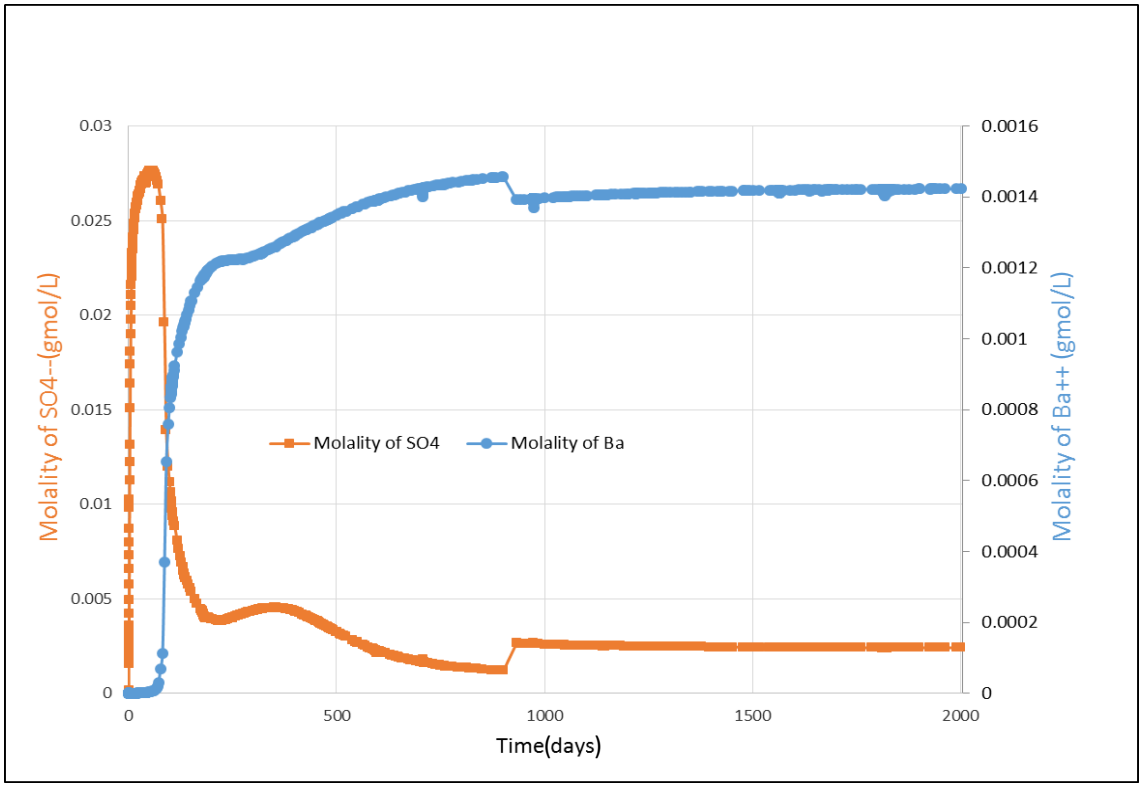

Figure 4.5 Molality of Ba and SO_4 in flowback water vs time, assuming mineral reactions can occur

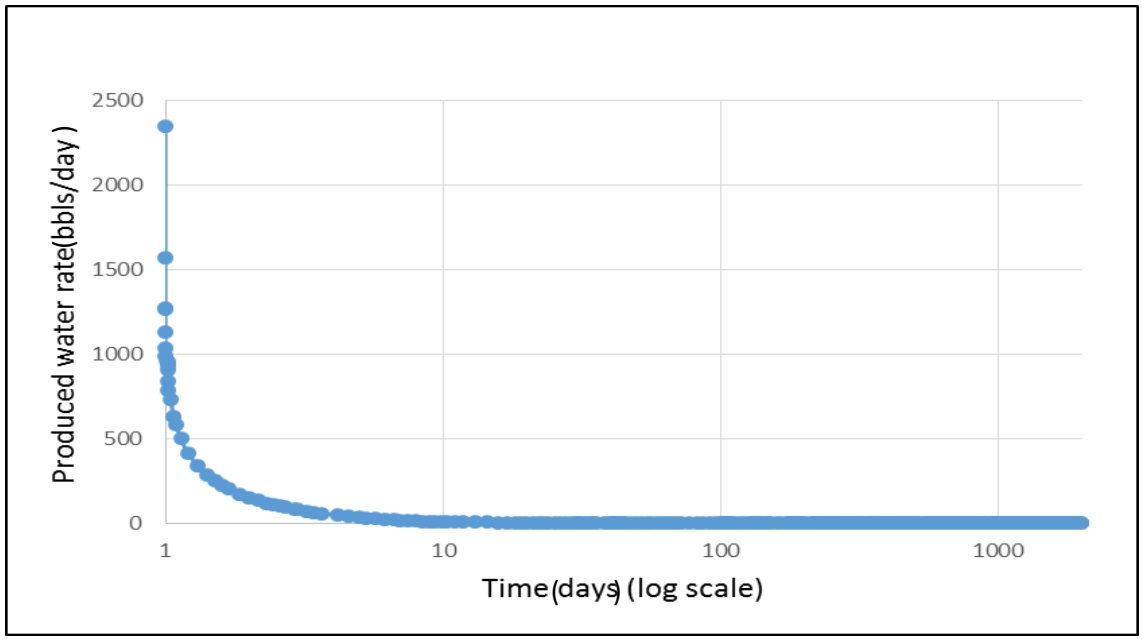

Figure 4.6 Produced water rate vs time on log scale

Figure 4.5 shows the molality of barium and sulphate in flowback water during production. It can be seen that significant concentrations of sulphate have been produced at the early period of production due to the fraction of fracture fluid in flowback water being high at the beginning; there is abundant sulphate in the fracture fluid by comparison with the sulphate concentration in the formation water. This contributes to the retardation of barium during the same period, since there is $BaSO_4$ precipitation due to the commingled flow of the two brines containing barium and sulphate. The chemical equation for depositing barium sulphate precipitation is shown as below.

$$\mathbf{Ba^{2+} + SO_4^{2-} = BaSO_4}$$

Once the sulphate reaches a peak concentration it then drops very sharply, which is in response to the fast decrease of the fracture fluid fraction in the flowback water during the early stages of production. However, the peak concentration of sulphate is much higher than the initial sulphate concentration in the fracture fluid, which indicates that both deposition and dissolution processes are taking place during the early period of production.

During the following production, a trend can be observed with the molality of barium increasing and sulphate decreasing, ending with both concentrations reaching a plateau value. Meanwhile, higher sulphate and lower barium are observed at the end points compared to the initial ion concentrations in the fracture fluid and formation water. This can be also interpreted as evidence that the whole process includes a combination of precipitation and dissolution taking place.

Figure 4.7 shows a 3D view of the mass of $BaSO_4$ deposition change at the end of production (mass change is indicated by the unit of gram mole minerals – zero value represents there is no precipitation nor dissolution taking place and positive value represents the generation of mineral deposition). It can be observed that the greatest $BaSO_4$ precipitation has taken place in the area along the production well and adjacent to the bottom of the fracture zone. The interpretation of this observation is that it is due to the refined perforations being switched open during the production to enhance the communication between the secondary fracture zone and the horizontal section of the well, and also the application of a variable conductivity zone at the bottom of the fracture area to simulate the process of secondary fracture closure. In other words, the

simulation results indicated in **Figure 4.7** do meet our expectations of where the worst scale deposition could take place – the whole fracture area (primary hydraulic fracture and secondary induced fractures) where the major fluid transportation and storage occurs.

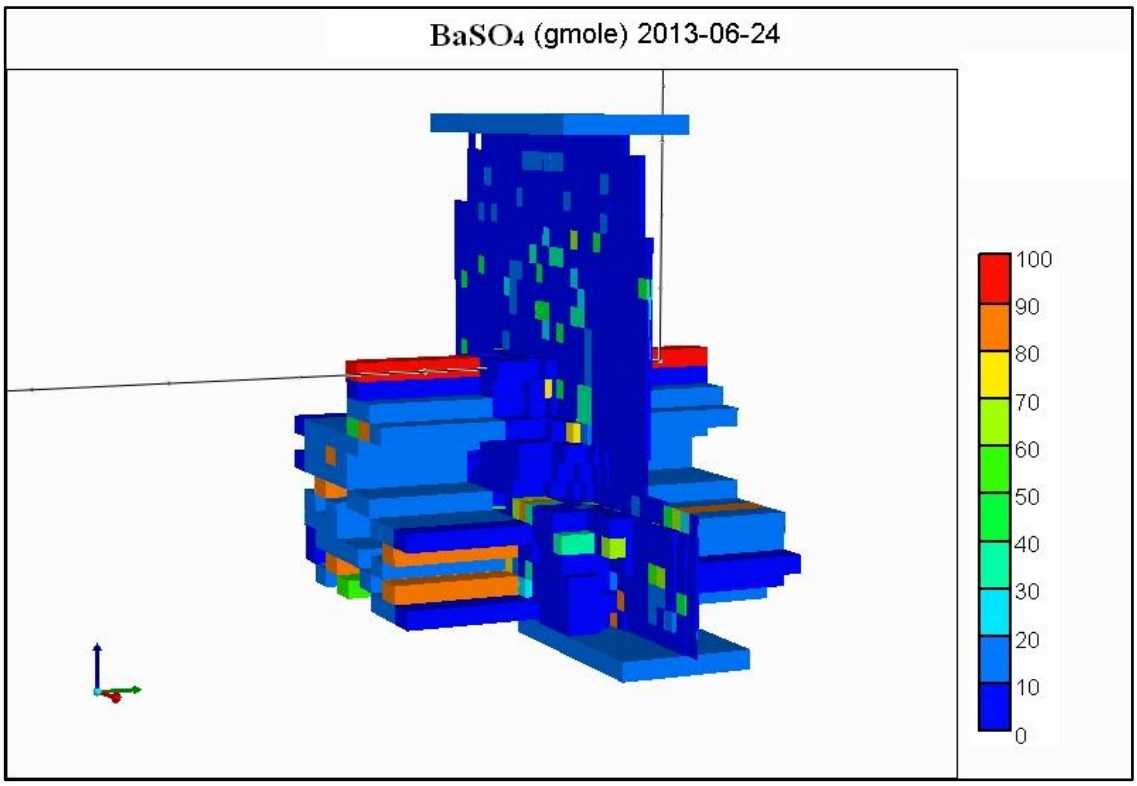

Figure 4.7 3D view of $BaSO_4$ deposition at the end of production

The exact mass of barium and sulphate in the flowback water should be calculated in order to better predict the scaling tendency. The produced water rate (shown in **Figure 4.6**) is also required to calculate the exact mass of ions flowing back in the produced water. A calculation based on **Equation 4.1** is used to obtain the results for further analysis.

$$Mass\ of\ ion\ \left(\frac{gmol}{day}\right) = Molality\ of\ ion\ \left(\frac{gmol}{L(water)}\right) * Produced\ water\ rate\ \left(\frac{bbls}{day}\right) * \frac{L}{bbls}$$

Equation 4.1 Mass of ion calculation

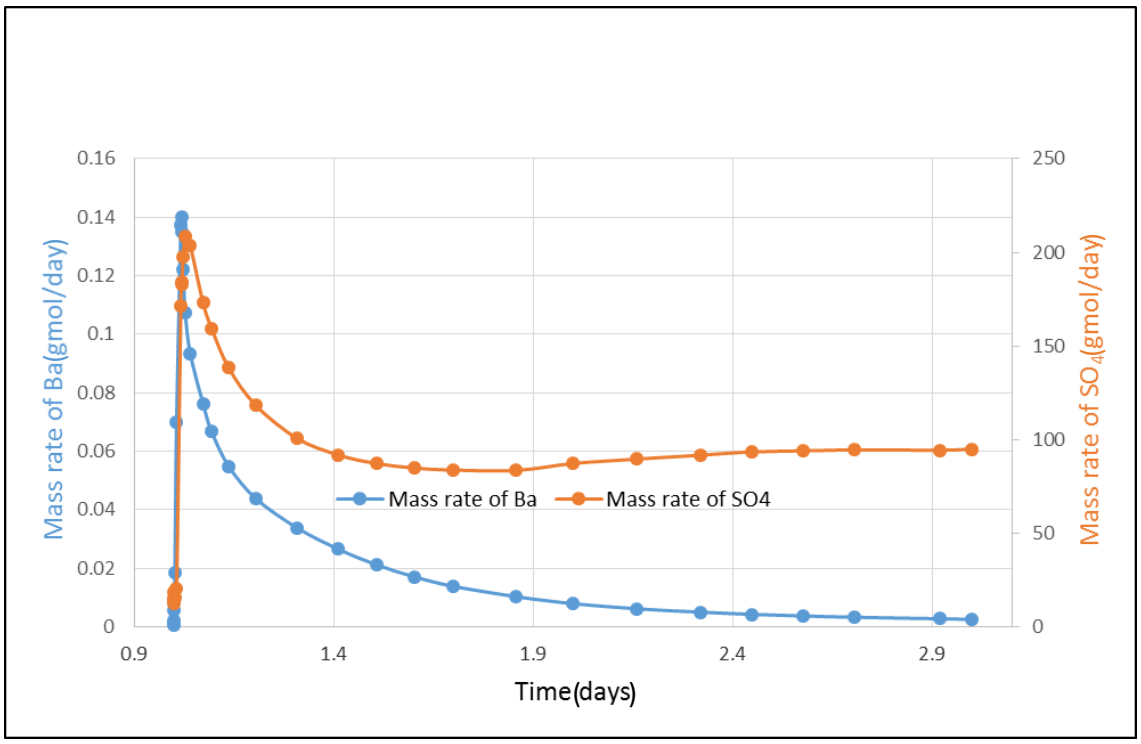

Figure 4.8 Mass rates of Ba and SO_4 vs time, assuming mineral reactions can occur

The calculation results for the mass of ions in the flowback water are shown in **Figure 4.8**. Although the barium concentration (1522 ppm) in the formation water is much higher than the sulphate concentration (100 ppm) in the fracture fluid, the maximum mass flux of sulphate is still significantly more than the mass flux of barium. The interpretation for this is that the majority of the water flows back during the early stages when it is composed mainly of fracture fluid (as indicated in **Figure 4.6**). The plot also indicates that both of the ions reach their peak values very soon after the well is brought onto production (around 44 minutes into the production period).

4.4.2 Two phase 3D GEM modelling without mineral reactions

The maximum mass of ions flowing does not reflect the "worst" scaling risk, since there is precipitation taking place in the reservoir and fracture, and so another GEM model is required to help to obtain the possible "worst" case scaling tendency, which would occur if scale inhibitor were applied in the frac fluid, and thus the ions remained in solution – and so it would be important to know the maximum possible scaling tendency of the produced brine. In conventional production we do not face this issue, as scale deposition deep within the reservoir could not be impacted by application of scale inhibitor; however, in the case of fracture fluid injection, it is possible that all scaling ions could be kept in solution until the brines are being produced into the wellbore.

As discussed previously, it can be seen from **Table 4.6** and **Figure 4.5** that there would be a scaling tendency for $BaSO_4$ precipitation during production due to the existence of high barium and sulphate concentrations in the fluids, and this has also been demonstrated by analysis of the geochemical simulation results previously. Taking this into consideration, the simplified GEM compositional model only includes the ions of Ba, SO_4, Na and Cl in the aqueous phase to calculate the "worst" case amount of barium and sulphate in the flowback water so that the scaling risk can be evaluated and addressed. The simulation parameters are the same as shown in **Table 4.5** but without applying any mineral reactions. No mineral or aqueous reactions have been included in this model, which assumes the fracture fluid and formation water are involved in a simple mixing process, but without any chemical reaction or mineral dissolution taking place. The same methodology and calculations have been applied to obtain the "true" mass of barium and sulphate in the flow back water, and the simulation results are shown in **Figure 4.9**. The calculated mass fluxes of ions in the flowback water have been plotted in **Figure 4.10** (according to **Equation 4.1**).

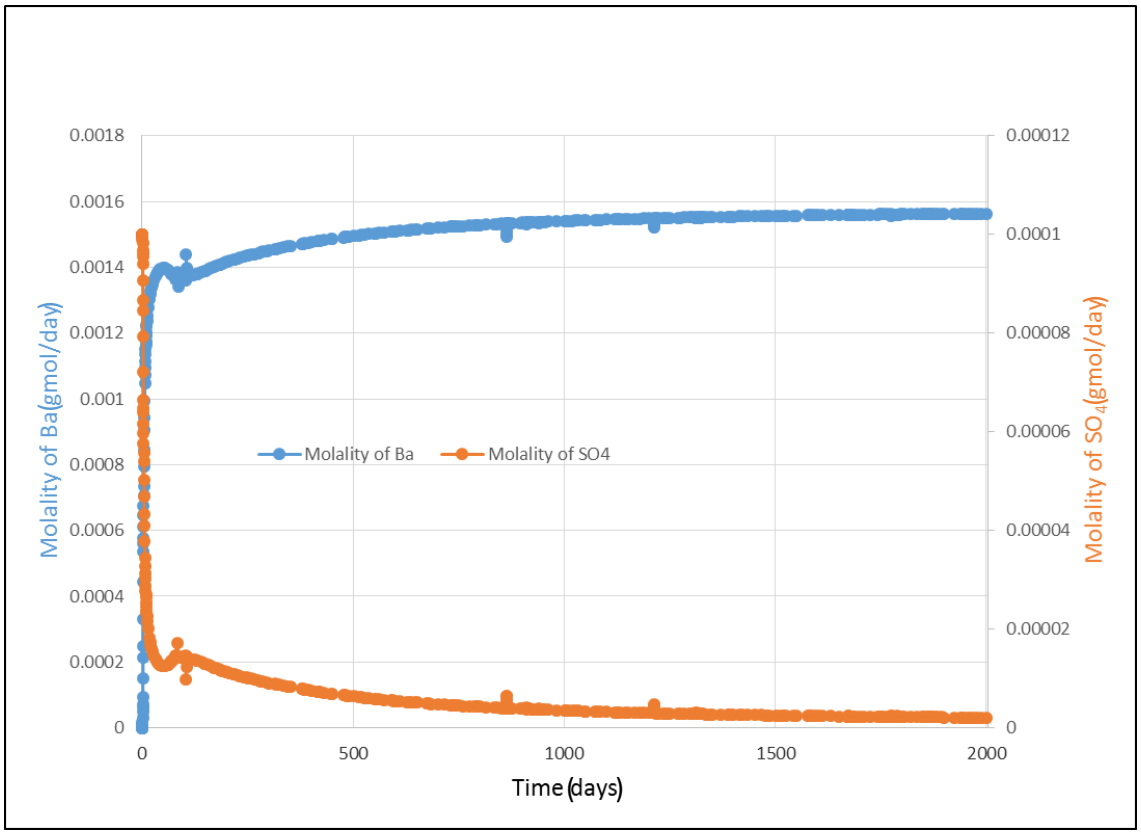

Figure 4.9 Molality of Ba and SO_4 vs time, assuming mineral reactions do <u>not</u> occur

Figure 4.9 shows the molality of barium and sulphate in the flowback water from the simplified GEM model. It can be readily seen that the change of barium and sulphate in

the flowback water is symmetrical throughout the whole production period – i.e. concentrations are affected only by mixing and dilution, and not by reactions. The concentration of sulphate at the beginning along with the concentration of barium at the end is consistent with the initial concentrations of barium and sulphate in the fracture fluid and the formation water, respectively. In other words, this simplified model eliminated the effect of the precipitation and dissolution processes during production, which provides an endpoint "worst" scaling case scenario in the flowback water for the next step of analysis.

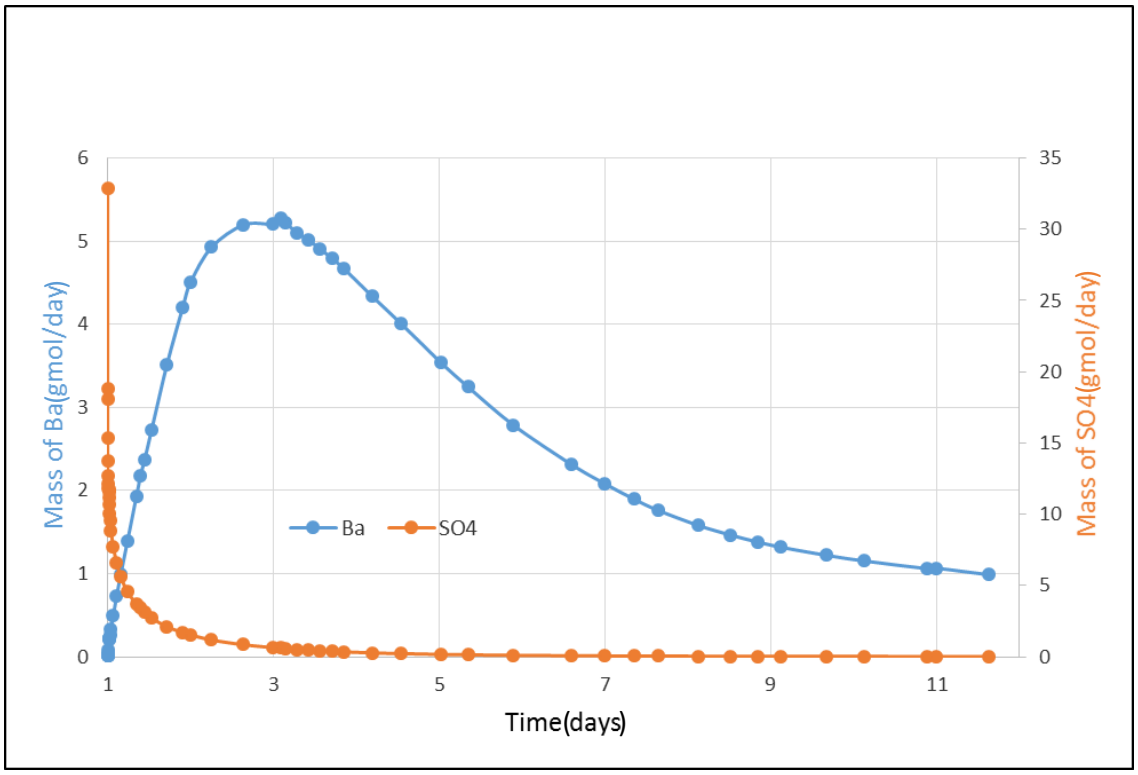

Figure 4.10 Mass of Ba and SO_4 vs time, assuming mineral reactions do <u>not</u> occur

As shown in **Figure 4.10**, the mass flux of barium and sulphate in the flowback water has been calculated. It can be seen that for the first two days of production the mass flux of barium in the flowback water increases, reaches a peak value, and then declines. The mass flux of sulphate instantly reaches a maximum value as soon as the injection process completed, and then decreases very quickly. Thus, while removing the mineral reactions might appear to create a "worst" case scenario, the precipitation of minerals and then subsequent gradual dissolution of these minerals into the flowing brine stream might result in scaling ions flowing into the well for much longer (**Figure 4.5** and **Figure 4.7**) than if no reactions were to take place (**Figure 4.9** and **Figure 4.10**).

4.4.3 Multi-stage hydraulic fracturing introductions

According to the analysis of the mass flux of barium and sulphate in the flowback water above, it can be seen that there may be a serious scaling risk due to the commingled flow from two hydraulic fractures if they are simultaneously producing flowback water from different stages of the hydraulic fracturing process. In this section, a brief review on multistage hydraulic fracturing technologies will be introduced first, and then an updated two stages hydraulic fracturing GEM model will be developed and studied in the following section.

There is significant resistance for the fluid flowing within a low permeability reservoir, of which a shale reservoir is typical. As geological time passed by, geochemical and geophysical processes acted on the low-perm reservoir rock; some of the actions narrowed or blocked the flow paths in the rock. In addition, if there is a system of natural fractures existing in the shale reservoir, the high capillary pressure will also imbibe the fluid and trap it within. Under these circumstances, hydraulic fracturing is necessary for stimulation in low-perm reservoirs to increase the conductivity of the gas shales system and create/ connect paths for fluid flowing within the shale matrix or even from the shale matrix up to the well. The diagram of **Figure 4.11** (Janszen, 2015) represents a typical hydraulic fractured horizontal well design for the multi-stage fracturing in comparison with a vertical well design.

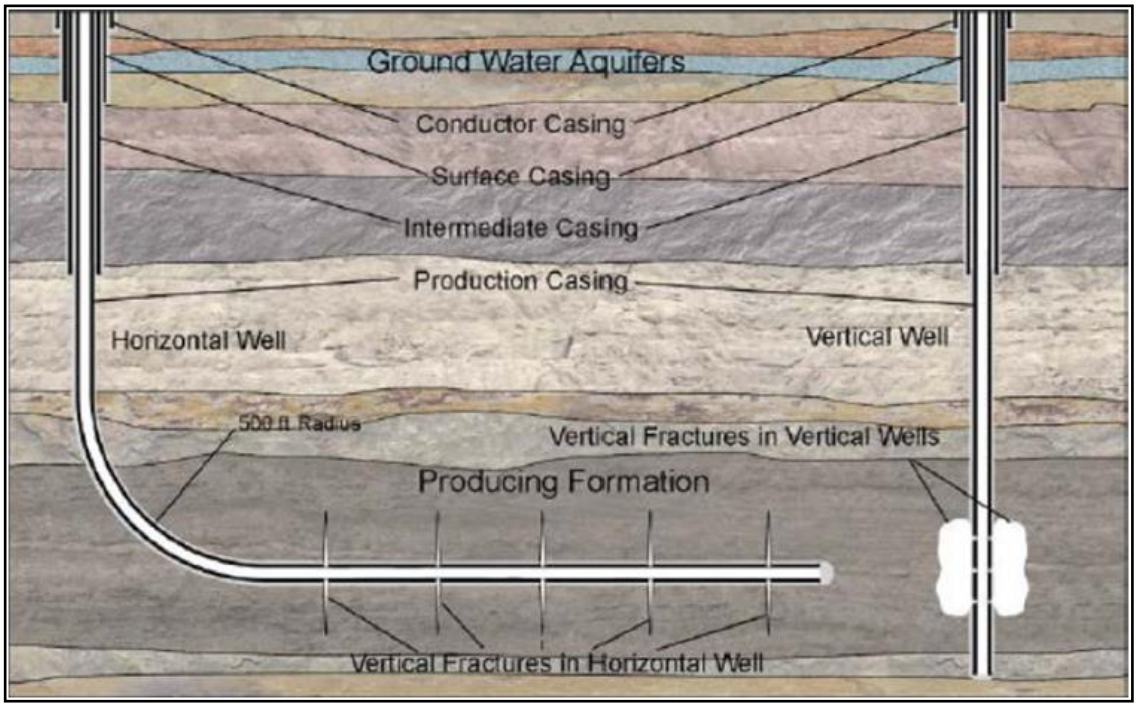

Figure 4.11 Hydraulic fractured horizontal well and vertical well design (Janszen, 2015)

The horizontal section of horizontal well extends to thousands of feet within the most hydrocarbon-rich intervals in shale reservoirs to enlarge the contact area between the well and the shale matrix. The perforation holes along the lateral length allow the fracture fluid to create a single fracture or even, ideally, a fracture network at each stage of the process (Janszen, 2015). The hydraulic fracturing fluid is normally water-based, from the rivers, melted snow or the underground water only if the water source is sufficient; it also contains proppants (such as fine-grained sand and ceramic particles) and varieties of chemical additives (biocide, surfactant, inhibitors, friction reducer, etc.).

As it is isolated for each of the fracturing stages, the fracturing fluid is able to be pumped into the reservoir to create fractures with every single stage; and after the designed multi-stage fracturing process is completed, the well will be put back on production. For the shale gas hydraulic fracturing, high pumping pressure is needed, and as a result, only one fracture is able to be created at a time (Janszen, 2015). The perforation for the horizontal length should be ideally towards the direction of the least principal stress, so that the fluid can penetrate the formations to create fractures to be held open by proppants.

On the one hand, for the horizontal well hydraulic fracturing process, if the lateral section is too long, it is not possible to fracture the whole lateral section at one time, and so a multi-stage hydraulic fracturing process needs to be operated; on the other hand, in order to meet the demands of the designed production target, a multi-stage hydraulic fracturing process will be needed to raise the productivity efficiency. For the "Plug and Perf" fracturing, a single stage normally takes between one to two days, although sometimes two stages can be completed in one day (Themig, 2011). Furthermore, for the "Continuous Pumping" multi-stage hydraulic fracturing, it is more effective with the open-hole and ball-actuated system which can allow shut-off after the production or fracturing processes and also it is easier to do the re-fracturing process if it is required (Packers, 2011); it is even more economical to operate compared to the "Plug and Perf" fracturing process (Bobrosky, 2010).

Another important objective that needs to be mentioned is the optimization of hydraulic fracturing. It is considered that a good optimization and successful operation of hydraulic fracturing process is the key to manage an economical shale gas production. According to the basic IMEX shale model study from the last chapter, it can be found that decreasing fracture spacing, enlarging the fracture size (longer hydraulic fracture

half-length and higher height – shown in **Figure 3.7**) and also optimizing the proppant-transportation (lighter proppants are used) are all useful to increase the productivity of shale gas production.

4.4.4 Dual fractured GEM modelling study

4.4.4.1 Dual fractured GEM modelling without mineral reactions

As an extension to the modelling study to investigate the "worst" scaling risk scenarios, a dual fractured GEM model has been developed to extend the scaling tendency prediction and scale management discussion. The parameters for this dual fractured GEM model are showing in **Table 4.7** and a vertical cross sectional plane (JK) view of a dual fractured GEM model is shown in **Figure 4.12**.

Table 4.7 Summary of main parameters used for dual fractured modelling

Parameter	Value	Unit	Definition
D	7000	ft	Reservoir top
G_p	0.5	psi/ft	Reservoir pressure gradient
K_{mi}	0.0001	mD	Matrix initial permeability
C_{fi}	50	mD*ft	Fracture initial conductivity
K_{sf}	0.001	mD	Secondary fracture initial permeability
Φ_m	0.05	N.A.	Matrix porosity
Φ_f	0.001	N.A.	Fracture porosity
P_i	4500	psi	Reservoir initial pressure
T	135	°C	Reservoir temperature
H_f	250	ft	Fracture height
H_{Lf}	500	ft	Fracture half length
S_f	0.45	N.A.	Fracture initial water saturation
S_{sf}	0.2	N.A.	Secondary fracture initial water saturation
R_{sf}	10~30, 5, 18~20 (lower layers); 10~30, 7, 18~20 (lower layers);	N.A.	Secondary fracture closure zones location
M_r	No reactions	N.A.	Mineral reactions in model
L_{1hf}	20, 5, 16	N.A.	Center block location of 1st hydraulic frac
L_{2hf}	20, 7, 16	N.A.	Center block location of 2nd hydraulic frac

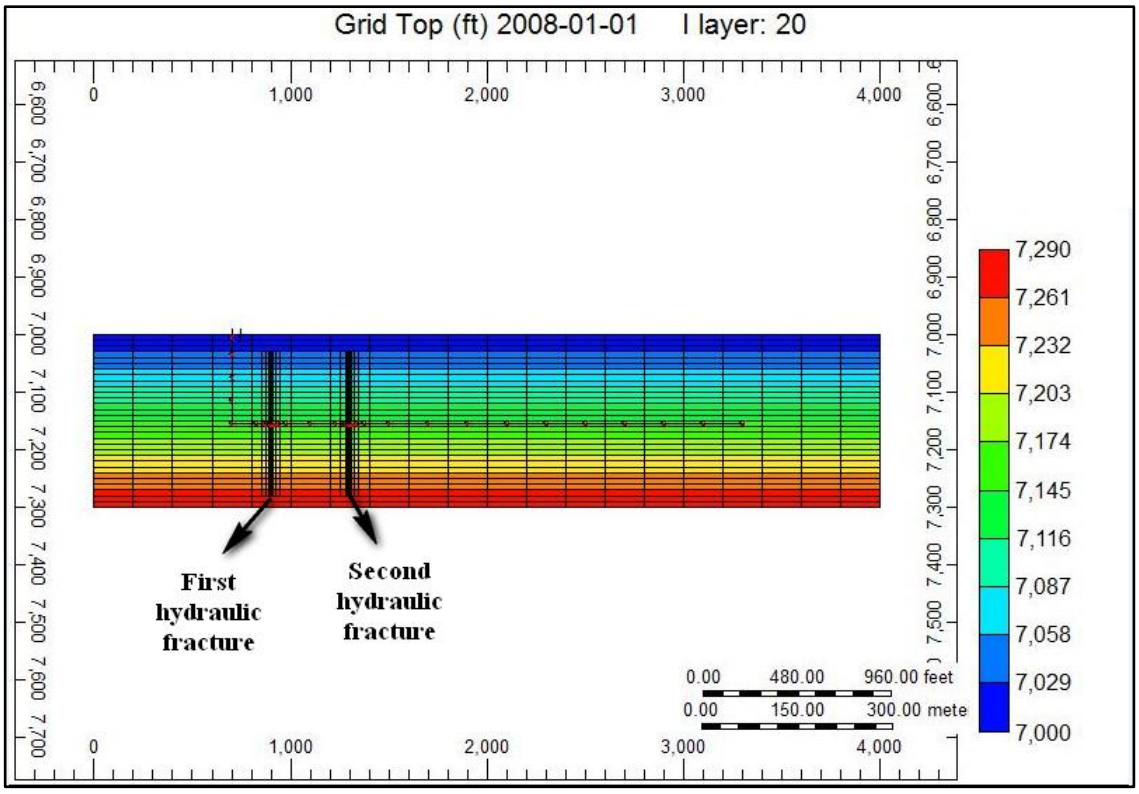

Figure 4.12 Vertical cross section (JK) view of dual fractured GEM model

This dual fractured GEM model includes the first hydraulic fracture established at the beginning of the simulation, through which fracture fluid is injected for one day (3000 bbls) and which is then brought back on production for a further two days and then this production is followed by a one day shut-in. The second hydraulic fracture has been established two blocks away from the first fracture in the J direction. Fracture fluid is injected in it as soon as the perforations in the first hydraulic fracture are closed during the shut-in. The amount of fracture fluid injected in the second hydraulic fracture is also 3000 bbls (considering the same fracture volume has been applied for both of fracture zones), and the whole process also lasts for one day. After the injection process is completed in the second hydraulic fracture, the well is brought back on production and both of the hydraulic fractures remain open for fluid to flow back during the entire production period.

This dual fractured GEM model has been developed without including any aqueous or mineral reactions in the base case, to observe the scaling tendency from the point of view of pure mixing. The concentrations of barium and sulphate in flowback water are plotted in **Figure 4.13** and produced water flow rate against time is shown in **Figure 4.14**.

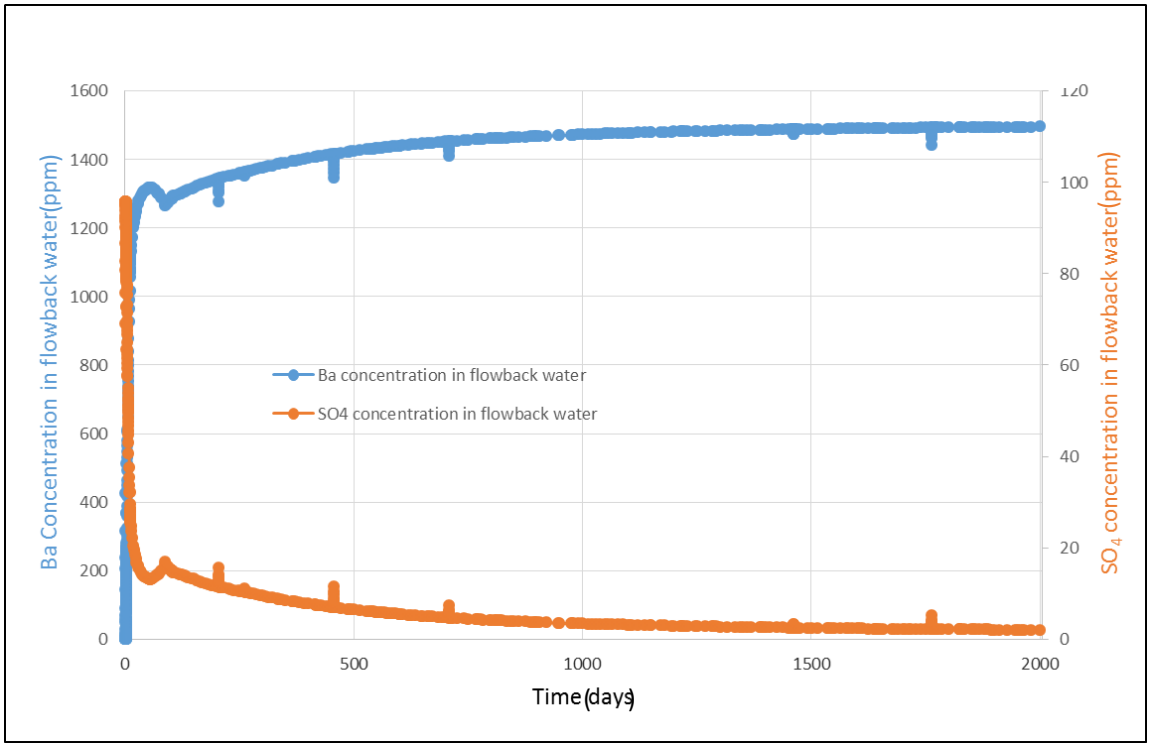

Figure 4.13 Concentration of Ba&SO_4 in flowback water vs time in dual frac GEM

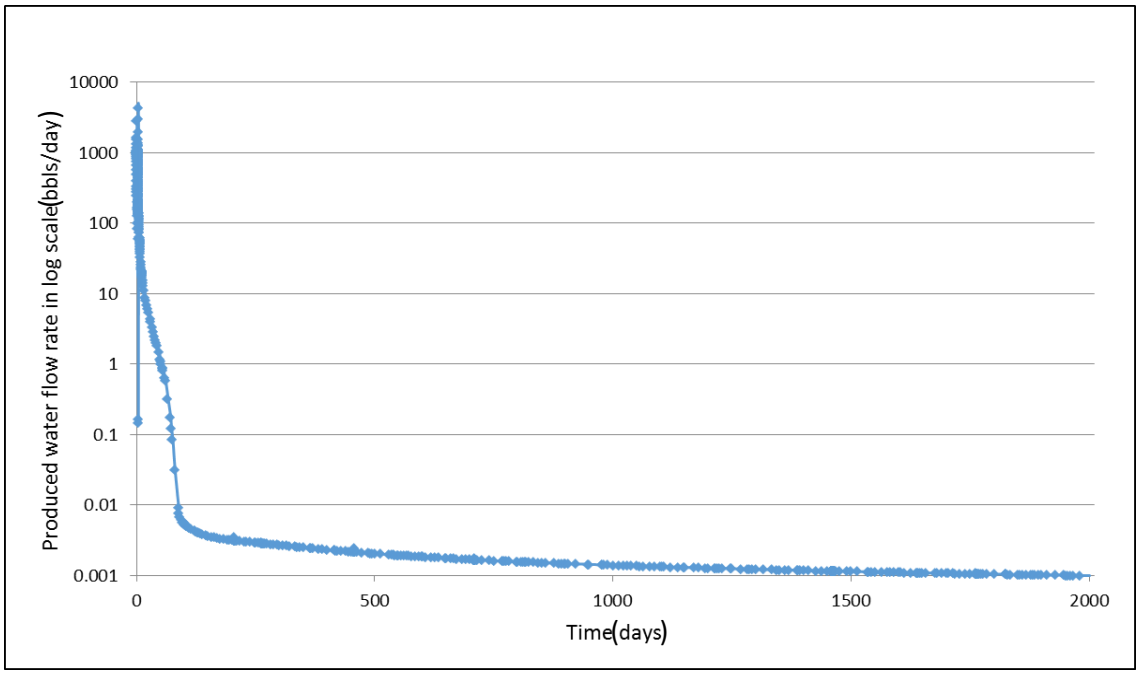

Figure 4.14 Produced water flow rate vs time in dual frac GEM model

The simulation results for each ion's concentration exported as molality. As a result, the concentrations in units of mg/L from **Figure 4.13** have been calculated from **Equation 4.2** and **5.3** by using the exported molalities from simulation results.

$$I_{con} = I_{mola} \times H_2O_{con} \quad \text{…Equation 4.2}$$

$$H_2O_{con} = 1{,}000{,}000 / H_2O_{MW} - \sum I_{mm} \quad \text{…Equation 4.3}$$

Where I_{con} is calculated ion concentration in mg/L, I_{mola} is exported ion molality in flowback water from simulation results, H_2O_{con} is calculated solution in mg/L, H_2O_{MW} is solution molecular weight which is 18 g/mol for water and $\sum I_{mm}$ is summation of ion concentrations in mmole/L (TDS in unit of mmole/L)

From **Figure 4.13** it can be observed that the change of concentrations in barium and sulphate are identical to each other in terms of the behaviour of increase in barium and decrease in sulphate and then both reach a plateau at the end of production. This observation could be accounted for by the application of a pure mixing process without any reactions taking place. The mass fluxes of both ions in flowback water are also calculated from **Equation 4.1** and shown in **Figure 4.15**.

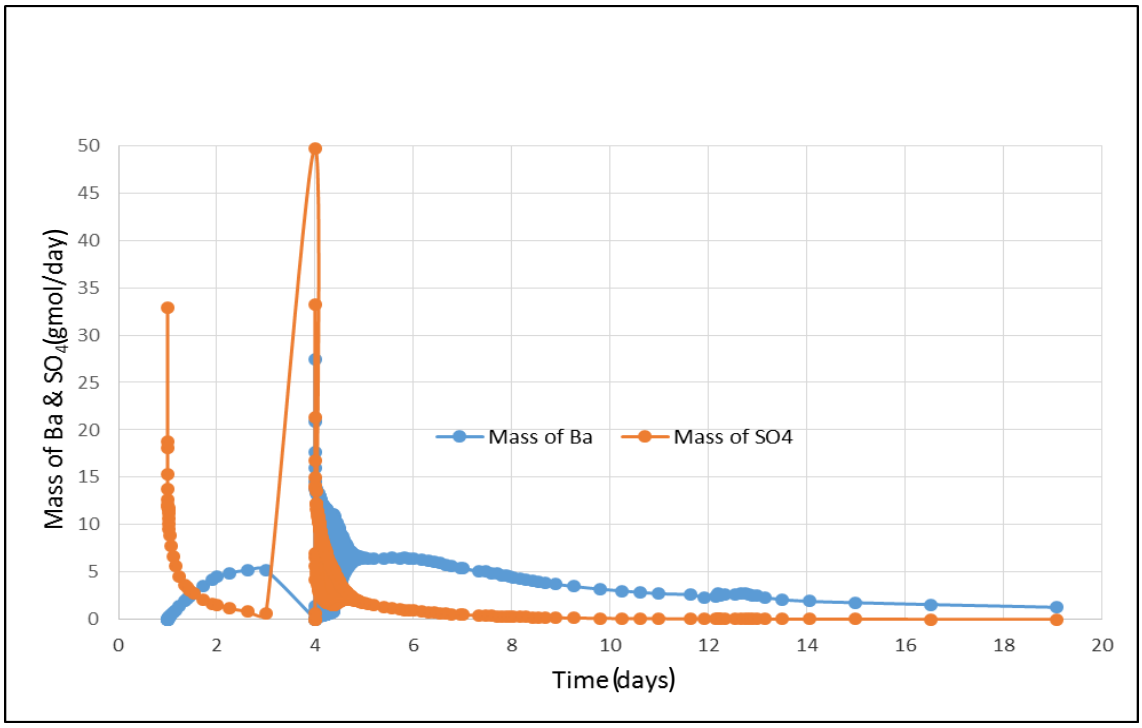

Figure 4.15 Mass of Ba and SO_4 in dual fractured model vs time, assuming mineral reactions do not occur

As shown in **Figure 4.15**, the mass flux of sulphate starts with a high value straight after the injection of fracture fluid in the first fracture, and then it drops due to the fraction of fracture fluid decreasing in the flowback water. Meanwhile, as soon as the injection is completed in the second hydraulic fracture, the mass flux of sulphate

reaches a peak value, which is even higher than the starting point; this is on account of the fluid mixing between the initial flowback water produced from the second hydraulic fracture and the subsequent flowback water produced from the first hydraulic fracture after a recovery of three days.

It can be also observed that mass flux of barium reaches the maximum amount as soon as the production is brought back on for both of the hydraulic fractures. This is due to the abundant barium produced back from the previous recovery of the first hydraulic fracture, which is shown in **Figure 4.10**. In conclusion, the fact that large amounts of barium and sulphate flow back during the production period means that the $BaSO_4$ scaling risk is quite significant.

4.4.4.2 Dual fractured GEM modelling with mineral reactions

4.4.4.2.1 Dual fractured GEM modelling with $BaSO_4$ reaction

A further series of dual fractured geochemical models, now including aqueous and minerals reactions, has been developed to examine the mineral dissolution and scaling risk during shale gas production.

First of all, the dual fractured GEM model including $BaSO_4$ reactions has been developed to observe the scaling tendency from a mixing of commingled flow produced in the two hydraulic fractures. The parameters are the same as shown in **Table 4.7** but with mineral reaction of $BaSO_4$.

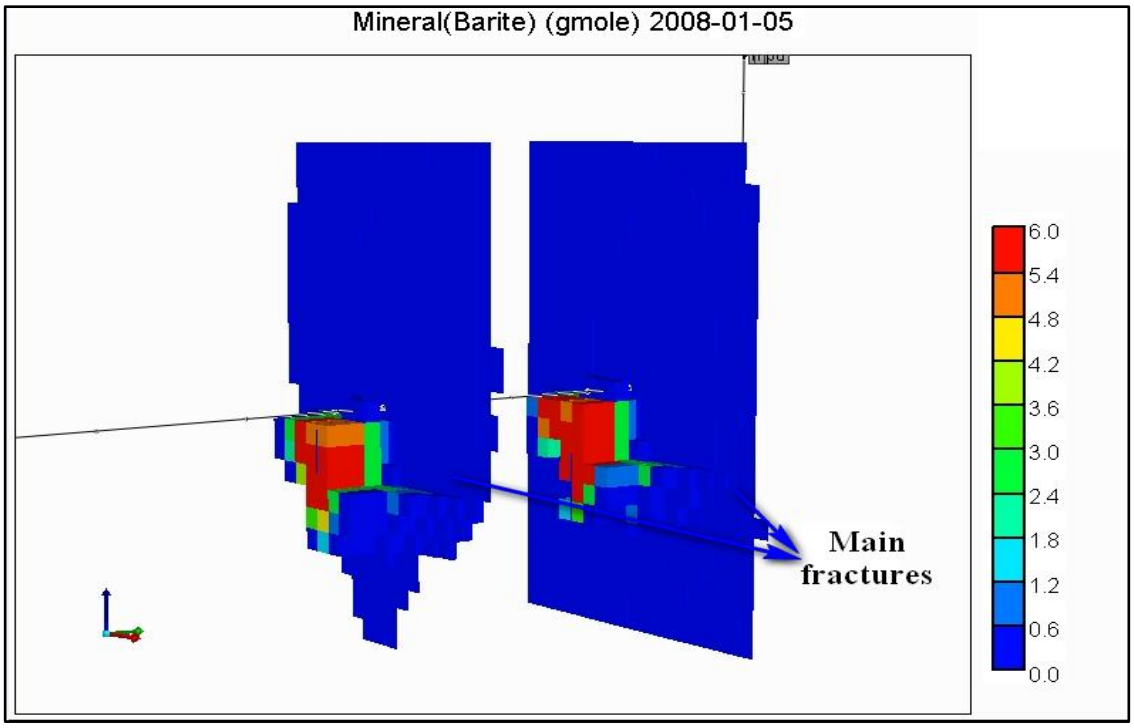

Figure 4.16 3D view of the mass change of $BaSO_4$ in the dual fractured GEM model

Figure 4.16 illustrates a 3D view of dual fractured GEM model, which includes the $BaSO_4$ aqueous reaction and barite as a primary mineral initially present in the system. It shows that the scaling tendency along the primary hydraulic fractures is low, whereas the greatest precipitation occurs in the adjacent fracture zones located in the deeper layers of the reservoir.

This is consistent with the comparison in the previous analysis:

1) The impact of gravity segregation drives water downwards, and so scale tends to accumulate at the bottom of the fracture zone;

2) Larger contact area has been provided due to the existence of zones of variable conductivity located at greater depth in the reservoir, so where major fluid transport takes place;

3) More fluid has been retained in place because of the multiple impacts due to the high conductivity, high capillary pressure and fracture closure in the adjacent secondary fracture zones.

Another finding from the simulation results is that the formation of $BaSO_4$ precipitation around the first hydraulic fracture at the end of production has become greater than the deposition around the second hydraulic fracture. This can be accounted for by the higher

concentration of ions that can be observed adjacent to the first fracture zone, due to the produced water flow back from the second fracture after a longer period of production (differential of reservoir pressure drives the communication of fluids flow back from two fractures). The fluid mixing leads to an increased mass flux of ions around the first fracture, which could lead to a worse scaling risk.

4.4.4.2.2 Dual fractured GEM modelling with anhydrite as initial mineral

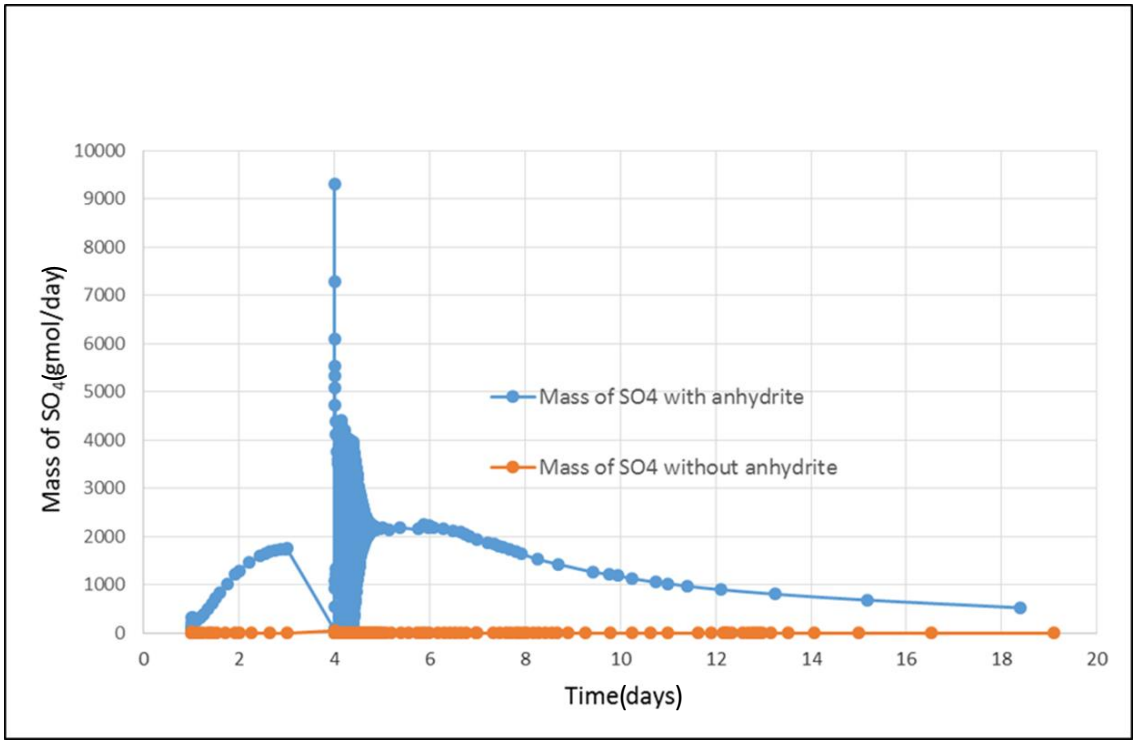

Figure 4.17 Comparison of mass of SO_4 from cases with and without anhydrite

Another dual fractured GEM model has been developed to look into the impact of the presence of anhydrite initially in the simulation. The parameters are the same as shown in **Table 4.7** but with anhydrite mineral reaction. The comparison of simulation results is plotted in **Figure 4.17**.

It can be seen that the mass flux of sulphate in the flowback water from the anhydrite case is significantly higher by comparison with the case with no primary minerals. It can also be observed that there is only a minor difference at the start point, whereas there is a large difference after the injection period was completed in the second hydraulic fracture. This can be interpreted as signifying that the major mineral dissolution process taking place during the fracture fluid injection is due to under-saturated low salinity brine dissolving anhydrite, and this can yield a high concentration

of sulphate in the flowing system (similar conclusions were also drawn from 1D GEM model study before).

Figure 4.18 illustrates a 3D view of anhydrite change in this GEM model, and it can be readily seen that all the change values are presented as negative, which means there is mineral dissolution taking place. In addition, a large loss of anhydrite has also been observed after the injection period is completed in the second fracture, which is also consistent with the discussion above.

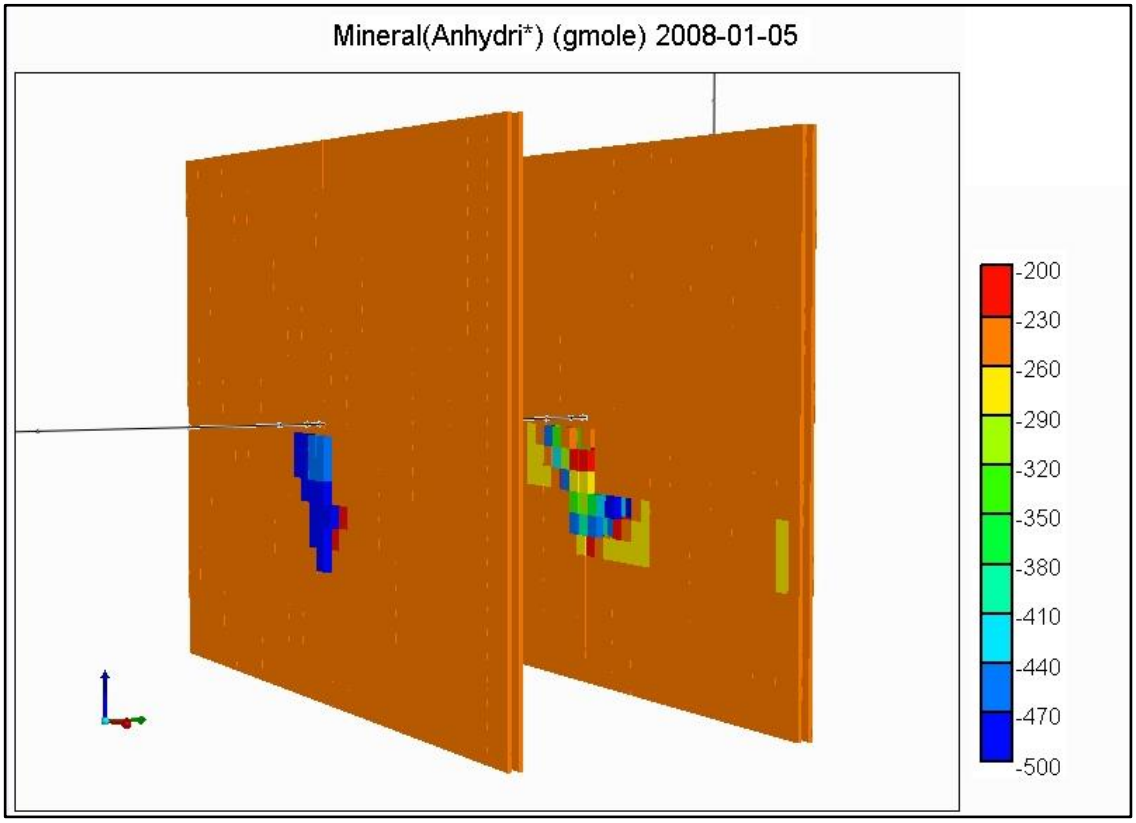

Figure 4.18 3D view of dual fractured GEM model for the mass change of anhydrite

4.5 CONCLUSIONS

As mentioned in the first section of this chapter, the aim of it is to take advantage of geochemical modelling to make further improvement in answering the question of what caused the altered high salinity in flowback water and also to further observe and predict scaling risk during shale gas production. The conclusions are drawn as below:

- According to the development of mineral dissolution model in PHREEQC, the high salinity in the flowback water in the HRB area is due to the mixing with high salinity formation water, whereas mineral dissolution is insufficient to

account for it.

- A single phase 1D GEM model has been developed to study the equilibration of initial formation water with the primary minerals. The simulation results offer more information about the *in situ* water composition and also provide further proof for the previously addressed question – the reason for the high salinity of the flowback water is not purely the result of dissolution of minerals into the fracture fluid.

- Another two phase 3D geochemical model has also been developed to observe the scaling risk due to the high salinity of the flowback water -

    - Firstly, from the simulation results of single fractured GEM modelling, the highest scaling risk is identified at the early stage of production (after injection process completed).
    - Secondly, a dual fractured GEM model is developed without applying mineral reactions to simulate the "worst" scaling scenario and it is observed this happens after two days production from first hydraulic fracture and the very beginning of the production from the second hydraulic fracture.
    - Finally, several cases with mineral reactions in GEM has been simulated to demonstrate the scaling tendency and the impact of mineral dissolution during production – low scaling tendency along the primary fracture zone in addition with the greatest precipitation occurring in the adjacent fracture zones located in the deeper layers of the reservoir; anhydrite dissolution will introduce abundant sulphate into the system which could lead to a worse scaling risk along with high concentration of barium in the formation water.

CHAPTER 5 SCALE INHIBITOR INJECTION MODELLING

5.1 INTRODUCTION AND CHAPTER CONTENT

Being an important chemical reagent to reduce or prevent inorganic scale from forming during the production process, scale inhibitor has been commonly introduced into reservoirs, not only for conventional hydrocarbon recovery but also for hydraulic fracturing operations in unconventional production.

According to the chemical compositional data analysis and modelling study presented in previous chapters, a serious scaling risk has been identified in the Horn River Basin area, and also in some other shale plays around the world (Towers, 2011; Elisabeth, 2015; Kuijvenhoven, 2013; Slutz, 2012; Blanch, 2009). As a consequence of this, the management of scale requires a control strategy to be designed and operated to prevent the potential damage that could be caused during shale gas production.

There are two basic scale control strategies to be followed based on the study to date – scale inhibitor squeeze treatment and scale inhibitor injection during fracturing. On the one hand, for the conventional reservoirs, scale inhibitor squeeze treatments have been widely studied and applied; however, with unconventional reservoirs, the management of the squeeze process could be quite difficult due to the uncertainties of extremely low matrix permeability. On the other hand, under the circumstances that the scaling tendency has been well predicted and the scaling risk is well defined, pumping scale inhibitor as an additive along with fracture fluid during hydraulic fracturing is another effective option that can be selected.

The aim of this chapter is to explore scale control management based on the development of a scale inhibitor retention model, which is based on the history matched hydraulic fractured shale modelling set up previously. In completing the discussion of this modelling study, some general recommendations will be provided for inorganic scale risk control during shale gas production.

First of all, we briefly introduce some fundamental properties and adsorption theory applied in this model, and then we focus on the discussions of the impact of applying different adsorption levels and strategies on the retention of scale inhibitors in shale

systems. The whole scale inhibitor retention modelling study in this chapter is presented just as a starting point for scale control management, and further studies will be required in the future.

5.2 INTRODUCTION OF SCALE INHIBITOR INJECTION MODELLING

Scale inhibitors are commonly used to prevent or control the deposition of scale within a completed well or reservoir. A squeeze treatment is one of the most widely used processes to deliver scale inhibitor into the production system (Kan, 2012). During a squeeze treatment the scale inhibitor is injected into the production system and retained (Tomson et al., 2006). When the well is brought back onto production, the free inhibitors in the fluid will flow back along with the produced water.

The application of scale inhibitor during the hydraulic fracturing process is similar to a squeeze treatment, and the operators normally pump scale inhibitor into the reservoir under high pressures along with hydraulic fracture fluid before the production commences (Fei, 2015). It is reported that around 10 to 25% of all shale fracturing uses scale inhibitor as an additive during fracture fluid injection (King, 2012).

A scale inhibitor injection model has been developed to examine the impact of inhibitor retention on well protection. This model is set up on the basis of the history matched shale modelling presented in Chapter 3 and the scale inhibitor is only applied in the injected fracture fluid as a component that can be adsorbed onto the shale matrix; what is not simulated is the that actual inhibition of mineral precipitation. In other words, the retention of injected scale inhibitor in this modelling study is due to a reversible process (a combination of closure of secondary fractures and matrix adsorption). The detailed simulation models have been included in **Appendix 3**.

The base case for this new model includes scale inhibitor in the fracture fluid which is injected for one day. The concentration of scale inhibitor in the fracture fluid is 1000 ppm (it has been converted into field units in the model - 0.3498 lb/bbls) and it has been injected continuously throughout the whole injection period in the initial simulation. Permeability and porosity for the matrix are set to be a constant value, which means changes of any matrix properties during production are not considered in the simulation.

The basic concept used to retain scale inhibitor within the shale system is to include scale inhibitor adsorption in the simulation. This is applied to evaluate the treatment process to control the scaling risk. The application of the adsorption process in this modelling study is by means of a derived inhibitor-rock interaction table which is calculated by **Equation 5.1**.

$$\Gamma = KC^n$$

Equation 5.1 Scale inhibitor adsorption isotherm – Freundlich function

*Where **Γ** is actual adsorbed amount of scale inhibitor, **K** and **n** are constants which identify the adsorption level and **C** is the scale inhibitor concentration in solution.*

This equation determines the mass of scale inhibitor adsorbed or retained within the reservoir rock at different levels of concentration, and is described as a Freundlich function (Mackay, 1999; Vazquez, 2012). The reason for choosing the Freundlich function is due to its wide application as a commonly used adsorption isotherm, but a Langmuir isotherm can also be used (Wang and Hung, 2006). The Langmuir isotherm assumes that the adsorption thermal level is constant, the adsorbent surface is homogenous and a monolayer and the adsorbed elements do not interact with each other (Li et al., 2015).

It is well documented that the Langmuir isotherm is the most extensively used adsorption isotherm, not only for coal bed methane studies, but also it can be applied in shale reservoir modelling. However, the main disadvantage is that the adsorption assumption of this theory is too ideal to represent the complex adsorption mechanisms in real shale reservoirs (Li et al., 2015). Although this adsorption isotherm has been commonly applied for gas adsorption in unconventional system modelling, it is still selected as our SI adsorption isotherm to account for the simulation study of SI retention.

Table 5.1 Calculated adsorption results for base case simulation

Concentraion of SI in frac fluid	ppm(mg/l)	0	200	400	600	800	1000
Concentraion of SI in frac fluid	lb/STB	0	0.069954	0.139909	0.209863	0.279818	0.349772
Γ	lb/STB	0	180.0962	221.7244	250.4038	272.9748	291.8741

Following previous studies, the constants K and n have been defined as 400 and 0.3, this representing a typical adsorption level that accounts for the scale inhibitor retention. The calculated adsorption table (shown in **Table 5.1**) is then applied in the model and the produced water rate and scale inhibitor mass flux in the flow back water can be obtained from the simulation results. Thus the concentration of scale inhibitor in the flowback water could be calculated by **Equation 5.2**. The results of the calculated scale inhibitor concentration in flowback water are plotted in **Figure 5.1** and **Figure 5.2** indicates the produced water flow rate from the simulation results of this model.

$$C_{sifw} = \frac{N_{si}}{N_{fw}}$$

Equation 5.2 Calculation of scale inhibitor concentration in flowback water

Where $\boldsymbol{C_{sifw}}$ *is concentration of scale inhibitor in flowback water,* $\boldsymbol{N_{si}}$ *is scale inhibitor produced mass flux rate and* $\boldsymbol{N_{fw}}$ *is produced water volumetric rate.*

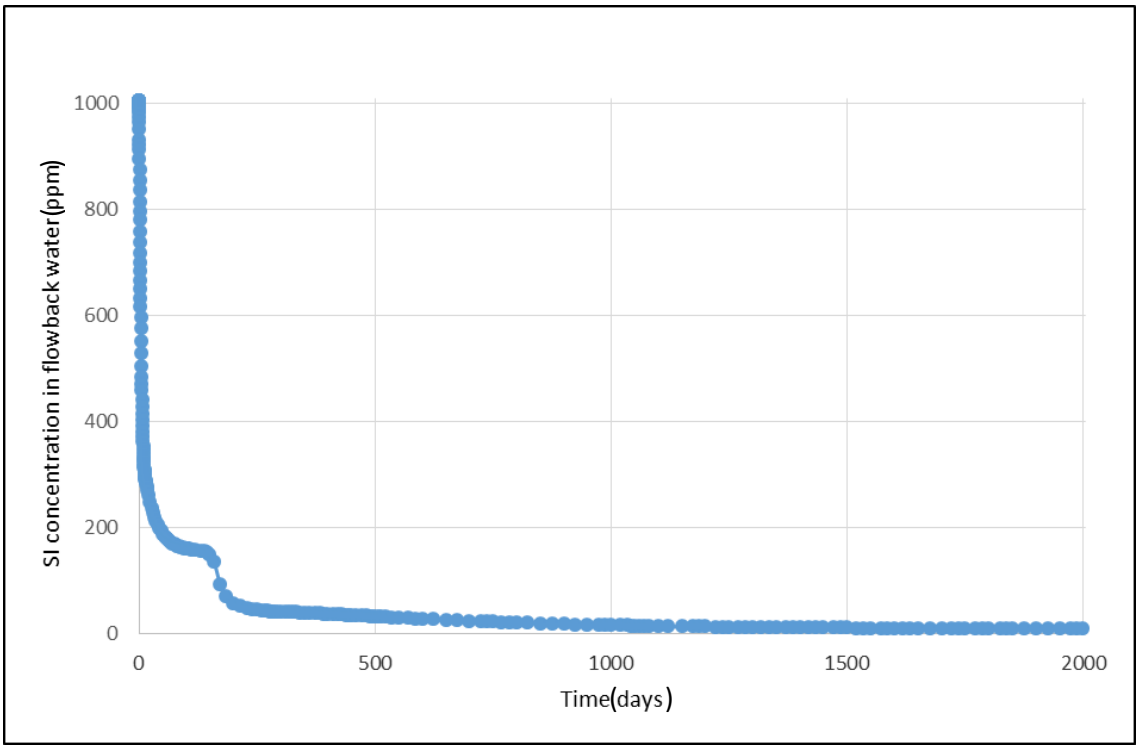

Figure 5.1 Scale inhibitor concentrations in flowback water vs time

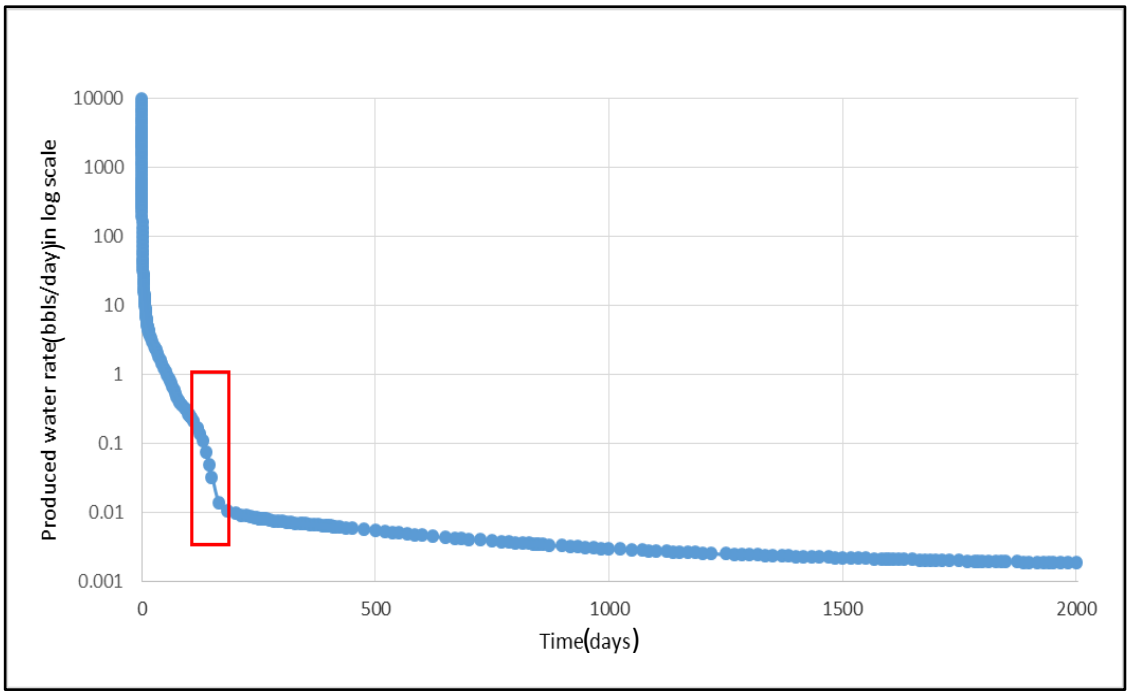

Figure 5.2 Produced water rate vs time in SI injection base case

From **Figure 5.1** it can be seen that the scale inhibitor return concentration is similar in profile to the typical return results from a conventional squeeze treatment – it reaches a peak value right after the injection process is completed, and then this is followed by a gradual decrease throughout the entire lifetime of production (shown in **Figure 5.3** by Vazquez, 2012). Meanwhile, return concentration will continue to decrease by the end of the production period (minimum inhibitor concentration (MIC) tested in the lab can be satisfied at certain time point during the flowback process).

The scale inhibitor return profile is normally considered as criterion to decide whether or not an inhibition treatment is successful. As indicated in **Figure 5.1** it can be observed that if the MIC for this inhibitor system is 50 ppm, then this treatment design can be considered as satisfactory by approaching this target at around four months of production after the treatment has been accomplished. This inhibition treatment can be optimised to accommodate different requirements of MIC in different production period.

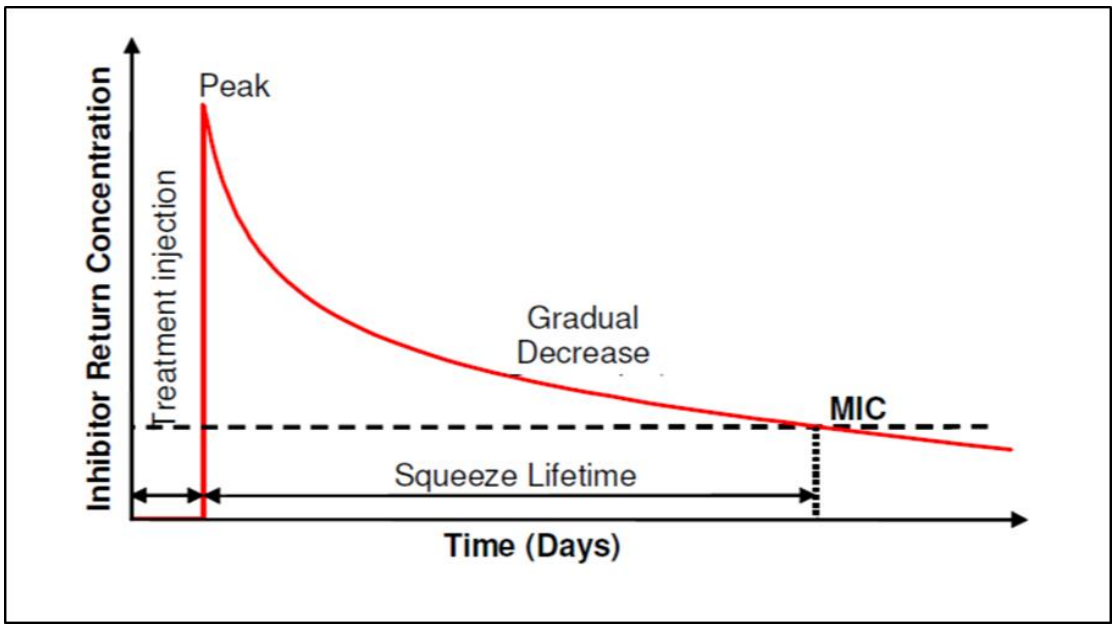

Figure 5.3 Illustration of the SI field return concentration profile

Another observation from the trend plot in **Figure 5.1** is that a significant decrease of return SI in flowback water can be observed at the beginning of the production and is followed by a sharp decrease from around 120 days to 180 days. This is attributable to variations in water flow due to the variable conductivity zones, and this will result in significant fluctuations during early stages of production. Meanwhile, the sharp drop of SI in flowback water can account for the response of the change of produced water flow rate. As shown in **Figure 5.2**, it can be readily seen that there is also an obvious decrease in the flow rate of produced water during the same time period (the red square area highlighted in the plot) which coincides with a significant decline in scale inhibitor concentration in **Figure 5.1**. The further explanation for this sharp drop could also account for the variation of the fraction of fracture fluid in the flowback water due to the application of secondary fracture zones. It is known that at the early stage of shale gas production the majority of flowback water is the injected fracture fluid and this fraction of the injected fracture fluid in the flowback water will gradually decrease after the significant drop happened in the beginning. However, due to the existence of secondary fractures adjacent to the primary fracture, a transition region of injected fracture fluid fraction could be observed in consideration of brine mixing gradient (well mixed brine in the primary zone produces back first and then brine mixed in the secondary fracture zones flows back and finally the formation water at the boundary of fracture zone will be drained last). Due to this, a retardation of the water produced from the boundary of

the secondary fracture zones can be observed; this will result in a sharp drop in the returned SI concentration.

5.3 SENSITIVITY STUDY OF SI INJECTION MODELLING

5.3.1 Variable conductivity zones sensitivity

As a start to the sensitivity cases study with the SI retention model, the impact of the variable conductivity area in the fracture zone will be assessed first. A series of sensitivity cases have been developed by applying different locations of the variable conductivity area to observe the effect on SI return concentration (the SI concentration in fracture fluid is 1,000 ppm). Two representative scenarios are selected and the simulation results are shown in **Figure 5.4**, in which the Y axis is plotted on a log scale for better representation.

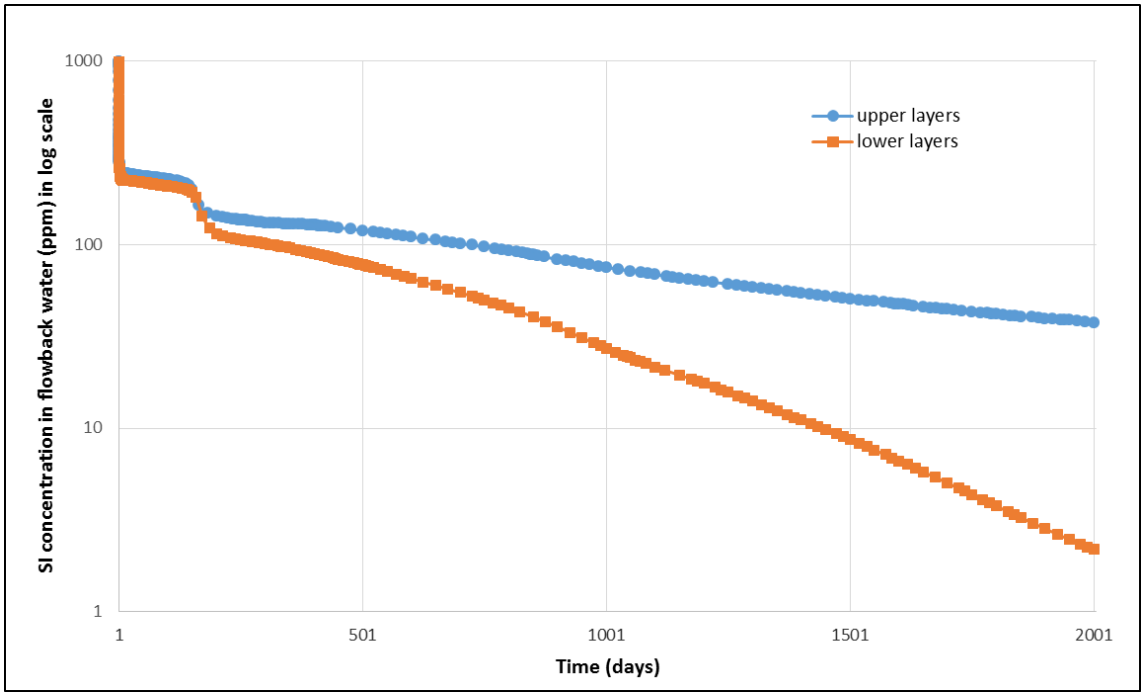

Figure 5.4 Return SI concentrations in flowback water in upper& lower layers cases

As indicated in **Figure 5.4**, it can be readily found that the case with application of variable conductivity zones in the lower layers retains more scale inhibitor within the system. This retention difference is more noticeable especially at the late stages of production. In contrast with this, both cases produce back approximately the same amount of SI at the early stages of the production. It can be interpreted that the impact of gravity segregation and matrix adsorption has more impact on scale inhibitor retention at the late stage of production.

More injected fracture fluid has been trapped in the reservoir due to the impact of gravity segregation along with the application of secondary fracture closure (presented and discussed in Chapter 3), and this will impact the return of SI in flowback water. Also, as discussed before, the impact is relatively less sensitive with regards to holding back fracture fluid during the early stages rather than the late stages.

5.3.2 Different SI injection adsorption level sensitivity

Some further models have been developed by applying different adsorption levels to study their impact on SI return concentrations in flowback water. It is known that the shale matrix normally contain high levels of clay content, which could result in stronger adsorption compared with conventional reservoirs. Therefore, two cases are going to be presented here to discuss the sensitivity of different adsorption levels – a base case with normal adsorption level and a comparison case with stronger adsorption level.

The stronger adsorption level case has been applied with the same adsorption isotherm as in the base case (shown in **Equation 5.1**) and the values used to calculate adsorption table has been referenced by Spicka, (2017) (a shale reservoir adsorption case based on the Bakken shale play study). According to **Equation 5.1**, the constants K and n have been defined as 700 and 0.32, respectively, to represent a stronger adsorption level and the calculated adsorption table applied in the simulation is shown in **Table 5.2**.

Table 5.2 Calculated adsorption results for stronger adsorption simulation

Concentraion of SI in frac fluid	ppm(mg/l)	0	200	400	600	800	1000
Concentraion of SI in frac fluid	lb/STB	0	0.069954	0.139909	0.209863	0.279818	0.349772
r	lb/STB	0	298.8401	373.0512	424.7346	465.6912	500.1604

The comparisons of simulation results from both cases are plotted in **Figure 5.5** and **Figure 5.6**. From the plots it can be observed that more SI has been retained within the system when applying a stronger adsorption level; furthermore, this behaviour is even more significant after completing the injection process. **Figure 5.6** provides a better display for this changing trend – the difference on returned SI concentration between two cases is narrowing during the production process.

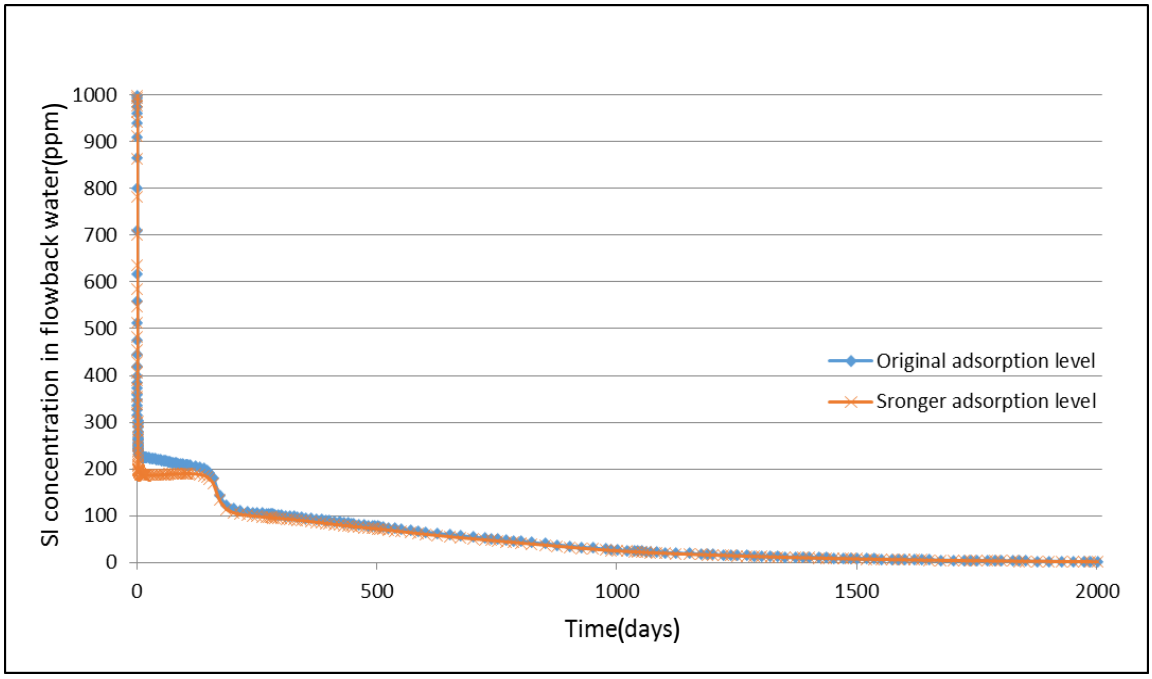

Figure 5.5 SI concentrations in flowback water in different adsorption level cases

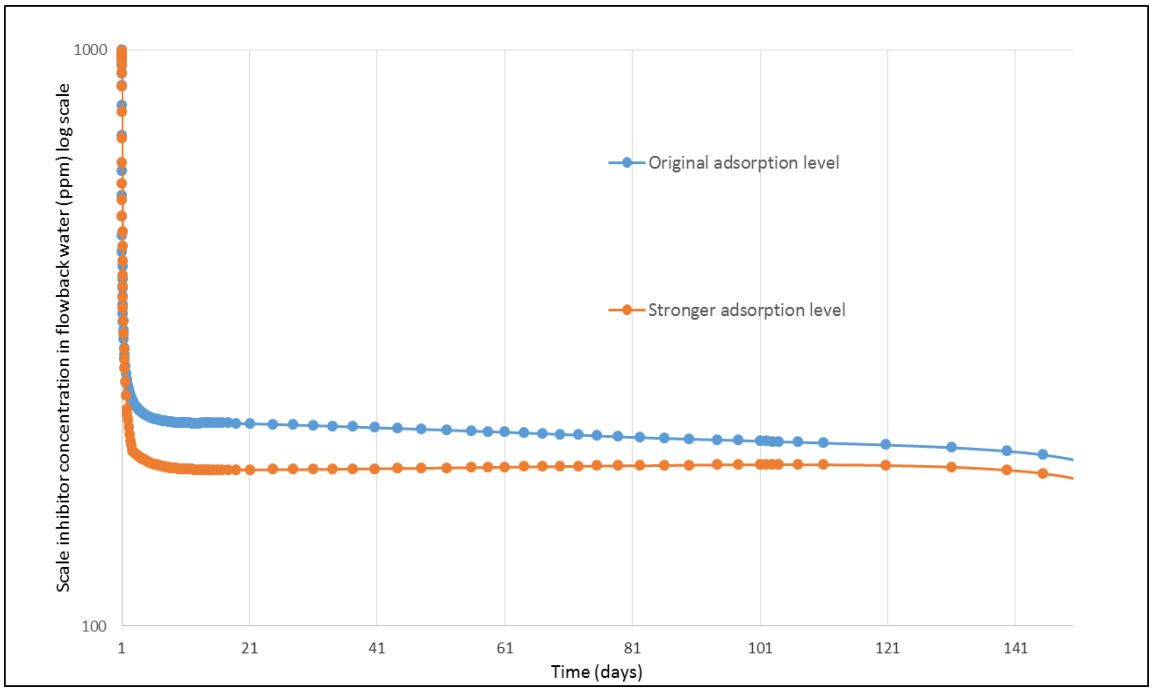

Figure 5.6 SI concentrations in flowback water in different adsorption level cases at early stage of production

The observation of this difference for SI retention is expected since a significant amount of fluid transport takes place at the beginning of the production process due to the high fraction of injected fracture fluid in flowback water when the impact of stronger adsorption will be evident immediately. Whereas at the end of the production, most of the water that flows back is formation water with extremely low flow rate, the impact of

different adsorption level will be fairly small or even could be neglected. Meanwhile, the maximum adsorption capacity will be reached after the early stage of production due to the limited contact area has been provided in the system. The final inhibitor return concentration for both cases are 2.17 ppm (original case) and 2.02 ppm (stronger adsorption case), which also confirms that the sensitivity of different adsorption level at the end of production is small. However, the $BaSO_4$ scaling period identified in Chapter 5 is immediately after the well starts production, and so a poorer adsorbing inhibitor may be much more favourable.

5.3.3 Different SI injection strategy sensitivity

5.3.3.1 Injection of SI in different concentrations

More sensitivity scenarios have been developed by pumping SI under different injection strategies. These cases are simulated simply to show the impact of applying different injection designs on SI returns in flowback water.

First of all, several cases are simulated by injecting fracture fluid with different SI concentrations. In order to obtain better comparison results, these cases are applied with the SI concentrations of 10 ppm, 100 ppm, 1,000 ppm (original case) and 10,000 ppm. All the injections are continuously operated for one day and the matrix adsorption level is also applied in consistent with each other (the same as the original case). The simulation results of returned SI in flowback water are shown in **Figure 5.7** and **Figure 5.8**; both figures have the Y axis plotted on log scales.

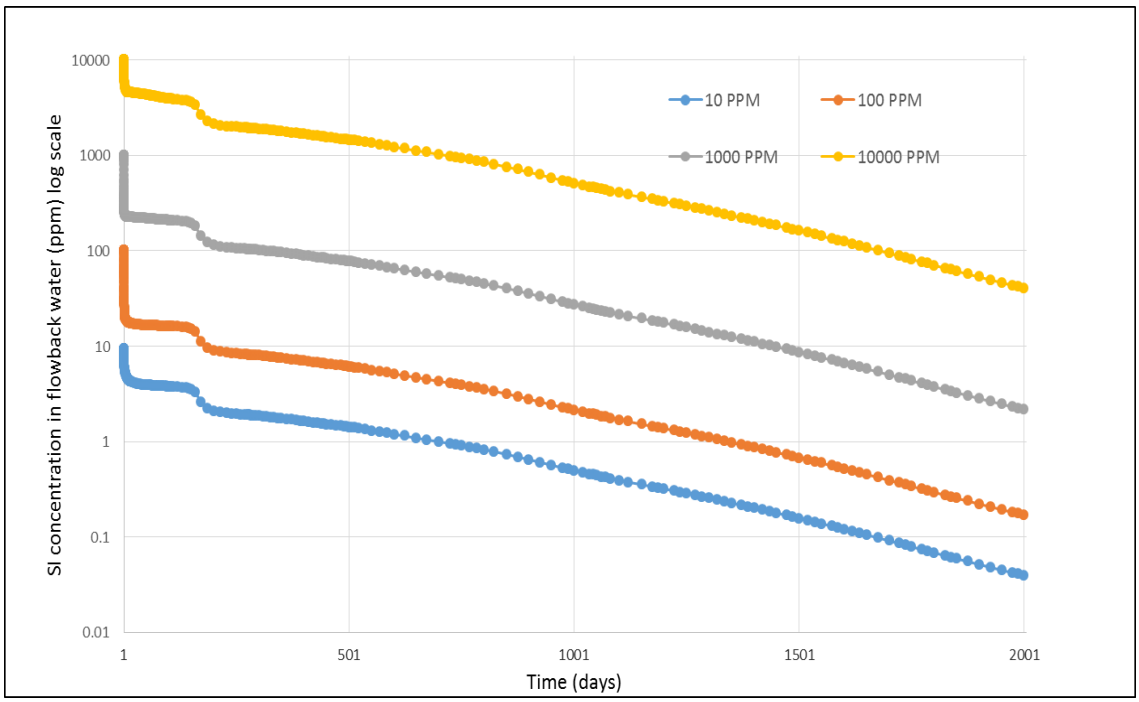

Figure 5.7 Return SI concentrations in flowback water vs time

From **Figure 5.7** it can be readily seen that the entire trend of returned SI concentration in the flowback water from different cases are identical to each other, which is consistent with the predictions due to the location of secondary fractures closure and matrix adsorption isotherm are uniform between each simulations. It can be also observed that the two cases with original concentration of SI injected at 100 ppm and 1,000 ppm behave a more significant drop on the returned SI during the earliest production period, which could be in response to variable adsorption capacity corresponding to different SI concentrations.

Figure 5.7 can also provide some data for an initial discussions on the selection of optimal SI concentration in the fracture fluid in consideration of the requirement of MIC in different scenarios. For instance, if the MIC is 5 ppm, the case with 10 ppm SI in fracture fluid approaches this threshold after around 200 days production. By contrast, the case with 100 ppm SI in fracture fluid takes almost 5 times longer production time (around 1,000 days production) to reach the same MIC, whereas the case with 1,000 ppm requires almost 2,000 days of production to meet this threshold. According to the simulation results showing in **Figure 5.7**, it can be considered that the optimal SI concentration in the fracture fluid can be variable due to the specific MIC.

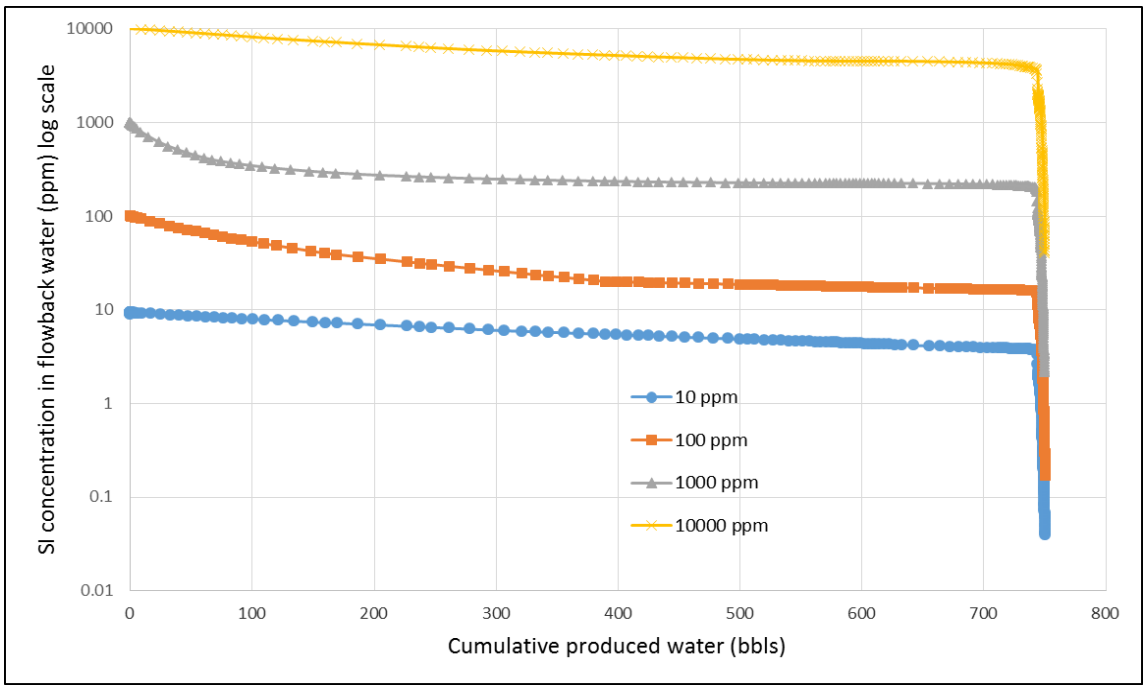

Figure 5.8 Return SI concentrations in flowback water vs cumulative produced water

Figure 5.8 indicates the returned profiles of SI concentration in different cases plotted against cumulative produced water. It is plotted to obtain the comparison trends of returned SI in response of the changing of total volume of water produced. As discussed previously, both the case with 100 ppm and with 1,000 ppm SI injected present more obvious declines, compared with the other two cases (10 ppm and 10,000 ppm); meanwhile, all the returned SI shows a significant drop during the production period with extremely low produced water rate (the late stage of production), which is due to the majority of flowback water produced at this stage being almost pure formation water (including only low concentration of SI).

5.3.3.2 Pumping SI during different injection period

As a further discussion of this section, three cases are simulated by pumping scale inhibitor during different injection period (early, middle and late stage of injection) and all of them are performed by pumping the same mass of SI along with the same total volume of fracture fluid into the system. In the meantime, the total injection process is also maintained to be uniform for only one day (all the injection constraints are controlled by the comparison of the original SI injection case).

Case 1 injects fracture fluid that includes 3,000 ppm SI for the first 1/3 day and followed with the injection of regular fracture fluid (without adding SI) until the one

day injection period is completed; case 2 injects regular fracture fluid for the beginning 1/3 days and then starts to inject fracture fluid contains 3,000 ppm SI for a further 1/3 days and completes the rest of the process with the injection of regular fracture fluid; case 3 applies the injection of 3,000 ppm SI during the last 1/3 days along with injecting regular fracture fluid for the first 2/3 days . As mentioned previously, all three cases are with a total volume injection of 3,000 barrels and the mass of SI injected is 477,000 grams. All the scenarios are also modelled using the same matrix adsorption isotherm as the original base case. The simulation results are shown in **Figure 5.9** and **Figure 5.10** with both Y axes plotted as log scales.

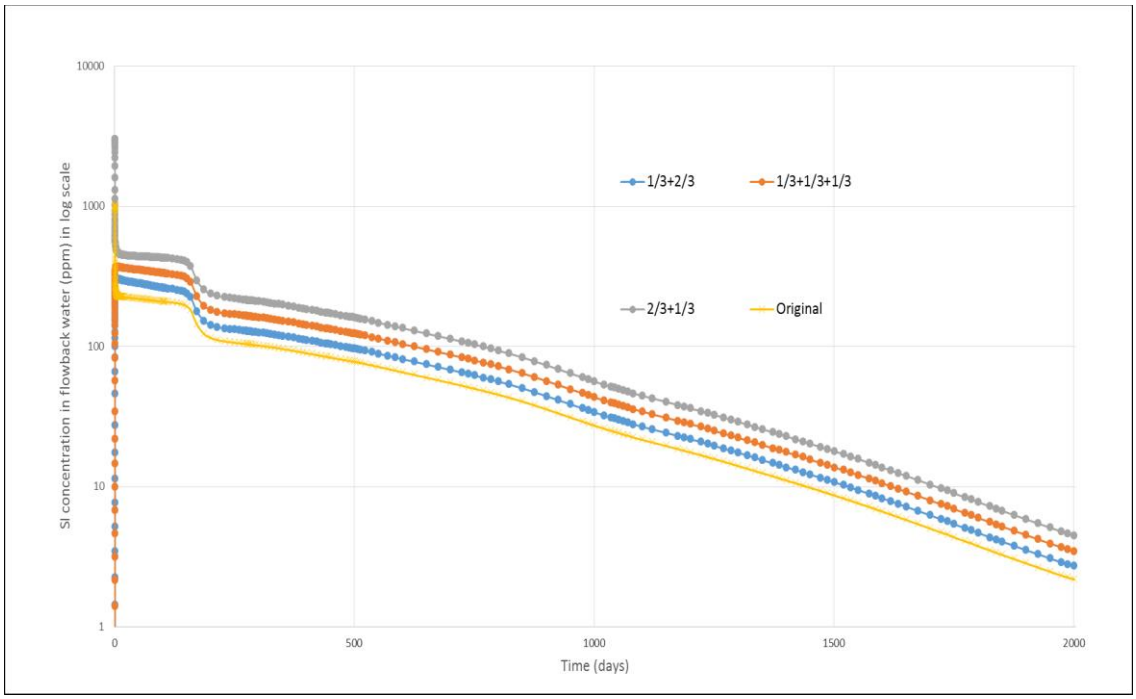

Figure 5.9 Return SI concentrations in flowback water vs time

As indicated in **Figure 5.9**, it can be seen that the overall trend for all four cases are similar to each other; however, the original case yields the worst return profile among them all (provides the worst protection especially during early stage of production). This can be interpreted by comparing with the continuous scale inhibitor injection, and all the cases that include a pre/post-injection treatment. Even squeezing a large volume of SI in a short period before production can provide a better inhibitor return profile due to the worst scaling risk occurring at the very early stage of production (higher level of protection is required during this period). The maximum returned SI concentrations in case 1 and case 2 are less than 600 ppm due to the post flush of fracture fluid injection which means more SI has been retained in the system during the very early

stage of production. Case 3 thus offers the best protection among all three cases. It can be seen that the maximum SI concentration in the flowback water at the beginning reaches 3,000 ppm due to the pumping of high concentration of SI at the late stage of injection. This high returned inhibitor concentration not only provides extra protection for the well at early production stages, but could also offer longer protection (under the condition of injecting the same mass of SI for each scenario).

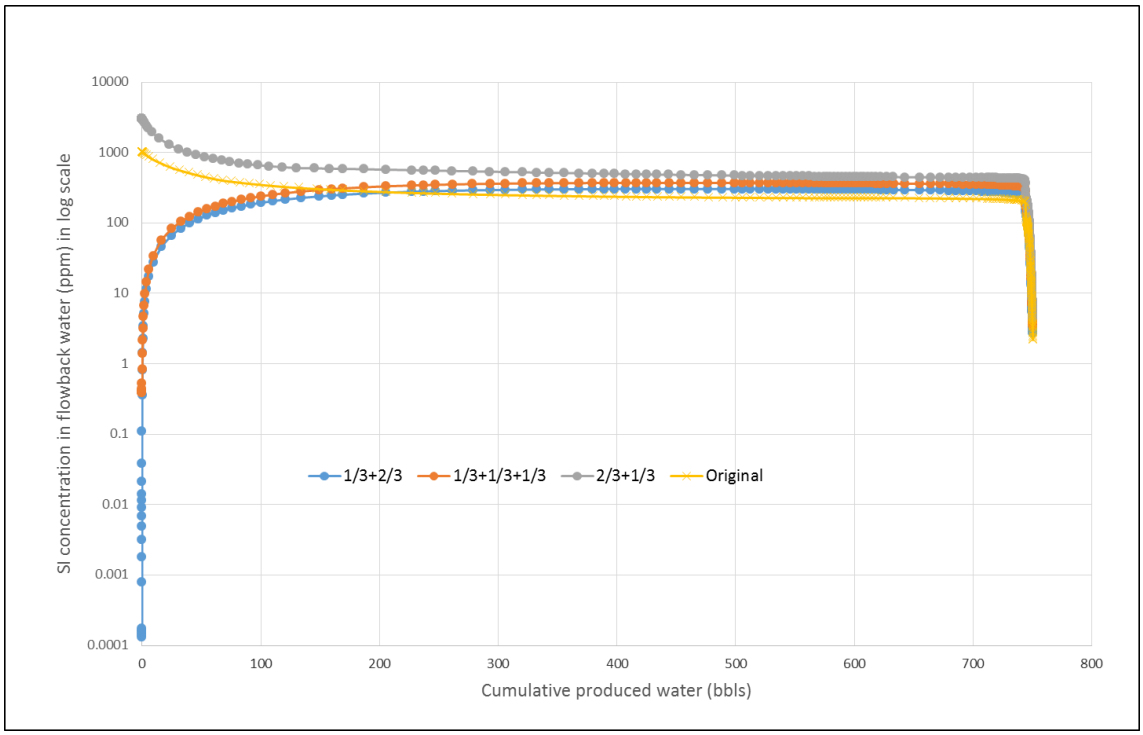

Figure 5.10 Return SI concentrations in flowback water vs cumulative produced water

Figure 5.10 indicates SI concentration in flowback water plotted against total volume of water produced. Two major return behaviours can be readily observed (cases 1 & 2 and case 3 & original case). As discussed previously, on the one hand, at the early stage of production the return concentrations for cases 1 & 2 are increasing due to the operation of post-injection process (fracture fluid pumped into the system at late stage of injection contains zero SI but produced back prior to the injected fracture fluid with high concentration of SI). On the other hand, case 3 and the original case start with a high concentration of returned SI and it decreases while production brings it back on. This decline of the concentration can be accounted for by the injection of age proportion of SI directly before the production process (high concentration of the injected fracture fluid will flow back first, followed by the production of brine with low SI concentration). Another obvious behaviour can be observed is the sharp decline that happened where an extremely low produced water rate appears, this can be considered

consistent with the analysis above since the majority of water that flows back during the low water rate period is formation water with a negligible concentration of SI.

To observe the capability of SI retention for every single scenario, the cumulative mass of SI produced for all three cases have been calculated. According to the calculation results, even with the poorest SI retention among them all, case 3 still produces back a total 14.3% of SI, meanwhile case 1 presents the strongest SI retention scenario, with only a total of 6.6% of injected SI flowing back. Therefore, it can be concluded that all the cases applied with different injection strategies can offer a significant retention of SI, which can be considered as satisfactory for conventional scaling control, yet may not be ideal to manage a scaling risk in a shale gas system due to the significant SI adsorption on the matrix rock.

5.4 CONCLUSIONS

As mentioned in the first section of this chapter, the aim is to explore scale control management based on a development of scale inhibitor injection model. This study is considered as a start of future scale inhibitor modelling studies and only provides a few basic discussions by comparing some simple sensitivity simulation cases. The conclusions are as below:

- A base case has been developed to simulate scale inhibitor injection and to examine the impact of inhibitor retention on well protection (with the applications of matrix adsorption isotherm). The base case also demonstrates that there is the potential to design a satisfactory scale inhibitor treatment by applying a Langmuir adsorption isotherm (without considering SI chemical reaction process).

- Some sensitivity study cases have been performed and discussed, some observations are listed here in terms of the conclusion for each study:

    - Different location of variable conductivity zones have been applied to investigate the impact on SI return– both of cases provide acceptable return concentration whereas the impact of lower location on retaining SI is less sensitive in the early stages compared with the late stages of production.
    - Different adsorption levels have been applied in various SI injection cases – it indicates that stronger adsorption can result in less SI flowing back

however, the impact is more sensitive at the beginning of the production period.

- Different SI injection strategies have been developed to observe the change of SI concentration in flowback water – this work suggests a large volume of SI pumped in a relatively short period at late injection stage can provide poorer SI retention but better protection overall for the well (higher SI concentration returned) during the early production period (when a high scaling risk is observed).

In conclusion, operating a post-water injection along with a system with a stronger adsorption level could offer greater SI retention at the early stages of production. However, this may be undesirable, as in fact this early period may be the time when highest concentrations of SI in solution are required. In this perspective, late stage injection with higher SI concentration is favourable to protect the well from inorganic scale precipitating at early stage of production.

CHAPTER 6 CONCLUSIONS AND SUGGESTED FUTURE WORK

6.1 OVERVIEW OF STUDY

The objective of this project is to provide recommendations for inorganic scale control management during shale gas production. A series of studies has been carried out to achieve this final aim. The detailed conclusions have been presented in each chapter of this thesis, and the overall workflow is shown in **Figure 6.1**.

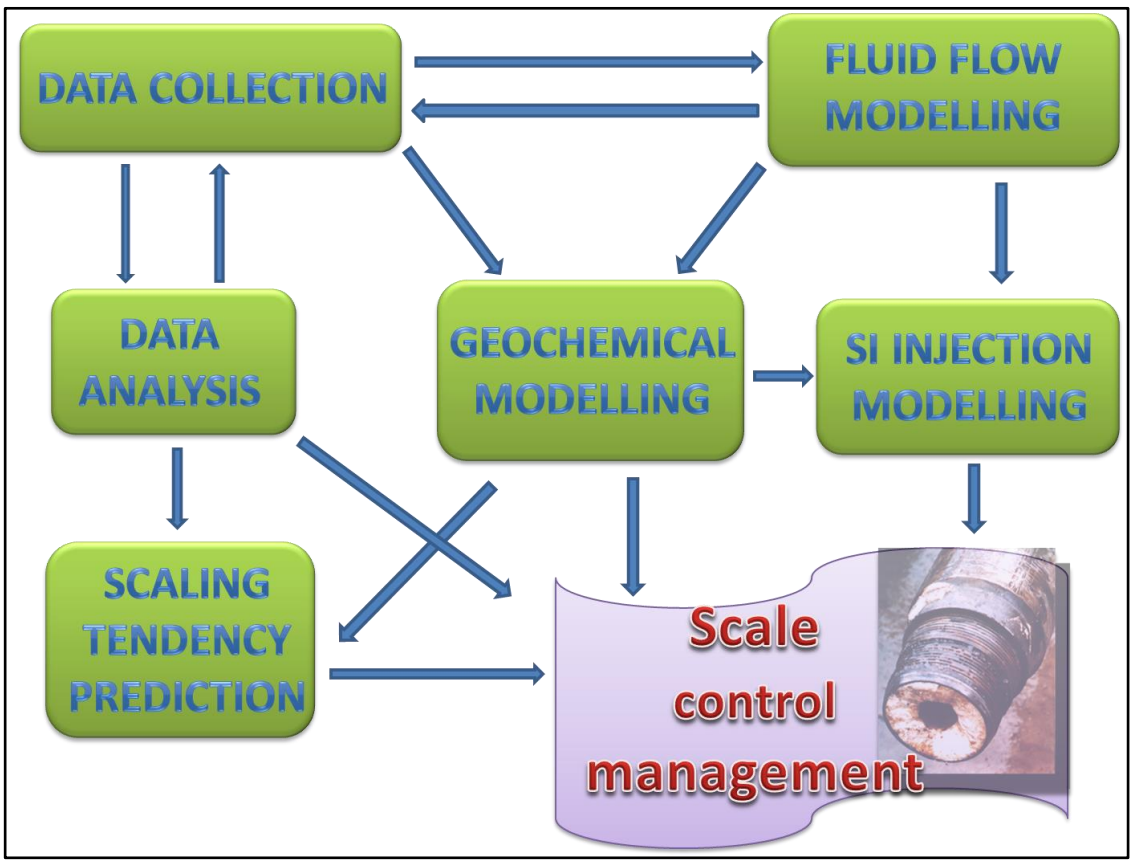

Figure 6.1 Workflow for inorganic scale control management during shale gas production

According to the workflow shown above, the study should start with data collection as a preparation for the modelling studies (simulation parameters and field data to be collected to provide a basis for creating a history match) and data analysis (geochemical compositional data to be collected). Thereafter the scaling tendency can be evaluated (formation water composition should also be predicted) and fluid flow modelling can be developed so that further geochemical models and scale inhibitor injection models can be run based on the previous studies. From the workflow chart, it can readily be found

that all of these studies head to an ultimate outcome, which is the design of a scale control management strategy.

6.2 CONCLUSIONS

The principal conclusions of this thesis are presented in this section. These conclusions have been divided into two parts for better classification – conclusions on data analysis and outcomes of simulation results according to modelling study.

6.2.1 Conclusions for data analysis

The aim of the data analysis was to use the established knowledge about shale gas systems to perform basic predictions of scaling tendency so that the *in situ* formation water composition can be calculated and validated, and also to better develop the hydraulic fractured shale gas models (both the fluid flow model and the geochemical model) to further evaluate the scaling risk; thus optimal scale control management can be achieved.

First of all, a database of parameters pertinent to shale gas systems has been set up based on the literatures review. As mentioned in Chapter 2, this dataset does not only provide reservoir properties but also includes geochemical compositional data collected from hydraulic fracturing and production processes.

Then these data are used for analysis to provide evidence that significant $CaCO_3$ scaling has been observed in the HRB area. In addition, the scaling risk of $BaSO_4$ has also been identified, this being due to the mixing of commingled fluids carrying high concentrations of barium and sulphate, not only in the HRB area but also in some other shale plays in US.

According to the scaling tendency prediction for $CaCO_3$ precipitation, the calculation of *in situ* formation water compositions has been performed and validated. It is important to know the formation water composition so that the calculations of the fraction of injected fracture fluid in flowback water can be performed. Both of these play an important role in the ensuing modelling studies.

6.2.2 Conclusions for modelling study

Firstly, the modelling study of the fractured shale system starts with a fluid flow simulation developed using the CMG IMEX simulator. A simplified hydraulic fractured

shale system is modelled to represent the production process during shale gas recovery, and a satisfactory history matched case has been achieved by comparing with the field data supplied for the HRB area. The fluid flow modelling identifies that including the closure of secondary fractures (by applying variable conductivity zones in the fracture area), along with considering the impact of gravity segregation in the fracture zone, can achieve a good history match.

Secondly, a series of geochemical models has been developed using the CMG GEM simulator and PHREEQC. The 1D GEM models and the PHREEQC mineral dissolution model are used to demonstrate that the altered high salinity in the flowback water in the HRB area is due to the mixing with high salinity *in situ* formation water, whereas mineral dissolution is insufficient to explain the observed behaviour. The 3D GEM models are developed by including aqueous and mineral reactions to further identify that a serious $BaSO_4$ scaling risk can be observed, especially at the early stage of shale gas production, and that the greatest precipitation can be found at the bottom of the fracture zone in addition to the perforations along the horizontal section of the well.

Finally, a scale inhibitor injection model has been developed on the basis of the history matched fluid flow model built using CMG IMEX. This simulation study is developed to explore an optimum scale control strategy. The base case demonstrates that there is the potential to design a satisfactory scale inhibitor treatment using an adsorption isotherm to describe retention. Meanwhile, to achieve a better performance of SI retention during the early stages of production, injecting a larger volume of SI in a relative short period followed by a post flush water injection process is required. If the shale matrix has a stronger adsorption level capacity then this retention behaviour will be enhanced.

6.3 RECOMMONDATIONS ON FUTURE WORK

Further research is required to be able to derive general principles and to apply the methodology to specific scenarios.

As discussed previously, the aim of this study was to be able to model scale inhibitor propagation, retention and release in shale systems, so that scale control treatment designs can be optimised. In consideration of this, two major areas of future work are proposed here:

1) Further research:
    - Further analysis of brines from this and other fields to identify maximum scale risk and the evolution of scale risk over the lifetime of the well.
    - If shale gas field data are available (in terms of scale inhibitor return concentrations in the flowback water), these could be collected and analysed to be used for optimising future scale inhibitor propagation models.
    - If experimental data related to interactions between fracture fluid and shale rock pertinent to scale management are available, these data can be recorded and analysed as preparation for future modelling studies.
2) Field application – scale control design:
    - Developing further scale inhibitor injection models to identify whether inhibitor application is necessary or not. If scale control management is necessary, the inhibitor design should be optimized based on the results of the modelling study.
    - Using laboratory scale inhibitor test data to assist with scale inhibitor selection, including inhibition efficiency, chemical compatibility, inhibitor adsorption on shale samples, etc. This could be used for the selection of an adsorption isotherm for a modelling study as well as developing a squeeze treatment design, in addition to formation damage prevention due to the application of scale inhibitors.

In conclusion, the main aim of the proposed future work would be to improve the understanding of the application of scale inhibitors in shale systems by using further data analysis along with scale inhibitor modelling to provide a tool to enable engineers to optimise scale control designs to prevent formation and wellbore damage from mineral precipitations in a cost effective way and minimising wastage of scale inhibitor chemicals.

References

Abdul Majid A.B., Hansen J.E., Al-Dahlan M.N., Malik A.R., Alharbi M.M., Al-Suwaigh M.K., Atwi M.A., Shammari N.S., Alkhaldi M.H., Abel J.T. and Alsalman M.A., 2017. Seawater Based Fracturing Fluid: A Game Changer in Hydraulic Fracturing Applications in Saudi Arabia, SPE-184015-MS.

Allen N., Aplin A. and Thomas M., 2009. Introduction to gas shale storage [Internal presentation].

Alramahi, B. and Sundberg, M. I., 2012. Proppant Embedment and Conductivity of Hydraulic Fractures in Shales. ARMA-2012-291.

Amitosh T., Prashant F., Ankit M., NeelMani S., Chandran M., Sarang L., Aastha S. and Anindya S., 2017. Development and Operational Implementation of Scale Management Strategy in a Mature Field, SPE-186910-MS.

Ardiansyah N., Amgad S., Shuyu S., Mokhtar E., Yushu W., 2015, Numerical Simulation of Natural Gas Flow in Anisotropic Shale Reservoirs, Abu Dhabi International Petroleum Exhibition and Conference, 9-12 November, Abu Dhabi, UAE, SPE-177481-MS.

Ashkan Z., Yingzhe T., Jordan H., Mojtaba B., Hassan D., Bearinger D., 2015, Chemical Analysis of Flowback Water and Downhole Gas Shale Samples, SPE/CSUR Unconventional Resources Conference, 20-22 October, Calgary, Alberta, Canada, SPE-175925-MS.

Ballard, T.J., Beare, S.P., Lawless, T.A., 1994. Fundamentals of Shale Stabilization: Water Transport through Shales. SPE Formation Eval, 129-134.

BCMEMPR, "Looking into the Future: Development in the Horn River Basin", 2009. British Columbia Oil and Gas Commission, Hydrocarbon and By-Product Reserves in British Columbia, 2003 and 2004.

BCMEMPR, "Ultimate Potential for Unconventional Natural Gas in Northeastern British Columbia's Horn River Basin", (http://www.neb-one.gc.ca/nrg/sttstc/ntrlgs/rprt/archive/ncnvntnlntrlgshrnrvrbsnhrnrvr2011/ncnvntnlntrlg

shrnrvrbsnhrnrvr2011-eng.pdf) British Columbia Ministry of Energy and Mines & National Energy Board, Oil and Gas Report 2011 – 1 (May 2011), Accessed May 2013..

Bearinger, D., 2013. Message in a Bottle, Paper URTeC 1618676, presented at the Unconventional Resources Technology Conference held in Denver, Colorado, USA, 12-14 August.

Bicheng Y., Lidong M., Yuhe W., Hewei T., Cheng A., John E. K., Mechanistic Simulation Workflow in Shale Gas Reservoirs, 2017, SPE Reservoir Simulation Conference, 20-22 February, Montgomery, Texas, USA, SPE-182623-MS.

Blauch, M.E., Myers R.R., Moore T.R., Lipinski B.A., and Houston N.A., 2009. Marcellus Shale post-frac flowback waters: Where is all the salt coming from and what are the implications?, SPE 125740.

Bobrosky, D., 2010. Multi-Stage Fracturing of Horizontal Wells - case studies: Alberta, Swan Lake, Fort Worth, Pembina, Saskatchewan, Packers Plus Presentation Lake Louise, January 28/29 2010.

Bowker, K.A., 2007. Barnett Shale gas production, Fort Worth Basin: Issues and discussion. AAPG Bulletin, v. 91, no. 4, pp. 523-533.

Brad J. Hayes, 2011. Water Source and Disposal for Unconventional Gas Plays in N. E. British Columbia, presentation to CSUG Water Workshop, 20th April.

Brian LeCompte, Javier A. Franquet and David Jacobi, 2009, Evaluation of Haynesville Shale Vertical Well Completions with a Mineralogy Based Approach to Reservoir Geomechanics, SPE 124227.

Brown A.D.F., Merrett S.J., and Putnam J.S., 1991. Coil-Tubing Milling/Underreaming of Barium Sulphate Scale and Scale Control in the Forties Field, SPE 23106.

Byrnes, A.P., 2011. Role of induced and natural imbibition in frac fluid transport and fate in gas shales: EPA Technical Workshops for Hydraulic Fracturing Study, Fate and Transport, March 28–29, 2011. presented at the US EPA Conference Center, Arlington, VA, 9 p., 19 PowerPoint slides, accessed February 4, 2014.

CCME (Canadian Council of Ministers of the Environment), 2013. Barium – Canadian Soil Quality Guidelines for the Protection of Environmental and Human Health, 2013.

Chaohua G., Mingzhen W., Haowei C., Xiaoming H., Baojun B., 2014, Improved Numerical Simulation for Shale Gas Reservoirs, Offshore Technology Conference-Asia, 25-28 March, Kuala Lumpur, Malaysia, OTC-24913-MS.

Chao Yan, Amy T. Kan, Wei Wang, Fei Yan, Lu Wang, Mason B. Tomson, Huiguang Zhu and Ross Tomson, 2013. Boehmite Based Sulphonated Polymer Nanoparticles with Improved Squeeze Performance for Deepwater Scale Control, OTC 24252, presented at the Offshore Technology Conference held in Houston, Texas, USA, 6–9 May.

Chenevert M., Shale alteration by water adsorption. J Pet Technol 1970; 22:1141–1148.

Cipolla, C.L., Lolon, E., Mayerhofer, M.J. and Warpinski, N.R., 2009. The Effect of Proppant Distribution and Un-propped Fracture Conductivity on Well Performance in Unconventional Gas Reservoir. Presented at the SPE Hydraulic Fracturing Technology Conference, The Woodlands, Texas, USA, 19-21 January. SPE-119368-MS.

Clemmit A.F., Ballance D.C. and Hunton A.G., 1985. The Dissolution of Scales in Oilfield Systems, SPE14010/l.

Crafton J.W., Gunderson D., Stimulation Flowback Management: Keeping a Good Completion Good. Paper SPE 110851 presented at the 2007 SPE Annual Technical Conference and Exhibition; November 11–14; Anaheim, CA; 2007.

Crain, Crain's Petrophysical Handbook – Dual porosity model for fractured reservoirs. (https://www.spec2000.net/23-fracmath5.htm) Accessed 10 April 2017.

Crain, Crain's Petrophysical Handbook – Editing logs with the log response equation. (https://www.spec2000.net/10-mechsyn.htm) Accessed 3 April 2017.

Crain, Crain's Petrophysical Handbook – Fracture porosity from aperture data. (https://www.spec2000.net/12-phifrac.htm) Accessed 10 April 2017.

Crain, Crain's Petrophysical Handbook – Special Cases – Tight Gas Reservoirs. (https://www.spec2000.net/17-tightgas.htm) Accessed 19 October 2016.

Curtis Crowe, McConnell S.B., Hinkel J.J., and Ken Chapman, 1994. Scale Inhibition in Wellbores, SPE 27996.

David Eslinger, Ashley B. Johnson, Aaron Mcdonough and Mark Oettli, 2000. A Hybrid Milling/Jetting Tool - The Safe Solution to Scale Milling, SPE 60700, presented at the Coiled Tubing Roundtable held in Houston, TX, 5–6 April.

Davis, W.E., "National Inventory of Sources and Emissions: Barium, Boron, Copper, Selenium and Zinc", presented at the U.S. Environmental Protection Agency, Washington, D.C. Report EPA-68-02-0100. P.56. In: WHO, 1990 and ATSDR, 1992.

Dershowitz W.S., Cottrell M.G., Lim D-H, Doe T.W., 2010. A discrete fracture network approach for evaluation of hydraulic fracture stimulation of naturally fractured reservoirs. presented at the 44th U.S. Rock Mechanics Symposium and 5th U.S.-Canada Rock Mechanics Symposium, 27–30 June, Salt Lake City, Utah; 2010. 8 p.

Doe T, Lacazette A, Dershowitz W, Knitter C., 2013. Evaluating the effect of natural fractures on production from hydraulically fractured wells using Discrete Fracture Network models. Paper SPE 168823/ URTeC 1581931, presented at the First Unconventional Resources Technology Conference. Society of Petroleum Engineers, 12–14 August, Denver, CO, USA.

Dong Shen, Sumit Bhaduri, Minh V.O., Paul Carman, D. V. Satya Gupta, and Yash Pandey, 2017. A Novel Solid Inhibitor for Anhydrite Scale Control under Extreme Well Conditions, SPE-184525-MS, presented at the SPE International Conference on Oilfield Chemistry held in Montgomery, Texas, USA, 3–5 April.

Dresel, P.E., and Rose, A.W., 2010. Chemistry and Origin of Oil and Gas Well Brine in Western Pennsylvania, Open file report.

Dresser Atlas. Log Interpretation Charts. Houston (TX): Dresser Atlas Publication; 1983.

Du, C., Zhang, X., Melton, B., Fullilove, D., Suliman, B., Grant, D. and Calvez, J., 2009. "A Workflow for Integrated Barnett Shale Gas Reservoir Modeling and Simulation," paper SPE 122934, presented at the 2009 SPE Latin American & Caribbean Petroleum Engineering Conference, Cartagena, Colombia, 31 May -3 Jun.

Ebrahim Ghanbari, Majid Ali Abbasi, Hassan Dehghanpour and Doug Bearinger, 2013. Flowback volumetric and chemical analysis for evaluating load recovery and its impact on early-time production, SPE 167165-MS.

Edwards KL, Weissert S., Jackson JB. et al., 2011. Marcellus Shale Hydraulic Fracturing and Optimal Well Spacing to Maximize Recovery and Control Costs. Paper SPE 140463-MS presented at SPE Hydraulic Fracturing Technology Conference; January 1, 2011; Woodlands, TX.

Elisabeth L. Rowan, Mark A. Engle, Thomas F. Kraemer, Karl T. Schroeder, Richard W. Hammack, and Michael W. Doughten, 2015. Geochemical and isotopic evolution of water produced from Middle Devonian Marcellus shale gas wells, Appalachian basin, Pennsylvania, AAPG BULLETIN, V. 99, NO. 2 (February 2015), pp. 181-206.

Eric Towers, 2011. "C-1-J Pad Hydraulic Fracturing Chemical Analysis Project", August 22nd 2011.

Fan, L., Thompson, J.W. and Robinson, J.R., 2010. Understanding Gas Production Mechanism and Effectiveness of Well Stimulation in the Haynesville Shale through Reservoir Simulation. Paper SPE 136696 presented at Canadian Unconventional Resources and International Petroleum Conference, Calgary, Alberta, Canada, 19-21 October.

Fei Yan, Fangfu Zhang, Narayan Bhandari, Ya Liu, Lu Wang, Zhaoyi Dai, Zhang Zhang, Valerie Bolanos, Amy Kan, and Mason Tomson, 2015. Interaction between Scale Inhibitors and Shale and Sandstone Formations, SPE-173769-MS, presented at the SPE International Symposium on Oilfield Chemistry held in The Woodlands, Texas, USA, 13–15 April.

Fredd, C. N., McConnell, S. B., Boney, C. L. et al., 2001. Experimental Study of Fracture Conductivity for Water-fracturing and Conventional Fracturing Applications. SPE Journal, 6(03): 288-298. SPE-74138-PA, 2001.

Gdanski, R. D. and Walters, H. G., 2010. Impact of Fracture Conductivity and Matrix Relative Permeability on Load Recovery. Presented at the SPE Annual Technical Conference and Exhibition, Florence, Italy, 19-22 Spetember. SPE-133057-MS.

Geoscience BC Report, 2015. Horn River Basin Surface Water Monitoring Program – Final Report, Geoscience BC Report 2016-13, December 2016, KWL Project No. 2692.002-300.

Gluyas J. and Swarbrick R., Petroleum Geoscience. Malden: Blackwell Publishing; 2009.

Ghanbari E, Abbasi M.A., Dehghanpour H. and Bearinger D., 2013. Flowback volumetric and chemical analysis for evaluating load recovery and its impact on early-time production, presented at the SPE Canadian Unconventional Resources Conference 2013, 5–7 November, Calgary, Alberta, Canada, 1, p 533–548.

Graham G.M. and Collins I.R., 2004. Assessing Scale Risks and Uncertainties for Subsea Marginal-Field Development, SPE 87460, presented at the SPE International Symposium on Oilfield Scale, Aberdeen, 26–27 May.

Gregory K.B., Vidic R.D. and Dzombak D.A., 2011. Water management challenges associated with the production of shale gas by hydraulic fracturing. Elements 2011;7 (3):181–186.

Hao S., Adwait C., Hussein H., Xundan S., Lin L., 2015, Understanding Shale Gas Flow Behavior Using Numerical Simulation, SPE-167753-PA.

Hassan Dehghanpour, Mingxiang Xu and Ali Habibi, 2015. Chapter 16 Wettability of Gas Shale Reservoirs, Fundamentals of Gas Shale Reservoirs, First Edition. Edited by Reza Rezaee. Pg 348-349, 2015.

Hensen EJM, Smit B., Why clays swell. J Phys Chem B., 2002; 106:12664–12667.

Hernandes R., Melo V.L.A., Santos J.A.M., Rosário F.F., Bezerra M.C.M., and Rosa K.R.S.A., 2008. Scale Management in Espadarte Field, SPE 114112, presented at the SPE International Oilfield Scale Conference held in Aberdeen, UK, 28–29 May 2008.

Holditch, S.A., Tight Gas Sand, SPE Distinguished Author Series, JPT, Jun 2006.

HRN, "Encana estimates up to 500 trillion cubic feet in Horn River Basin", (http://hornrivernews.com/2009/09/10/encana-estimates-up-to-500-trillion-cubic-feet-in-horn-river-basin/) Horn River News – Shale Gas in Northern British Columbia and elsewhere, September 10 2009, Accessed October 2015.

HRN, "Horn River Producers Group", (http://hornrivernews.com/companies/) Horn River News – Shale Gas in Northern British Columbia and elsewhere, 2012, (Accessed October 2015).

Hua Guan, 2015. Scale Deposition Control and Management in Subsea Fields, Paper NO. 5480, presented at the NACE International.

Hua Guan, 2016. Flow Assurance Risk Evaluation and Chemical Management in a Shale Gas Field, Paper NO. 7674, presented at the NACE International.

Igor Kocis, Tomas Kristofic, Matus Gajdos, Gabriel Horvath and Slavomir Jankovic, 2015. Utilization of Electrical Plasma for Hard Rock Drilling and Casing Milling, SPE-173016-MS, presented at the SPE/IADC Drilling Conference and Exhibition, 17-19 March, London, England, UK.

IHRDC, 2016. Critical water saturation and irreducible water saturation training - (http://www.ihrdc.com/els/ipims-demo/t26/offline_IPIMS_s23560/resources/data/G4108.htm) Accessed October 2016.

Iman O. K., Tim L., Jason M., Meaghan C. Y., Adebola T. A., Usman A., Reza B., Imre K., Murray R., Mike C., James M., Dave W., 2016, Examination of Water Management Challenges and Solutions in Shale Resource Development - Could Waterless Fracturing Technologies Work?, SPE/AAPG/SEG Unconventional Resources Technology Conference, 1-3 August, San Antonio, Texas, USA, URTEC-2461040-MS.

Ishkov, O., Mackay, E. and Sorbie, K., 2015. The Analysis of Chemical Processes in Reservoirs on the Basis of the Identification of Injection-Water Fraction in Produced Brine, presented at the SPE Production & Operations, August, Page 229-235.

Janszen M., Bakker T. and Zitha P. L. J., 2015. Hydraulic fracturing in the Dutch Posedonia Shale, SPE 174231-MS.

Jaremalm, M., Hifab A.B. and Kohler, S., 2013. Precipitation of barite in the biosphere and its consequences for the mobility of Ra in Forsmark and Simpevarp, presented at the Swedish Nuclear Fuel and Waste Management Co., Technical Report, TR-13-28, December.

Jenkins, C.D., Boyer M., 2008. Coalbed and Shale Gas Reservoirs, SPE 103514, 2008.

Jordan M.M., Feasey N.D, and Johnston C.J., 2005. Inorganic Scale Control Within MEG/Methanol-Treated Produced Fluids, SPE 95034, presented at the SPE International Symposium on Oilfield Scale held in Aberdeen, United Kingdom, 11–12 May 2005.

Juan Felipe A. P., Faruk C., Deepak D., Richard F. S., 2010, Accurate Simulation of Shale-Gas Reservoirs, SPE Annual Technical Conference and Exhibition, 19-22 September, Florence, Italy, SPE-135564-MS.

Kaasa, B., 1998. Prediction of pH, mineral precipitation and multiphase equilibria during oil recovery: IUK-PhD Thesis. The Norwegian University of Science and Technology, Trondheim, Norway.

Kan, A.T., Tomson, M.B., 2012. Scale Prediction for Oil and Gas Production. SPE J 17(2): 362-378. SPE-132237-PA, 2012.

Kennedy R.B., 2015. Chapter 17 Gas Shale Challenges Over the Asset Life Cycle in Fundamentals of Gas Shale Reservoirs First Edition, Pg 376, 2015.

King G.E., 2010. Thirty years of Gas Shale Fracturing: What Have We learned? Paper SPE 133456 presented at the SPE Annual Technical Conference and Exhibition; September 19–22; Florence, Italy.

King, G.E., 2012. "Hydraulic Fracturing 101: What Every Representative, Environmentalist, Regulator, Reporter, Investor, University Researcher, Neighbor, and Engineer Should Know About Hydraulic Fracturing Risk", Paper SPE 152596 MS, Presented at the SPE Hydraulic Fracturing Technology Conference held in The Woodlands, Texas, USA, 6-8 February.

Kurtoglu B., 2013. Integrated reservoir characterization and modeling in support of enhanced oil recovery for Bakken [PhD Thesis]. Petroleum Engineering, Colorado School of Mines.

Lacazette A., Dershowitz W. and Vermilye J., 2014. Geomechanical and flow simulation of hydraulic fractures using high-resolution passive seismic images, presented at the SPE/AAPG/SEG Unconventional Resources Technology Conference, 25–27 August, Denver, CO, URTeC 1935902; 2014. 10 p.

Lensie Owlen Paugh, 2008, Marcellus Shale Water Management Challenges in Pennsylvania, SPE Shale Gas Production Conference, 16-18 November, Fort Worth, Texas, USA, SPE-119898-MS.

Leonard J. Kalfayan, Clyde A. McAfee, and Lawrence M. Cenegy, Hess Corporation, 2013. Field Wide Implementation of Proppant-Based Scale Control Technology in the

Bakken Field, SPE 165201, presented at the SPE European Formation Damage Conference and Exhibition held in Noordwijk, The Netherlands, 5–7 June.

Lexicon of Canadian Geological Units, "Muskwa Formation", (http://www.nrcan.gc.ca/energy/crude-petroleum/4559) Natural Resources Canada, 2009, Accessed May 2015.

Li Jianchao, Lie Hui Zhang, and Yulin Chen, 2015. Adsorption Behavior Study of Shale Gas: Models and New Combination Approach, SPE-176880-MS, presented at the SPE Asia Pacific Unconventional Resources Conference and Exhibition held in Brisbane, Australia, 9–11 November.

Lu XC, Li FC, 1995. Adsorption measurements in Devonian shales. Fuel 1995; 74:599–603.

Mackay E.J., Jordan M.M., Feasey N.D., Nalco, Shah D., Kumar P. and Ali S.A., 2004. Integrated Risk Analysis for Scale Management in Deepwater Developments, SPE-87459-MS, presented at the SPE International Symposium on Oilfield Scale, 26-27 May, Aberdeen, United Kingdom.

Mackay Eric J., 2010. Comparison of Scale Control Challenges between Production and PWRI Wells, SPE 129181, presented at the SPE International Symposium and Exhibition on Formation Damage Control held in Lafayette, Louisiana, USA, 10–12 February.

Mackay, E.J., and Sorbie, K., 1999. An Evaluation of Simulation Techniques for Modelling Squeeze Treatments. SPE 56775.

Maricel Marquez, Laura Anne Schafer and William David Norman, 2011. Preemptive Scale Management: Treating with Scale Inhibitor While Frac Packing a Well, SPE-147006-MS, presented at the SPE Annual Technical Conference and Exhibition, 30 October-2 November, Denver, Colorado, USA.

Matus Gajdos, Mostenicky, Igor Kocis, Tomas Kristofic, Michal Plichta, Gamalel Bannan and Islam Taha, 2016. Plasma-Based Milling Tool for Light Well Intervention, SPE-178179-MS, presented at the SPE/IADC Middle East Drilling Technology Conference and Exhibition, 26-28 January, Abu Dhabi, UAE.

Meyer B.R. and Bazan L.W., 2011. A Discrete Fracture Network Model for Hydraulically Induced Fractures: Theory, Parametric, and Case Studies, Paper SPE 140514 presented at the SPE Hydraulic Fracturing Technology Conference; January 24–26; The Woodlands, TX, 2011.

Michel G., Civan F., Sigal R.F. and Devegowda D., 2011. Parametric Investigation of Shale Gas Production Considering Nano-scale Pore Size Distribution, Formation Factor, and Non Darcy Flow Mechanisms. SPE-147438-PP, presented at the 2011 SPE Annual Technical Conference and Exhibition (ATCE), Denver, CO, USA; 2011b 30th Oct–2nd Nov.

Michele S., Ivan C., 2011, Use of Reservoir Simulation to Help Gas Shale Reserves Estimation, International Petroleum Technology Conference, 15-17 November, Bangkok, Thailand, IPTC-14798-MS.

Mohamed M. and Salaheldin E., 2017. Towards a Complete Removal of Barite Weighted Water and Oil Based-Drilling Fluids in Single Stage, SPE-187122-MS, presented at the SPE Annual Technical Conference and Exhibition, 9-11 October, San Antonio, Texas, USA, 2017.

Mossop, G.D. and Shetsen, I., 1994. "The Geological Atlas of the Western Canada Sedimentary Basin, Chapter 11: Devonian Beaverhill Lake Group of the Western Canada Sedimentary Basin", Alberta Geological Survey, (http://www.ags.gov.ab.ca/publications/wcsb_atlas/a_ch11/ch_11.html), Accessed May 2016.

Nathan R. Hutchings, Eric W. Appleton and Robert A. McGinnis, 2010. Making High Quality Frac Water out of Oilfield Waste, SPE-135469-MS, presented at the SPE Annual Technical Conference and Exhibition, 19-22 September, Florence, Italy 2010.

NEB, 2009. "Energy Briefing Note - A Primer for Understanding Canadian Shale Gas", (https://www.neb-one.gc.ca/nrg/sttstc/ntrlgs/rprt/archive/prmrndrstndngshlgs2009/prmrndrstndngshlgs2009-eng.pdf) National Energy Board, November, 2009, Accessed April 2013.

Norris M.R., Gulrajani S.N., Mathur A.K., Price J. and May D., 2001. Hydraulic Fracturing for Reservoir Management: Production Enhancement, Scale Control and

Asphaltine Prevention, SPE 71655, presented at the SPE Annual Technical Conference and Exhibition held in New Orleans, Louisiana, 30 September–3 October 2001.

Obinna Akuanyionwu and Fazrie Wahid, 2011. Consideration Factors in Defining an Effective Scale Management Strategy during Early Stages of Field Development Planning, SPE 144502, presented at the SPE Offshore Europe Oil and Gas Conference and Exhibition held in Aberdeen, UK, 6–8 September 2011.

Oddo J.E., Reizer J.M., and Sitz C.D., 1999. A Comprehensive Field and Laboratory Study of Scale Control and Scale Squeezes in Sumatra, Indonesia, Paper NO. 115, presented at the NACE International.

Packers Plus, 2011. A Case Study: Packers Plus StackFRAC doubles production in the Horn River shale gas play.

Parmer, J.S. and H., Kuru. E., 2013. Drainage against Gravity: Factors Impacting the Load Recovery in Fractures, SPE 164530-MS, presented at the SPE Unconventional Resources Conference - USA, Woodlands, TX, USA, 10-12 April, 2013.

Parkhurst, D.L., and Appelo, C.A.J., 1999. User's guide to PHREEQC (version 2) – a computer program for speciation, batch-reaction, one-dimensional transport, and inverse geochemical calculations: U.S. Geological Survey, Water-Resources Investigations Report 99-4259, US Geological survey, Denver, Colorado.

Passey, Q. R., Bohacs K. M., Esch W. L., Klimentidi R., and Sinha S., 2010. From oil-prone source rock to gas-producing shale reservoir geologic and petrophysical characterization and unconventional shale-gas reservoirs: Society of Petroleum Engineers, SPE 131350, 2010.

Patrick H., Brent H., James A. S., 2011, Shale Gas Water Treatment Value Chain - A Review of Technologies, including Case Studies, SPE Annual Technical Conference and Exhibition, 30 October-2 November, Denver, Colorado, USA, SPE-147264-MS.

Peng W., Roberto A., 2013, Uncertainty Analysis of Shale Gas Simulation: Consideration of Basic Petrophysical Properties, SPE Unconventional Resources Conference Canada, 5-7 November, Calgary, Alberta, Canada, SPE-167236-MS.

Pervukhina M., Gurevich B., Dewhurst D.N. and Siggins A.F., 2010. Experimental verification of the physical nature of velocity stress relationship for isotropic porous rocks. Geophys J Int 2010; 181:1473–1479.

Ragulin V., Mikhailov A., Latipov O., Voloshin A., Tyabayeva N., Yukos and Mackay E., 2004. Scale Management of Production Wells via Inhibitor Application in Supporting Injection Wells, SPE 87461, presented at the 6th International Symposium on Olfield Scale held in Aberdeen, UK, 26-27 May 2004.

Rakhimov A., Vazquez O., Sorbie K.S. and Mackay E.J., 2010. Impact of Fluid Distribution on Scale Inhibitor Squeeze Treatments in Pattern Floods and Fractured Wells, SPE 131724.

Reynolds, M.M. and Munn, D.L., 2010. Development Update for an Emerging Shale Gas Giant Field - Horn River Basin British Columbia Canada, presented at the SPE Unconventional Gas Conference. Society of Petroleum Engineers, January.

Reza Rezaee, 2015. Fundamental of Gas Shale Reservoirs, first edition published in May 2015.

Richardson N, Gottlirb M, Krupnick A, Wiseman H., 2013. The state of shale gas regulation by state – Resources for the Future, presented at the Center for Energy Economics and Policy, May 2013.

Roger M. Slatt, 2015. Sequence Stratigraphy of Unconventional Resource Shales, Fundamentals of Gas Shale Reservoirs, First Edition, Published 2015, pg 71-72.

Rogers, S., Elmo, D., Dunphy, R., Bearinger, D., 2010. Understanding Hydraulic Fracture Geometry and Interactions in the Horn River Basin through DFN and Numerical Modeling. Paper SPE 137488-MS, presented at the Canadian Unconventional Resources and International Petroleum Conference, Calgary, Alberta, Canada, 19-21 October, 2010.

Rogers L.A., Varughese K., Prestwich S.M., Salimi M.H., Oddo J.E., Street Jr. E.H. and Tomson M.B., 1990. Use of Inhibitors for Scale Control in Brine-Producing Gas and Oil Wells, presented at the SPE Production Engineering. February 1990, Pg 77-82.

Samuelsen E.H. and Frederiksen R.A., Hess Denmark ApS, Heath S.M., Thornton A., Sim M., Arefjord A. and McAra E.K., 2009. Downhole Scale Control Through

Continuous Injection of Scale Inhibitor in the Water Injection – A Field Case, presented at the International Oilfield Chemistry Symposium, Geilo, Norway, 23–25 March.

Satya Gupta D.V., Mike Brown J. and Steve Szymczak, 2008. Multi-Year Scale Inhibition from a Solid Inhibitor Applied during Stimulation, SPE 115655, presented at the SPE Annual Technical Conference and Exhibition held in Denver, Colorado, USA, 21–24 September.

Shapiro SA., 2003. Elastic piezo sensitivity of porous and fractured rocks. Geophysics 2003; 68 (2):482–486.

Shaw J.C., Reynolds M.M. and Burke L. H., 2006. Shale Gas Production Potential and Technical Challenges in Western Canada, presented at the Petroleum Society's 7th Canadian International Petroleum Conference (57th Annual Technical Meeting), Calgary, Alberta, Canada, 13 – 15 June.

Simon Mauger, Dana Bozbiciu, 2011. "How Changing Gas Supply Costs Leads to Surging Production: A Ziff Energy White Paper", presented at the Calgary, Alberta, April 2011.

Sitz C.D., Barbin D.K. and Hampton B.J., 2003. Scale Control in a Hydrogen Sulfide Treatment Program, SPE 80235, presented at the SPE International Symposium on Oilfield Chemistry held in Houston, Texas, U.S.A., 5–7 February.

Spooner, Victoria E., Stalker Robert, Wright Rob and Graham Gordon M., 2014. Improving Scale Inhibitor Squeeze Design for Naturally Fractured Reservoirs, SPE-169755-MS, presented at the SPE International Oilfield Scale Conference and Exhibition, 14-15 May, Aberdeen, Scotland, 2014.

Staff, 2025 Unconventional gas outlook, the next wave. Volume 1. Draft for participant review. Core Energy Group, 2010.

Sunil L. Kokal, Krishnam U. Raju and Hector Bayona, 1996. Cost Effective Design of Scale Inhibitor Squeeze Treatments Using a Mathematical Model, SPE-29819-PA, presented at the SPE Production & Facilities, Volume 11, Issue 2, May 1996, Pg 77-82.

Themig, D.J., 2011. New Technologies Enhance Efficiency of Horizontal, Multistage Fracturing, JPT, April 2011.

Thomas C. Weedmark and Ronald J. Spencer, 2012. “Applications of Portable XRF, Chemical Stratigraphy and SEM in the Horn River Basin”, GeoConvention 2012: Vision.

Tollefson, J., 2013. Secrets of fracking fluids pave way for cleaner recipe. Nature, 501(7466) (2013), pp. 146–147.

Tomson, M.B., Kan, A.T. and Fu, G., 2006. Control of Inhibitor Squeeze through Mechanistic Understanding of Inhibitor Chemistry. SPE J 11(3): 283-293. SPE-87450-PA.

Vazquez, O., Corne, D., Jordan, M.M., Mackay, E.J., 2012. Automatic Isotherm Derivation from Field Data for Oilfield Scale Inhibitor. SPE 154954, 2012.

Vetter O.J., 1976. Oilfield Scale - Can We Handle It?, SPE-5879-PA, Journal of Petroleum Technology, Volume 28, Issue 12, December 1976, pg 1402-1408.

Vetter O.J., Lankford S., Nilssen T., and Shelton M., 1988. Well Stimulations and Scale Inhibitors, SPE 17284, presented at the SPE Permian Basin Oil and Gas Recovery Conference held in Midland, Texas, March 10-11, 1988.

Wang, L.K., Y. Hung, et al., 2006. Advanced Physicochemical Treatment Processes, Humana Press.

Warren J.E. and Root P.J., 1963. The Behavior of Naturally Fractured Reservoirs. SPE J 1963;3(3):245–255. SPE-426-PA.

Wayne W. Frenier, David Wilson, Druce Crump and Ladell Jones, 2000. Use of Highly Acid-Soluble Chelating Agents in Well Stimulation Services, SPE 63242, presented at the SPE Annual Technical Conference and Exhibition held in Dallas, Texas, 1–4 October 2000.

Weedmark, T.C. and Spencer, R.J., 2012. Applications of Portable XRF, Chemical Stratigraphy and SEM in the Horn River Basin, GeoConvention 2012: Vision.

Williams-Stroud, S., 2008. "Using Microseismic Events to Constrain Fracture Network Models and Implications for Generating Fracture Flow Properties for Reservoir Simulation," paper SPE 119895, presented at the 2008 SPE Shale Gas Production Conference, Dallas, Texas, USA, 16-18 November 2008.

Williams-Stroud S., 2013. Ozgen C, Billingsley R.L., Microseismicity-constrained discrete fracture network models for stimulated reservoir simulation. Geophysics 2013; 78 (1, January-February): B37–B47.

Duccini Y., Dufour A., NorsoHaas S.A., Harm W.M., Sanders T.W., 1997. High Performance Oilfield Scale Inhibitors, NACE-97169, presented at the NACE InternationalSourceCorrosion97, 9-14 March, New Orleans, Louisiana, 1997.

Yongzan Liu, Juliana Y. Leung, and Rick Chalaturnyk, Claudio J.J. Virues, 2017. Fracturing Fluid Distribution in Shale Gas Reservoirs Due to Fracture Closure, Proppant Distribution and Gravity Segregation. SPE-185043-MS, presented at the SPE Unconventional Resources Conference held in Calgary, Alberta, Canada, 15-16 February 2017.

Zahid Amjad, 1996. Scale Inhibition in Desalination Applications: An Overview, Paper No. 230, presented at the NACE International Annual Conference and Exposition 1996.

Zhang, X., Du, C., Deimbacher, F., Crick, M. and Harikesavanallur, A., 2009. Sensitivity Studies of Horizontal Wells with Hydraulic Fractures in Shale Gas Reservoirs. IPTC 13338.

Appendix

Appendix 1 Examples of shale gas system properties data collection

1. Matrix Permeability – Km

Value (mD)	Reference
10^{-5}	Moridis G.J., Blasingame T.A. and Freeman C.M., 2010. Analysis of Mechanisms of Flow in Fractured Tight-Gas and Shale-Gas Reservoirs, SPE 139250
10^{-5} - 10^{-4}	Zhang, X., Du, C., Deimbacher, F., Crick, M. and Harikesavanallur, A., 2009. Sensitivity Studies of Horizontal Wells with Hydraulic Fractures in Shale Gas Reservoirs. IPTC 13338.
10^{-6} - 10^{-3}	Bustin R.M., Bustin A.M.M., Cui X., Ross D.J.K., and Murthy Pathi V.S., 2008. Impact of Shale Properties on Pore Structure and Storage Characteristics, SPE 119892.
10^{-4}	Oliver H., Eric T., Vincent A., 2010. The Analysis of Dynamic Data in Shale Gas Reservoirs – Part 1 (Version 2), KAPPA, December 2010.
10^{-9} - 10^{-6}	Luffel D.L., Hopkins C.W. and Schettler Jr. P.D., 1993. Matrix Permeability Measurement of Gas Productive Shales, SPE 26633.
10^{-5} - 10^{-3}	Darishchev L. P., and Rouvroy P., 2013. On Simulation of Flow in Tight and Shale Gas Reservoirs, SPE 163990.
$5*10^{-4}$	Mauricio F. and Emesto F., 2013. Hydraulic Fracturing Simulation Case Study and Post Frac Analysis in the Haynesville Shale, SPE 163847.
10^{-4}	Hamed L., Greg J. and Nnamdi A., 2013. A Novel Approach to Modeling and Forecasting Frac Hits in Shale Gas Wells, SPE 164898.
10^{-5}	Karl-Heinz Frohne and James C. Mercer, 1984. Fractured Shale Gas Reservoir Performance Study-An Offset Well Interference Field Test, JPT, February 1984, 291-300
$3*10^{-5}$	Haghshenas B., Clarkson C. R., and Chen S., 2013. Multi-Porosity, Multi-Permeability Models for Shale Gas Reservoirs, SPE 167220.
10^{-4}	Tunde Osholake Jr., John Yilin Wang and Tuygay Ertekin, 2011. Factors Affecting Hydraulically Fractured Well Performances in the Marcellus Shale Gas Reservoirs, SPE 144076.
10^{-4}	Cipolla, C.L., Lolon E. P., and M. J., 2009. Reservoir Modeling and Production Evaluation in Shale – Gas Reservoirs, IPTC 13185.

$1.5*10^{-4}$	Ahmad Alkouh, Steven McKetta and Robert A. Wattenbarger, 2013. Estimation of Effective Fracture Volume Using Water Flowback and Production Data for Shale Gas Wells, SPE 166279.

2. Matrix porosity – Φ_m

Value (%)	Reference
5	Moridis G.J., Blasingame T.A. and Freeman C.M., 2010. Analysis of Mechanisms of Flow in Fractured Tight-Gas and Shale-Gas Reservoirs, SPE 139250
2 - 8	Zhang, X., Du, C., Deimbacher, F., Crick, M. and Harikesavanallur, A., 2009. Sensitivity Studies of Horizontal Wells with Hydraulic Fractures in Shale Gas Reservoirs. IPTC 13338.
2 - 6	Jacobi D., Gladkikh M., LeCompte B., Hursan G., Mendez F., Longo J. and Ong S., 2008. Integrated Petrophysical Evaluation of Shale Gas Reservoirs, SPE 114925.
3	Oliver Houze, Eric Tauzin, Vincent Artus, Leif Larsen, 2010. The Analysis of Dynamic Data in Shale Gas Reservoirs – Part 1 (Version 2), KAPPA, December 2010.
≤ 5	Dewhurst, D.N., Bunger, A., Josh, M., Sarout, J., C., Esteban, L. and Clennell, M.B, 2010. Perth, Western Australia, Mechanics, Physics, Chemistry and Shale Rock Properties, ARMA 13-151.
1.6 - 6	Luffel D.L., Hopkins C.W. and Schettler Jr. P.D., 1993. Matrix Permeability Measurement of Gas Productive Shales, SPE 26633.
4 - 15	Darishchev, Lemouzy P. and Rouvroy P., 2013. On Simulation of Flow in Tight and Shale Gas Reservoirs, SPE 163990.
8	Mauricio Farinas and Emesto Fonseca, 2013. Hydraulic Fracturing Simulation Case Study and Post Frac Analysis in the Haynesville Shale, SPE 163847.
8	Hamed Lawal, Greg Jackson and Nnamdi Abolo, 2013. A Novel Approach to Modeling and Forecasting Frac Hits in Shale Gas Wells, SPE 164898.
2 - 5	Jacobi D., Breig J., LeCompte B., Kopal M. and Hursan G., 2009. Effective Geochemical and Geomechanical Characterization of Shale Gas

	Reservoirs from the Wellbore Environment: Caney and the Woodford Shale, SPE 124231.
1 - 4	Karl-Heinz Frohne and James C. Mercer, 1984. Fractured Shale Gas Reservoir Performance Study-An Offset Well Interference Field Test, JPT, February 1984, 291-300.
3	Tunde Osholake Jr., John Yilin Wang and Tuygay Ertekin, 2011. Factors Affecting Hydraulically Fractured Well Performances in the Marcellus Shale Gas Reservoirs, SPE 144076.
3	Cipolla C.L., Lolon E. P., and M. J., 2009. Reservoir Modeling and Production Evaluation in Shale – Gas Reservoirs, IPTC 13185.
8	Xiuling Han, Fujian Zhou, Chunming Xiong, Xiongfei Liu and Xianyou Yang, 2013. The Optimal Design of Hydraulic Fracture Parameters in Fractured Gas Reservoirs with Low Porosity, Proceedings of the 2nd International Conference on Computer Science and Electronics Engineering (ICCSEE 2013), Page 0328 – 0332.
6	Ahmad Alkouh, Steven McKetta and Robert A. Wattenbarger, 2013. Estimation of Effective Fracture Volume Using Water Flowback and Production Data for Shale Gas Wells, SPE 166279.

3. Connate water saturation – Swc

Swc (%)	Reference
30	Oliver Houze, Eric Tauzin, Vincent Artus, Leif Larsen, 2010. The Analysis of Dynamic Data in Shale Gas Reservoirs – Part 1 (Version 2), KAPPA, December 2010.
20 – 40 in gas zone	Darishchev, Lemouzy P. and Rouvroy P., 2013. On Simulation of Flow in Tight and Shale Gas Reservoirs, SPE 163990.
30	Mauricio Farinas and Emesto Fonseca, 2013. Hydraulic Fracturing Simulation Case Study and Post Frac Analysis in the Haynesville Shale, SPE 163847.
30	Cipolla C.L., Lolon E. P., and M. J., 2009. Reservoir Modeling and Production Evaluation in Shale – Gas Reservoirs, IPTC 13185.

4. Rock Compressibility

Cr (1/psi)	Reference

3E-06	Oliver Houze, Eric Tauzin, Vincent Artus, Leif Larsen, 2010. The Analysis of Dynamic Data in Shale Gas Reservoirs – Part 1 (Version 2), KAPPA, December 2010.
1E-06	Haghshenas B., Clarkson C. R. and Chen S., 2013. Multi-Porosity, Multi-Permeability Models for Shale Gas Reservoirs, SPE 167220.
1E-06	Ahmad Alkouh, Steven McKetta and Robert A. Wattenbarger, 2013. Estimation of Effective Fracture Volume Using Water Flowback and Production Data for Shale Gas Wells, SPE 166279.

5. Water viscosity at reservoir temperature

μ_w (cp)	Reference
0.2	Mauricio Farinas and Emesto Fonseca, 2013. Hydraulic Fracturing Simulation Case Study and Post Frac Analysis in the Haynesville Shale, SPE 163847.
0.86	Schepers K. C., Gonzalez R. J., Koperna G. J. and Oudinot A.Y., 2009. Advanced Resources International, Reservoir Modelling in Support of Shale Gas Exploration, SPE 123057.

6. Shale matrix rel-perm curves

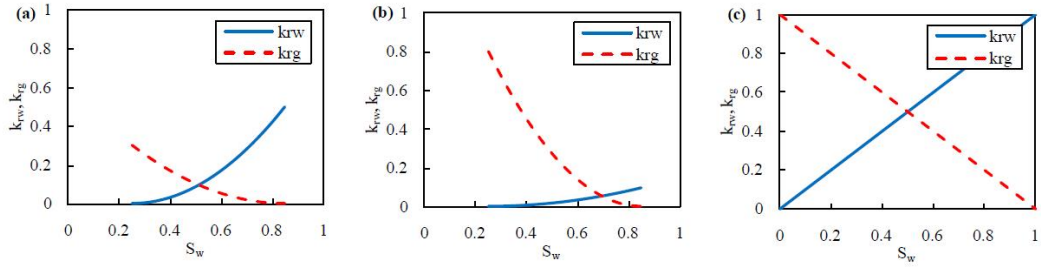

Fig ative permeability diagrams of (a) gas-wet matrix grids, (b) water-wet matrix grids, and (c) natural fractures.

Reference: Haghshenas B., Clarkson C. R. and Chen S., 2013. Multi-Porosity, Multi-Permeability Models for Shale Gas Reservoirs, SPE 167220.

7. Hydraulic Fracture properties

1.) Spacing

Values ft	Reference
100 - 700	Cipolla C.L., Lolon E. P., and M. J., 2009. Reservoir Modeling and Production Evaluation in Shale – Gas Reservoirs, IPTC 13185.
500	Schepers K. C., Gonzalez R. J., Koperna G. J. and Oudinot A.Y., 2009. Advanced Resources International, Reservoir Modeling in Support of Shale Gas Exploration, SPE 123057.
200 - 600	Zhang, X., Du, C., Deimbacher, F., Crick, M. and Harikesavanallur, A., 2009. Sensitivity Studies of Horizontal Wells with Hydraulic Fractures in Shale Gas Reservoirs. IPTC 13338.

500	Ahmad Alkouh, Steven McKetta and Robert A. Wattenbarger, 2013. Estimation of Effective Fracture Volume Using Water Flowback and Production Data for Shale Gas Wells, SPE 166279.

2.) Half length

Value (ft)	Reference
100 - 500	Zhang, X., Du, C., Deimbacher, F., Crick, M. and Harikesavanallur, A., 2009. Sensitivity Studies of Horizontal Wells with Hydraulic Fractures in Shale Gas Reservoirs. IPTC 13338.
350	Hamed Lawal, Greg Jackson and Nnamdi Abolo, 2013. A Novel Approach to Modeling and Forecasting Frac Hits in Shale Gas Wells, SPE 164898.
500	Tunde Osholake Jr., John Yilin Wang and Tuygay Ertekin, 2011. Factors Affecting Hydraulically Fractured Well Performances in the Marcellus Shale Gas Reservoirs, SPE 144076.
50 m – 200 m ≈ 164 ft – 656 ft	Xiuling Han, Fujian Zhou, Chunming Xiong, Xiongfei Liu and Xianyou Yang, 2013. The Optimal Design of Hydraulic Fracture Parameters in Fractured Gas Reservoirs with Low Porosity, Proceedings of the 2nd International Conference on Computer Science and Electronics Engineering (ICCSEE 2013), Page 0328 – 0332.
250	Schepers K. C., Gonzalez R. J., Koperna G. J. and Oudinot A.Y., 2009. Advanced Resources International, Reservoir Modeling in Support of Shale Gas Exploration, SPE 123057.
550	Ahmad Alkouh, Steven McKetta and Robert A. Wattenbarger, 2013. Estimation of Effective Fracture Volume Using Water Flowback and Production Data for Shale Gas Wells, SPE 166279.

3.) Width

Value (ft)	Reference
0.01	Zhang, X., Du, C., Deimbacher, F., Crick, M. and Harikesavanallur, A., 2009. Sensitivity Studies of Horizontal Wells with Hydraulic Fractures in Shale Gas Reservoirs. IPTC 13338.

4.) Height

Value (ft)	Reference
100 – 300	Zhang, X., Du, C., Deimbacher, F., Crick, M. and Harikesavanallur, A., 2009. Sensitivity Studies of Horizontal Wells with Hydraulic Fractures in Shale Gas Reservoirs. IPTC 13338.
300	Cipolla C.L., Lolon E. P., and M. J., 2009. Reservoir Modeling and Production Evaluation in Shale – Gas Reservoirs, IPTC 13185.
50(m) ≈ 164 ft	Mike Du C., Lang Zhan, James Li, Xu Zhang, Stefan Church, Keith Tushingham, and Brad Hay, 2011. Generalization of Dual-Porosity-System Representation and Reservoir Simulation of Hydraulic Fracturing-Stimulated Shale Gas Reservoirs, SPE 146534.

5.) Primary hydraulic fracture conductivity

<table>
<tr><th colspan="2">Value (md-ft)</th><th>Reference</th></tr>
<tr><td colspan="2">1 – 50</td><td>Zhang, X., Du, C., Deimbacher, F., Crick, M. and Harikesavanallur, A., 2009. Sensitivity Studies of Horizontal Wells with Hydraulic Fractures in Shale Gas Reservoirs. IPTC 13338.</td></tr>
<tr><td>Shale play</td><td>Kh(md-ft)</td><td rowspan="6">Creties D. Jenkins, DeGolyer, Mac Naughton and Charles M. Boyer, 2008. Coalbed- and Shale-Gas Reservoirs, JPT February 2008, 92-99.</td></tr>
<tr><td>Antrim</td><td>1 – 5,000</td></tr>
<tr><td>Ohio</td><td>0.2 – 50</td></tr>
<tr><td>New Albany</td><td>1 – 1,8000</td></tr>
<tr><td>Barnett</td><td>0.01– 2</td></tr>
<tr><td>Lewis</td><td>6 – 400</td></tr>
<tr><td colspan="2">2 – 200</td><td>Cipolla C.L., Lolon E. P., and M. J., 2009. Reservoir Modeling and Production Evaluation in Shale – Gas Reservoirs, IPTC 13185.</td></tr>
<tr><td colspan="2">4</td><td>Ahmad Alkouh, Steven McKetta and Robert A. Wattenbarger, 2013. Estimation of Effective Fracture Volume Using Water Flowback and Production Data for Shale Gas Wells, SPE 166279.</td></tr>
<tr><td colspan="2">5 - 30</td><td>Xiuling Han, Fujian Zhou, Chunming Xiong, Xiongfei Liu and Xianyou Yang, 2013. The Optimal Design of Hydraulic Fracture Parameters in Fractured Gas Reservoirs with Low Porosity, Proceedings of the 2nd International Conference on Computer Science and Electronics Engineering (ICCSEE 2013), Page 0328 – 0332.</td></tr>
</table>

8. Gas properties

1.) Gravity

Values	Reference
0.6	Cipolla C.L., Lolon E. P., and M. J., 2009. Reservoir Modeling and Production Evaluation in Shale – Gas Reservoirs, IPTC 13185.
0.55	Schepers K. C., Gonzalez R. J., Koperna G. J. and Oudinot A.Y., 2009. Advanced Resources International, Reservoir Modeling in Support of Shale Gas Exploration, SPE 123057.
0.65	Ahmad Alkouh, Steven McKetta and Robert A. Wattenbarger, 2013. Estimation of Effective Fracture Volume Using Water Flowback and Production Data for Shale Gas Wells, SPE 166279.

2.) Viscosity

μ_g (cp)	Reference
0.016	Mauricio Farinas and Emesto Fonseca, 2013. Hydraulic Fracturing Simulation Case Study and Post Frac Analysis in the Haynesville Shale, SPE 163847.

3.) Gas compressibility

Values psi^{-1}	Reference
$3.9*10^{-6}$	Ahmad Alkouh, Steven McKetta and Robert A. Wattenbarger, 2013. Estimation of Effective Fracture Volume Using Water Flowback and Production Data for Shale Gas Wells, SPE 166279.

Appendix 2 Examples of geochemistry compositional data collection

1. Flowback water data for wells in south Texas

	Injection water	Flowback Well 1 - AF1					Flowback Well 2 - AF2			
		Flowback water					Flowback water			
	07/08/2013	13/01/2012	18/07/2012	19/02/2013	10/05/2013	23/10/2013	13/01/2012	18/07/2012	26/02/2013	10/05/2013
Sample Point		Heater	Heater	Separator	Separator	Wellhead	Heater	Heater	Separator	Separator
Dissolved CO2 (mg/L)):	0	154	220	480	810	352	286.00	220.00	144.00	267.30
Bicarbonate (HCO3):	1384.7	134.2	122	366	854	322	256.20	244.00	286.70	335.50
Lead (Pb):	0.54	0.88	0.04	0	0.1	0.02	0.61	0.12	0.00	0.05
H2S in Gas (%):	no data	0.03	0.07	0.0006	0.001	0.002	0.00	0.02	0.00	0.00
H2S in Water (mg/L):	2.5	1.5	1	1	2	4	0.05	1.00	2.00	1.00
pH:	8.1	6.7	6.7	7.3	7.3	7.4	6.9	6.7	7.5	7
Calculated Density (g/ml):	0.999	1.03	1.025	1.016	1.024	1.026	1.03	1.031	1.017	1.021
Calculated TDS (mg/L):	2570.57	43854.61	39655	26430.13	38103.05	41723.39	40493.31	48901.19	28816.5	33889.7
Cations	mg/L	mg/L	mg/L	mg/L	mg/L	mg/L	mg/L	mg/L	mg/L	mg/L
Calcium (Ca):	4.19	1060.2	1863.78	1236.66	1885.32	2151.05	1168.93	2567.38	1078.90	1297.93
Barium (Ba):	0.26	4.47	4.79	5.63	8.43	8.41	4.64	7.94	4.17	4.39
Iron (Fe):	1.02	9.03	66.09	214.81	480.05	104.52	8.82	18.23	22.02	28.11
Magnesium (Mg):	1.13	107.21	174.73	111.17	171.52	192.14	117.93	229.57	99.46	129.74
Manganese (Mn):	0.01	0.25	7.18	3.58	7.58	1.52	0.21	0.95	0.57	0.87
Sodium (Na):	761	15650.79	12932.19	8435.69	11814.1	13254.67	14074.34	15733.19	9757.55	11434.64
Potassium (K):	2.53	304.76	147.14	85.33	121.72	154.06	301.32	158.66	92.56	92.48
Strontium (Sr):	0.65	15.69	236.96	168.22	258.19	337.97	153.12	241.05	134.57	167.97
Zinc (Zn):	14.36	0.13	0	0.04	0.04	0.03	0.20	0.00	0.00	0.02
Anions	mg/L	mg/L	mg/L	mg/L	mg/L	mg/L	mg/L	mg/L	mg/L	mg/L
Sulfate (SO4):	0	67	0.1	3	2	97	107.00	0.10	140.00	98.00
Chloride (Cl):	400	26500	24100	15800	22500	25100	24300.00	29700.00	17200.00	20300.00

	Injection water	Flowback Well 3 - AF3				Flowback Well 4 - AF4				
		Flowback water				Flowback water				
	07/08/2013	13/01/2012	18/07/2012	19/02/2013	10/05/2013	13/01/2012	18/07/2012	19/02/2013	10/05/2013	23/10/2013
Sample Point		Heater	Heater	Separator	Separator	Heater	Heater	Separator	Separator	Wellhead
Dissolved CO2 (mg/L)):	0	220.00	220.00	344.00	176.00	176.00	220.00	400.00	480.00	256.00
Bicarbonate (HCO3):	1384.7	122.00	122.00	201.30	549.00	109.80	122.00	366.00	378.20	305.00
Lead (Pb):	0.54	0.00	0.09	0.00	0.00	0.00	0.02	0.00	0.07	0.07
H2S in Gas (%):	no data	0.00	0.00	0.00	0.00	0.01	0.05	0.00	0.00	0.00
H2S in Water (mg/L):	2.5	0.50	1.00	6.00	8.50	0.50	1.00	2.00	1.00	4.00
pH:	8.1	6.7	6.7	6.4	7.1	6.3	6.5	6.5	6.5	6.9
Calculated Density (g/ml):	0.999	1.02	1.029	1.029	1.007	1.03	1.034	1.029	1.037	1.027
Calculated TDS (mg/L):	2570.57	39393.67	44894.8	45252.76	14246.35	50015.11	52721.23	46256.52	57424.01	41848.47
Cations	mg/L	mg/L	mg/L	mg/L	mg/L	mg/L	mg/L	mg/L	mg/L	mg/L
Calcium (Ca):	4.19	1618.25	2310.88	2410.02	262.81	2148.54	2763.53	2284.70	2810.88	2215.36
Barium (Ba):	0.26	5.84	6.33	6.60	1.15	8.99	10.29	7.53	9.87	8.24
Iron (Fe):	1.02	8.86	408.59	19.79	7.55	60.90	34.78	120.10	120.38	71.88
Magnesium (Mg):	1.13	163.05	208.08	213.80	24.94	220.44	250.70	213.54	268.62	202.13
Manganese (Mn):	0.01	0.34	7.25	0.70	0.18	0.91	1.05	2.15	1.58	1.11
Sodium (Na):	761	13015.59	14147.55	14517.60	5111.45	16400.41	16954.81	14919.94	18601.93	13265.72
Potassium (K):	2.53	366.71	165.90	149.77	39.76	380.50	159.45	135.93	145.73	127.30
Strontium (Sr):	0.65	212.84	218.03	225.16	40.47	312.19	289.60	247.54	303.71	343.63
Zinc (Zn):	14.36	0.19	0.00	0.02	0.04	0.42	0.00	0.09	0.04	0.03
Anions	mg/L	mg/L	mg/L	mg/L	mg/L	mg/L	mg/L	mg/L	mg/L	mg/L
Sulfate (SO4):	0	80.00	0.10	8.00	109.00	72.00	35.00	59.00	83.00	108.00
Chloride (Cl):	400	23800.00	27300.00	27500.00	8100.00	30300.00	32100.00	27900.00	34700.00	25200.00

	Injection water	Injection water	Flowback Well 5 - AF5		Flowback Well 6 - AF6
			Flowback water		Flowback water
	07/08/2013	19/02/2014	08/01/2013	30/10/2013	01/08/2013
Sample Point			Separator	Separator	Separator
Dissolved CO2 (mg/L)):	0	0	472.00	384.00	416.00
Bicarbonate (HCO3):	1384.7	1384.7	366.00	305.00	372.10
Lead (Pb):	0.54	0.54	0.00	0.03	0.04
H2S in Gas (%):	no data	no data			
H2S in Water (mg/L):	2.5	2.5			
pH:	8.1	8.1	7.3	6.8	7.2
Calculated Density (g/ml):	0.999	0.999	1.025	1.029	1.022
Calculated TDS (mg/L):	2570.57	2570.57	40222.56	45100.82	35208.89
Cations	mg/L	mg/L	mg/L	mg/L	mg/L
Calcium (Ca):	4.19	4.19	1815.47	2387.57	1710.45
Barium (Ba):	0.26	0.26	7.00	8.16	6.41
Iron (Fe):	1.02	1.02	85.42	69.74	78.41
Magnesium (Mg):	1.13	1.13	164.66	224.90	156.17
Manganese (Mn):	0.01	0.01	1.29	0.92	1.03
Sodium (Na):	761	761	13194.51	14377.12	11505.36
Potassium (K):	2.53	2.53	103.21	127.03	97.29
Strontium (Sr):	0.65	0.65	225.99	266.33	21.60
Zinc (Zn):	14.36	14.36	0.01	0.02	0.03
Anions	mg/L	mg/L	mg/L	mg/L	mg/L
Sulfate (SO4):	0	0	159.00	134.00	160.00
Chloride (Cl):	400	400	24100.00	27200.00	21100.00

2. Produced water data in north America

Typical Ranges of Components Present in Produced Water of shale gas from north America			
Parameters, mg/L	Produced water (> 2 weeks)	Parameters, mg/L	Produced water (> 2 weeks)
TDS	10000- 336000	Acetate	0- 2500
Sodium	4000- 135000	Propionate	0- 400
Potassium	0- 1000	Butyrate	0- 75
Calcium	0- 40000	BTEX	0- 100
Magnesium	0- 4000	Specific gravity	1000- 1250
Barium	0- 20000	Dissolved oxygen	0
Strontium	0- 10000	Ammonia	10- 200
Iron	0- 200	Dissolved H2S	0- 1000
Chloride	6000- 200000	Temperature	20- 150
Sulfate	0- 5000	TSS	1- 500
Carbonate	0- 1000	Oil in water	5- 1000
Bicarbonate	100- 6000	Bacteria (total) / ml	0- 10^10

Reference: Kuijvenhoven C., Fedotov V., Gallo D. and Hagemeijer P., 2013. Water Management Approach for Shale Operations in North America, SPE 167057.

3. Flowback water data in various US Shale Plays

Example Flowback Analysis from various US Shale Plays								
	Shale Play							
Component			BARNETT	EAGLEFORD	FAYETTEVILLE	HAYNESVILLE	MARCELLUS	BAKKEN
Sodium	Na	mg/L	10741	10900	13804	34879	24445	45100
Potassium	K	mg/L	484	192	256	735	190	3550
Magnesium	Mg	mg/L	316	111	293	828	263	720
Calcium	CA	mg/L	2916	1270	1046	7052	2921	9020
Strontium	Sr	mg/L	505	203	267	1354	347	
Barium	Ba	mg/L	15	10	18	1121	679	13
Iron	Fe	mg/L	28	112	0	147	26	77
Cloride	Cl	mg/L	23797	19318	23856	71143	43578	91300
Sulphate	SO4	mg/L	309	163	13	-	4	440
Bicarbonate	HCO3	mg/L	405	736	6161	382	261	126
Total Dissolved Solids	TDS	mg/L	39516	33015	45715	117641	72714	150346
Total Suspended Solids	TSS	mg/L	1272	840	700	868		

Reference: James Slutz, Jeffrey Anderson, 2012. Key Shale Gas Water Management Strategies: An Economic Assessment Tool, SPE 157532.

4. Flowback water data in Marcellus shales

Marcellus Shale Well a Late Stage Flowback Water Chemical Characterization Data				
FlowbackVol(bbl)	12000	13000	14000	15000
pH	6.22	6.08	5.98	5.88
Alkalinity (HCO3-Only in mg/L of CaCO3)	280	240	200	160
Cl-, mg/L	54000	59000	62900	67800
SO42-, mg/L	31	20	20	24
Na+,mg/L	26220	28630	31810	35350
K+,mg/L	1119	1201	1350	1480
Ca2+, mg/L	7160	7680	8880	9720
Mg2+, mg/L	341	463	488	805
Ba2+, mg/L	28.9	43.3	99.6	175.7
Sr2+, mg/L	1110	1305	1513	1387

Fe3+,mg/L	0.4	0.9	1.1	3.3
Fe Total, mg/L	63	66	72	78
TSS, mg/L	144	175	498	502
LangelierIndex	1.02	0.84	0.72	0.55
Microbial Count	Low	Low	Low	Low

Reference: Blauch M.E., Myers R. R. and Moore T. R., 2009. Marcellus Shale Post-Frac Flowback Waters - Where is All the Salt Coming From and What are the Implications, SPE 125740.

45 Days Flowback Water Chemical Characterization Data												
Data 3	TDS	Ca	Mg	CaCO3	Na	K	Fe	Ba	Sr	Mn	SO4	Cl
Sample Date		mg/L	mg/L		mg/L	mg/L	mg/L	mg/L	mg/L	mg/L	mg/L	mg/L
4/15 pre-frac	224.38	15	2.73	49.44	18	1.65	0.25	0.23	0.46	0.06	3	183
4/26	84839	7100	603	23286	22800	326	3.93	2000	1400	6.69	0	50600
4/27	89861	7640	651	24952	24300	346	7.8	1990	1510	7.07	8.87	53400
4/27	105169	8490	714	27432	25100	352	9.7	1870	1670	7.44	156	66800
4/28	116266	10500	893	33879	29400	410	35.3	1980	2200	9.1	139	70700
4/29	123902	11700	996	38419	31100	437	16.2	2480	2860	9.5	2.94	74300
4/30	164081	16700	1400	52071	41700	579	23.5	2230	2570	13	165	98700
5/1	140169	14000	1150	44358	34300	477	28.7	2290	2590	11	22.7	85300
5/2	146539	16700	1380	53473	39400	535	30.2	3000	3380	13.1	0.19	82100
5/3	161636	17100	1410	54446	40400	543	35.2	2950	3280	13.3	4.97	95900
5/4	164902	16700	13000	103026	37000	496	32.9	3850	4310	12.3	1.15	89500
5/28	39706	2920	243	9281	11500	187	26.5	607	472	2.79	47.6	23700
5/29	50019	3140	273	10187	13000	189	31.4	776	568	2.28	619	
5/30	94665	9590	906	31580	35300	518	44.7	2500	1800	7.44	199	43800
5/31	93207	7080	672	23552	24000	340	7.65	2090	1370	5.85	41.5	57600
6/1	108047	7860	751	26258	26500	367	7.49	2400	1550	6.08	205	68400
6/8	124303	10200	901	33669	30500	425	34.9	3100	1930	6.76	64.8	Nd

Reference: Blauch M.E., Myers R. R. and Moore T. R., 2009. Marcellus Shale Post-Frac Flowback Waters - Where is All the Salt Coming From and What are the Implications, SPE 125740.

Appendix 3 Simulation codes

A3.1 CMG IMEX

```
RESULTS SIMULATOR IMEX 201210

*TITLE1

'3D 2-PHASE'

*INUNIT *FIELD

*DIM  *MAX_ROCK_TYPES  2

RESULTS XOFFSET          0.0000

RESULTS YOFFSET          0.0000

RESULTS ROTATION          0.0000  **  (DEGREES)

RESULTS AXES-DIRECTIONS 1.0 -1.0 1.0

GRID VARI 40 20 30

KDIR DOWN

DI IVAR

 40*50

DJ JVAR

 20*200

DK ALL

 24000*10

DTOP

 800*7000

*MDPLNRBK 575

** Please don't remove these RESULTS PLNRTEMPLATE keywords.

RESULTS PLNRTEMPLATE NAME 'Template (I - Frac 1)'

RESULTS PLNRTEMPLATE PRIMFRACWIDTH 0.01

RESULTS PLNRTEMPLATE PRIMFRACPERM 10000

RESULTS PLNRTEMPLATE ORIGINALREFINEINTO 3 15 1

RESULTS PLNRTEMPLATE ORIGINALHALFLENGTH 500

RESULTS PLNRTEMPLATE ORIGINAL_LAYERUP 12

RESULTS PLNRTEMPLATE ORIGINAL_LAYERDOWN 12

RESULTS PLNRTEMPLATE END
```

```
*PLNRFRAC_TEMPLATE 'Template (I - Frac 1)'
  *PLNR_REFINE *INTO  3 15 1
    *BWHLEN 500
    *IDIR
    *INNERWIDTH 2
    *LAYERSUP 12
    *LAYERSDOWN 12
  *PERMI MATRIX *FZ 50
  *PERMJ MATRIX *FZ 50
  *PERMK MATRIX *FZ 50
*END_TEMPLATE
NULL CON           1
*PERMI *ALL
24000*0.0001
*PERMJ *ALL
24000*0.0001
*PERMK *ALL
24000*0.0001
PINCHOUTARRAY CON          1
*POR *ALL
24000*0.05
*CPOR 1.45E-06
*PRPOR 4500.0
** Please don't remove these RESULTS PLNRSTAGE keywords.
RESULTS PLNRSTAGE NAME 'Planar Stage 1'
RESULTS PLNRSTAGE WELL 'I'
RESULTS PLNRSTAGE DATE 2008-01-01
RESULTS PLNRSTAGE BASENAME 'I - Frac'
RESULTS PLNRSTAGE FRACS 'I - Frac_2'
RESULTS PLNRSTAGE SLABS '5'
RESULTS PLNRSTAGE PERFOPTION 0
RESULTS PLNRSTAGE LAYERMIN 16
RESULTS PLNRSTAGE LAYERMAX 16
```

RESULTS PLNRSTAGE END

*PLNRFRAC 'Template (I - Frac 1)' 20,5,16 *BG_NAME 'I - Frac_2'

*PERMI MATRIX BG 'I - Frac_2' *NFZ 0.0005

*PERMJ MATRIX BG 'I - Frac_2' *NFZ 0.0005

*PERMK MATRIX BG 'I - Frac_2' *NFZ 0.0005

*MODEL BLACKOIL_SEAWATER

TRES 113

PVT BG 1

**$ p	Rs	Bo	Bg	viso	visg
1674	706.49717	1.06162	0.00198	1.06274	0.0162
2031	859.9811558	1.07233	0.00162	1.04846	0.0171
2530	1060.092277	1.0873	0.0013	1.0285	0.0184
2991	1230.604288	1.10113	0.00111	1.01006	0.0197
3553	1420.693433	1.11799	0.000959	0.98758	0.0213
4110	1590.800531	1.1347	0.000855	0.9653	0.023
4544	1711.389981	1.14772	0.000795	0.94794	0.0244
4935	1811.5121	1.15945	0.000751	0.9323	0.0255
5255	1887.704956	1.16905	0.00072	0.9195	0.0265
5545	1952.462254	1.17775	0.000696	0.9079	0.0274
7000	2221	1.2214	0.0006	0.8497	0.033

BWI 1.0037

CO 1.0E-5

CVO 4.6E-5

CVW 0

CW 5.8E-05

DENSITY OIL 44.986

DENSITY WATER 63

DENSITY GAS 0.01

REFPW 1.034

VWI 0.607

SVISC 1.1

*ROCKFLUID

*KROIL *SEGREGATED

RPT 1

** Sw krw krow Pcow

SWT

0.05 0 1 949.1237

0.08 0.0032 0.765177106 845.1237

0.1 0.007 0.63540829 767.8247

0.15 0.0175 0.391119705 497.3465

0.18 0.0264 0.288969162 378.7831

0.2 0.033 0.23551488 318.7831

0.25 0.051 0.141749805 210.5835

0.28 0.064 0.106188841 166.5435

0.3 0.07 0.08875667 143.1604

0.35 0.09 0.060592829 98.03826

0.38 0.103 0.050675057 78.03826

0.4 0.118 0.04578976 66.31738

0.45 0.147 0.036702028 48.85232

0.48 0.165 0.032019366 40.85232

0.5 0.18 0.02885625 36.30661

0.55 0.216 0.020300053 26.3625

0.58 0.238 0.014732765 20.8625

0.6 0.253 0.01095104 18.04625

0.65 0.295 0.001945752 11.1688

0.68 0.323 0 7.7888

0.7 0.342 0 5.881897

0.75 0.401 0 2.48962

0.78 0.441 0 1.88202

0.8 0.466 0 0.78202

0.85 0.537 0 0.535352

0.88 0.589 0 0.485352

0.9 0.627 0 0.467084

0.95 0.75 0 0.10416

0.98 0.86 0 0.05816

1 1 0 0

**	Sl	krg	krog	Pcog
SLT				
0.05	1	0	0	
0.08	0.765177106		0.0009	0
0.1	0.63540829		0.0013	0
0.15	0.391119705		0.002	0
0.18	0.288969162		0.0045	0
0.2	0.23551488		0.007	0
0.25	0.141749805		0.015	0
0.28	0.106188841		0.0193	0
0.3	0.08875667		0.024	0
0.35	0.060592829		0.037	0
0.38	0.050675057		0.042	0
0.4	0.04578976		0.049	0
0.45	0.036702028		0.067	0
0.48	0.032019366		0.076	0
0.5	0.02885625		0.088	0
0.55	0.020300053		0.116	0
0.58	0.014732765		0.135	0
0.6	0.01095104		0.154	0
0.65	0.001945752		0.2	0
0.68	0	0.228	0	
0.7	0	0.251	0	
0.75	0	0.312	0	
0.78	0	0.355	0	
0.8	0	0.392	0	
0.85	0	0.49	0	
0.88	0	0.558	0	
0.9	0	0.601	0	
0.95	0	0.731	0	
0.98	0	0.854	0	
1	0	1	0	
RPT 2				

```
**       Sl      krg      krog      Pcog
SLT
         0     1.000         0         0
       1.00         0     1.000         0
**       Sw       krw         krow      Pcow
SWT
         0        0           1         0
         1        1           0         0
*RTYPE *ALL 24000*1
*RTYPE MATRIX BG 'I - Frac_2' *NFZ 1
*RTYPE MATRIX BG 'I - Frac_2' *FZ 2
*INITIAL
*USER_INPUT
*INCLUDE 'include-files/PRES.DAT'
PB   *CON 3000
SO   *CON     0
SW   *CON  0.05
*SW MATRIX BG 'I - Frac_2' *NFZ 0.21
*SW MATRIX BG 'I - Frac_2' *FZ 0.45
SEAWATFRC *CON 0.0
NUMERICAL
NCUTS 100
CONVERGE *MAXRES *SEAWATER  0.0001
*RUN
*DATE 2008 1 1
DTMIN  1.0E-10
DTMAX  50
DTWELL 0.0001
GROUP 'G' ATTACHTO 'FIELD'
WELL  'I' ATTACHTO 'G'
INJECTOR MOBWEIGHT 'I'
INCOMP  SEAWATER
OPERATE  MAX  STW  3000.0  CONT REPEAT
```

```
**        rad  geofac  wfrac  skin
GEOMETRY  K  0.0365  0.37  1.0  0.0
    PERF     GEOA  'I'
** UBA                ff        Status  Connection
   20 4 1             1.0  CLOSED  FLOW-FROM  'SURFACE'  REFLAYER
   20 4 4             1.0  CLOSED  FLOW-FROM  1
   20 4 8             1.0  CLOSED  FLOW-FROM  2
   20 4 12            1.0  CLOSED  FLOW-FROM  3
   20 4 16            1.0  CLOSED  FLOW-FROM  4
   20 5 16 / 2 1 1      1.0  CLOSED  FLOW-FROM  5
   20 5 16 / 2 2 1      1.0  CLOSED  FLOW-FROM  6
   20 5 16 / 2 3 1      1.0  CLOSED  FLOW-FROM  7
   20 5 16 / 2 4 1      1.0  CLOSED  FLOW-FROM  8
   20 5 16 / 2 5 1      1.0  CLOSED  FLOW-FROM  9
   20 5 16 / 2 6 1      1.0  CLOSED  FLOW-FROM  10
   20 5 16 / 2 7 1      1.0  CLOSED  FLOW-FROM  11
   20 5 16 / 2 8 1      1.0  OPEN    FLOW-FROM  12
   20 5 16 / 2 9 1      1.0  CLOSED  FLOW-FROM  13
   20 5 16 / 2 10 1     1.0  CLOSED  FLOW-FROM  14
   20 5 16 / 2 11 1     1.0  CLOSED  FLOW-FROM  15
   20 5 16 / 2 12 1     1.0  CLOSED  FLOW-FROM  16
   20 5 16 / 2 13 1     1.0  CLOSED  FLOW-FROM  17
   20 5 16 / 2 14 1     1.0  CLOSED  FLOW-FROM  18
   20 5 16 / 2 15 1     1.0  CLOSED  FLOW-FROM  19
   20 6 16            1.0  CLOSED  FLOW-FROM  20
   20 7 16            1.0  CLOSED  FLOW-FROM  21
   20 8 16            1.0  CLOSED  FLOW-FROM  22
   20 9 16            1.0  CLOSED  FLOW-FROM  23
   20 10 16           1.0  CLOSED  FLOW-FROM  24
   20 11 16           1.0  CLOSED  FLOW-FROM  25
   20 12 16           1.0  CLOSED  FLOW-FROM  26
   20 13 16           1.0  CLOSED  FLOW-FROM  27
   20 14 16           1.0  CLOSED  FLOW-FROM  28
```

```
   20 15 16              1.0  CLOSED  FLOW-FROM  29

   20 16 16              1.0  CLOSED  FLOW-FROM  30

   20 17 16              1.0  CLOSED  FLOW-FROM  31

XFLOW-MODEL 'I' ZERO-FLOW

BHPDEPTH 'I' 7000.0

PERMI   RG 30 5 22 ALL

 14*50 50.0001 15*50

PERMI   RG 29 5 22 ALL

 14*50 2*50.0001 14*50

PERMI   RG 28 5 22 ALL

 14*50 2*50.0001 14*50

PERMI   RG 27 5 22 ALL

 14*50 2*50.0001 14*50

PERMI   RG 26 5 22 ALL

 14*50 2*50.0001 14*50

PERMI   RG 25 5 22 ALL

 14*50 2*50.0001 14*50

PERMI   RG 24 5 22 ALL

 14*50 2*50.0001 14*50

PERMI   RG 23 5 22 ALL

 14*50 2*50.0001 14*50

PERMI   RG 22 5 22 ALL

 14*50 2*50.0001 14*50

PERMI   RG 21 5 22 ALL

 14*50 2*50.0001 14*50

PERMI   RG 20 5 22 ALL

 21*50 3*50.0001 21*50

  PERMI   RG 30 5 21 ALL

 14*50 50.0001 15*50

PERMI   RG 29 5 21 ALL

 14*50 2*50.0001 14*50

PERMI   RG 28 5 21 ALL

 14*50 2*50.0001 14*50
```

PERMI RG 27 5 21 ALL

14*50 2*50.0001 14*50

PERMI RG 26 5 21 ALL

14*50 2*50.0001 14*50

PERMI RG 25 5 21 ALL

14*50 2*50.0001 14*50

PERMI RG 24 5 21 ALL

14*50 2*50.0001 14*50

PERMI RG 23 5 21 ALL

14*50 2*50.0001 14*50

PERMI RG 22 5 21 ALL

14*50 2*50.0001 14*50

PERMI RG 21 5 21 ALL

14*50 2*50.0001 14*50

PERMI RG 20 5 21 ALL

21*50 3*50.0001 21*50

PERMI RG 30 5 20 ALL

14*50 50.0001 15*50

PERMI RG 29 5 20 ALL

14*50 2*50.0001 14*50

PERMI RG 28 5 20 ALL

14*50 2*50.0001 14*50

PERMI RG 27 5 20 ALL

14*50 2*50.0001 14*50

PERMI RG 26 5 20 ALL

14*50 2*50.0001 14*50

PERMI RG 25 5 20 ALL

14*50 2*50.0001 14*50

PERMI RG 24 5 20 ALL

14*50 2*50.0001 14*50

PERMI RG 23 5 20 ALL

14*50 2*50.0001 14*50

PERMI RG 22 5 20 ALL

14*50 2*50.0001 14*50

PERMI RG 21 5 20 ALL

14*50 2*50.0001 14*50

PERMI RG 20 5 20 ALL

21*50 3*50.0001 21*50

PERMI RG 20 5 19 ALL

21*50 3*50.0001 21*50

PERMI RG 19 5 19 ALL

14*50 2*50.0001 14*50

PERMI RG 18 5 19 ALL

14*50 2*50.0001 14*50

PERMI RG 17 5 19 ALL

14*50 2*50.0001 14*50

PERMI RG 16 5 19 ALL

14*50 2*50.0001 14*50

PERMI RG 15 5 19 ALL

14*50 2*50.0001 14*50

PERMI RG 14 5 19 ALL

14*50 2*50.0001 14*50

PERMI RG 13 5 19 ALL

14*50 2*50.0001 14*50

PERMI RG 12 5 19 ALL

14*50 2*50.0001 14*50

PERMI RG 11 5 19 ALL

14*50 2*50.0001 14*50

PERMI RG 10 5 19 ALL

15*50 50.0001 14*50

PERMI RG 20 5 18 ALL

21*50 3*50.0001 21*50

PERMI RG 19 5 18 ALL

14*50 2*50.0001 14*50

PERMI RG 18 5 18 ALL

14*50 2*50.0001 14*50

PERMI RG 17 5 18 ALL

14*50 2*50.0001 14*50

PERMI RG 16 5 18 ALL

14*50 2*50.0001 14*50

PERMI RG 15 5 18 ALL

14*50 2*50.0001 14*50

PERMI RG 14 5 18 ALL

14*50 2*50.0001 14*50

PERMI RG 13 5 18 ALL

14*50 2*50.0001 14*50

PERMI RG 12 5 18 ALL

14*50 2*50.0001 14*50

PERMI RG 11 5 18 ALL

14*50 2*50.0001 14*50

PERMI RG 10 5 18 ALL

15*50 50.0001 14*50

PERMI RG 20 5 17 ALL

21*50 3*50.0001 21*50

PERMI RG 19 5 17 ALL

14*50 2*50.0001 14*50

PERMI RG 18 5 17 ALL

14*50 2*50.0001 14*50

PERMI RG 17 5 17 ALL

14*50 2*50.0001 14*50

PERMI RG 16 5 17 ALL

14*50 2*50.0001 14*50

PERMI RG 15 5 17 ALL

14*50 2*50.0001 14*50

PERMI RG 14 5 17 ALL

14*50 2*50.0001 14*50

PERMI RG 13 5 17 ALL

14*50 2*50.0001 14*50

PERMI RG 12 5 17 ALL

14*50 2*50.0001 14*50

PERMI RG 11 5 17 ALL

14*50 2*50.0001 14*50

PERMI RG 10 5 17 ALL

15*50 50.0001 14*50

PERMJ RG 30 5 22 ALL

14*50 50.0001 15*50

PERMJ RG 29 5 22 ALL

14*50 2*50.0001 14*50

PERMJ RG 28 5 22 ALL

14*50 2*50.0001 14*50

PERMJ RG 27 5 22 ALL

14*50 2*50.0001 14*50

PERMJ RG 26 5 22 ALL

14*50 2*50.0001 14*50

PERMJ RG 25 5 22 ALL

14*50 2*50.0001 14*50

PERMJ RG 24 5 22 ALL

14*50 2*50.0001 14*50

PERMJ RG 23 5 22 ALL

14*50 2*50.0001 14*50

PERMJ RG 22 5 22 ALL

14*50 2*50.0001 14*50

PERMJ RG 21 5 22 ALL

14*50 2*50.0001 14*50

PERMJ RG 20 5 22 ALL

21*50 3*50.0001 21*50

PERMJ RG 30 5 21 ALL

14*50 50.0001 15*50

PERMJ RG 29 5 21 ALL

14*50 2*50.0001 14*50

PERMJ RG 28 5 21 ALL

14*50 2*50.0001 14*50

PERMJ RG 27 5 21 ALL

14*50 2*50.0001 14*50

PERMJ RG 26 5 21 ALL

14*50 2*50.0001 14*50

PERMJ RG 25 5 21 ALL

14*50 2*50.0001 14*50

PERMJ RG 24 5 21 ALL

14*50 2*50.0001 14*50

PERMJ RG 23 5 21 ALL

14*50 2*50.0001 14*50

PERMJ RG 22 5 21 ALL

14*50 2*50.0001 14*50

PERMJ RG 21 5 21 ALL

14*50 2*50.0001 14*50

PERMJ RG 20 5 21 ALL

21*50 3*50.0001 21*50

PERMJ RG 30 5 20 ALL

14*50 50.0001 15*50

PERMJ RG 29 5 20 ALL

14*50 2*50.0001 14*50

PERMJ RG 28 5 20 ALL

14*50 2*50.0001 14*50

PERMJ RG 27 5 20 ALL

14*50 2*50.0001 14*50

PERMJ RG 26 5 20 ALL

14*50 2*50.0001 14*50

PERMJ RG 25 5 20 ALL

14*50 2*50.0001 14*50

PERMJ RG 24 5 20 ALL

14*50 2*50.0001 14*50

PERMJ RG 23 5 20 ALL

14*50 2*50.0001 14*50

PERMJ RG 22 5 20 ALL

14*50 2*50.0001 14*50

PERMJ RG 21 5 20 ALL

14*50 2*50.0001 14*50

PERMJ RG 20 5 20 ALL

21*50 3*50.0001 21*50

PERMJ RG 20 5 19 ALL

21*50 3*50.0001 21*50

PERMJ RG 19 5 19 ALL

14*50 2*50.0001 14*50

PERMJ RG 18 5 19 ALL

14*50 2*50.0001 14*50

PERMJ RG 17 5 19 ALL

14*50 2*50.0001 14*50

PERMJ RG 16 5 19 ALL

14*50 2*50.0001 14*50

PERMJ RG 15 5 19 ALL

14*50 2*50.0001 14*50

PERMJ RG 14 5 19 ALL

14*50 2*50.0001 14*50

PERMJ RG 13 5 19 ALL

14*50 2*50.0001 14*50

PERMJ RG 12 5 19 ALL

14*50 2*50.0001 14*50

PERMJ RG 11 5 19 ALL

14*50 2*50.0001 14*50

PERMJ RG 10 5 19 ALL

15*50 50.0001 14*50

PERMJ RG 20 5 18 ALL

21*50 3*50.0001 21*50

PERMJ RG 19 5 18 ALL

14*50 2*50.0001 14*50

PERMJ RG 18 5 18 ALL

14*50 2*50.0001 14*50

PERMJ RG 17 5 18 ALL

14*50 2*50.0001 14*50

PERMJ RG 16 5 18 ALL

14*50 2*50.0001 14*50

PERMJ RG 15 5 18 ALL

14*50 2*50.0001 14*50

PERMJ RG 14 5 18 ALL

14*50 2*50.0001 14*50

PERMJ RG 13 5 18 ALL

14*50 2*50.0001 14*50

PERMJ RG 12 5 18 ALL

14*50 2*50.0001 14*50

PERMJ RG 11 5 18 ALL

14*50 2*50.0001 14*50

PERMJ RG 10 5 18 ALL

15*50 50.0001 14*50

PERMJ RG 20 5 17 ALL

21*50 3*50.0001 21*50

PERMJ RG 19 5 17 ALL

14*50 2*50.0001 14*50

PERMJ RG 18 5 17 ALL

14*50 2*50.0001 14*50

PERMJ RG 17 5 17 ALL

14*50 2*50.0001 14*50

PERMJ RG 16 5 17 ALL

14*50 2*50.0001 14*50

PERMJ RG 15 5 17 ALL

14*50 2*50.0001 14*50

PERMJ RG 14 5 17 ALL

14*50 2*50.0001 14*50

PERMJ RG 13 5 17 ALL

14*50 2*50.0001 14*50

PERMJ RG 12 5 17 ALL

14*50 2*50.0001 14*50

PERMJ RG 11 5 17 ALL

14*50 2*50.0001 14*50

PERMJ RG 10 5 17 ALL

15*50 50.0001 14*50

PERMK RG 30 5 22 ALL

14*50 50.0001 15*50

PERMK RG 29 5 22 ALL

14*50 2*50.0001 14*50

PERMK RG 28 5 22 ALL

14*50 2*50.0001 14*50

PERMK RG 27 5 22 ALL

14*50 2*50.0001 14*50

PERMK RG 26 5 22 ALL

14*50 2*50.0001 14*50

PERMK RG 25 5 22 ALL

14*50 2*50.0001 14*50

PERMK RG 24 5 22 ALL

14*50 2*50.0001 14*50

PERMK RG 23 5 22 ALL

14*50 2*50.0001 14*50

PERMK RG 22 5 22 ALL

14*50 2*50.0001 14*50

PERMK RG 21 5 22 ALL

14*50 2*50.0001 14*50

PERMK RG 20 5 22 ALL

21*50 3*50.0001 21*50

PERMK RG 30 5 21 ALL

14*50 50.0001 15*50

PERMK RG 29 5 21 ALL

14*50 2*50.0001 14*50

PERMK RG 28 5 21 ALL

14*50 2*50.0001 14*50

PERMK RG 27 5 21 ALL

14*50 2*50.0001 14*50

PERMK RG 26 5 21 ALL

14*50 2*50.0001 14*50

PERMK RG 25 5 21 ALL

14*50 2*50.0001 14*50

PERMK RG 24 5 21 ALL

14*50 2*50.0001 14*50

PERMK RG 23 5 21 ALL

14*50 2*50.0001 14*50

PERMK RG 22 5 21 ALL

14*50 2*50.0001 14*50

PERMK RG 21 5 21 ALL

14*50 2*50.0001 14*50

PERMK RG 20 5 21 ALL

21*50 3*50.0001 21*50

PERMK RG 30 5 20 ALL

14*50 50.0001 15*50

PERMK RG 29 5 20 ALL

14*50 2*50.0001 14*50

PERMK RG 28 5 20 ALL

14*50 2*50.0001 14*50

PERMK RG 27 5 20 ALL

14*50 2*50.0001 14*50

PERMK RG 26 5 20 ALL

14*50 2*50.0001 14*50

PERMK RG 25 5 20 ALL

14*50 2*50.0001 14*50

PERMK RG 24 5 20 ALL

14*50 2*50.0001 14*50

PERMK RG 23 5 20 ALL

14*50 2*50.0001 14*50

PERMK RG 22 5 20 ALL

14*50 2*50.0001 14*50

PERMK RG 21 5 20 ALL

14*50 2*50.0001 14*50

PERMK RG 20 5 20 ALL

21*50 3*50.0001 21*50

PERMK RG 20 5 19 ALL

21*50 3*50.0001 21*50

PERMK RG 19 5 19 ALL

14*50 2*50.0001 14*50

PERMK RG 18 5 19 ALL

14*50 2*50.0001 14*50

PERMK RG 17 5 19 ALL

14*50 2*50.0001 14*50

PERMK RG 16 5 19 ALL

14*50 2*50.0001 14*50

PERMK RG 15 5 19 ALL

14*50 2*50.0001 14*50

PERMK RG 14 5 19 ALL

14*50 2*50.0001 14*50

PERMK RG 13 5 19 ALL

14*50 2*50.0001 14*50

PERMK RG 12 5 19 ALL

14*50 2*50.0001 14*50

PERMK RG 11 5 19 ALL

14*50 2*50.0001 14*50

PERMK RG 10 5 19 ALL

15*50 50.0001 14*50

PERMK RG 20 5 18 ALL

21*50 3*50.0001 21*50

PERMK RG 19 5 18 ALL

14*50 2*50.0001 14*50

PERMK RG 18 5 18 ALL

14*50 2*50.0001 14*50

PERMK RG 17 5 18 ALL

14*50 2*50.0001 14*50

PERMK RG 16 5 18 ALL

14*50 2*50.0001 14*50

PERMK RG 15 5 18 ALL

14*50 2*50.0001 14*50

PERMK RG 14 5 18 ALL

14*50 2*50.0001 14*50

PERMK RG 13 5 18 ALL

14*50 2*50.0001 14*50

PERMK RG 12 5 18 ALL

14*50 2*50.0001 14*50

PERMK RG 11 5 18 ALL

14*50 2*50.0001 14*50

PERMK RG 10 5 18 ALL

15*50 50.0001 14*50

PERMK RG 20 5 17 ALL

21*50 3*50.0001 21*50

PERMK RG 19 5 17 ALL

14*50 2*50.0001 14*50

PERMK RG 18 5 17 ALL

14*50 2*50.0001 14*50

PERMK RG 17 5 17 ALL

14*50 2*50.0001 14*50

PERMK RG 16 5 17 ALL

14*50 2*50.0001 14*50

PERMK RG 15 5 17 ALL

14*50 2*50.0001 14*50

PERMK RG 14 5 17 ALL

14*50 2*50.0001 14*50

PERMK RG 13 5 17 ALL

14*50 2*50.0001 14*50

PERMK RG 12 5 17 ALL

```
 14*50 2*50.0001 14*50
PERMK   RG 11 5 17 ALL
 14*50 2*50.0001 14*50
PERMK   RG 10 5 17 ALL
 15*50 50.0001 14*50
*TIME 0.1
*TIME 0.2
*TIME 0.3
*TIME 0.4
*TIME 0.5
*TIME 0.6
*TIME 0.7
*TIME 0.8
*TIME 0.9
*TIME 1
SHUTIN 'I'
**$
WELL  'I_pd' ATTACHTO 'G'
** HEAD-METHOD 'I_pd' *ZERO-HEAD
PRODUCER 'I_pd'
OPERATE  MAX  STG  25000000.0  CONT
OPERATE  MAX  STW  1e+020  CONT
OPERATE  MAX  STL  10000.0  CONT
OPERATE  MAX  BHF  100000.0  CONT
OPERATE  MIN  BHP  2500.0  CONT
**         rad  geofac  wfrac  skin
GEOMETRY  K  0.0365  0.37  1.0  0.0
     PERF      GEOA  'I_pd'
** UBA                    ff         Status  Connection
   20 4 1                1.0  CLOSED  FLOW-TO  'SURFACE'  REFLAYER
   20 4 4                1.0  CLOSED  FLOW-TO  1
   20 4 8                1.0  CLOSED  FLOW-TO  2
   20 4 12               1.0  CLOSED  FLOW-TO  3
```

```
   20 4 16              1.0  CLOSED  FLOW-TO  4
   20 5 16 / 2 1 1      1.0  OPEN    FLOW-TO  5
   20 5 16 / 2 2 1      1.0  OPEN    FLOW-TO  6
   20 5 16 / 2 3 1      1.0  OPEN    FLOW-TO  7
   20 5 16 / 2 4 1      1.0  OPEN    FLOW-TO  8
   20 5 16 / 2 5 1      1.0  OPEN    FLOW-TO  9
   20 5 16 / 2 6 1      1.0  OPEN    FLOW-TO  10
   20 5 16 / 2 7 1      1.0  OPEN    FLOW-TO  11
   20 5 16 / 2 8 1      1.0  OPEN    FLOW-TO  12
   20 5 16 / 2 9 1      1.0  OPEN    FLOW-TO  13
   20 5 16 / 2 10 1     1.0  OPEN    FLOW-TO  14
   20 5 16 / 2 11 1     1.0  OPEN    FLOW-TO  15
   20 5 16 / 2 12 1     1.0  OPEN    FLOW-TO  16
   20 5 16 / 2 13 1     1.0  OPEN    FLOW-TO  17
   20 5 16 / 2 14 1     1.0  OPEN    FLOW-TO  18
   20 5 16 / 2 15 1     1.0  OPEN    FLOW-TO  19
   20 6 16              1.0  CLOSED  FLOW-TO  20
   20 7 16              1.0  CLOSED  FLOW-TO  21
   20 8 16              1.0  CLOSED  FLOW-TO  22
   20 9 16              1.0  CLOSED  FLOW-TO  23
   20 10 16             1.0  CLOSED  FLOW-TO  24
   20 11 16             1.0  CLOSED  FLOW-TO  25
   20 12 16             1.0  CLOSED  FLOW-TO  26
   20 13 16             1.0  CLOSED  FLOW-TO  27
   20 14 16             1.0  CLOSED  FLOW-TO  28
   20 15 16             1.0  CLOSED  FLOW-TO  29
   20 16 16             1.0  CLOSED  FLOW-TO  30
   20 17 16             1.0  CLOSED  FLOW-TO  31
XFLOW-MODEL 'I_pd' ZERO-FLOW
BHPDEPTH 'I_pd' 7000.0
PERMI   RG 30 5 22 ALL
 14*0.0000001 50.0001 15*0.0000001
PERMI   RG 29 5 22 ALL
```

14*0.0000001 2*50.0001 14*0.0000001

PERMI RG 28 5 22 ALL

14*0.0000001 2*50.0001 14*0.0000001

PERMI RG 27 5 22 ALL

14*0.0000001 2*50.0001 14*0.0000001

PERMI RG 26 5 22 ALL

14*0.0000001 2*50.0001 14*0.0000001

PERMI RG 25 5 22 ALL

14*0.0000001 2*50.0001 14*0.0000001

PERMI RG 24 5 22 ALL

14*0.0000001 2*50.0001 14*0.0000001

PERMI RG 23 5 22 ALL

14*0.0000001 2*50.0001 14*0.0000001

PERMI RG 22 5 22 ALL

14*0.0000001 2*50.0001 14*0.0000001

PERMI RG 21 5 22 ALL

14*0.0000001 2*50.0001 14*0.0000001

PERMI RG 20 5 22 ALL

21*0.0000001 3*50.0001 21*0.0000001

PERMI RG 30 5 21 ALL

14*0.0000001 50.0001 15*0.0000001

PERMI RG 29 5 21 ALL

14*0.0000001 2*50.0001 14*0.0000001

PERMI RG 28 5 21 ALL

14*0.0000001 2*50.0001 14*0.0000001

PERMI RG 27 5 21 ALL

14*0.0000001 2*50.0001 14*0.0000001

PERMI RG 26 5 21 ALL

14*0.0000001 2*50.0001 14*0.0000001

PERMI RG 25 5 21 ALL

14*0.0000001 2*50.0001 14*0.0000001

PERMI RG 24 5 21 ALL

14*0.0000001 2*50.0001 14*0.0000001

PERMI RG 23 5 21 ALL

14*0.0000001 2*50.0001 14*0.0000001

PERMI RG 22 5 21 ALL

14*0.0000001 2*50.0001 14*0.0000001

PERMI RG 21 5 21 ALL

14*0.0000001 2*50.0001 14*0.0000001

PERMI RG 20 5 21 ALL

21*0.0000001 3*50.0001 21*0.0000001

PERMI RG 30 5 20 ALL

14*0.0000001 50.0001 15*0.0000001

PERMI RG 29 5 20 ALL

14*0.0000001 2*50.0001 14*0.0000001

PERMI RG 28 5 20 ALL

14*0.0000001 2*50.0001 14*0.0000001

PERMI RG 27 5 20 ALL

14*0.0000001 2*50.0001 14*0.0000001

PERMI RG 26 5 20 ALL

14*0.0000001 2*50.0001 14*0.0000001

PERMI RG 25 5 20 ALL

14*0.0000001 2*50.0001 14*0.0000001

PERMI RG 24 5 20 ALL

14*0.0000001 2*50.0001 14*0.0000001

PERMI RG 23 5 20 ALL

14*0.0000001 2*50.0001 14*0.0000001

PERMI RG 22 5 20 ALL

14*0.0000001 2*50.0001 14*0.0000001

PERMI RG 21 5 20 ALL

14*0.0000001 2*50.0001 14*0.0000001

PERMI RG 20 5 20 ALL

21*0.0000001 3*50.0001 21*0.0000001

PERMI RG 20 5 19 ALL

21*0.0000001 3*50.0001 21*0.0000001

PERMI RG 19 5 19 ALL

14*0.0000001 2*50.0001 14*0.0000001

PERMI RG 18 5 19 ALL

14*0.0000001 2*50.0001 14*0.0000001

PERMI RG 17 5 19 ALL

14*0.0000001 2*50.0001 14*0.0000001

PERMI RG 16 5 19 ALL

14*0.0000001 2*50.0001 14*0.0000001

PERMI RG 15 5 19 ALL

14*0.0000001 2*50.0001 14*0.0000001

PERMI RG 14 5 19 ALL

14*0.0000001 2*50.0001 14*0.0000001

PERMI RG 13 5 19 ALL

14*0.0000001 2*50.0001 14*0.0000001

PERMI RG 12 5 19 ALL

14*0.0000001 2*50.0001 14*0.0000001

PERMI RG 11 5 19 ALL

14*0.0000001 2*50.0001 14*0.0000001

PERMI RG 10 5 19 ALL

15*0.0000001 50.0001 14*0.0000001

PERMI RG 20 5 18 ALL

21*0.0000001 3*50.0001 21*0.0000001

PERMI RG 19 5 18 ALL

14*0.0000001 2*50.0001 14*0.0000001

PERMI RG 18 5 18 ALL

14*0.0000001 2*50.0001 14*0.0000001

PERMI RG 17 5 18 ALL

14*0.0000001 2*50.0001 14*0.0000001

PERMI RG 16 5 18 ALL

14*0.0000001 2*50.0001 14*0.0000001

PERMI RG 15 5 18 ALL

14*0.0000001 2*50.0001 14*0.0000001

PERMI RG 14 5 18 ALL

14*0.0000001 2*50.0001 14*0.0000001

PERMI RG 13 5 18 ALL

14*0.0000001 2*50.0001 14*0.0000001

PERMI RG 12 5 18 ALL

14*0.0000001 2*50.0001 14*0.0000001

PERMI RG 11 5 18 ALL

14*0.0000001 2*50.0001 14*0.0000001

PERMI RG 10 5 18 ALL

15*0.0000001 50.0001 14*0.0000001

PERMI RG 20 5 17 ALL

21*0.0000001 3*50.0001 21*0.0000001

PERMI RG 19 5 17 ALL

14*0.0000001 2*50.0001 14*0.0000001

PERMI RG 18 5 17 ALL

14*0.0000001 2*50.0001 14*0.0000001

PERMI RG 17 5 17 ALL

14*0.0000001 2*50.0001 14*0.0000001

PERMI RG 16 5 17 ALL

14*0.0000001 2*50.0001 14*0.0000001

PERMI RG 15 5 17 ALL

14*0.0000001 2*50.0001 14*0.0000001

PERMI RG 14 5 17 ALL

14*0.0000001 2*50.0001 14*0.0000001

PERMI RG 13 5 17 ALL

14*0.0000001 2*50.0001 14*0.0000001

PERMI RG 12 5 17 ALL

14*0.0000001 2*50.0001 14*0.0000001

PERMI RG 11 5 17 ALL

14*0.0000001 2*50.0001 14*0.0000001

PERMI RG 10 5 17 ALL

15*0.0000001 50.0001 14*0.0000001

PERMJ RG 30 5 22 ALL

14*0.0000001 50.0001 15*0.0000001

PERMJ RG 29 5 22 ALL

14*0.0000001 2*50.0001 14*0.0000001

PERMJ RG 28 5 22 ALL

14*0.0000001 2*50.0001 14*0.0000001

PERMJ RG 27 5 22 ALL

14*0.0000001 2*50.0001 14*0.0000001

PERMJ RG 26 5 22 ALL

14*0.0000001 2*50.0001 14*0.0000001

PERMJ RG 25 5 22 ALL

14*0.0000001 2*50.0001 14*0.0000001

PERMJ RG 24 5 22 ALL

14*0.0000001 2*50.0001 14*0.0000001

PERMJ RG 23 5 22 ALL

14*0.0000001 2*50.0001 14*0.0000001

PERMJ RG 22 5 22 ALL

14*0.0000001 2*50.0001 14*0.0000001

PERMJ RG 21 5 22 ALL

14*0.0000001 2*50.0001 14*0.0000001

PERMJ RG 20 5 22 ALL

21*0.0000001 3*50.0001 21*0.0000001

PERMJ RG 30 5 21 ALL

14*0.0000001 50.0001 15*0.0000001

PERMJ RG 29 5 21 ALL

14*0.0000001 2*50.0001 14*0.0000001

PERMJ RG 28 5 21 ALL

14*0.0000001 2*50.0001 14*0.0000001

PERMJ RG 27 5 21 ALL

14*0.0000001 2*50.0001 14*0.0000001

PERMJ RG 26 5 21 ALL

14*0.0000001 2*50.0001 14*0.0000001

PERMJ RG 25 5 21 ALL

14*0.0000001 2*50.0001 14*0.0000001

PERMJ RG 24 5 21 ALL

14*0.0000001 2*50.0001 14*0.0000001

PERMJ RG 23 5 21 ALL

14*0.0000001 2*50.0001 14*0.0000001

PERMJ RG 22 5 21 ALL

14*0.0000001 2*50.0001 14*0.0000001

PERMJ RG 21 5 21 ALL

14*0.0000001 2*50.0001 14*0.0000001

PERMJ RG 20 5 21 ALL

21*0.0000001 3*50.0001 21*0.0000001

PERMJ RG 30 5 20 ALL

14*0.0000001 50.0001 15*0.0000001

PERMJ RG 29 5 20 ALL

14*0.0000001 2*50.0001 14*0.0000001

PERMJ RG 28 5 20 ALL

14*0.0000001 2*50.0001 14*0.0000001

PERMJ RG 27 5 20 ALL

14*0.0000001 2*50.0001 14*0.0000001

PERMJ RG 26 5 20 ALL

14*0.0000001 2*50.0001 14*0.0000001

PERMJ RG 25 5 20 ALL

14*0.0000001 2*50.0001 14*0.0000001

PERMJ RG 24 5 20 ALL

14*0.0000001 2*50.0001 14*0.0000001

PERMJ RG 23 5 20 ALL

14*0.0000001 2*50.0001 14*0.0000001

PERMJ RG 22 5 20 ALL

14*0.0000001 2*50.0001 14*0.0000001

PERMJ RG 21 5 20 ALL

14*0.0000001 2*50.0001 14*0.0000001

PERMJ RG 20 5 20 ALL

21*0.0000001 3*50.0001 21*0.0000001

PERMJ RG 20 5 19 ALL

21*0.0000001 3*50.0001 21*0.0000001

PERMJ RG 19 5 19 ALL

14*0.0000001 2*50.0001 14*0.0000001

PERMJ RG 18 5 19 ALL

14*0.0000001 2*50.0001 14*0.0000001

PERMJ RG 17 5 19 ALL

14*0.0000001 2*50.0001 14*0.0000001

PERMJ RG 16 5 19 ALL

14*0.0000001 2*50.0001 14*0.0000001

PERMJ RG 15 5 19 ALL

14*0.0000001 2*50.0001 14*0.0000001

PERMJ RG 14 5 19 ALL

14*0.0000001 2*50.0001 14*0.0000001

PERMJ RG 13 5 19 ALL

14*0.0000001 2*50.0001 14*0.0000001

PERMJ RG 12 5 19 ALL

14*0.0000001 2*50.0001 14*0.0000001

PERMJ RG 11 5 19 ALL

14*0.0000001 2*50.0001 14*0.0000001

PERMJ RG 10 5 19 ALL

15*0.0000001 50.0001 14*0.0000001

PERMJ RG 20 5 18 ALL

21*0.0000001 3*50.0001 21*0.0000001

PERMJ RG 19 5 18 ALL

14*0.0000001 2*50.0001 14*0.0000001

PERMJ RG 18 5 18 ALL

14*0.0000001 2*50.0001 14*0.0000001

PERMJ RG 17 5 18 ALL

14*0.0000001 2*50.0001 14*0.0000001

PERMJ RG 16 5 18 ALL

14*0.0000001 2*50.0001 14*0.0000001

PERMJ RG 15 5 18 ALL

14*0.0000001 2*50.0001 14*0.0000001

PERMJ RG 14 5 18 ALL

14*0.0000001 2*50.0001 14*0.0000001

PERMJ RG 13 5 18 ALL

14*0.0000001 2*50.0001 14*0.0000001

PERMJ RG 12 5 18 ALL

14*0.0000001 2*50.0001 14*0.0000001

PERMJ RG 11 5 18 ALL

14*0.0000001 2*50.0001 14*0.0000001

PERMJ RG 10 5 18 ALL

15*0.0000001 50.0001 14*0.0000001

PERMJ RG 20 5 17 ALL

21*0.0000001 3*50.0001 21*0.0000001

PERMJ RG 19 5 17 ALL

14*0.0000001 2*50.0001 14*0.0000001

PERMJ RG 18 5 17 ALL

14*0.0000001 2*50.0001 14*0.0000001

PERMJ RG 17 5 17 ALL

14*0.0000001 2*50.0001 14*0.0000001

PERMJ RG 16 5 17 ALL

14*0.0000001 2*50.0001 14*0.0000001

PERMJ RG 15 5 17 ALL

14*0.0000001 2*50.0001 14*0.0000001

PERMJ RG 14 5 17 ALL

14*0.0000001 2*50.0001 14*0.0000001

PERMJ RG 13 5 17 ALL

14*0.0000001 2*50.0001 14*0.0000001

PERMJ RG 12 5 17 ALL

14*0.0000001 2*50.0001 14*0.0000001

PERMJ RG 11 5 17 ALL

14*0.0000001 2*50.0001 14*0.0000001

PERMJ RG 10 5 17 ALL

15*0.0000001 50.0001 14*0.0000001

PERMK RG 30 5 22 ALL

14*0.0000001 50.0001 15*0.0000001

PERMK RG 29 5 22 ALL

14*0.0000001 2*50.0001 14*0.0000001

PERMK RG 28 5 22 ALL

14*0.0000001 2*50.0001 14*0.0000001

PERMK RG 27 5 22 ALL

14*0.0000001 2*50.0001 14*0.0000001

PERMK RG 26 5 22 ALL

14*0.0000001 2*50.0001 14*0.0000001

PERMK RG 25 5 22 ALL

14*0.0000001 2*50.0001 14*0.0000001

PERMK RG 24 5 22 ALL

14*0.0000001 2*50.0001 14*0.0000001

PERMK RG 23 5 22 ALL

14*0.0000001 2*50.0001 14*0.0000001

PERMK RG 22 5 22 ALL

14*0.0000001 2*50.0001 14*0.0000001

PERMK RG 21 5 22 ALL

14*0.0000001 2*50.0001 14*0.0000001

PERMK RG 20 5 22 ALL

21*0.0000001 3*50.0001 21*0.0000001

PERMK RG 30 5 21 ALL

14*0.0000001 50.0001 15*0.0000001

PERMK RG 29 5 21 ALL

14*0.0000001 2*50.0001 14*0.0000001

PERMK RG 28 5 21 ALL

14*0.0000001 2*50.0001 14*0.0000001

PERMK RG 27 5 21 ALL

14*0.0000001 2*50.0001 14*0.0000001

PERMK RG 26 5 21 ALL

14*0.0000001 2*50.0001 14*0.0000001

PERMK RG 25 5 21 ALL

14*0.0000001 2*50.0001 14*0.0000001

PERMK RG 24 5 21 ALL

14*0.0000001 2*50.0001 14*0.0000001

PERMK RG 23 5 21 ALL

14*0.0000001 2*50.0001 14*0.0000001

PERMK RG 22 5 21 ALL

14*0.0000001 2*50.0001 14*0.0000001

PERMK RG 21 5 21 ALL

14*0.0000001 2*50.0001 14*0.0000001

PERMK RG 20 5 21 ALL

21*0.0000001 3*50.0001 21*0.0000001

PERMK RG 30 5 20 ALL

14*0.0000001 50.0001 15*0.0000001

PERMK RG 29 5 20 ALL

14*0.0000001 2*50.0001 14*0.0000001

PERMK RG 28 5 20 ALL

14*0.0000001 2*50.0001 14*0.0000001

PERMK RG 27 5 20 ALL

14*0.0000001 2*50.0001 14*0.0000001

PERMK RG 26 5 20 ALL

14*0.0000001 2*50.0001 14*0.0000001

PERMK RG 25 5 20 ALL

14*0.0000001 2*50.0001 14*0.0000001

PERMK RG 24 5 20 ALL

14*0.0000001 2*50.0001 14*0.0000001

PERMK RG 23 5 20 ALL

14*0.0000001 2*50.0001 14*0.0000001

PERMK RG 22 5 20 ALL

14*0.0000001 2*50.0001 14*0.0000001

PERMK RG 21 5 20 ALL

14*0.0000001 2*50.0001 14*0.0000001

PERMK RG 20 5 20 ALL

21*0.0000001 3*50.0001 21*0.0000001

PERMK RG 20 5 19 ALL

21*0.0000001 3*50.0001 21*0.0000001

PERMK RG 19 5 19 ALL

14*0.0000001 2*50.0001 14*0.0000001

PERMK RG 18 5 19 ALL

14*0.0000001 2*50.0001 14*0.0000001

PERMK RG 17 5 19 ALL

14*0.0000001 2*50.0001 14*0.0000001

PERMK RG 16 5 19 ALL

14*0.0000001 2*50.0001 14*0.0000001

PERMK RG 15 5 19 ALL

14*0.0000001 2*50.0001 14*0.0000001

PERMK RG 14 5 19 ALL

14*0.0000001 2*50.0001 14*0.0000001

PERMK RG 13 5 19 ALL

14*0.0000001 2*50.0001 14*0.0000001

PERMK RG 12 5 19 ALL

14*0.0000001 2*50.0001 14*0.0000001

PERMK RG 11 5 19 ALL

14*0.0000001 2*50.0001 14*0.0000001

PERMK RG 10 5 19 ALL

15*0.0000001 50.0001 14*0.0000001

PERMK RG 20 5 18 ALL

21*0.0000001 3*50.0001 21*0.0000001

PERMK RG 19 5 18 ALL

14*0.0000001 2*50.0001 14*0.0000001

PERMK RG 18 5 18 ALL

14*0.0000001 2*50.0001 14*0.0000001

PERMK RG 17 5 18 ALL

14*0.0000001 2*50.0001 14*0.0000001

PERMK RG 16 5 18 ALL

14*0.0000001 2*50.0001 14*0.0000001

PERMK RG 15 5 18 ALL

14*0.0000001 2*50.0001 14*0.0000001

PERMK RG 14 5 18 ALL

14*0.0000001 2*50.0001 14*0.0000001

PERMK RG 13 5 18 ALL

14*0.0000001 2*50.0001 14*0.0000001

PERMK RG 12 5 18 ALL

14*0.0000001 2*50.0001 14*0.0000001

PERMK RG 11 5 18 ALL

14*0.0000001 2*50.0001 14*0.0000001

PERMK RG 10 5 18 ALL

15*0.0000001 50.0001 14*0.0000001

PERMK RG 20 5 17 ALL

21*0.0000001 3*50.0001 21*0.0000001

PERMK RG 19 5 17 ALL

14*0.0000001 2*50.0001 14*0.0000001

PERMK RG 18 5 17 ALL

14*0.0000001 2*50.0001 14*0.0000001

PERMK RG 17 5 17 ALL

14*0.0000001 2*50.0001 14*0.0000001

PERMK RG 16 5 17 ALL

14*0.0000001 2*50.0001 14*0.0000001

PERMK RG 15 5 17 ALL

14*0.0000001 2*50.0001 14*0.0000001

PERMK RG 14 5 17 ALL

14*0.0000001 2*50.0001 14*0.0000001

PERMK RG 13 5 17 ALL

14*0.0000001 2*50.0001 14*0.0000001

PERMK RG 12 5 17 ALL

14*0.0000001 2*50.0001 14*0.0000001

PERMK RG 11 5 17 ALL

14*0.0000001 2*50.0001 14*0.0000001

PERMK RG 10 5 17 ALL

15*0.0000001 50.0001 14*0.0000001

*TIME 1.5

*TIME 2

*TIME 3

*TIME 7

*TIME 11

*TIME 31

*TIME 61

*TIME 101

*TIME 102

*TIME 103

*TIME 104

*TIME 107

*TIME 111

*TIME 131

*TIME 151

*TIME 201

*TIME 251

*TIME 301

*TIME 351

*TIME 401

*TIME 451

*TIME 501

*TIME 551

*TIME 601

*TIME 651

*TIME 701

*TIME 751

*TIME 801

*TIME 851

*TIME 901

*TIME 951

*TIME 1001

*TIME 1051

*TIME 1101

*TIME 1151

*TIME 1201

*TIME 1251

*TIME 1301

*TIME 1351

*TIME 1401

*TIME 1451

*TIME 1501

*TIME 1551

*TIME 1601

*TIME 1651

*TIME 1701

*TIME 1751

*TIME 1801

*TIME 1851

*TIME 1901

*TIME 1951

*TIME 2001

*STOP

A3.2 CMG GEM

```
RESULTS SIMULATOR GEM 201410

DIM MDNRXN 6

INUNIT FIELD

WSRF WELL 1

OUTSRF GRID MINERAL 'Anhydri*' MINERAL 'Barite' MINERAL 'Calcite' MOLALITY 'Ba++' MOLALITY
'CH4' MOLALITY 'CO2' MOLALITY 'CO3--' MOLALITY 'Ca++' MOLALITY 'CaOH+' MOLALITY 'Cl-'
MOLALITY 'H+'

      MOLALITY 'HCO3-' MOLALITY 'Na+' MOLALITY 'SO4--' PRES SG SW PERM

*MOLALITY 'Na+' *MOLALITY 'Cl-' *MOLALITY 'CO3--' *DPORMNR *MINERAL 'Calcite'

OUTSRF RES NONE

OUTSRF WELL

      MOLALITYW 'Cl-' 'I_pd'


      MOLALITYW 'Ba++' 'I_pd'


      MOLALITYW 'SO4--' 'I_pd'


      MOLALITYW 'CO3--' 'I_pd'


      MOLALITYW 'Ca++' 'I_pd'


      MOLALITYW 'HCO3-' 'I_pd'

OUTPRN GRID NONE

OUTPRN RES NONE

OUTPRN WELL BRIEF

RESULTS XOFFSET          0.0000

RESULTS YOFFSET          0.0000

RESULTS ROTATION         0.0000  **  (DEGREES)

RESULTS AXES-DIRECTIONS 1.0 -1.0 1.0

… …

… …

… …
```

```
**********************************************************************************************
**The same as CMG IMEX basecase for the start until model section (define phase compositions and
**mineralreactions)

**********************************************************************************************

*MODEL   *PR

*NC   2   2

*TRES      235.000

*COMPNAME

        'CO2'         'CH4'

*SG        8.1800000E-01  3.0000000E-01

*TB       -1.0921000E+02 -2.5861000E+02

*PCRIT     7.2800000E+01  4.5400000E+01

*VCRIT     9.4000000E-02  9.9000000E-02

*TCRIT     3.0420000E+02  1.9060000E+02

*AC        2.2500000E-01  8.0000000E-03

*MW        4.4010000E+01  1.6043000E+01

*HCFLAG    0              0

*BIN 1.0500000E-01

*VSHIFT    0.0000000E+00  0.0000000E+00

*VISCOR *HZYT

*MIXVC     1.0000000E+00

*VISVC     9.4000000E-02  9.9000000E-02

*VISCOEFF   1.0230000E-01  2.3364000E-02  5.8533000E-02 -4.0758000E-02 9.3324000E-03

*OMEGA     4.5723553E-01  4.5723553E-01

*OMEGB     7.7796074E-02  7.7796074E-02

*PCHOR     7.8000000E+01  7.7000000E+01

*ENTHCOEF

         9.6880000E-02  1.5884300E-01 -3.3712000E-05  1.4810500E-07

        -9.6620300E-11  2.0738320E-14

        -2.8385700E+00  5.3828500E-01 -2.1140900E-04  3.3927600E-07

        -1.1643220E-10  1.3896120E-14

*HENRYC    5902.60260877    1.0132500E+22

*REFPH     493.461633358  493.461633358

*VINFINITY  0              0
```

```
**********
*AQUEOUS-DENSITY  *ROWE-CHOU
*AQUEOUS-VISCOSITY  *KESTIN
*DER-CHEM-EQUIL  *ANALYTICAL
*DER-REACT-RATE  *ANALYTICAL
*PERM-VS-POR   OFF
*ACTIVITY-MODEL  *B-DOT
*SALINITY-CALC  *OFF
*SALINITY   0.00000
*AQFILL  *OFF
 *NC-AQUEOUS    9
*COMPNAME-AQUEOUS
'H+' 'Ca++' 'Ba++' 'SO4--' 'Na+'
'Cl-' 'HCO3-' 'CO3--' 'CaOH+'
*MW-AQUEOUS
    1.0079    40.0800   137.3300    96.0576    22.9898
   35.4530    61.0171    60.0092    57.0873
*ION-SIZE-AQUEOUS
   9.00    6.00    5.00    4.00    4.00
   3.00    4.50    4.50    4.00
*CHARGE-AQUEOUS
    1.0     2.0     2.0    -2.0     1.0
   -1.0    -1.0    -2.0     1.0
 *NC-MINERAL    3
*COMPNAME-MINERAL
'Barite' 'Anhydri*' 'Calcite'
*MW-MINERAL
  233.3876   136.1376   100.0892
*MASSDENSITY-MINERAL
   4479.61    2963.38    2709.95
 *N-CHEM-EQUIL    3
*N-RATE-REACT    3
**REACTION NO.   1: CO2(aq) + H2O = (H+) + (HCO3-)
```

*STOICHIOMETRY

-1.000 0.000 -1.000 1.000 0.000

0.000 0.000 0.000 0.000 1.000

0.000 0.000 0.000 0.000 0.000

*LOG-CHEM-EQUIL-COEFS

-6.549243E+00 9.001740E-03 -1.021150E-04 2.761879E-07 -3.561421E-10

**REACTION NO. 2: (CO3--) + (H+) = (HCO3-)

*STOICHIOMETRY

0.000 0.000 0.000 -1.000 0.000

0.000 0.000 0.000 0.000 1.000

-1.000 0.000 0.000 0.000 0.000

*LOG-CHEM-EQUIL-COEFS

1.060796E+01 -1.276757E-02 1.202580E-04 -3.017310E-07 2.693718E-10

**REACTION NO. 3: (CaOH+) + (H+) = (Ca++) + H2O

*STOICHIOMETRY

0.000 0.000 1.000 -1.000 1.000

0.000 0.000 0.000 0.000 0.000

0.000 -1.000 0.000 0.000 0.000

*LOG-CHEM-EQUIL-COEFS

1.370810E+01 -4.388997E-02 1.340774E-04 -2.357931E-07 9.750535E-11

**REACTION NO. 4: Barite = (Ba++) + (SO4--)

*STOICHIOMETRY

0.000 0.000 0.000 0.000 0.000

1.000 1.000 0.000 0.000 0.000

0.000 0.000 -1.000 0.000 0.000

*LOG-CHEM-EQUIL-COEFS

-1.047962E+01 2.521499E-02 -2.151593E-04 7.214753E-07 -1.179685E-09

*REACTIVE-SURFACE-AREA 23.23

*ACTIVATION-ENERGY 41870.00

*LOG-TST-RATE-CONSTANT -8.79588

*REF-TEMP-RATE-CONST 113.00

**REACTION NO. 5: Anhydrite = (Ca++) + (SO4--)

*STOICHIOMETRY

```
    0.000     0.000     0.000     0.000     1.000
    0.000     1.000     0.000     0.000     0.000
    0.000     0.000     0.000    -1.000     0.000
*LOG-CHEM-EQUIL-COEFS
 -4.069059E+00  -5.737552E-03  -1.101507E-04   4.993139E-07  -9.869430E-10
*REACTIVE-SURFACE-AREA       23.23
*ACTIVATION-ENERGY    41900.00
*LOG-TST-RATE-CONSTANT    -5.00000
*REF-TEMP-RATE-CONST      113.00

**REACTION NO.   6: Calcite + (H+) = (Ca++) + (HCO3-)
*STOICHIOMETRY
    0.000     0.000     0.000    -1.000     1.000
    0.000     0.000     0.000     0.000     1.000
    0.000     0.000     0.000     0.000    -1.000
*LOG-CHEM-EQUIL-COEFS
  2.068889E+00  -1.426678E-02  -6.060961E-06   1.459215E-07  -4.189284E-10
*REACTIVE-SURFACE-AREA       23.23
*ACTIVATION-ENERGY    41900.00
*LOG-TST-RATE-CONSTANT    -5.00000
*REF-TEMP-RATE-CONST      113.00
*ANNIH-MATRIX
  1.00  0.00  0.00  0.00  0.00  0.00  0.00  0.00  0.00  1.00  0.00  0.00
  0.00  1.00  0.00  0.00  0.00  0.00  0.00  0.00  0.00  0.00  0.00  0.00
  0.00  0.00  1.00  0.00  0.00  0.00  0.00  0.00  0.00  1.00  0.00  1.00
  0.00  0.00  0.00  1.00  0.00  0.00  0.00  0.00  0.00 -1.00 -1.00 -1.00
  0.00  0.00  0.00  0.00  1.00  0.00  0.00  0.00  0.00  0.00  0.00  1.00
  0.00  0.00  0.00  0.00  0.00  1.00  0.00  0.00  0.00  0.00  0.00  0.00
  0.00  0.00  0.00  0.00  0.00  0.00  1.00  0.00  0.00  0.00  0.00  0.00
  0.00  0.00  0.00  0.00  0.00  0.00  0.00  1.00  0.00  0.00  0.00  0.00
  0.00  0.00  0.00  0.00  0.00  0.00  0.00  0.00  1.00  0.00  0.00  0.00
********** Rockfluid section is the same as CMG IMEX**********
USER_INPUT
```

```
*INCLUDE 'include-files/PRES.DAT'
SW CON         0.05
*SW MATRIX BG 'I - Frac_1' *NFZ 0.21
*SW MATRIX BG 'I - Frac_1' *FZ 0.45
*SW MATRIX BG 'I - Frac_2' *NFZ 0.21
*SW MATRIX BG 'I - Frac_2' *FZ 0.45
ZGLOBALC 'CO2' CON         0.01
ZGLOBALC 'CH4' CON         0.99
*MOLALITY-AQUEOUS
**'H+' 'Ca++' 'Ba++' 'SO4--' 'Na+'
**'Cl-' 'HCO3-' 'CO3--' 'CaOH+'
0.0000001       0.00577  0.001597   0   0.023661
0.0499  0.000555 0          0
*VOLUMEFRACTION-MINERAL
0 0 1
NUMERICAL
*MAXCHANGE *PRESS 1E+05
RUN
DATE 2008 1  1.00000
DTWELL 0.0001
WELL  'I'
**   'CO2'          'CH4'
**'H+' 'Ca++' 'Ba++' 'SO4--' 'Na+'
**'Cl-' 'HCO3-' 'CO3--' 'CaOH+'
INJECTOR 'I'
INCOMP  AQUEOUS  0.0  0.0  1e-007  0.000296184  0.0  0.000100062  9.40584e-005  0.000740459  0.0  0.0  0.0
OPERATE  MAX  STW  3000.0  CONT REPEAT
GEOMETRY  K  0.0365  0.37  1.0  0.0
     PERF      GEOA  'I'
** UBA                    ff         Status  Connection
   20 4 1                1.0  CLOSED  FLOW-FROM  'SURFACE'  REFLAYER
   20 4 4                1.0  CLOSED  FLOW-FROM  1
   20 4 8                1.0  CLOSED  FLOW-FROM  2
```

20 4 12 1.0 CLOSED FLOW-FROM 3

20 4 16 1.0 CLOSED FLOW-FROM 4

20 5 16 / 2 1 1 1.0 CLOSED FLOW-FROM 5

20 5 16 / 2 2 1 1.0 CLOSED FLOW-FROM 6

20 5 16 / 2 3 1 1.0 CLOSED FLOW-FROM 7

20 5 16 / 2 4 1 1.0 CLOSED FLOW-FROM 8

20 5 16 / 2 5 1 1.0 CLOSED FLOW-FROM 9

20 5 16 / 2 6 1 1.0 CLOSED FLOW-FROM 10

20 5 16 / 2 7 1 1.0 CLOSED FLOW-FROM 11

20 5 16 / 2 8 1 1.0 OPEN FLOW-FROM 12

20 5 16 / 2 9 1 1.0 CLOSED FLOW-FROM 13

20 5 16 / 2 10 1 1.0 CLOSED FLOW-FROM 14

20 5 16 / 2 11 1 1.0 CLOSED FLOW-FROM 15

20 5 16 / 2 12 1 1.0 CLOSED FLOW-FROM 16

20 5 16 / 2 13 1 1.0 CLOSED FLOW-FROM 17

20 5 16 / 2 14 1 1.0 CLOSED FLOW-FROM 18

20 5 16 / 2 15 1 1.0 CLOSED FLOW-FROM 19

20 6 16 1.0 CLOSED FLOW-FROM 20

20 7 16 / 2 1 1 1.0 CLOSED FLOW-FROM 21

20 7 16 / 2 2 1 1.0 CLOSED FLOW-FROM 22

20 7 16 / 2 3 1 1.0 CLOSED FLOW-FROM 23

20 7 16 / 2 4 1 1.0 CLOSED FLOW-FROM 24

20 7 16 / 2 5 1 1.0 CLOSED FLOW-FROM 25

20 7 16 / 2 6 1 1.0 CLOSED FLOW-FROM 26

20 7 16 / 2 7 1 1.0 CLOSED FLOW-FROM 27

20 7 16 / 2 8 1 1.0 CLOSED FLOW-FROM 28

20 7 16 / 2 9 1 1.0 CLOSED FLOW-FROM 29

20 7 16 / 2 10 1 1.0 CLOSED FLOW-FROM 30

20 7 16 / 2 11 1 1.0 CLOSED FLOW-FROM 31

20 7 16 / 2 12 1 1.0 CLOSED FLOW-FROM 32

20 7 16 / 2 13 1 1.0 CLOSED FLOW-FROM 33

20 7 16 / 2 14 1 1.0 CLOSED FLOW-FROM 34

20 7 16 / 2 15 1 1.0 CLOSED FLOW-FROM 35

```
   20 8 16              1.0  CLOSED  FLOW-FROM  36
   20 9 16              1.0  CLOSED  FLOW-FROM  37
   20 10 16             1.0  CLOSED  FLOW-FROM  38
   20 11 16             1.0  CLOSED  FLOW-FROM  39
   20 12 16             1.0  CLOSED  FLOW-FROM  40
   20 13 16             1.0  CLOSED  FLOW-FROM  41
   20 14 16             1.0  CLOSED  FLOW-FROM  42
   20 15 16             1.0  CLOSED  FLOW-FROM  43
   20 16 16             1.0  CLOSED  FLOW-FROM  44
   20 17 16             1.0  CLOSED  FLOW-FROM  45
XFLOW-MODEL 'I' ZERO-FLOW
DTMIN 1.0E-16
DTMAX 50
********secondary fracture conductivity is the same as CMG IMEX so is well section for production well*********
```

A3.3 CMG IMEX – SI adsorption model

RESULTS SIMULATOR IMEX 201210

********Grid sections, hydraulic fracture and reservoir settings are all the same as IMEX base case**********

**********polymer option has been applied to simulate matrix adsorption of SI**********

MODEL POLY

TRES 113

PVT BG 1

1674	706.49717	1.06162	0.00198	1.06274	0.0162
2031	859.9811558	1.07233	0.00162	1.04846	0.0171
2530	1060.092277	1.0873	0.0013	1.0285	0.0184
2991	1230.604288	1.10113	0.00111	1.01006	0.0197
3553	1420.693433	1.11799	0.000959	0.98758	0.0213
4110	1590.800531	1.1347	0.000855	0.9653	0.023
4544	1711.389981	1.14772	0.000795	0.94794	0.0244
4935	1811.5121	1.15945	0.000751	0.9323	0.0255
5255	1887.704956	1.16905	0.00072	0.9195	0.0265
5545	1952.462254	1.17775	0.000696	0.9079	0.0274
7000	2221	1.2214	0.0006	0.8497	0.033

BWI 1.0037

CO 1.0E-5

CVO 4.6E-5

CVW 0

CW 5.8E-05

DENSITY OIL 44.986

DENSITY WATER 63

DENSITY GAS 0.01

```
REFPW 1.034

VWI 0.607

*PADSORP                    ** Enter polymer adsorption table.

  **  p_con       adsop_level     ** values should appear in increasing order, top to bottom.

      0               0

      0.06995441      180.096188

      0.13990882      221.7244157

      0.209863229     250.4037894

      0.279817639     272.9747757

      0.349772049     291.8740751

*PMIX *LINEAR

*PPERM

  **  perm    max_ad   res_ad    p_pore   rrf

   0.0001    291.8740751  0       1.0     1.0

   1000      291.8740751  0       1.0     1.0

PVISC 0.607

PREFCONC 0.349772049

*******************************Rockfluid section is the same as IMEX basecase************************

*INITIAL

*USER_INPUT

*INCLUDE 'include-files/PRES.DAT'

PB   *CON 3000

SO   *CON     0

SW   *CON  0.05

*SW MATRIX BG 'I - Frac_2' *NFZ 0.21

*SW MATRIX BG 'I - Frac_2' *FZ 0.45

POLYCONC CON 0.0
```

```
NUMERICAL

NCUTS 100

**********Run section is the same as IMEX base case**********

GROUP 'G' ATTACHTO 'FIELD'

WELL  'I' ATTACHTO 'G'

INJECTOR MOBWEIGHT 'I'

**********SI concentration in the fracture fluid is defined here**********

INCOMP  WATER 0.349772049

OPERATE  MAX  STW  3000.0  CONT REPEAT

GEOMETRY  K  0.0365  0.37  1.0  0.0

    PERF      GEOA  'I'

   20 4 1                1.0  CLOSED  FLOW-FROM  'SURFACE'  REFLAYER

   20 4 4                1.0  CLOSED  FLOW-FROM  1

   20 4 8                1.0  CLOSED  FLOW-FROM  2

   20 4 12               1.0  CLOSED  FLOW-FROM  3

   20 4 16               1.0  CLOSED  FLOW-FROM  4

   20 5 16 / 2 1 1       1.0  CLOSED  FLOW-FROM  5

   20 5 16 / 2 2 1       1.0  CLOSED  FLOW-FROM  6

   20 5 16 / 2 3 1       1.0  CLOSED  FLOW-FROM  7

   20 5 16 / 2 4 1       1.0  CLOSED  FLOW-FROM  8

   20 5 16 / 2 5 1       1.0  CLOSED  FLOW-FROM  9

   20 5 16 / 2 6 1       1.0  CLOSED  FLOW-FROM  10

   20 5 16 / 2 7 1       1.0  CLOSED  FLOW-FROM  11

   20 5 16 / 2 8 1       1.0  OPEN    FLOW-FROM  12

   20 5 16 / 2 9 1       1.0  CLOSED  FLOW-FROM  13

   20 5 16 / 2 10 1      1.0  CLOSED  FLOW-FROM  14

   20 5 16 / 2 11 1      1.0  CLOSED  FLOW-FROM  15
```

```
   20 5 16 / 2 12 1        1.0  CLOSED  FLOW-FROM  16

   20 5 16 / 2 13 1        1.0  CLOSED  FLOW-FROM  17

   20 5 16 / 2 14 1        1.0  CLOSED  FLOW-FROM  18

   20 5 16 / 2 15 1        1.0  CLOSED  FLOW-FROM  19

   20 6 16              1.0  CLOSED  FLOW-FROM  20

   20 7 16              1.0  CLOSED  FLOW-FROM  21

   20 8 16              1.0  CLOSED  FLOW-FROM  22

   20 9 16              1.0  CLOSED  FLOW-FROM  23

   20 10 16              1.0  CLOSED  FLOW-FROM  24

   20 11 16              1.0  CLOSED  FLOW-FROM  25

   20 12 16              1.0  CLOSED  FLOW-FROM  26

   20 13 16              1.0  CLOSED  FLOW-FROM  27

   20 14 16              1.0  CLOSED  FLOW-FROM  28

   20 15 16              1.0  CLOSED  FLOW-FROM  29

   20 16 16              1.0  CLOSED  FLOW-FROM  30

   20 17 16              1.0  CLOSED  FLOW-FROM  31

XFLOW-MODEL 'I' ZERO-FLOW

BHPDEPTH 'I' 7000.0

**********************************The rest of Well section is the same as IMEX basecase**********
```